Catalyst Deactivation in Copper-Catalysed C-N Cross-Coupling Reactions

Grant John Sherborne

Submitted in accordance with the requirements for the degree of

Doctor of Philosophy

School of Chemistry

University of Leeds

April 2017

The candidate confirms that the work submitted is his/her own, except where work which has formed part of jointly authored publications has been included. The contribution of the candidate and the other authors to this work has been explicitly indicated below. The candidate confirms that appropriate credit has been given within the thesis where reference has been made to the work of others.

References for jointly-authored publications:

The work in Chapter 5 of the thesis has appeared in publications as follows:

Grant J. Sherborne, Michael R. Chapman, A. John Blacker, Richard A. Bourne, Thomas W. Chamberlain, Benjamin D. Crossley, Stephanie J. Lucas, Patrick C. McGowan, Mark A. Newton, Thomas E. O Screen, Paul Thompson, Charlotte E. Willans, and Bao N. Nguyen*, '*Activation and Deactivation of a Robust Immobilized Cp*Ir-Transfer Hydrogenation Catalyst: A Multielement in Situ X-ray Absorption Spectroscopy Study*', *J. Am. Chem. Soc.* **2015,** 137 (12), pp 4151–4157.

The work described within this publication is presented in Chapter 5 of this thesis. The candidate was responsible for preparation of iridium complexes, preparation of the flow cell for *in situ* XAFS experiments, taking part in data collection and lab-based experiments. Dr Bao N Nguyen was responsible for data processing, Yorkshire Process Technology supplied fresh immobilised catalysts, Dr Stephanie Lucas synthesised 2 iridium complexes and data collection was a collaborative effort.

Acknowledgements

First and foremost, I would like to thank my supervisors Drs Bao Nguyen and Charlotte Willans for the opportunity to undertake this PhD project. I am thoroughly grateful for the training that I received and I have learned a huge amount over the past three and a half years. I am also grateful for the opportunities afforded me as part of this research, including two long(!) weeks in Grenoble, and my placement in Macclesfield with AstraZeneca, where my industrial supervisor Dr Mark Fielding deserves thanks for helping me make the most of my time there.

I would like to give thanks to the technical staff at the University of Leeds, particularly Mr. Simon Barrett for enabling Bao and I to try out all of our wacky NMR experiments, after a bit of convincing. I must also thank Dr Chris Pask for running and solving single-crystal X-ray diffractions samples, and assistance with powder diffraction.

To the many people who have made the past three and a half years much less painful, thank you for all the pub trips and procrastination along the way. A special thanks to all of the members of iPRD for endless assistance with equipment and great discussion, to go with the walks, cakes and pints. Which leads me thank the many members of the organic section who have been a part of many beer-fuelled Friday nights. Special mentions must also go to Ryan and Seb, who made sure my living arrangements in the final year were never simple.

A massive thank you goes to all of the members of the Nguyen and Willans groups past and present, as well as the Fishwicks who shared the G39j office: Lewis, James G and Ryan. Thanks to Mike for going through that first trip to Grenoble with me, featuring two 5 hour stints in airport bars. To James and Rachel, it has been a pleasure to go through almost everything together during this PhD, you both have made the past few years easier and much more enjoyable.

My biggest thanks must go to my family, who are hugely important in this achievement. You have provided me with everything I have needed to succeed, from life experiences to that little loan before payday, I could not have done this without your support, guidance and encouragement. Last, I would like to acknowledge my Grandad, Ian Hunt, who always took an interest in my work and inspired me with his positive attitude and humour. This achievement is dedicated to you.

Abstract

This thesis details research into the mechanism of the copper-catalysed cross-coupling reaction, with a focus on the *N*-arylation of secondary amines and amides (Ullmann-Goldberg reaction). Issues limiting the application of the Ullmann-Goldberg reaction on industrial scale are uncovered and understood from a mechanistic point of view, to provide a platform for more efficient copper catalysts.

In situ kinetic monitoring using ^{1}H NMR spectroscopy is used to understand the role of each key component in the *N*-arylation of piperidine using a copper catalyst in a fully homogeneous system. Key roles of the amine and catalyst are observed, whilst product inhibition was found to significantly inhibit the reaction. Solvent effects are evaluated by repeating the *in situ* kinetic investigation in d_7-DMF and d_3-MeCN. The kinetic findings indicate deviation of the mechanism from the accepted literature mechanism, with a rate-limiting amine coordination proposed.

Kinetic studies are also used to show the key role that the solubility of inorganic bases such as Cs_2CO_3 and K_3PO_4 play in rate-determining equilibria between copper species. Slow catalyst turnover was observed for up to 14 hours at lowered catalyst loadings, before a dramatic increase in the rate of reaction. A link between particle size, solubility and the deprotonation of the cyclic amide substrate are made, with the results having important implications on the use of inorganic bases in cross-coupling reactions.

Inhibition of the reaction from inorganic side products and precipitation of copper from solution is combined with findings of a novel interaction between copper and cesium cation to give evidence for a non-innocent role of the cesium cation in copper-catalysed *N*-arylation. Heterogeneous catalysis is explored, where it is shown that copper precipitated from the reaction is capable of catalysis, introducing a question of a pseudo-heterogeneous mechanism and phase equilibria.

A multi-edge XAFS (X-ray absorption fine structure) study is combined with laboratory experiments to uncover the activation, deactivation and reactivation pathways of an immobilised iridium transfer hydrogenation catalyst. The key role of an Ir-Cl bond is shown, where initial ligand exchange activates the catalyst, followed by further, slow ligand exchange, leading to deactivation of the catalyst.

Table of contents

Chapter 6 - *Experimental*

Appendix

Abbreviations

$^{13}C\{^1H\}$	Proton-decoupled carbon (NMR)
Å	Angstrom, 1.0×10^{-10} metres
AAS	Atomic absorption spectroscopy
API	Active pharmaceutical ingredient
br	Broad (NMR spectroscopy)
COSY	Correlation spectroscopy
CuTC	Cu(I)-thiophene-2-carboxylate
d	Doublet (NMR spectroscopy)
dd	Doublet of doublets (NMR spectroscopy)
DFT	Density funtional theory
DMEDA	*N,N′*-Dimethylethylenediamine
DMF	*N,N*-Dimethyl formamide
DMSO	Dimethyl sulfoxide
e.g.	*Exempli gratia* (for the sake of example)
EDX	Energy-dispersive X-ray spectroscopy
EPR	Electron paramagnetic resonance
ESI	Electrospray ionisation
et al.	*et alia (and others)*
EXAFS	Extended X-ray absorption fine structure
GC/MS	Gas chromatography/mass spectrometry (coupled)
HCl	Hydrochloric acid
HRMS	High resolution mass spectrometry
Hz	Hertz
ICP	Inductive coupled plasma
IR	Infrared
J	Coupling constant (NMR)
kcal	Kilocalorie
KHMDS	Potassium *bis*(trimethylsilyl)amide
L	Ligand
m	Multiplet (NMR spectroscopy)
m/z	Mass to charge ratio
MS	Mass spectrometry

NHC	*N*-Heterocyclic carbene
ppm	Parts per million
PTFE	Polytetrafluoroethylene
q	Quartet (NMR spectroscopy)
quint	Quintet (NMR spectroscopy)
rt	Room temperature
s	Singlet (NMR spectroscopy)
SEM	Scanning electron microscope
SET	Single electron transfer
t	Triplet (NMR spectroscopy)
t_0	Time-zero (reaction initiation)
TBAA	Tetrabutylammonium adipate
TBPA	Tetrabutylphosphonium adipate
TBPM	Tetrabutylphosphonium malonate
TOF	Turnover frequency
TON	Turnover number
TsDPEN	*N-p*-Tosyl-1,2-diphenylethylenediamine
XAFS	X-ray absorption fine structure
XANES	X-ray absorption near edge structure
XAS	X-ray absorption spectroscopy
δ	Chemical shift

Introduction

### 1.1. Metal-catalysed cross-coupling reactions

Transition metal catalysis is one of the most important fields of chemical research, where it is claimed that 90 % of all commercial chemicals are formed with at least one catalyst being used in the synthesis.[1] The importance of transition metal-catalysed reactions in modern chemistry is highlighted by the award of Nobel Prizes in 2001, 2005, and most recently, in 2010, for the revolutionary methods developed by Heck, Negishi and Suzuki in the field of palladium-catalysed cross-coupling reactions.[2]

Cross-coupling reactions involve the formation of a bond between two organic fragments, often promoted by a transition metal catalyst. The reactions usually require a leaving group, most commonly a halide, but phosphates and sulfonates are amongst others which have been demonstrated.[3-5] Cross-coupling reactions are now possible between a broad range of substrates and a wide range of transition metal catalysts have been developed for use in industrial and academic labs worldwide (Scheme 1.1).
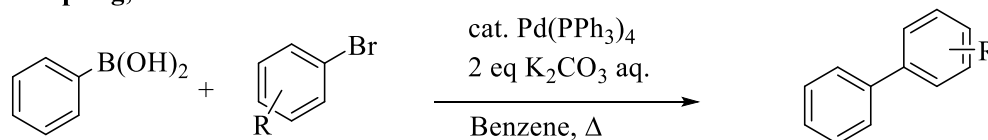
Ullmann Ether Synthesis, 1905
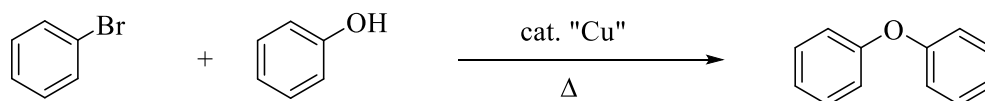
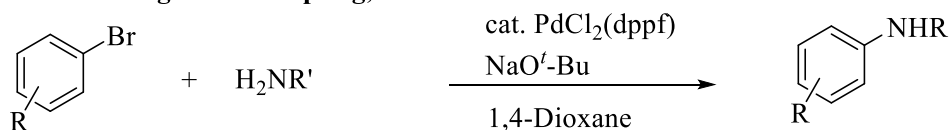**Heck Coupling, 1972**
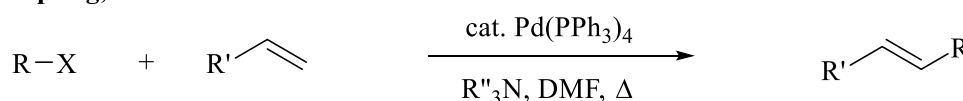
Suzuki Coupling, 1979

Buchwald-Hartwig Cross-coupling, 1994

Scheme 1.1 - Cross-coupling reactions widely used in synthesis. Ullmann (1905),[6] Heck (1972),[7] Suzuki (1979),[8, 9] and Buchwald-Hartwig (1994).[10, 11]

In addition to copper and palladium examples, many other transition metal elements have gained significant attention in the field of cross-coupling, including nickel, cobalt and iron.[12] Ni-catalysed cross-coupling reactions, such as the Kumada coupling has been known for decades,[13] however interest in Nickel as a catalyst remains prominent.[14] Iron catalysts, similar to copper, are particularly attractive due to their low cost and toxicity, and high natural abundance.[15] Recent examples of enantioselective Fe- and Ni-catalysed cross-coupling with Grignard reagents represents an advance for cross-coupling reactions, which have mostly been limited to achiral centres.[16, 17]

1.1.1. Cross-coupling reactions in the pharmaceutical industry

Since the latter half of the 20th century, metal-catalysed cross-coupling reactions have been an indispensable tool to the pharmaceutical industry, providing reliable routes to complex molecules. Use of metals such as Pd, Cu, Ni, Zn, Co, Rh, Ru and Mo has simplified many syntheses of marketed drugs, as well as playing a huge role in many drugs currently under development.[18] The formation of C-C, C-N and C-O bonds is vitally important in the synthesis of organic compounds and the development of new, highly active catalytic systems is a constant goal, in order to increase efficiency and scope whilst reducing costs.

Continued work in the field of cross-coupling since the initial work of the 2010 Nobel Prize Laureates has led to the development of palladium catalysts with turnover numbers (TONs) up to 10^6, making palladium the most efficient catalyst choice in many cases. With strong mechanistic understanding and expansion of scope, implementation of palladium-catalysed coupling reactions on the large-scale synthesis of active pharmaceutical ingredients (APIs) has been realised over recent years.[19]

Table 1.1 summarises the "mainstream" publications which report the use of transition-metal catalysed coupling reactions in large scale (> 100 mmol) reactions. Important to note is the drastic rise in reports since the turn of the century as understanding and substrate scope has developed greatly. Also of note is the numbers for C-N bond formation, where its importance to industry is observed through a rise in reported examples, likely corresponding with the development of the Buchwald-Hartwig *N*-arylation reaction.

Table 1.1 – Data collected on the publication of large-scale (greater than 100 mmol) usage of cross-coupling reactions. Data collected and reported by Dunetz[20].

Type of coupling	Large-scale reports of transition metal-catalysed coupling reactions		
	Pre-2000	**2001-2010**	**2011-Dec 2013**
Suzuki-Miyaura	5	53	16
Heck	10	20	2
Sonogashira	4	17	5
Kumada-Corriu	3	3	3
Negishi	0	10	1
Stille	1	1	0
Hayashi-Miyaura	0	3	0
Tsuji-Trost	1	3	3
Carbonylation	5	8	1
Cyanation	1	14	0
Nozaki-Hiyami-Kishi	0	1	1
Ring-closing metathesis	0	6	3
C-N bond formation	**0**	**13**	**9**
Migita	0	2	3

Brown and Boström have also discussed the impact of cross-coupling reaction in modern medicinal chemistry,[21] evaluating the chemical reactions used in medicinal chemistry and how this has developed with time. The authors found that in the period from 1984 to 2014, the trends in reactions that are used in this field are surprisingly similar. The most recent reaction which was found to be commonly used was the Buchwald-Hartwig amination, first reported in 1994.[10, 11] The only other "recently developed" reaction regularly used in medicinal synthesis was the Suzuki-Miyaura reaction, first reported in 1981.[22] The conclusions of this study are that there are a handful of reactions which are prominent in the area of drug discovery, and of those, only the cross-coupling reactions have been developed since 1980, emphasising the importance of these in synthetic chemistry and the need for more efficient catalytic systems.

1.1.1.1. Suzuki-Miyaura reaction in pharmaceutical synthesis

The Suzuki-Miyaura reaction is a reliable and widely used cross-coupling reaction in modern chemistry, utilising mild conditions, broad functional group compatibility and wide availability of boronic acid coupling partners. Many important pharmacophores, drug intermediates and final drug compounds have been synthesised using Suzuki reactions.[23] The pharmacophore 3-amino-2-phenylpyridine, shown in Scheme 1.2, is synthesised from 3-amino-2-chloropyridine through a one-pot protection of the amine to an imine and a Suzuki reaction with phenylboronic acid.[24]
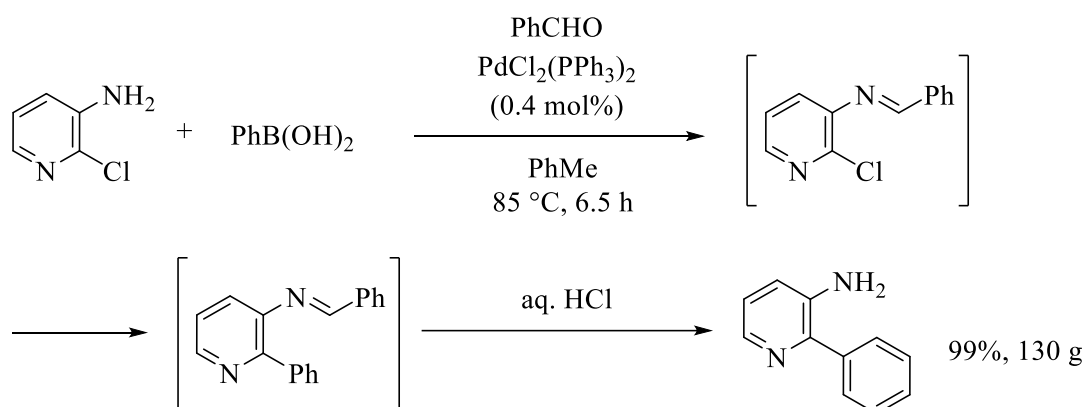
Scheme 1.2 - One-pot synthesis of 3-amino-2-phenylpyridine from 3-amino-2-chloropyridine.[24]

Work performed at Novartis in 2010 reports the coupling of the aryl chloride precursor with 4-carboxyphenylboronic acid to yield a phosphodiesterase-4 inhibitor in 88% yield, using the palladium dimer [PdP(t-Bu)$_3$Br]$_2$ as a catalyst (Scheme 1.3).[25] The mild conditions, stability of the Pd(I)-dimer complex in H$_2$O and the conservation of stereochemistry during these conditions made this an effective reaction to give the final API.
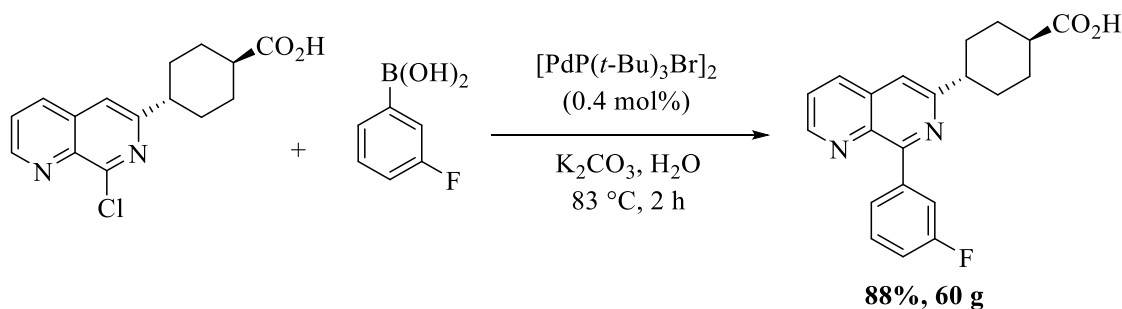
Scheme 1.3 - Novartis' synthesis of a phosphodiesterase-4 inhibitor using a Suzuki coupling.[25]

4

Elsewhere, Merck published the synthesis of GABA α2/3 agonist (**B** in Scheme 1.4). This synthesis involves the C-C coupling of 2-bromo-5-fluorobenzonitrile with an arylboronic acid to yield the precursor **A** in 92%, with just 0.3 mol% catalyst loading.[26]
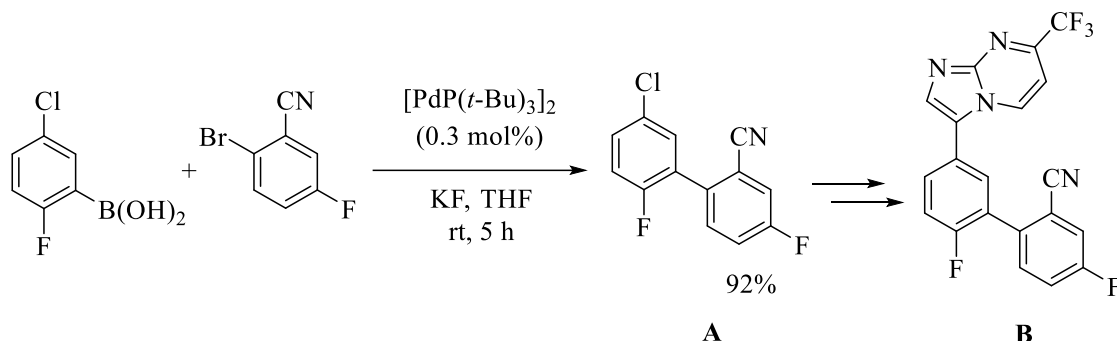
Scheme 1.4 – Suzuki coupling to make compound **A**, reported by Merck.[26]

1.1.1.2. Other coupling reactions for pharmaceuticals

Many other drugs involve coupling reactions as key steps in their synthesis, a few examples are depicted in Figure 1.1, for example the migraine treatment Eletriptan, marketed as Relpax by Pfizer, which is formed with a Heck C-C coupling between a phenyl vinyl sulfone and its bromoindole precursor.[27] Elsewhere, Gegentech developed a synthesis for Vismodegib involving a Negishi coupling with a palladium catalyst and zinc to assist in transmetallation.[28] An example of a Buchwald-Hartwig C-N bond formation can be found in a synthetic procedure published by Novartis for the leukemia treatment Imatinib, of which the mesylate salt is marketed.[29]
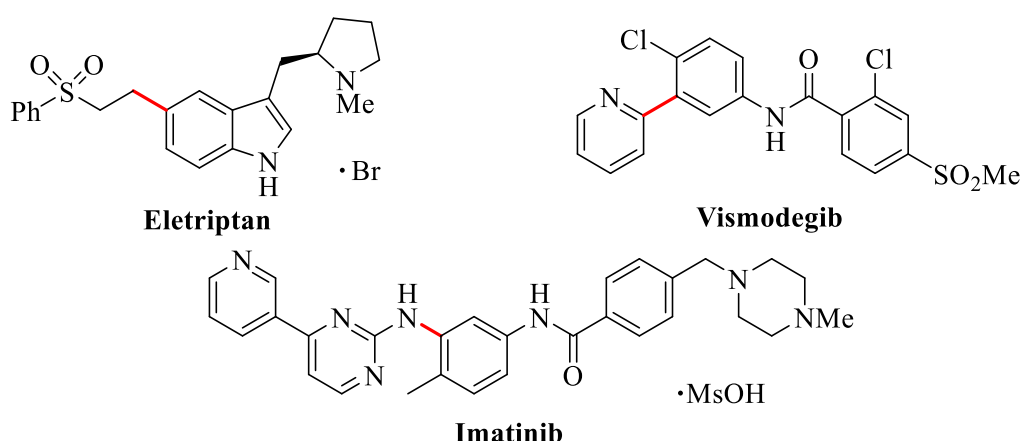

Figure 1.1 - Important drug molecules which feature bonds constructed by transition-metal catalysed coupling reactions. Eletriptan (Heck coupling)[27], Vismodegib (Negishi coupling)[28] and Imatinib (Buchwald-Hartwig coupling)[29].

With a large proportion of synthetic drug-like molecules requiring the construction of C-C, C-N, C-O or other C-heteroatom functionality, cross-coupling reactions are often the best option for the formation of these bonds. There is however both economic and toxicity drives to ensure that these reactions are performed with mild conditions such as low catalyst loadings, "green" solvents and without the formation of unwanted byproducts. It is for this reason that constant research in alternative catalytic systems is still widespread, particularly in base metal and metal-free cross-coupling reactions.

1.2. Copper-catalysis in synthesis

Copper salts are inexpensive, possess low toxicity and are able to mediate a range of reactions catalytically (Scheme 1.5).[30] Various copper sources are known to act as catalysts for organic transformations. For example, Cu(0) powder in Ullmann-type coupling reactions,[6, 31] and Cu nanoparticles in cross-coupling reactions and reductive cleavage reactions.[32, 33] Cu(I) salts are widely prevalent in many catalytic procedures, such as Ullmann etherification and amination reactions,[34, 35] click chemistry,[36] Grignard coupling,[37] and conjugate addition reactions.[38] Cu(II) salts are the most common form of copper, and a number of procedures have been developed to harness the catalytic competence of these, such as the Chan-Lam coupling and even water oxidation.[39-41]
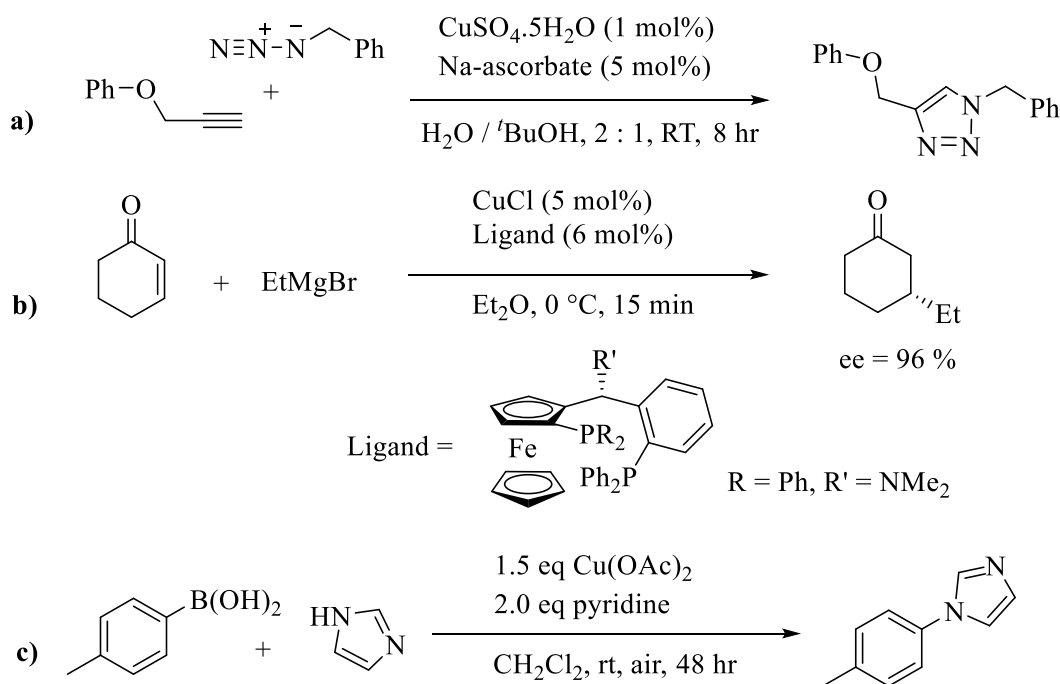
Scheme 1.5 – Showcase of copper catalysis in a) click chemistry,[42] b) asymmetric conjugate additions,[38] and c) Chan-Lam cross-coupling.[40]

1.2.1.1. Copper-catalysed mechanisms

As a catalyst for many different reactions, copper catalysts have been reported to proceed through a variety of mechanistic pathways Copper has been shown to be catalytically active in all the well-known oxidation states, from Cu(0) to Cu(III), and is often able to shuttle between these *via* one-electron or two-electron processes.[43]   As a result of this, copper catalysts are often expected to react as organometallic reagents, similar to the behaviour of palladium in coupling reactions,[44] or through single electron transfer (SET). Typically, a two electron process is expected to occur from Cu(I) to Cu(III), as Cu(IV) complexes have only been discussed and experimentally observed in rare cases.[45, 46] Distinguishing between SET and two electron processes can be difficult, common techniques employed to achieve this include radical clock reactions,[47] kinetic isotope effects,[48] and computational studies.[49-51] Yu combined some of these techniques in 2006 to determine a SET pathway in the C-H functionalisation of a pyridine-bearing aryl rings (Scheme 1.6).
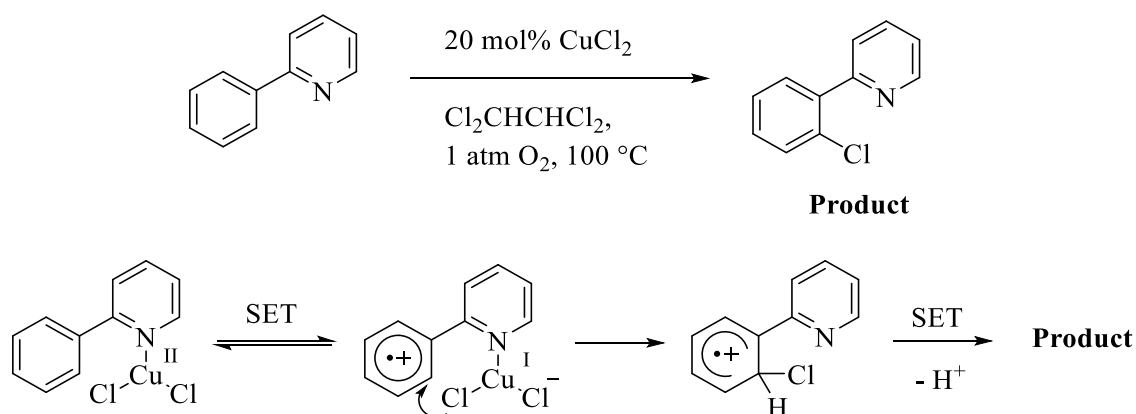
Scheme 1.6 - Yu's proposed SET mechanism in the Cu(II)-catalysed chlorination of aryl C-H bonds.[48]

Stahl reported the divergence between an organometallic and SET pathways in the Cu(II)-mediated aerobic oxidation of *N*-(8-quinolinyl)benzamide.[49]   Under acidic conditions it was found that a chlorination occurs on the quinoline group in the presence of a Cu(I) catalyst, whilst under basic conditions, mediated by Cu(II), methoxylation of the benzamide is favoured. These results highlight the varied chemistry of copper as a catalyst and mediator for various organic transformations.
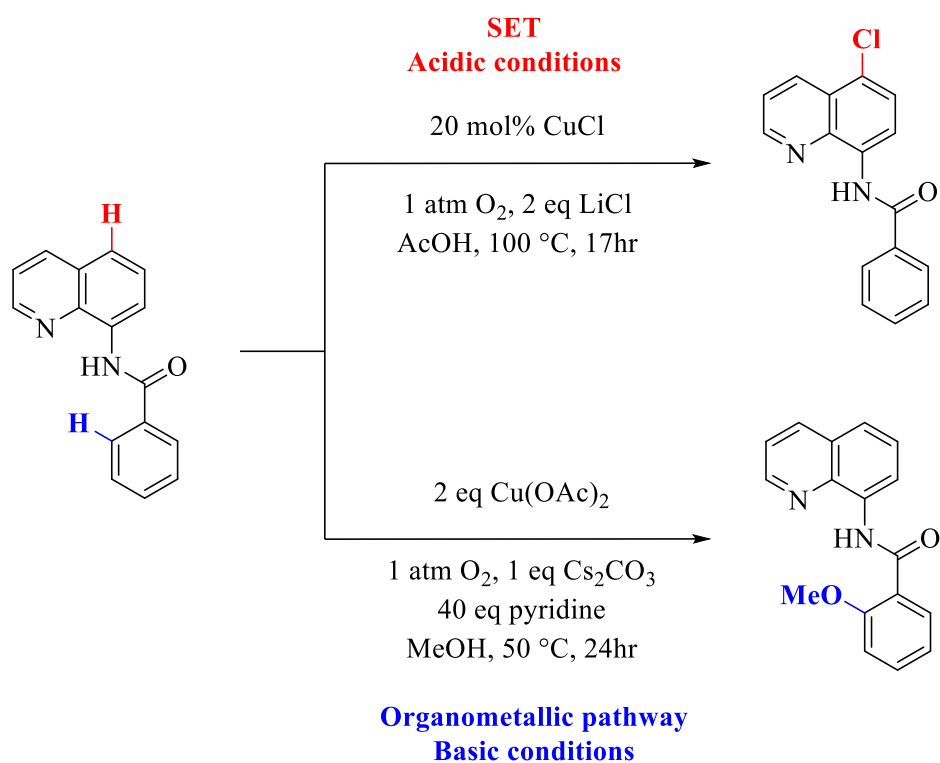
Scheme 1.7 - Condition-dependant selectivity of C-H activation mechanism as reported by Stahl.[49]

1.2.2. Copper-catalysed cross-coupling reactions

Copper-mediated coupling reactions were initially discovered in the late 19th century and have developed significantly over following years. The use of copper-mediated cross-couplings have expanded from Ullmann's initial aryl-aryl coupling,[52] to carbon-amide bond formation pioneered by both Ullmann and Goldberg,[53, 54] followed by carbon-carbon coupling reactions shown in Scheme 1.8.[6, 55] Throughout much of the 20th century, copper was the primary metal used to mediate coupling reactions; however due to poor efficiency, limited substrate scope and extreme conditions, industrial implementation was scarce.
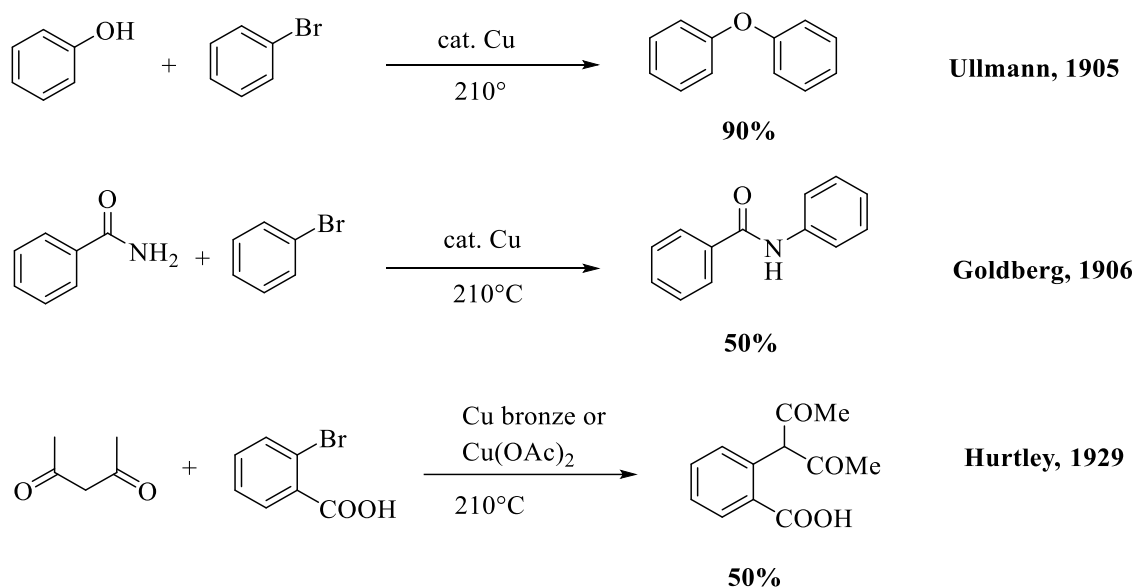
Scheme 1.8 - Early development of copper-catalysed coupling reactions.

The emergence of palladium as an efficient catalyst for cross-coupling reactions in the 1970's resulted in widespread use of palladium catalysts in academic and industrial syntheses.[44] Much of the focus of research into cross-coupling reactions was put onto palladium chemistry, leading to a good understanding of mechanistic behaviour and a broad range of synthetic applications.[56]

At the turn of the 21st century, copper-catalysed coupling reactions have seen somewhat of a resurgence, when it was initially observed that ancillary ligands boosted reactivity.[57] The development of more robust catalytic systems for C-N and C-O cross-couplings has led the way for an increase in research on the topic. This work is fuelled by the drive to reduce the cost of processes which use the precious metals, such as palladium, whilst avoiding toxic metals which require added processes to be removed downstream. Copper is an ideal target as it has the benefit of being a much cheaper and having a higher toxicity threshold in active pharmaceutical ingredients (API), as reported by the European Medicine agency (Table 1.2).[58]

Table 1.2 - Daily oral exposure limits for selected metals.

Classification	Oral Exposure PDE (μg/day)
Metals of significant safety concern	
Class 1A: **Pd**, Pt	100
Class 1B: Ir, Rh, Ru, Os	100
Class 1C: Mo, Ni, Cr, V	250
Metals with low safety concern	
Class 2: **Cu**, Mg	2500
Metals with minimal safety concern	
Class 3: Fe, Zn	13000

1.2.3. Modern advances in copper-catalysed cross-coupling reactions

Recent developments to the copper-catalysed C-C, C-N and C-O cross-coupling reactions have been somewhat restrained by limited mechanistic understanding when compared to the understanding of palladium cross-coupling reactions. Ligand design and nanoparticle catalysts are two of the areas which have been investigated in the past 5 years,[59, 60] however furthering the mechanistic understanding is necessary for advancements to be made.

An important new methodology which has been reported in recent years is the light-mediated copper-catalysed cross-coupling reaction, reported by Creutz and Fu,[61, 62] and von Wangelin.[63] These reactions may be expected to follow a different mechanistic pathway to the classical Ullmann-type coupling reactions, as they can be performed under ambient conditions, or low temperatures (-40 °C). Further to this, Fu has reported the first light-mediated asymmetric copper-catalysed C-N coupling in 2016, harnessing visible light and a chiral phosphine ligand, to couple tertiary alkyl chlorides with secondary amines (Scheme 1.9).[64]
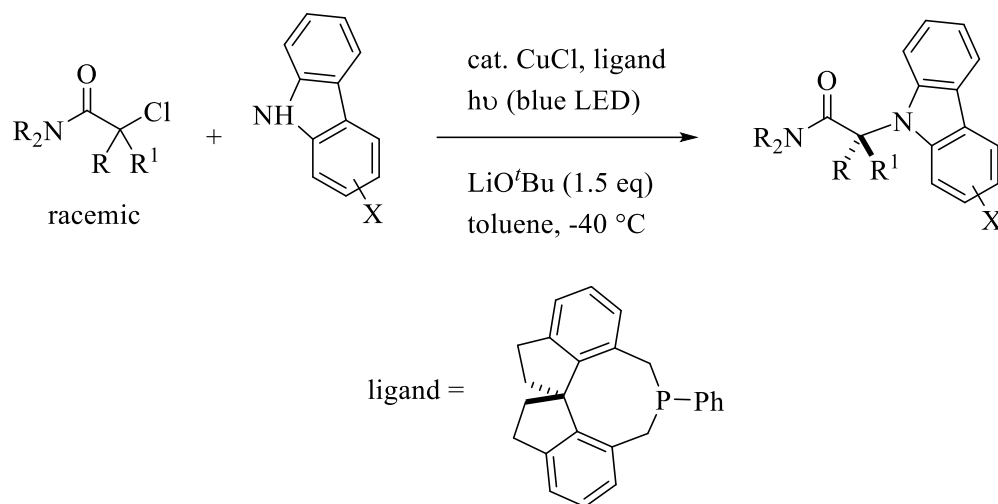
Scheme 1.9 - Asymmetric light-driven copper-catalysed C-N coupling reported by Fu.[64]

1.2.4. Limitations of copper-catalysed coupling reactions

Despite the benefits that copper can offer over more established metals, such as palladium, there is still a lack of efficiency in the copper-catalysed systems. As a result, there are a number of hurdles that need to be overcome if widespread industrial implementation is to be realised.[65] These include irreproducibility of results, high catalyst loadings (typically 10 mol %), high reaction temperatures (> 100 ^{o}C) and poor efficiency.[66]

It is not well understood why copper catalysts often lack efficiency, with few sub-mol% examples available, however catalyst deactivation may be involved. If a high proportion of active catalyst species is lost throughout the reaction, it will slow the reaction rate and necessitate high catalyst loadings. Development of mechanistic understanding is vital to the production of more efficient catalysts, and in copper-catalysed cross-coupling reactions, there remain unanswered questions despite progress that has been made in recent years.

1.2.5. Copper-catalysed cross-coupling mechanism

1.2.5.1. Early mechanistic studies

Of the areas still widely debated, perhaps the aryl halide activation step is the most contentious issue currently. What is apparent, as is the case with palladium cross-coupling reactions, is that there is not a "one-size-fits-all" rule regarding the mechanism. Early work on the mechanism was first seen in the 1960's, with Weingarten studying the

catalytic condensation of potassium phenolate and bromobenzene.[67] In testing a number of Cu(I) and Cu(II) salts and through EPR studies, it was determined that Cu(I) is most likely the active copper species, which is still largely agreed upon today. Weingarten also used kinetic observations to propose a mechanism involving two phenoxide molecules coordinating to copper, followed by aryl halide activation, as shown in Scheme 1.10.
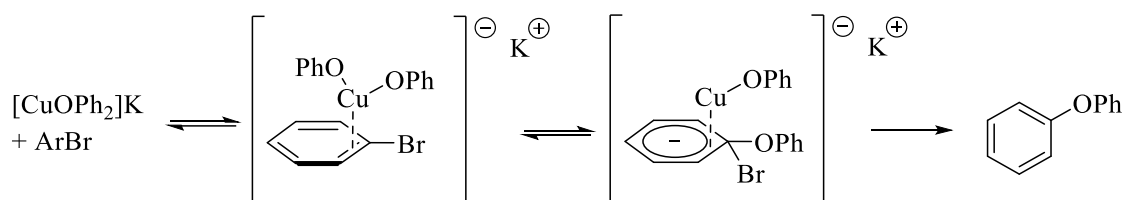
Scheme 1.10 - Early Cu(I) mechanism of aryl halide activation as proposed by Weingarten in 1964.[67]

1.2.5.2. Mode of aryl halide activation

Other studies performed prior to 1990 largely refer to the reaction as a catalytic aromatic nucleophilic substitution (S_NAr), although the reactivity order of the aryl halides follow the bond-dissociation energies of the halogens ($I > Br > Cl$), opposite of that expected in S_NAr reactions.[18] This trend is discussed by Paine in 1987 and is summarised in Table 1.3. It is observed that the uncatalysed S_NAr reactivity trend is consistent with a rate-limiting step of addition of a nucleophile to the carbon, but the copper-catalysed reaction indicates breaking the C-X bond is rate-limiting.[68]

π-Coordination of the $[Cu(Nucleophile)_2]^-$ species to the aryl halide, as proposed by Weingarten, was predicted to act as an activating group to promote the nucleophilic aromatic substitution, as seen with various metal-complexed halobenzenes.[69] Paine disputed this however, drawing attention to the known activating effect of a carboxylate group in the ortho position but not para, as well as the opposite order of halide reactivity seen between the copper-promoted reactions and those of the metal-complexed halobenzenes.[68]

Table 1.3 - Bond dissociation energies (KJ mol^{-1}) for various aryl halides and the reactivity order seen in cross-coupling reactions.

Aryl-X Bond	Bond Dissociation Energy (KJ mol^{-1})	Reactivity Order
Ph-F	533	Least reactive
Ph-Cl	407	
Ph-Br	346	
Ph-I	280	Most reactive

1.2.5.3. Single electron transfer

Van Koten *et al.* discussed the possibility of an oxidative addition/reductive elimination type mechanism but concludes that the formation of Cu(III) is unlikely and instead, proposes a single electron transfer (SET) mechanism, followed by concerted formation of the product (Scheme 1.11).[70] The theory of a SET pathway was first speculated in 1937 and further developed in the 1960s.[71,72,73] When Bunnett proposed the S$_{RN}$1 mechanism for unimolecular radical nucleophilic substitution,[74] it was a logical step to connect this to the knowledge that organometallics which were capable of electron transfer, such as copper, could act as catalysts for nucleophilic aromatic substitution.[75]
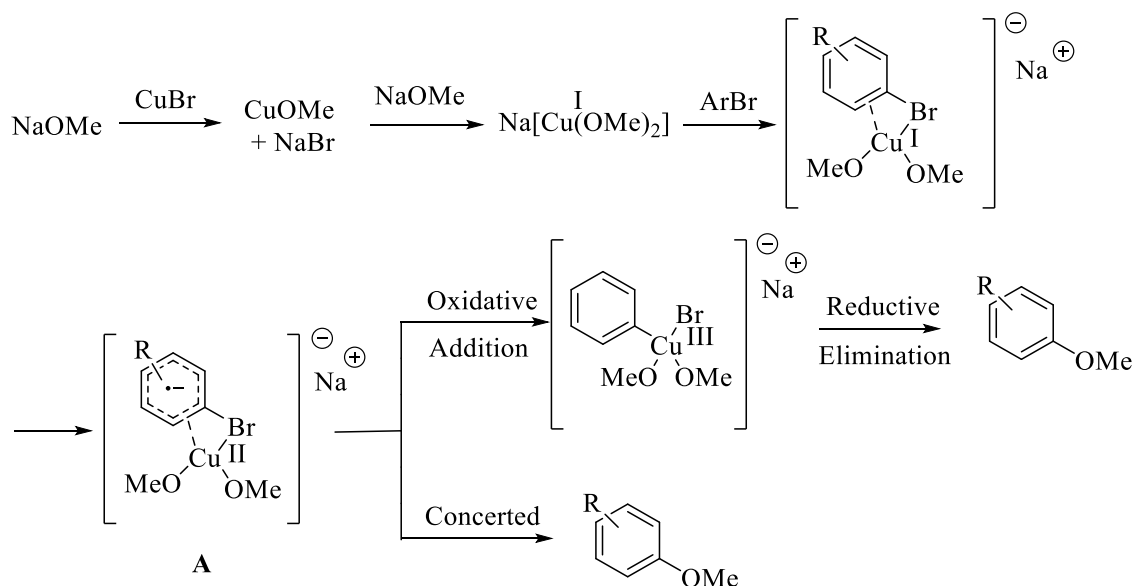
Scheme 1.11 - The proposed pathways possible for aryl-halide activation as reported by Van Koten. SET from Cu(I) to Cu(II) species (**A**) was concluded to precede concerted formation of the coupled product and Cu(I).[70]

13

Studies investigating a possible SET redox couple between Cu(I) and Cu(II) include reports by Bowman, who performed a number of experiments, including the radical clock investigation of an intramolecular ring closure seen in Scheme 1.12.[76] In this test, the reaction performed under photocatalytic $S_{RN}1$ conditions yielded the ring closing product, whilst the Cu-catalysed reaction only yielded the coupled product, giving evidence against aryl radicals being formed. This reaction is based on the theory that if aryl radicals are present, the formation of the ring-closed product would be the kinetically favoured product. The legitimacy of this radical clock type experiment and those alike has been questioned by Buchwald however, who introduces the idea that an aryl radical may exist in the form of a caged radical pair, unavailable for reaction with the alkene functional group.[77]

Radical pathway

Ring-closed product

Cross-coupling pathway

Coupling product
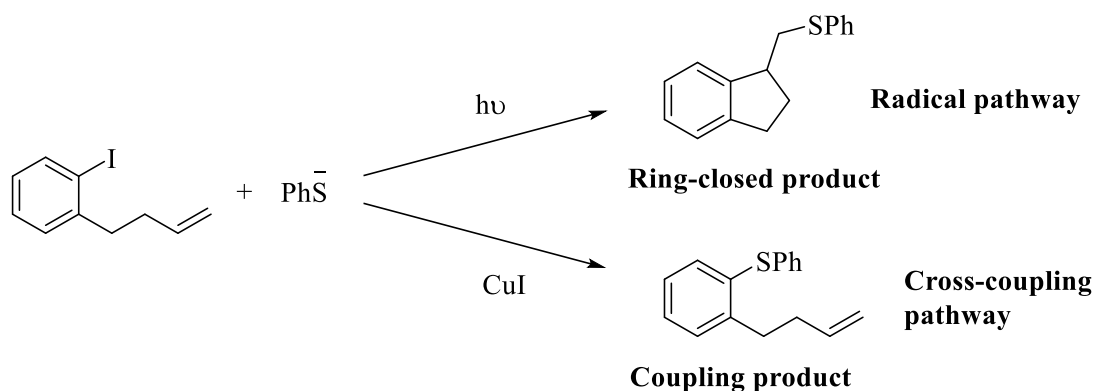
Scheme 1.12 - Radical clock experiment performed by Bowman to determine the likelihood of aryl radicals being involved in aryl halide activation and coupling.[76]

Norrby has also disputed the SET mechanism,[78] using DFT calculations and a Hammett study to conclude that aryl radicals are unlikely to be formed in the rate limiting step. A correlation between aromatic substituents and σ• values would be expected if aryl radicals were involved in the mechanism.[79] The DFT calculations in this study indicate that an oxidative addition and irreversible reductive elimination pathway is considerably lower than the calculated radical pathway, contradicting Buchwalds reports,[77] but agreeing with other computational reports.[80, 81]

1.2.5.4. A copper(I)/(III) cycle

Van Koten's work was not the first discussion of a Cu(I)/Cu(III) oxidative addition, Cohen hypothesised its involvement in copper-promoted halogen exchange reactions in 1979 and Bethell to an Ullmann amination in 1985.[82, 83] Both provided an argument for

addition of aryl halides to copper halide salts, to form Cu(III) species, which would undergo reductive elimination to yield the products and Cu(I). The presence of Cu(III) intermediates in the cross-coupling reactions is still widely debated, and whilst in many cases it is assumed that they likely play a role, there is little experimental evidence due to the inherent difficulty in observation or isolation of Cu(III) species. One study utilising a highly stabilising triazamacrocyclic ligand was reported in 2010 by Ribas as shown in Scheme 1.13, whereby they directly observe Cu(III) intermediates similar to those previously proposed.[84] The authors use *in situ* ^{1}H NMR and UV-visible spectroscopy to show the complexes relevance to an *N*-arylation reaction, however the application of this chemistry to typical reaction systems has been questioned.[66]
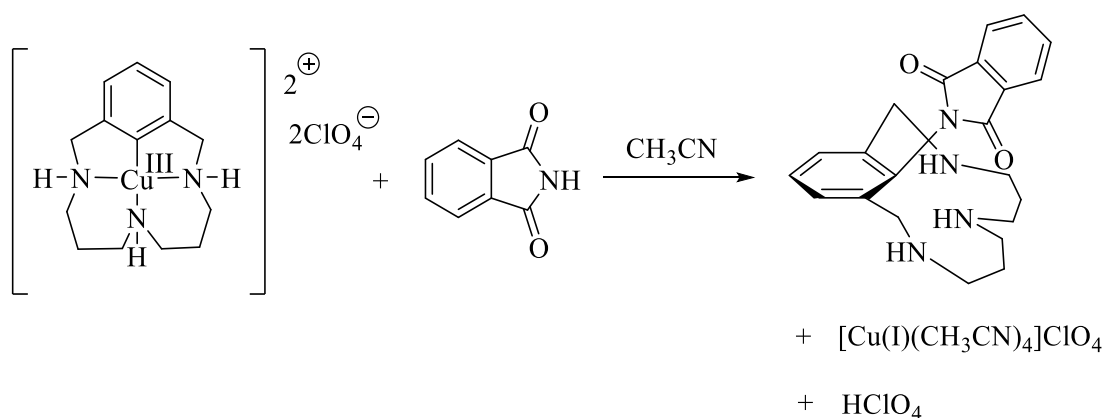
Scheme 1.13 - Cu(III) complex and its reaction with pthalimide, demonstrating possible role of Cu(III) as intermediates in Cu-catalysed cross-coupling with amides.[84]

1.2.5.5. Role of the ligand

Use of ancillary ligands to boost the efficiency of copper-catalysed cross-coupling reactions has been the key to the resurgence of research in the area since the late 20th century. The role that the ligand plays in the mechanism has been studied since their use by Liebeskind in biaryl syntheses,[85] and Buchwald in aryl ether synthesis,[86] followed by the *N*-arylation of heterocycles.[57] Liebeskind hypothesised that his preformed Cu(I) thiophene-2-carboxylate complex (CuTC) would stabilise a reversible oxidative addition of the aryl halide.

Buchwald, alternatively, proposed that 1,10-phenantholine added as a ligand stabilised the copper intermediates or improved solubility of the copper salts. Buchwald also found in the same work that *trans,trans*-dibenzylideneacetone (dba) stabilised the reaction to oxidation, possibly preventing disproportionation of Cu(I) to Cu(0)/(II) or just preserving the active Cu(I) intermediates. Now, there is a large pool of ligands available to choose from, with the majority of them being commercially available and easy to handle, some of the most popular ligands are depicted in Figure 1.2.[30]
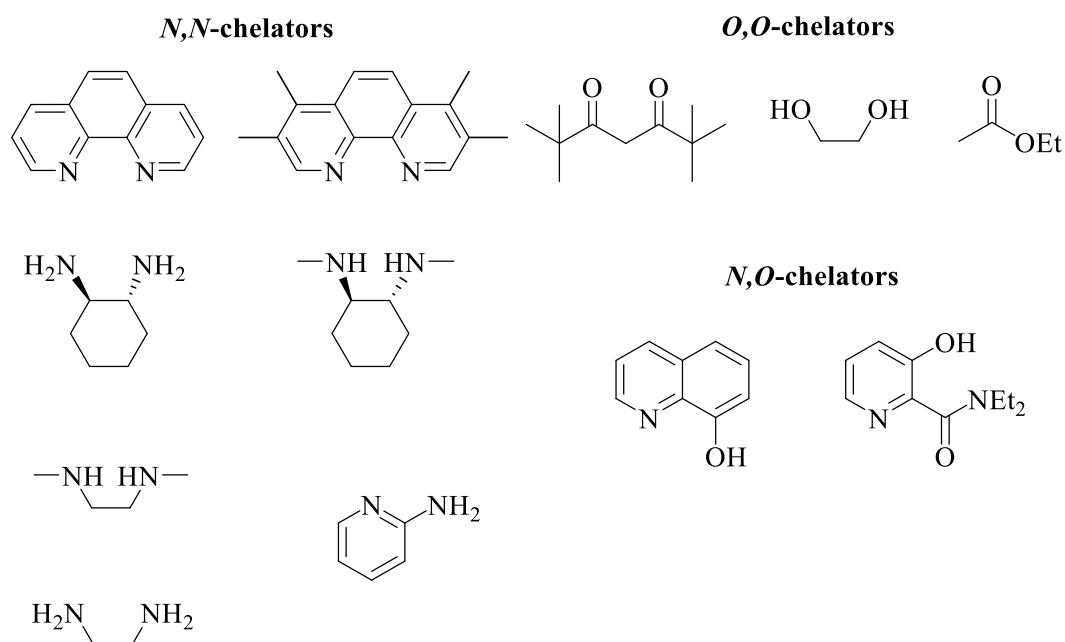
Figure 1.2 - Various ligands which have been reported to mediate Cu-catalysed cross-coupling reactions.[30]

More recent work has explored in-depth investigations, providing insight into structure-activity relationships[87] and chemoselectivity.[88] These studies discuss electron rich and electron poor copper complexes formed from different ligands and their influence on reactivity (Scheme 1.14). This knowledge may be useful in choosing systems for more complex molecules, in which *N*- and *O*-arylation may be competitive. A follow-up report from Buchwald used computational methods to show how the electron-rich *β*-diketone promotes a SET in both *N*-arylation and *O*-arlyation reactions, although with a faster rate in *N*-arylation. On the other hand, the less electron-rich phenanthroline ligand promotes SET in *N*-arylation but the faster iodine atom transfer (IAT) in *O*-arylation.[77]
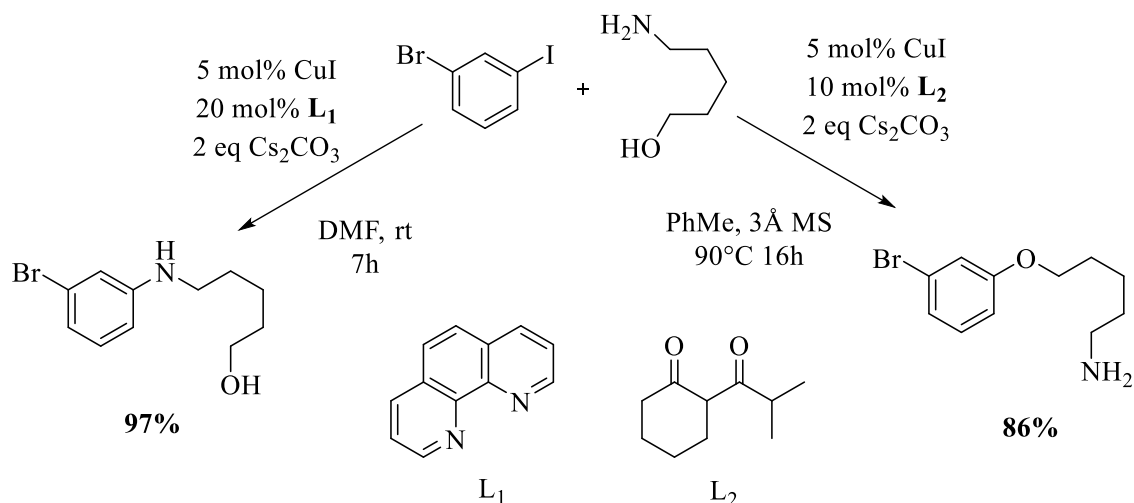
Scheme 1.14- Study reported by Buchwald in 2007 discussing how electronic effects of the copper centre can affect selectivity in C-N and C-O coupling.[88]

1.2.5.6. Kinetic studies

Perhaps the most powerful tool for mechanistic investigations into Ullmann-type catalyst systems involves kinetic studies. Buchwald and Blackmond published a key study in 2005 in which the reaction of 3,5-dimethyliodobenzene and 2-pyrrolidinone under copper-catalysed conditions was probed.[89] The reaction in Scheme 1.15 was chosen for its selective and highly efficient turnover, making it ideal for study by calorimetry.
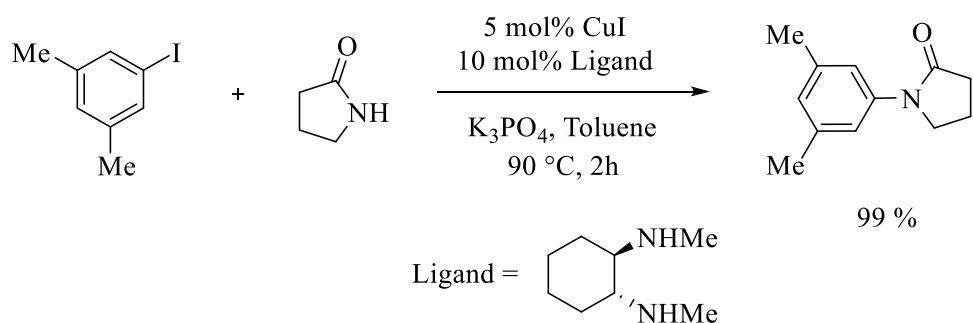
Scheme 1.15 - Coupling of 3,5-dimethyliodobenzene with 2-pyrrolidinone used for kinetic studies by Buchwald and Blackmond.[89]

The system studied showed a change in rate law when changing from low to high initial concentration of diamine ligand.[89] It was found that at low $[Ligand]_0$, a first order dependence on [Ligand] was observed. At high $[Ligand]_0$ however, a zero-order dependence of rate on $[Ligand]_0$ was observed. Buchwald explained these results by proposing the equilibrium shown in Scheme 1.16. In this equilibrium, low concentrations of the diamine ligand result in a multiply coordinated *bis*-amidate

complex (**A**), which has been shown to be inactive in the case of a pthalimidate example.[90] At high concentrations of the diamine ligand, the major species (**B**) is in rapid equilibrium with the copper(I) amidate (**C**), allowing the activation of the aryl halide to be the rate-limiting step.
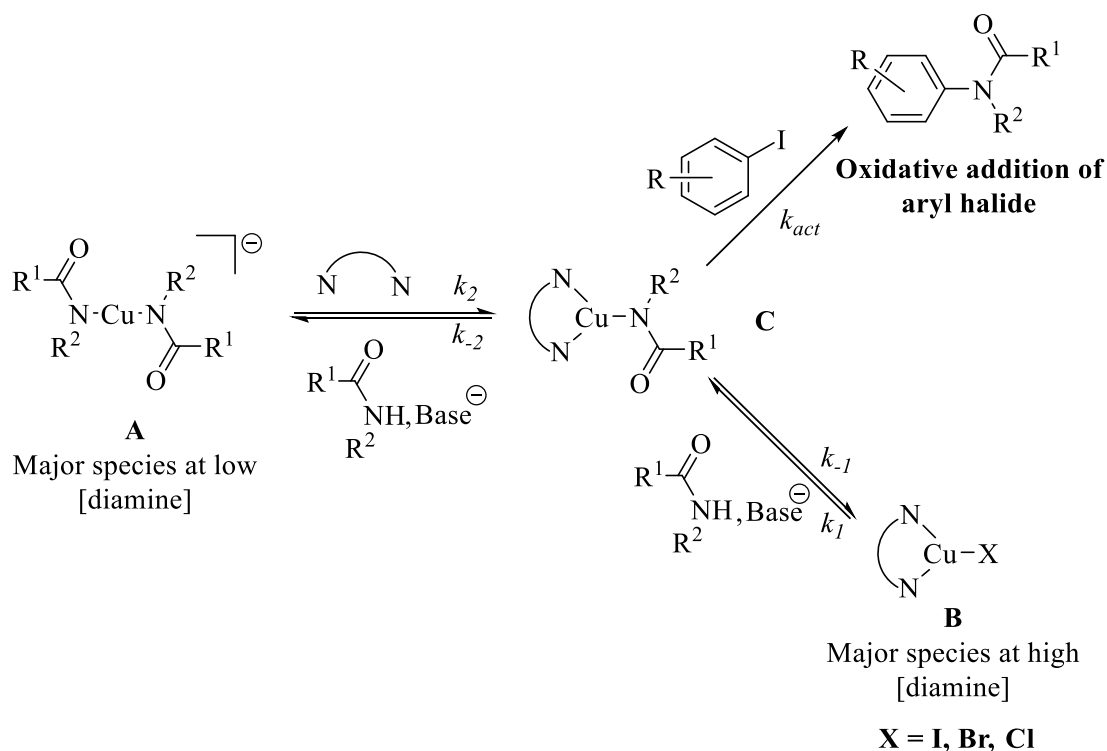
Scheme 1.16 – Buchwald's proposed equilibrium for copper-catalysed activation of aryl halides under varying [ligand] and [amide].[89]

Norrby has investigated the copper-catalysed C-N bond formation at sub-mol% levels of catalyst.[91] Using the *N*-arylation of pyrazole in the presence of $CuCl_2$ and *N,N*-dimethylethylenediamine (20 mol%), it was found that at very low levels (0.000625 – 0.04 mol%), the reaction was first order in [Cu], but zero order in [Cu] at higher loadings (0.16 – 0.64 mol%). It is hypothesised that at the higher loadings, the active copper in solution is in equilibrium with inactive heterogeneous copper species, such as nanoparticles. At 0.5 mol% copper loadings, a zero-order dependence on base (K_3PO_4) is observed, whilst a first-order dependence in aryl halide, a positive order in DMEDA and variable in pyrazole are also found. Though the catalyst loadings in this study are not entirely representative of a typical Ullmann-Goldberg coupling, the saturation of the soluble copper catalyst at > 0.16 mol% is an interesting result given the typically high (10 mol%) loadings usually used. Further work by Norrby showed that the positive order

in the DMEDA ligand is due to its dual role of ligand and mass transfer facilitator for the inorganic base.[78]

1.2.5.7. Copper(I)-nucleophile complexes

The unstable nature of many Cu(I) and particularly Cu(III) species has led to difficulty in directly observing intermediates in Cu-catalysed cross-coupling reactions. Key mechanistic studies since 2005 performed by Buchwald,[89, 92] Hartwig,[90, 93] and Jutand[80] dedicate much focus to the important balance between ligands and nucleophile.

An early example of a phosphine-stabilised Cu(I)-anilido complex was reported by Gunnoe in 2003,[94] and was shown to react with carbocationic species and alkyl halides. In attempts to show the relevance of complexes between Cu(I) and nucleophiles, Buchwald synthesised a Cu(I)-amidate complex (Scheme 1.17),[89] this was found to have broad signals in the ^{1}H NMR spectrum, relating to multiple oligomers, which are prone to formation with Cu(I) salts[95]. Upon the addition of a 1,2-diamine ligand, the NMR peaks sharpened, attributed to formation of monomeric species. This complex, in the presence of the ligand forms the C-N coupled product with 3,5-dimethyliodobenzene rapidly at 0 ℃, indicating strong relevance of the intermediate to the catalytic coupling reaction.
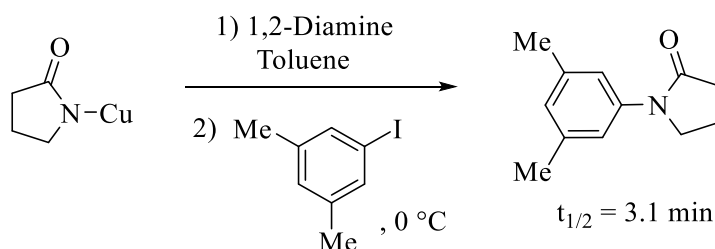
Scheme 1.17 - Reactivity of Cu-amidate complex with an 3,5-dimethyliodobenzene in the presence of a 1,2-diamine ligand.[89]

Hartwig explored a similar intermediate for the etherification reaction, forming various anionic [Cu(OPh)$_2$]$^-$ complexes and assessing the kinetic and chemical competency of the complexes for C-O bond formation.[96] Poor yield was obtained from the ligand-free reactions involving these complexes, with similar conclusions drawn to the copper-amidate complexes of Hartwig and Buchwald described previously.[89, 90]

The oligomeric form in which Cu(I) amine and amide complexes may exist in are typically regarded to be catalytically inactive, requiring conversion to a monomeric form.[57] Recent work from Davies has however shown the potential intermediary role that copper(I) amide complexes, existing in various aggregated forms, may play in the C-N cross-coupling of aryl iodides.[97] Ligand free, stoichiometric reactions of these complexes result in the significant turnover of less sterically bulky aggregates in when run in DMSO for the first time. This work may mean that a competing pathway, not involving coordination of an ancillary ligand is possible, with the work also shedding light on the issue of sterically hindered amines giving poor conversion.
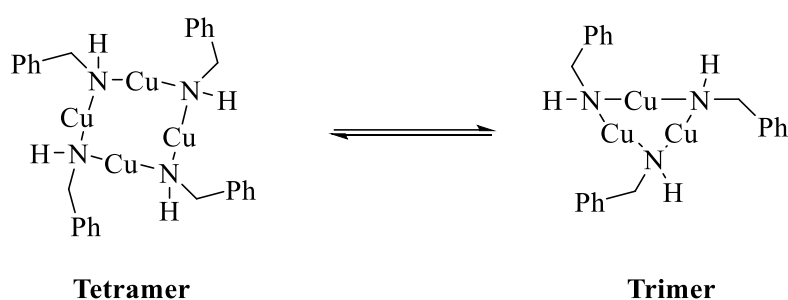
Scheme 1.18 - Tetramer and Trimer oligomers of a Cu(I)-benzylamine complex studies by Davies.[97]

1.2.5.8. Role of the base

The best choice of which base to use in cross-coupling reactions is often not predictable, where the chemist will be required to screen a number of bases for a certain reaction and use the best of these. Whilst this is an inefficient approach to the matter, the difficulty lies in the fact that different substrates, ligands and solvents all may interact with the base in a different manner. One important consideration is the possible presence of base-sensitive functional groups, such as esters, phenols or amides which can lead to numerous unwanted side products.

The role of the base in copper-catalysed C-N and C-O coupling reactions is primarily to deprotonate the nucleophile, although deprotonation of a ligand may also occur. Weak bases such as K_2CO_3, K_3PO_4 or Cs_2CO_3 are almost always utilised despite their poor solubility in organic solvents, which has made computational studies of the reaction somewhat difficult.[51] It is assumed that due to the disparity in pKa between base and nucleophile, coordination of the nucleophile to the copper centre is necessary before deprotonation can occur.

Buchwald has proposed that the low solubility of inorganic bases in organic solvents is vital to reactivity and it is necessary to match the rate of nucleophile deprotonation with bond formation. Evidence for this comes from observations that stronger bases such as KHMDS require slow addition to the reaction for adequate conversion to occur.[98] This is thought to be due to the catalytically inert *bis*-amido curprate which is hypothesised to dominate the reaction under these conditions.[89] These conclusions are mostly speculation however, with little experimental evidence available in determining the exact nature of the deprotonation step.

DFT calculations on the Pd-catalysed Buchwald-Hartwig reaction shows that whilst coordination of the *N*-nucleophile must coordinate to palladium before deprotonation, it is still unknown whether the base must also coordinate.[99] A similar topic is still debated in the copper-free Sonogashira cross-coupling reaction, where tertiary amine bases such as triethylamine (pKa = 10.75) are commonly used. A η^2-coordination of the metal to the alkyne is hypothesised to be necessary to activate the alkyne C-H bond ($pKa \approx 20 - 25$) for deprotonation by the weak base.[100, 101]

In 2017, Sharma reported spectroscopic evidence for phosphate and carbonate having a triple role of base, bidentate ligand and inhibitor for the reaction between aryl iodides and *N*-nucleophiles (Scheme 1.19).[102] The study combined DFT calculations and spectroscopic experiments to give evidence for a Cu(III) species, in which they calculated the octahedral complex (**B**) to be involved in the lowest energy pathway, facilitating the reductive elimination of the coupling product. The authors calculated a high energy barrier for the displacement of the carbonate moiety for the nucleophile (59.53 kcal^{-1}) (**A** to **B** below), and hypothesise inhibition of the catalytic cycle at high $[CO_3^{2-}]$. Characterisation of the Cu(III) species in this work is limited to comparison with literature spectra of similar complexes such as Ni^{2+}, if the proposed mechanism is to validated, further experiments such as kinetic studies are necessary.
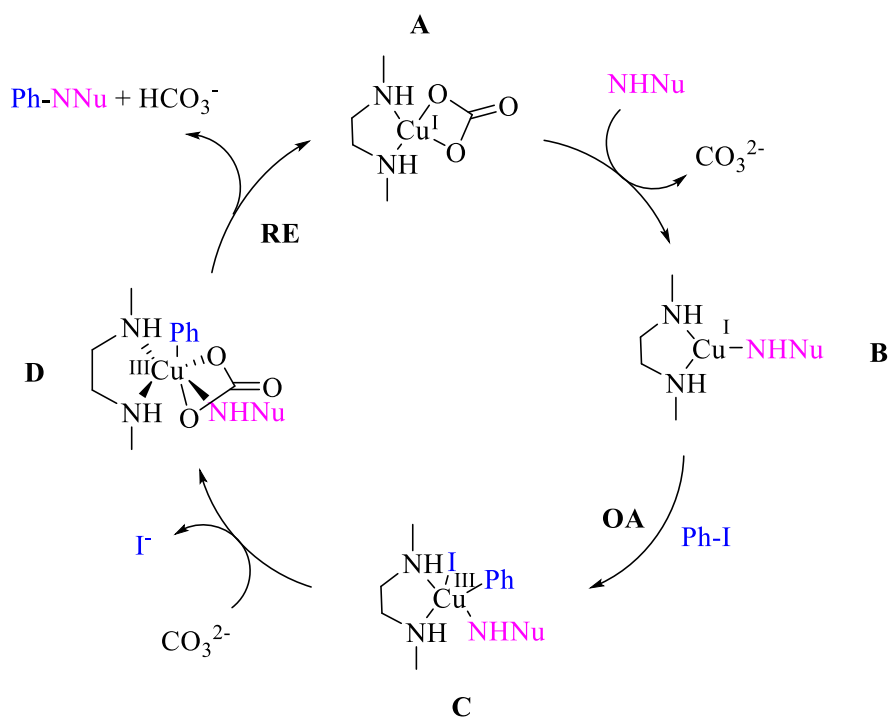
Scheme 1.19 – Cu(I)/(III) mechanism proposed by Sharma.[102]

1.2.5.9. Irreproducibility in copper-catalysed cross-coupling reactions

From an industrial standpoint, the irreproducibility associated with copper-catalysed cross-coupling reactions is a major hurdle which is necessary to overcome. Discussions regarding these reactions almost always come with stories of reproduction problems, however there is a lack of specific examples regarding the matter found in the literature. The air sensitive nature of the reaction may be one issue, although on scale-up trace amounts of O_2 is thought to have a negligible effect when compared to lab-scale. On a large scale, the amount of air needed to poison the reaction is likely to be much greater than that which would be typically introduced.

Buchwald has mentioned briefly the importance of storing bases adequately for Ullmann-type coupling reactions, stating that excess water in the hygroscopic bases may inhibit product formation.[35] Another report of reproducibility issues surrounding the base was again discussed by Buchwald, who reported a "time-lapse" at the beginning of the *N*-arylation of an aryl iodide.[92] This behaviour appeared as a plateau in the concentration vs time profiles for up to 15% conversion and varied based on how the base was stored, supplier and particle size. As these factors should not play a part in the catalytic cycle, the observations were noted and ignored from the kinetic study which was performed,

although these effects may go some way in explaining why there is a considerable concern regarding irreproducibility.

1.2.5.10. Well defined complexes for copper-catalysed cross-coupling reactions

A typical procedure for Ullmann-type reactions involves *in situ* formation of a catalytic species, typically through mixing a Cu(I)-halide with a bidentate ligand.[35] The complications of solution-based equilibria and clustering which are prominent with simple copper complexes, as discussed in Section 1.2.5.7. mean that development of well-defined, active copper catalysts is limited. Nevertheless, examples of pre-formed catalysts can be founds, such as the Cu(I)(Phen)(PPh$_3$)Br catalyst reported by Venkataraman,[103] CuTC,[85] and Cu(III) complexes previously discussed.[84, 104]

N-Heterocyclic carbenes (NHCs) have recently drawn attention as ligands in the field of catalysis, due to their similarities with phosphines, as strong σ-donators and weak π-acceptors to metal centres.[105] Examples of Cu-NHC complexes and their use in copper-catalysed coupling reactions have been reported in recent years.[106, 107] Whittlesey shows the formation of *tris*-Cu(I) μ_3-oxo complexes bearing NHC ligands,[108] and shows the catalytic competence of these complexes at 1 mol% in the coupling reaction between pyrazole and aryl halides. Willans has also reported the stability of Cu(II)-NHC complexes and their use in the Ullmann-etherification reaction, showing mild reactivity.[109]
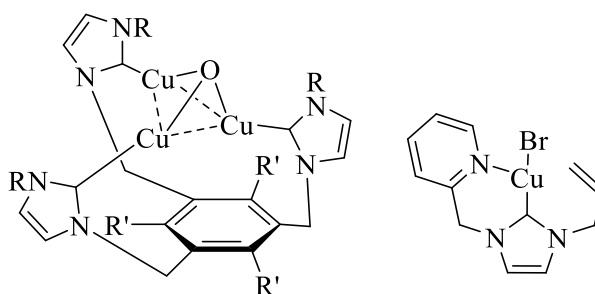
Figure 1.3 - Cu-NHC complexes used catalytically in Ullmann-type coupling reactions.[108, 109]

1.2.6. Summary of copper-catalysed cross-coupling reactions

Transition metal-catalysed coupling reactions are amongst the most important reactions in a synthetic chemists "toolbox". Studies in the past two decades have developed copper-catalysed coupling reactions from a historical relic, with stoichiometric copper

loadings, limited substrate scope and extreme conditions, to a useful alternative to palladium and other transition metal catalysed reactions. Part of this development may be attributed to the translation of mechanistic knowledge from the extensive work which has seen palladium-catalysed coupling reactions become important mainstays of pharmaceutical and fine chemical synthesis.

Despite this, many copper-catalysed coupling reactions are still underdeveloped from a mechanistic perspective. The typically cited Cu(I)/Cu(III) mechanism has significant grounding with important studies on intermediates and computational experiments, however some still argue a SET mechanism is still possible. The concepts of ligand design and well-defined Cu-catalysts are not widespread in the literature, which perhaps stems from a gap in the knowledge of the role of these components. Understanding these aspects further will allow the design of novel, efficient copper-catalysts, which can address issues of high catalyst loadings and the limitation of many systems to aryl iodides. Another gap in knowledge is seen in how catalyst deactivation may affect the reactivity of copper catalysts, which may be a significant cause of the problems which limit their efficiency.

1.3. Catalyst deactivation

Catalytic deactivation represents a serious concern for the industrial implementation of catalytic systems and can be defined as "the loss over time of catalytic activity and/or selectivity".[110] Whilst catalysts by definition are left unchanged at the end of a reaction, it is inevitable that any compound which is undergoing chemical change will be prone to decay over time. Catalyst deactivation can have huge implications on cost of production, with longer reaction times, lower catalytic turnover and higher loadings, as well as potential difficulty in separating side products formed.[111]

Many academic chemists neglect catalyst deactivation in favour of more rewarding pursuits in activity or selectivity of new catalysts, as discussed by Cavallo,[112] and Crabtree.[113] Despite the importance of catalytic deactivation in both homogeneous and heterogeneous catalysis, historically, a majority of the focus on it has been put on the deactivation of heterogeneous systems, studying coking, poisoning and decomposition.[110, 114] It is important for complete optimisation of any catalytic system that the mechanism is fully understood, including deactivation pathways.

### 1.3.1. Catalyst deactivation studies of palladium catalysts

The use of palladium catalysts is common in homogeneous catalysis due to its ability to promote a wide range of reactions, however the stability of some palladium catalysts is too low for large-scale industrial use, resulting from deactivation pathways.[115] A well-known deactivation process in palladium-catalysed reactions, such as cross-coupling or carbonylation reactions, is the formation of palladium black.

The Heck reaction is a widely used coupling reaction, forming C-C bonds in the presence of a palladium catalyst, formed from either Pd(0), such as [Pd(PPh$_3$)$_4$], or Pd(II) salts, such as acetate or chloride (Scheme 1.20).[116] The early systems devised for this reaction were found to be susceptible to severe catalytic deactivation due to clustering of palladium intermediates in the catalytic cycle, forming palladium black, which limited the lifetime of the active species. In the attempt to stabilise the metal species to this aggregation, it was found that stabilisation through the addition of phosphine ligands greatly improved the stability of the system.[117]
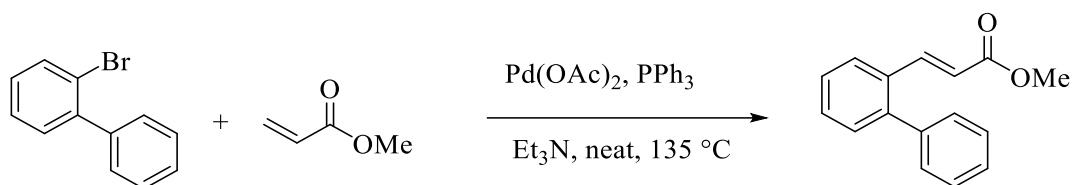
Scheme 1.20 – Early reported conditions for the Heck coupling reaction.[117]

Work performed by Koningsberger *et al.* on the Pd deactivation pathway utilised X-ray absorption fine structure (XAFS) and UV-*vis in situ* to elucidate a potential mechanism for the formation of palladium black.[115] The study found that a Pd-Pd interaction was seen to form over time with a bond distance of ~2.70 Å, indicating that the palladium intermediates were clustering together as previously hypothesised. Formation of dimer and trimer palladium species with the phosphine ligands and allyl group coordinated was observed from the initiation of catalysis (Scheme 1.21).
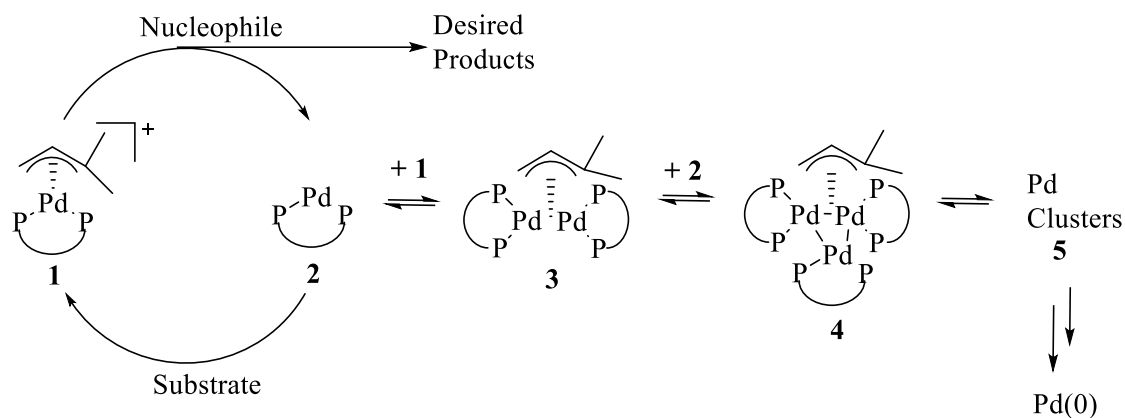
Scheme 1.21 – Formation of palladium black in Pd-catalysed nucleophilic addition reaction.[115]

Phosphines are widely used as ligands in palladium-catalysed cross-coupling reactions.[118] Phosphine ligands are not inert to side reactions and as a result, both deactivation of the metal centre and the phosphine ligands must be considered in many coupling reactions. Typical deactivation pathways for phosphine ligands are shown in Scheme 1.22, known as cyclometallation, P-C bond cleavage, and oxidation to the phosphine oxide.[113] It is important to understand these deactivation processes to prevent their occurrence and improve TONs of catalysts.
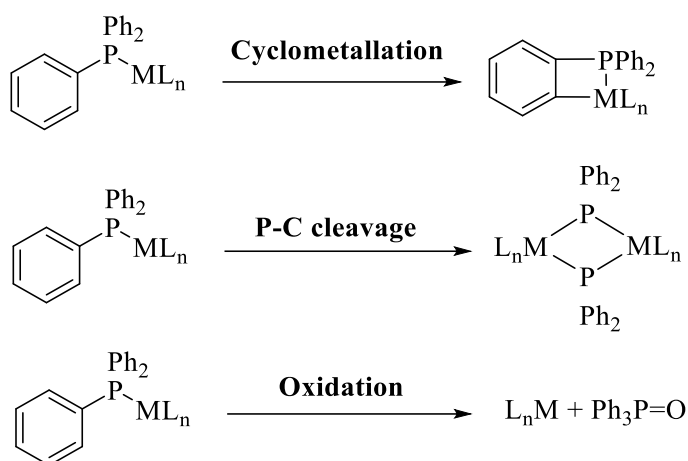
Scheme 1.22 – Deactivation modes for phosphine ligands.

1.3.2. Catalyst deactivation in copper-catalysed cross-coupling reactions

Catalyst deactivation studies are limited in copper-catalysed coupling reactions, as many of the kinetic investigations have relied on highly efficient systems, to provide insight into the coupling reaction only.[89] Whilst it is important to understand the primary catalytic cycle, deactivation pathways can change a cycle through off-cycle equilibria or

side products formed. The key deactivation route which has been proposed and investigated is the disproportionation of Cu(I) giving Cu(0)/Cu(II). As the precursor in many systems is a Cu(I) salt, the instability of many Cu(I) complexes to disproportionation is a necessary consideration.[119] In a kinetic study, Davies recently reported a negative order dependence of a malonate base in the organic-base mediated *N*-arylation of secondary amines.[120] A disproportionation reaction from a Cu(I)-malonate species is proposed, which agrees well with a XAFS/UV-*vis* study on the disproportionation of a Cu^I(acac) complex reported by Lei.[121]

$$[Cu^I Mal]^{\ominus} \underset{k_{-1}}{\overset{Mal \; k_1}{\rightleftharpoons}} [Cu^I Mal_2]^{3\ominus} \xrightarrow{k_{deact}} 1/2 \; Cu^0 + 1/2 \; Cu^{II} \; species$$

$$Mal = \quad {}^-O \overset{O \quad\quad O}{\diagup \diagdown \diagup} O^-$$
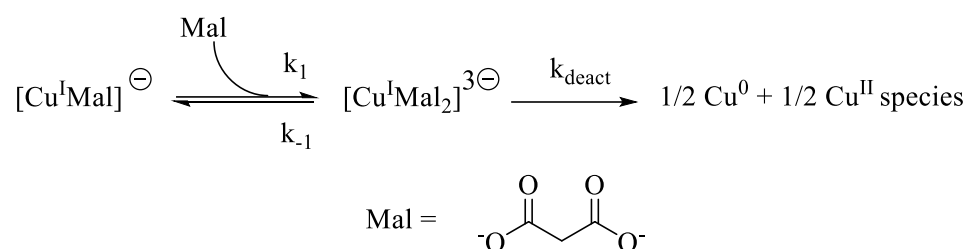
Scheme 1.23 - Cu(I) disproportionation mechansim as a deactivation pathway in copper-catalysed C-N coupling.[120]

1.4. The "cesium effect"

The cesium effect is a term used to describe the increased efficacy of cesium salts in organic and organometallic reactions compared to potassium and sodium salts. The relatively high cost of cesium salts can be offset by increased reactivity in organic reactions such as alkylations,[122, 123] macrocyclisations[124] and esterifications,[125] as well as many transition-metal catalysed reactions.[86, 126, 127] The increased yields and efficiency of using cesium in these reactions is regularly attributed to the higher solubility, basicity, and polarisability of cesium salts, due to the larger radius of the cesium cation.[122, 124] For example, formation of macrocycles with polyethylene glycol repeating units is found to be greatly enhanced in the presence of CsF (Scheme 1.24).[124]
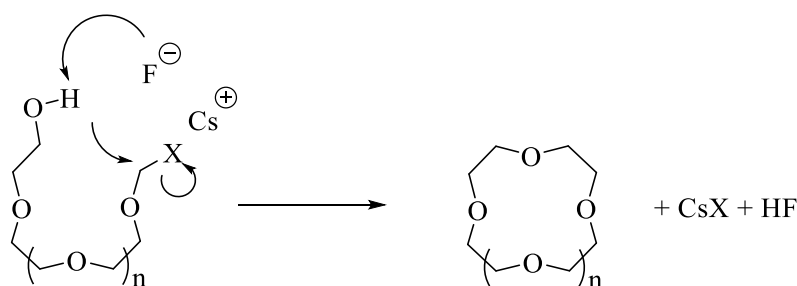

Scheme 1.24 - Schematic representation of the cesium effect stabilising the formation of macrocycles.

1.4.1. A role of the cesium cation in transition metal-catalysed transformations

Whilst increased solubility and stabilisation of charges are likely to be the main influences in organic systems, recent reports have hypothesised a more influential role of the cesium cation on transition metal intermediates.[128-131] In this section, recent computational studies into the interaction of cesium with various metal centres is discussed, in which a common theme throughout is a Cs-X-M motif, where X is an anion such as F^- or CO_3^{2-}. These reports could provide a mechanistic insight into the role of the cesium effect in transition metal-catalysed reactions.

In 2014, it was proposed by Sunoj and Schaefer that cesium fluoride plays a key role in stabilising a transition state in the a Pd-catalysed C-H activation of benzamides (Figure 1.4).[131] A -17.7 kcal/mol difference in energy of transition states is calculated in one of the proposed interactions, with and without Cs. In another palladium-catalysed reaction, Musaev and Yu used computation chemistry to undestand the importance of a Cs_2-I-F-

Pd cluster in assisting the C-H bond activation and the removal of an iodide ligand from the Pd centre for the Pd-catalysed C-H activation of a CH_3 group (Figure 1.5).[128]
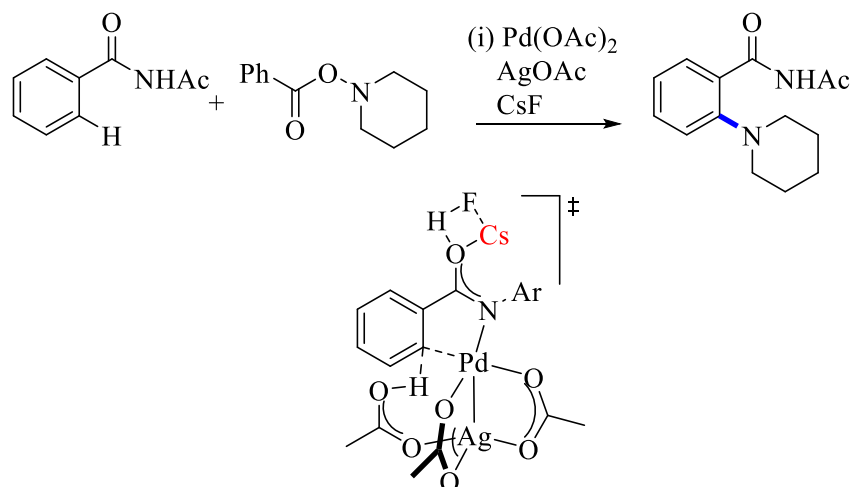
Figure 1.4 – Stabilisation effect of Cs-F in the transition state reported by Sunoj and Schaefer for a Pd-catalysed C-H activation.[131]
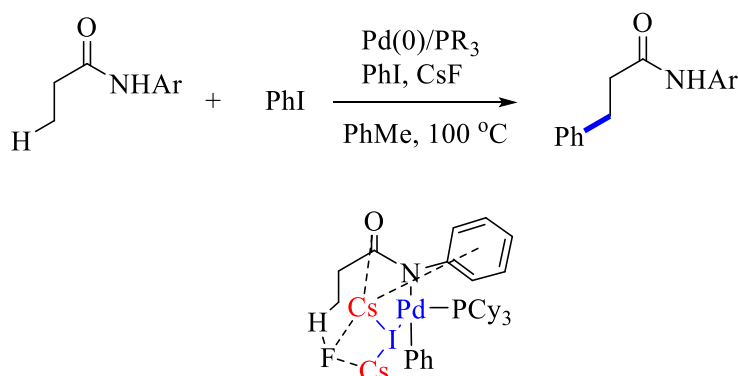
Figure 1.5 - Yu and Musaev reported complex **53** as a calculated intermediate in a C-H activation of a CH_3 group.[128]

In 2014, Musaev and Itami studied the Ni-catalysed C-H activation reaction, combining experimental and computation techniques.[129] The authors found that a Ni-CO_3^{2-}-Cs intermediate lowered the activation energy for the catalytic pathway from 34.7 kcal/mol with no base to 32.5 kcal/mol with K_2CO_3 as base and 31.1 kcal/mol with Cs_2CO_3 as base at 373.15 K (Figure 1.6).[129] Lastly, a similar bimetallic catalytic intermediate and a transition state were proposed by Luo and Zhang in a DFT study of Ag-catalysed carboxylation of terminal alkynes with CO_2 (Figure 1.7).[130]

29
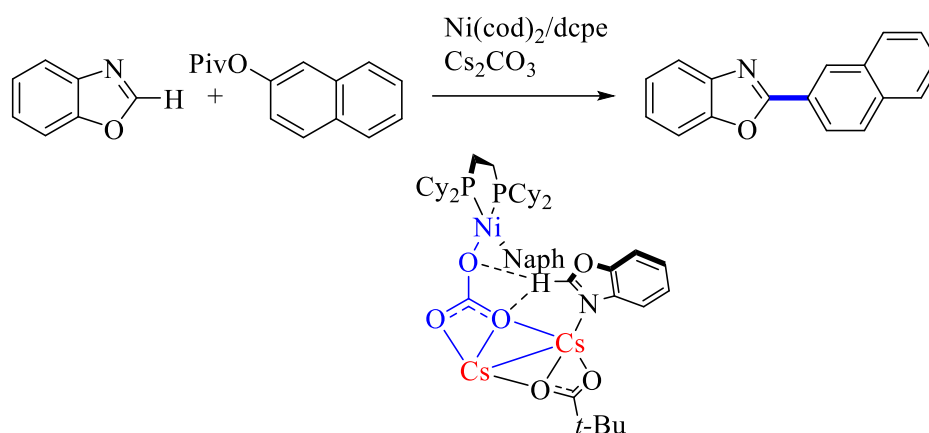
Figure 1.6 - Intermediate reported in DFT studies by Musaev and Itami featuring a Ni-CO_3-Cs interaction to stabilise the metal centre.[129]
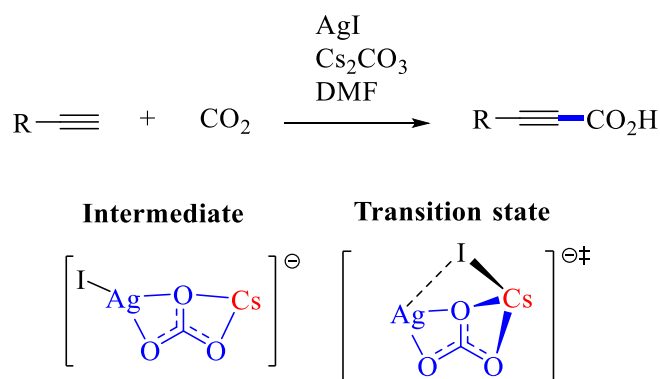
Figure 1.7 - Intermediate and transition state proposed in the DFT study of a silver-catalysed carboxylation of alkynes, featuring interaction of Cs.[132]

Although these studies are primarily computational, these interactions are proposed to stabilise intermediates or transition states, and may provide an insight into why cesium salts are often effective in transition metal catalysed systems. To many synthetic chemists, the cation of a base is a secondary thought, however, understanding the role that cations play in both intermediates and transition states of catalytic systems may lead to new reactions and catalysts.

1.5. Project outline

The primary target of this research aims to address issues of irreproducibility and poor efficiency in copper-catalysed C-N cross-coupling reactions. The key to achieving this is understanding of mechanistic concepts which are still debated in the literature, such as deactivation pathways, modes of aryl halide activation and rate-determining equilibria. By tackling the areas of poor understanding, an increase in awareness and solutions to common issues of the copper-catalysed cross-coupling reactions will be seen, which can have great implications for their use on an industrial scale.

In situ and sampling methods for kinetic monitoring will provide kinetic insight into the *N*-arylation of different nucleophiles, and investigation of different systems will expose the generality of mechanistic findings. Greater understanding of the kinetic dependence on the different components of the reaction will allow a more accurate prediction of optimal conditions for different substrates. By, broadening the study to a range of ligands and bases which have been widely reported, but are not well understood, it will provide relevance of the research to chemists who do not have an in depth knowledge of copper-catalysed cross-coupling.

Spectroscopy and crystallography is expected to allow the observation and isolation of potential reaction intermediates, deactivation species and side products in the reactions. A key aspect of the research will be the utilisation and combination of numerous analytical techniques to approach complex questions. This is relevant to the copper-catalysed systems and can be expanded to other metal catalysts, which will enable study of an immobilised iridium transfer hydrogenation catalyst, which has previously been shown to deactivate after > 20 uses.[133] Identification of activation and deactivation pathways in this research will provide a platform for further research into ligand and catalyst design, prevention of deactivation and ultimately, more efficient reactions.

1.6. References

1.   Q.L. Zhou, *Angew. Chem. Int. Ed.*, 2016, **55**, 5352-5353.

2.   A. Suzuki, *Angew. Chem. Int. Ed.*, 2011, **50**, 6722-6737.

3.   T. Hayashi, Y. Katsuro, Y. Okamoto and M. Kumada, *Tetrahedron Lett.*, 1981, **22**, 4449-4452.

4.   M.K. Lakshman, P.F. Thomson, M.A. Nuqui, J.H. Hilmer, N. Sevova and B. Boggess, *Org. Lett.*, 2002, **4**, 1479-1482.

5.   N. Miyaura and A. Suzuki, *Chem. Rev.*, 1995, **95**, 2457-2483.

6.   F. Ullmann and P. Sponagel, *Chem. Ber.*, 1905, **38**, 2211-2212.

7.   R.F. Heck and J.P. Nolley, *J. Org. Chem.*, 1972, **37**, 2320-2322.

8.   N. Miyaura, K. Yamada and A. Suzuki, *Tetrahedron Lett.*, 1979, **20**, 3437-3440.

9.   N. Miyaura and A. Suzuki, *J. Chem. Soc., Chem. Commun.*, 1979, 866-867.

10.   A.S. Guram and S.L. Buchwald, *J. Am. Chem. Soc.*, 1994, **116**, 7901-7902.

11.   F. Paul, J. Patt and J.F. Hartwig, *J. Am. Chem. Soc.*, 1994, **116**, 5969-5970.

12.   G. Cahiez and A. Moyeux, *Chem. Rev.*, 2010, **110**, 1435-1462.

13.   K. Tamao, K. Sumitani and M. Kumada, *J. Am. Chem. Soc.*, 1972, **94**, 4374-4376.

14.   S.Z. Tasker, E.A. Standley and T.F. Jamison, *Nature*, 2014, **509**, 299-309.

15.   A. Furstner, A. Leitner, M. Mendez and H. Krause, *J. Am. Chem. Soc.*, 2002, **124**, 13856-13863.

16.   M. Jin, L. Adak and M. Nakamura, *J. Am. Chem. Soc.*, 2015, **137**, 7128-7134.

17.   Y.F. Liang and G.C. Fu, *J. Am. Chem. Soc.*, 2015, **137**, 9523-9526.

18.   A. Alemagna, P. Delbuttero, C. Gorini, D. Landini, E. Licandro and S. Maiorana, *J. Org. Chem.*, 1983, **48**, 605-607.

19.   C. Torborg and M. Beller, *Adv. Synth. Catal.*, 2009, **351**, 3027-3043.

20.   J. Magano and J.R. Dunetz, ′CHAPTER 15 Recent Large-Scale Applications of Transition Metal-Catalyzed Couplings for the Synthesis of Pharmaceuticals′, in *New Trends in Cross-Coupling: Theory and Applications*, The Royal Society of Chemistry, 2015, 697-778.

21.   D.G. Brown and J. Bostrom, *J. Med. Chem.*, 2016, **59**, 4443-4458.

22.   N. Miyaura, T. Yanagi and A. Suzuki, *Synth. Commun.*, 1981, **11**, 513-519.

23.   J. Magano and J.R. Dunetz, *Chemical Reviews*, 2011, **111**, 2177-2250.

24.   M. Mikami and S. Shinkai, *J. Chem. Soc., Chem. Commun.*, 1995, 153-154.

25. X. Jiang, G.T. Lee, E.B. Villhauer, K. Prasad and M. Prashad, *Org. Process Res. Dev.*, 2010, **14**, 883-889.

26. M. Cameron, B.S. Foster, J.E. Lynch, Y.J. Shi and U.H. Dolling, *Org. Process Res. Dev.*, 2006, **10**, 398-402.

27. S.B. Madasu, N.A. Vekariya, M.N.V.D.H. Kiran, B. Gupta, A. Islam, P.S. Douglas and K.R. Babu, *Beilstein. J. Org. Chem.*, 2012, **8**, 1400-1405.

28. D.S. J. Gunzner, M. Stanley, L. Bao, G. Castanedo, R. Lalonde, S. Wang, M. Reynolds, S. Savage, K. Malesky and M. Dina, *PCT Int. Appl.*,WO 2006028958 A2 20060316, 2006.

29. D.K. O. Loiseleur, S. Abel, H. M. Buerger, M. Meisenbach, B. Schmitz and G. Sedelmeier, *PCT Int. Appl.*,WO 2003066613 A120030814 2003.

30. K. Kunz, U. Scholz and D. Ganzer, *Synlett*, 2003, 2428-2439.

31. J. Jiao, X.R. Zhang, N.H. Chang, J. Wang, J.F. Wei, X.Y. Shi and Z.G. Chen, *J. Org. Chem.*, 2011, **76**, 1180-1183.

32. K.S. Gayen, T. Sengupta, Y. Saima, A. Das, D.K. Maiti and A. Mitra, *Green Chem.*, 2012, **14**, 1589-1592.

33. J. Mondal, A. Biswas, S. Chiba and Y.L. Zhao, *Sci. Rep.*, 2015, **5**.

34. R.A. Altman, A. Shafir, A. Choi, P.A. Lichtor and S.L. Buchwald, *J. Org. Chem.*, 2008, **73**, 284-286.

35. R.A. Altman and S.L. Buchwald, *Nat. Protoc.*, 2007, **2**, 2474-2479.

36. J.E. Moses and A.D. Moorhouse, *Chem. Soc. Rev.*, 2007, **36**, 1249-1262.

37. F.J. Weiberth and S.S. Hall, *J. Org. Chem.*, 1987, **52**, 3901-3904.

38. B.L. Feringa, R. Badorrey, D. Pena, S.R. Harutyunyan and A.J. Minnaard, *P. Natl. Acad. Sci. USA*, 2004, **101**, 5834-5838.

39. D.M.T. Chan, K.L. Monaco, R.P. Wang and M.P. Winters, *Tetrahedron Lett.*, 1998, **39**, 2933-2936.

40. P.Y.S. Lam, C.G. Clark, S. Saubern, J. Adams, M.P. Winters, D.M.T. Chan and A. Combs, *Tetrahedron Lett.*, 1998, **39**, 2941-2944.

41. Z.F. Chen and T.J. Meyer, *Angew. Chem. Int. Ed.*, 2013, **52**, 700-703.

42. V.V. Rostovtsev, L.G. Green, V.V. Fokin and K.B. Sharpless, *Angew. Chem. Int. Ed.*, 2002, **41**, 2596-2599.

43. S.E. Allen, R.R. Walvoord, R. Padilla-Salinas and M.C. Kozlowski, *Chem. Rev.*, 2013, **113**, 6234-6458.

44. C.C.C.J. Seechurn, M.O. Kitching, T.J. Colacot and V. Snieckus, *Angew. Chem. Int. Ed.*, 2012, **51**, 5062-5085.

45. W. Harnischmacher and R. Hoppe, *Angew. Chem. Int. Ed.*, 1973, **12**, 582-583.

46. W. Sinha, M.G. Sommer, N. Deibel, F. Ehret, M. Bauer, B. Sarkar and S. Kar, *Angew. Chem. Int. Ed.*, 2015, **54**, 13769-13774.

47. R. Zhu and S.L. Buchwald, *Angew. Chem. Int. Ed.*, 2013, **52**, 12655-12658.

48. X. Chen, X.S. Hao, C.E. Goodhue and J.Q. Yu, *J. Am. Chem. Soc.*, 2006, **128**, 6790-6791.

49. A.M. Suess, M.Z. Ertem, C.J. Cramer and S.S. Stahl, *J. Am. Chem. Soc.*, 2013, **135**, 9797-9804.

50. B.E. Haines, T. Kawakami, K. Kuwata, K. Murakami, K. Itami and D.G. Musaev, *Chem. Sci.*, 2017, **8**, 988-1001.

51. H.Z. Yu, Y.Y. Jiang, Y. Fu and L. Liu, *J. Am. Chem. Soc.*, 2010, **132**, 18078-18091.

52. F. Ullmann and J. Bielecki, *Chem. Ber.*, 1901, **34**, 2174-2185.

53. F. Ullmann, *Chem. Ber.*, 1903, **36**, 2382-2384.

54. I. Goldberg, *Chem. Ber.*, 1906, **39**, 1691-1692.

55. W.R.H. Hurtley, *J. Chem. Soc.*, 1929, 1870-1873.

56. I.P. Beletskaya and A.V. Cheprakov, *Organometallics*, 2012, **31**, 7753-7808.

57. A. Kiyomori, J.F. Marcoux and S.L. Buchwald, *Tetrahedron Lett.*, 1999, **40**, 2657-2660.

58. C.f.M.P.f.H.U. (CHMP), Committee for Medicinal Products for Human Use (CHMP), London, 2008.

59. C. Sambiagio, R.H. Munday, S.P. Marsden, A.J. Blacker and P.C. McGowan, *Chem. Eur. J.*, 2014, **20**, 17606-17615.

60. K.H.V. Reddy, G. Satish, K. Ramesh, K. Karnakar and Y.V.D. Nageswar, *Tetrahedron Lett.*, 2012, **53**, 3061-3065.

61. S.E. Creutz, K.J. Lotito, G.C. Fu and J.C. Peters, *Science*, 2012, **338**, 647-651.

62. A.C. Bissember, R.J. Lundgren, S.E. Creutz, J.C. Peters and G.C. Fu, *Angew. Chem. Int. Ed.*, 2013, **52**, 5129-5133.

63. M. Majek and A. Jacobi von Wangelin, *Angew. Chem. Int. Ed.*, 2013, **52**, 5919-5921.

64. Q.M. Kainz, C.D. Matier, A. Bartoszewicz, S.L. Zultanski, J.C. Peters and G.C. Fu, *Science*, 2016, **351**, 681-684.

65. F. Bellina and R. Rossi, *Tetrahedron*, 2009, **65**, 10269-10310.

66. C. Sambiagio, S.P. Marsden, A.J. Blacker and P.C. McGowan, *Chem. Soc. Rev.*, 2014, **43**, 3525-3550.

67. H. Weingarten, *J. Org. Chem.*, 1964, **29**, 3624-3626.

68. A.J. Paine, *J. Am. Chem. Soc.*, 1987, **109**, 1496-1502.

69. A.C. Knipe, S.J. Mcguinness and W.E. Watts, *J. Chem. Soc., Chem. Commun.*, 1979, 842-843.

70. H.L. Aalten, G. Van Koten, D.M. Grove, T. Kuilman, O.G. Piekstra, L.A. Hulshof and R.A. Sheldon, *Tetrahedron*, 1989, **45**, 5565-5578.

71. D.H. Hey and W.A. Waters, *Chem. Rev.*, 1937, **21**, 169-208.

72. N. Kornblum, R.E. Michel and R.C. Kerber, *J. Am. Chem. Soc.*, 1966, **88**, 5662-5663.

73. G.A. Russell and W.C. Danen, *J. Am. Chem. Soc.*, 1966, **88**, 5663-5665.

74. J.K. Kim and J.F. Bunnett, *J. Am. Chem. Soc.*, 1970, **92**, 7463-7464.

75. S. Arai, M. Hida and T. Yamagishi, *Bull. Chem. Soc. Jpn.*, 1978, **51**, 277-282.

76. W.R. Bowman, H. Heaney and P.H.G. Smith, *Tetrahedron Lett.*, 1984, **25**, 5821-5824.

77. G.O. Jones, P. Liu, K.N. Houk and S.L. Buchwald, *J. Am. Chem. Soc.*, 2010, **132**, 6205-6213.

78. P.F. Larsson, C.J. Wallentin and P.O. Norrby, *Chemcatchem*, 2014, **6**, 1277-1282.

79. X. Creary, M.E. Mehrsheikhmohammadi and S. Mcdonald, *J. Org. Chem.*, 1987, **52**, 3254-3263.

80. G. Lefevre, G. Franc, A. Tlili, C. Adamo, M. Taillefer, I. Ciofini and A. Jutand, *Organometallics*, 2012, **31**, 7694-7707.

81. S.L. Zhang, L. Liu, Y. Fu and Q.X. Guo, *Organometallics*, 2007, **26**, 4546-4554.

82. T. Cohen, J. Wood and A.G. Dietz, *Tetrahedron Lett.*, 1974, 3555-3558.

83. D. Bethell, I.L. Jenkins and P.M. Quan, *J. Chem. Soc., Perk. Trans. 2*, 1985, 1789-1795.

84. A. Casitas, A.E. King, T. Parella, M. Costas, S.S. Stahl and X. Ribas, *Chem. Sci.*, 2010, **1**, 326-330.

85. S.J. Zhang, D.W. Zhang and L.S. Liebeskind, *J. Org. Chem.*, 1997, **62**, 2312-2313.

86.   J.F. Marcoux, S. Doye and S.L. Buchwald, *J. Am. Chem. Soc.*, 1997, **119**, 10539-10540.

87.   A. Ouali, J.F. Spindler, A. Jutand and M. Taillefer, *Adv. Synth. Catal.*, 2007, **349**, 1906-1916.

88.   A. Shafir, P.A. Lichtor and S.L. Buchwald, *J. Am. Chem. Soc.*, 2007, **129**, 3490-3491.

89.   E.R. Strieter, D.G. Blackmond and S.L. Buchwald, *J. Am. Chem. Soc.*, 2005, **127**, 4120-4121.

90.   J.W. Tye, Z. Weng, A.M. Johns, C.D. Incarvito and J.F. Hartwig, *J. Am. Chem. Soc.*, 2008, **130**, 9971-9983.

91.   P.F. Larsson, C. Bolm and P.O. Norrby, *Chem. Eur. J.*, 2010, **16**, 13613-13616.

92.   E.R. Strieter, B. Bhayana and S.L. Buchwald, *J. Am. Chem. Soc.*, 2009, **131**, 78-88.

93.   R. Giri and J.F. Hartwig, *J. Am. Chem. Soc.*, 2010, **132**, 15860-15863.

94.   E.D. Blue, A. Davis, D. Conner, T.B. Gunnoe, P.D. Boyle and P.S. White, *J. Am. Chem. Soc.*, 2003, **125**, 9435-9441.

95.   R.G.R. Bacon and H.A.O. Hill, *J. Chem. Soc.*, 1964, 1097-1107.

96.   J.W. Tye, Z.Q. Weng, R. Giri and J.F. Hartwig, *Angew. Chem. Int. Ed.*, 2010, **49**, 2185-2189.

97.   S. Sung, D.C. Braddock, A. Armstrong, C. Brennan, D. Sale, A.J.P. White and R.P. Davies, *Chem. Eur. J.*, 2015, **21**, 7179-7192.

98.   D.S. Surry and S.L. Buchwald, *Chem. Sci.*, 2010, **1**, 13-31.

99.   Y. Sunesson, E. Lime, S.O.N. Lill, R.E. Meadows and P.O. Norrby, *J. Org. Chem.*, 2014, **79**, 11961-11969.

100. T. Ljungdahl, T. Bennur, A. Dallas, H. Emtenas and J. Martensson, *Organometallics*, 2008, **27**, 2490-2498.

101. Z. Ahmadi, L.P.E. Yunker, A.G. Oliver and J.S. McIndoe, *Dalton Trans.*, 2015, **44**, 20367-20375.

102. K.K. Gurjar and R.K. Sharma, *Chemcatchem*, 2017, **9**, 862-869.

103. R.K. Gujadhur, C.G. Bates and D. Venkataraman, *Org. Lett.*, 2001, **3**, 4315-4317.

104. L.M. Huffman and S.S. Stahl, *J. Am. Chem. Soc.*, 2008, **130**, 9196-9197.

105. M.N. Hopkinson, C. Richter, M. Schedler and F. Glorius, *Nature*, 2014, **510**, 485-496.

106. C. Tubaro, A. Biffis, E. Scattolin and M. Basato, *Tetrahedron*, 2008, **64**, 4187-4195.

107. A. Biffis, C. Tubaro, E. Scattolin, M. Basato, G. Papini, C. Santini, E. Alvarez and S. Conejero, *Dalton Trans.*, 2009, 7223-7229.

108. C.E. Ellul, G. Reed, M.F. Mahon, S.I. Pascu and M.K. Whittlesey, *Organometallics*, 2010, **29**, 4097-4104.

109. B.R.M. Lake and C.E. Willans, *Organometallics*, 2014, **33**, 2027-2038.

110. C.H. Bartholomew, *Appl. Catal., A*, 2001, **212**, 17-60.

111. P.W.N.M. van Leeuwen, *Appl Catal a-Gen*, 2001, **212**, 61-81.

112. A. Poater and L. Cavallo, *Theor. Chem. Acc.*, 2012, **131**.

113. R.H. Crabtree, *Chem. Rev.*, 2015, **115**, 127-150.

114. P. Forzatti and L. Lietti, *Catal. Today*, 1999, **52**, 165-181.

115. M. Tromp, J.R.A. Sietsma, J.A. van Bokhoven, G.P.F. van Strijdonck, R.J. van Haaren, A.M.J. van der Eerden, P.W.N.M. van Leeuwen and D.C. Koningsberger, *Chem. Commun.*, 2003, 128-129.

116. I.P. Beletskaya and A.V. Cheprakov, *Chem. Rev.*, 2000, **100**, 3009-3066.

117. H.A. Dieck and R.F. Heck, *J. Am. Chem. Soc.*, 1974, **96**, 1133-1136.

118. R. Martin and S.L. Buchwald, *Acc. Chem. Res.*, 2008, **41**, 1461-1473.

119. E. Sperotto, G.P.M. van Klink, G. van Koten and J.G. de Vries, *Dalton Trans.*, 2010, **39**, 10338-10351.

120. S. Sung, D. Sale, D.C. Braddock, A. Armstrong, C. Brennan and R.P. Davies, *ACS Catal.*, 2016, **6**, 3965-3974.

121. C. He, G.H. Zhang, J. Ke, H. Zhang, J.T. Miller, A.J. Kropf and A.W. Lei, *J. Am. Chem. Soc.*, 2013, **135**, 488-493.

122. R.N. Salvatore, A.S. Nagle and K.W. Jung, *J. Org. Chem.*, 2002, **67**, 674-683.

123. J.P. Parrish, B. Sudaresan and K.W. Jung, *Synth. Commun.*, 1999, **29**, 4423-4431.

124. G. Dijkstra, W.H. Kruizinga and R.M. Kellogg, *J. Org. Chem.*, 1987, **52**, 4230-4234.

125. T. Sato, J. Otera and H. Nozaki, *J. Org. Chem.*, 1992, **57**, 2166-2169.

126. J.P. Wolfe and S.L. Buchwald, *J. Org. Chem.*, 2000, **65**, 1144-1157.

127. M. Wasa, K.M. Engle and J.Q. Yu, *J. Am. Chem. Soc.*, 2009, **131**, 9886-9887.

128. T.M. Figg, M. Wasa, J.Q. Yu and D.G. Musaev, *J. Am. Chem. Soc.*, 2013, **135**, 14206-14214.

129. H.Y. Xu, K. Muto, J. Yamaguchi, C.Y. Zhao, K. Itami and D.G. Musaev, *J. Am. Chem. Soc.*, 2014, **136**, 14834-14844.

130. C. Liu, Y. Luo, W.Z. Zhang, J.P. Qu and X.B. Lu, *Organometallics*, 2014, **33**, 2984-2989.

131. M. Anand, R.B. Sunoj and H.F. Schaefer, *J. Am. Chem. Soc.*, 2014, **136**, 5535-5538.

132. W.Z. Zhang, L.L. Shi, C. Liu, X.T. Yang, Y.B. Wang, Y. Luo and X.B. Lu, *Org Chem Front*, 2014, **1**, 275-283.

133. S.J. Lucas, B.D. Crossley, A.J. Pettman, A.D. Vassileiou, T.E.O. Screen, A.J. Blacker and P.C. McGowan, *Chem. Commun.*, 2013, **49**, 5562-5564.

Chapter 2

Use of Soluble Tetrabutylammonium Carboxylate Bases in Ullmann-Goldberg Reactions; Kinetics and Mechanism

2.1. Introduction

There have been a handful of kinetic studies for the purpose of investigating the mechanism of the copper-catalysed *N*-arylation reaction.[1-3] These studies have been vital in understanding reactivity and selectivity in the system, mainly utilising calorimetry to gathering kinetic data. Buchwald has focussed on the use of amides in these studies, whilst Davies explored the use of the alkyl amine, piperidine. The use of calorimetry in kinetics is an extremely useful technique for *in situ* measurements when dealing with highly efficient and homogeneous systems,[4] but in more complex systems, solubility and side products can have an effect on heat flow and influence the kinetics obtained.

The issue of catalyst deactivation in the copper-catalysed *N*-arylation reaction has not been investigated in great detail, despite the high catalyst loadings which are regularly employed when chemists perform these reactions. Davies *et al.* reported a deactivation pathway from a malonate counterion when using tetrabutylphosphonium salts as the base in this kinetic study (Chapter 1 - Scheme 1.23).[3] Most of the reported examples of copper-catalysed *N*-arylations employ the more common inorganic bases eg. Cs_2CO_3, K_2CO_3 and K_3PO_4, which indicates that other deactivation pathways might be possible in these systems as they lack a chelating base like a malonate.

### 2.1.1. Organic Bases in Copper-Catalyst *N*-Arylation

Organic bases have been used in transition metal catalysed cross-coupling reactions for many years and have a key feature of being soluble in many common organic solvents. In general organic bases such as trimethylamine have been found to be very poor when used in Ullmann-type couplings, despite having a pKa in a similar region to carbonate and phosphate. The major use of organic bases in the copper-catalysed *N*-arylation reaction stems from the study reported by Liu,[5] in which room temperature amination was found possible even when using aryl bromides, when utilising

tetrabutylphosphonium and tetrabutylammonium salts as bases. The authors reason that the unusually high reactivity of this system is a result of the ionisation ability of the salts. The reported kinetic study by Davies in 2016 also utilised this system, due to the high reactivity and homogeneity of the system.[3]

2.2. Synthesis of Organic Bases

Synthesis of tetrabutylammonium and tetrabutylphosphonium bases was initially performed as outlined by Liu.[5] The use of commercially purchased tetrabutylammonium and -phosphonium hydroxides (40 wt. % in H_2O) in a salt exchange reaction with the corresponding acid of the desired anion was followed by lyophilisation (freeze-drying) to obtain white powders which would then be dried further under vacuum. The obtained salts were extremely hygroscopic, visibly retaining water after minutes of exposure to air, thus the powders were stored under an atmosphere of either argon or nitrogen. Most success was had in the preparation of tetrabutylammonium adipate, **3** (TBAA) shown in Scheme 2.1, which gave a free flowing white-powder after lyophilisation.
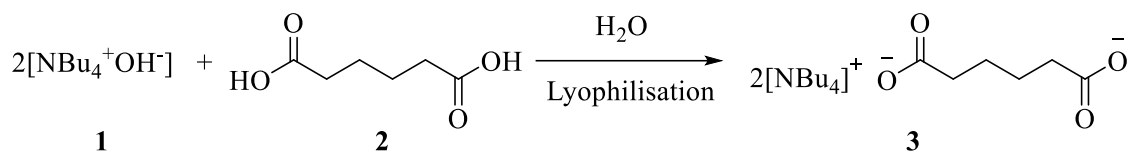
Scheme 2.1 - Preparation of TBAA from tetrabutylammonium hydroxide, **1** and adipic acid, **2**.

Other bases prepared through this method were tertrabuylammonium malonate (TBAM), tetrabutylammonium phosphate (TBAP) and tetrabutylphosphonium adipate (TBPA). Of these, only TBPA was successfully isolated and screened for catalyst activity. The difficulty in the preparation and isolation of these compounds stems from the requirement to use **1** as a solution, typically it is available in H_2O or MeOH. This is due to the predisposition of **1** to undergo Hofmann elimination, shown in Scheme 2.2, particularly when isolated. When using lyophilisation to remove water, mixed results were obtained leaving a thick, gelatinous residue on numerous occasions.
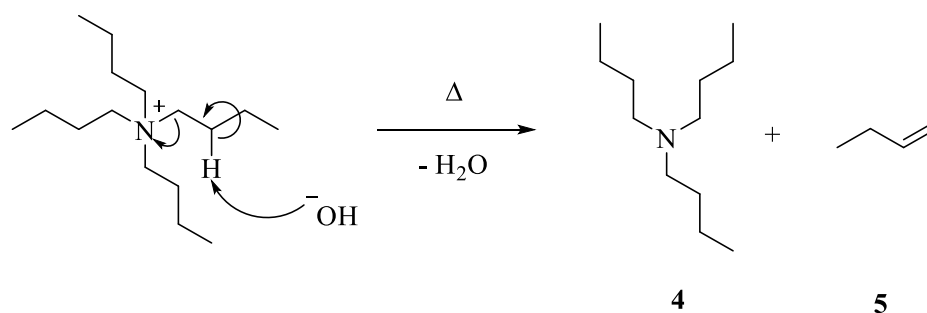
Scheme 2.2 - Hofmann elimination of the quaternary amine to give tributylamine (**3**) and 1-butene (**4**).

As a result of the difficulty in preparation, a solution of **1** in MeOH was used, eliminating much of the potential water content in the final base, although the byproduct of the reaction would remain H_2O. To counter this, activated 4 Å molecular sieves were used and filtered off prior to evaporation of the MeOH. The initial product of this procedure would be a sticky, pale yellow gel, which with repeated washes with toluene and evaporation would azeotrope the water to give a free flowing white powder. It is possible that these repeated washes were necessary to remove any **4** which contaminates the product.

2.3. Screening in *N*-arylation Reactions

To examine the efficiency of the organic bases, the *N*-arylation reaction between 4-iodoanisole **9** and piperidine **10** was initially chosen. Conditions were adapted from the protocol reported by Liu *et al.*[5] The ligand *N,N*-dimethylglycine **8** was found to be the most efficient by Liu, and so this was prepared through the synthesis shown in Scheme 2.3. The results of the initial screening are shown in Table 2.1.
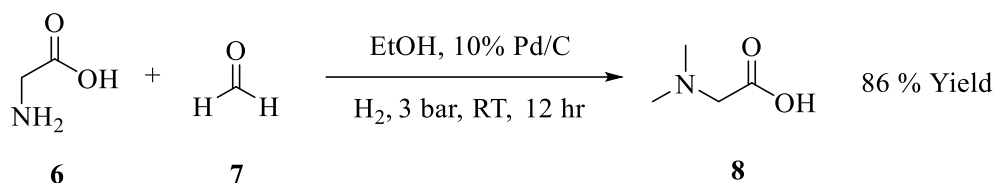
Scheme 2.3 - Preparation of *N,N*-dimethylglycine **8** through reductive amination of formaldehyde (**7**).

Table 2.1 - Initial screening of organic bases in *N*-arylation of piperidine (**10**).
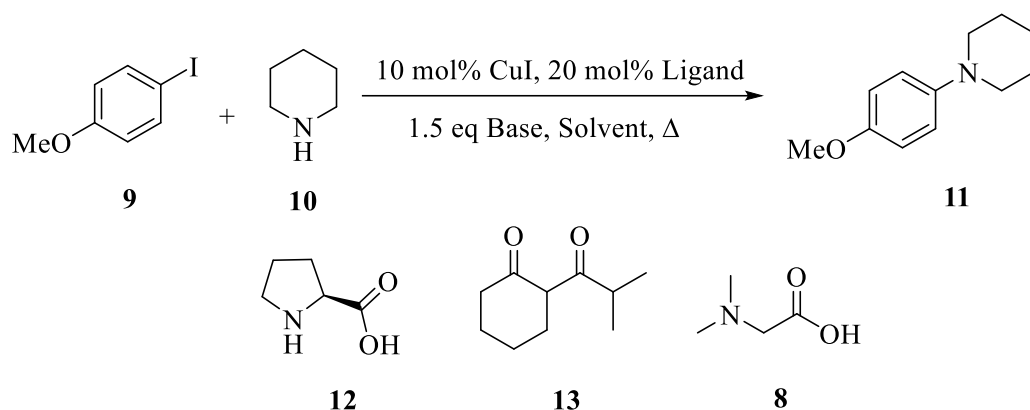
Entry	Base	Ligand	Solvent	Time (hours)	Temperature °C	Conversion % (to 11)
1[a]	TBAA	**12**	DMF	21	25	24 (22)
2[a]	TBPA	**13**	1,4-Dioxane	18	25	NR
3[a]	TBPA	**8**	DMF	17	90	69 (45)
4[a]	TBPA	**8**	DMF	16	25	50 (40)
5[a]	TBAA	**8**	DMF	23	90	>99 (63)
6[b]	TBAA	**8**	DMF	16	70	80 (64)
7[b]	TBAA	**8**	MeCN	16	70	95 (88)

9 (0.50 mmol), **10** (0.75 mmol), CuI (0.05 mmol), ligand (0.1 mmol), base (0.75 mmol), Solvent (2 mL). [a]Base prepared from H2O solutions of TBAH or TBPH and lyophilisation. [b]Base prepared from MeOH solutions of TBAH.

The results of the initial screen showed that these reactions have some interesting behaviour, particularly with regards to the side products formed. In most reports of the copper-cataylsed *N*-arylation reaction, there is little discussion of the formation of side products. These results show significant side reactions, for example, the conditions in Entry 5 gave quantitative conversion of the starting material, yet only 63 % of this was found to be the *N*-arylation product. It was also clear that there is a clear link between temperature and the ratio of side products to **11**. Entries 3 and 4 demonstrate the effect of running the reaction at room temperature versus 90 °C, with the former having

approximately 2 : 1 ratio of **11** to side products opposed to 4 : 1 when the reaction is run at room temperature.

It was found that the TBAA prepared from the MeOH solution of TBAH had better reactivity, which is hypothesised to be a result of the easier drying process. Reactions using both DMF and MeCN as solvent were found to have good reactivity for this reaction, whilst the reduction of the temperature from 90 °C to 70 °C was also seen to be beneficial, due to the greatly reduced side product formation. As in the previously reported work, the ligand **8** was found to be effective for this reaction and so was picked for further study.

2.4. Characterisation of Side Products

To understand the reactivity of the system better, characterisation of side products was necessary. It is well known in cross-coupling reactions that hydrodehalogenation is possible on aryl halides however it was clear from crude NMR spectra that a number of different aryl species were present. The spectra displayed in Figure 2.1a shows a significant peak in the aryl region at 6.76 ppm, along with the pair of doublet peaks belonging to the product and other, weaker signals. Following column purification, the impurity was isolated and characterised as 4-methoxyphenol **14**, shown in Figure 2.1c, matching the literature data for this compound.[6] It is hypothesised that this is present as a result of excess moisture adsorbed onto the organic bases used in this reaction. It was found that the level of **14** reduced significantly when moving away from using TBAH in H_2O to TBAH in MeOH. In the Chan-Lam reaction, isotopic labelling studies with O_2^{18} and H_2O^{18} has been used to show that the phenol side products arise from H_2O.[7]
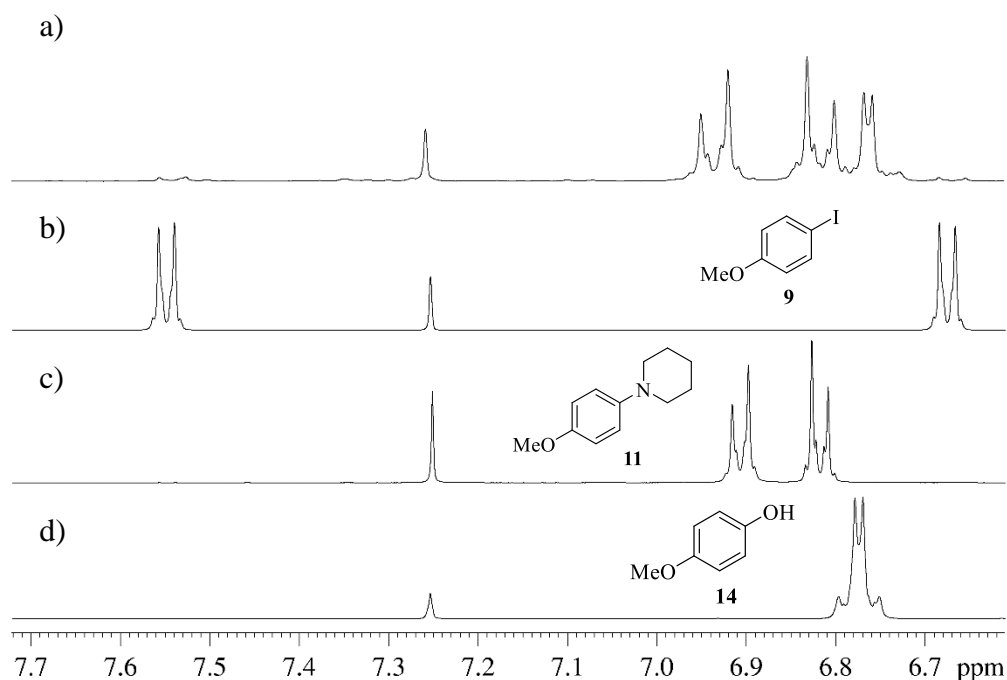
Figure 2.1 – NMR spectra (500 MHz, 25 °C). a) Crude NMR of the coupling reaction between **9** and **10** following work-up. b) Pure NMR of **9**. c) NMR spectra of the *N*-arylation product **11** d) NMR spectra of **14** following isolation.

The side products which were present in lower concentrations were not isolated from the reaction, so other analysis was needed to uncover the nature of these species. One surprising observation was the presence of a species when using TBPA, but not TBAA, which formed in high quantities. The crude NMR of the result of Entry 3 in Table 2.1 is shown in Figure 2.2, this shows the presence of two doublet peaks at 7.38 ppm and 6.78 ppm, which match the literature values for 4-bromoanisole.[8] The presence of this species is somewhat surprising and was confirmed with GC/MS analysis.
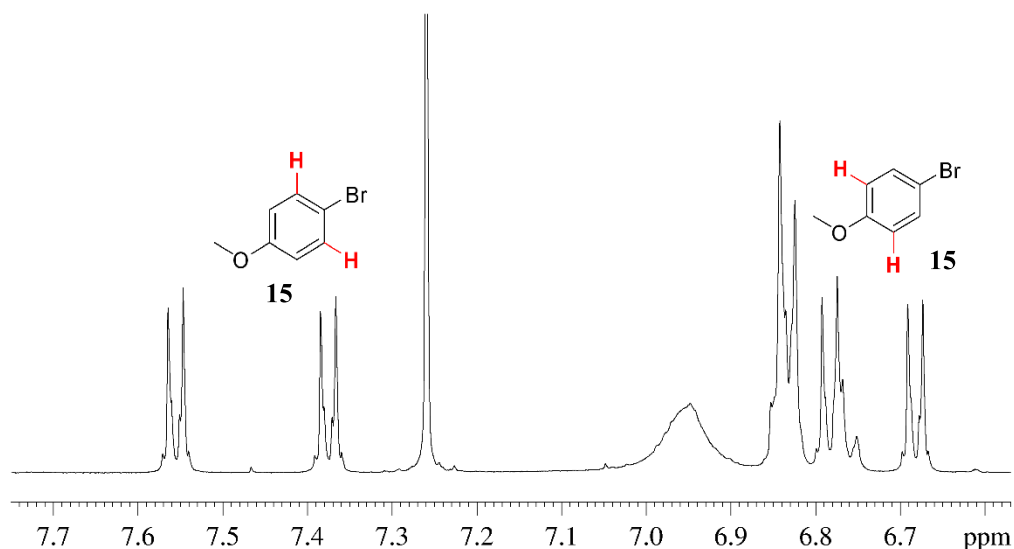
Figure 2.2 - Crude NMR (500 MHz, CDCl$_3$, 25 °C) of Entry 3 of Table 2.1.

The formation of 4-bromoanisole (**15**) accounted for 0.2 equivalents of **9**, which given that there was no obvious bromide species, was concerning. High-resolution mass spectrometry was used to explore the source of bromide in this reaction, which was found to be present in the TBPH (40 % in H$_2$O) used to prepare TBPA for this reaction. A large set of peaks at m/z = 597.4280 and 599.4283 was seen with the expected bromide isotope pattern which accounted for the species in Figure 2.3.

m/z: 597.42871 (100.0%), 599.42667 (97.3%), 598.43207 (34.6%), 600.43002 (33.7%), 599.43542 (5.8%), 601.43338 (5.6%)
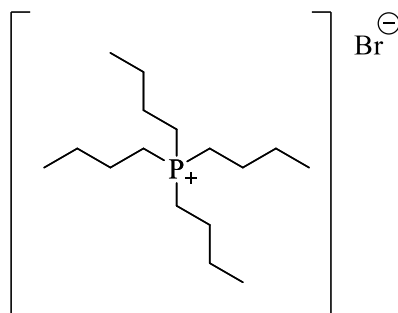
Figure 2.3 - Bromine contamination of TBPH solutions. Species seen at m/z 597.4280 and 599.4283 by HRMS.

It is likely that this contamination is a result of the process in which the chemical is made, where a literature search shows that it is possible to prepare it from tetrabutylphosphonium bromide.[9] Although purification through ion exchange could have been performed to ensure the purity of the TBPA used in the reactions, it was

45

decided that only TBAH, which appeared pure, would be used from this point on. The reaction shown in Scheme 2.4 was performed to gain further information regarding the nature of the unknown side products when using TBAA as a base.

Scheme 2.4 - *N*-Arylation of **10** using CuI/**8** catalyst and TBAA as the base in DMF.
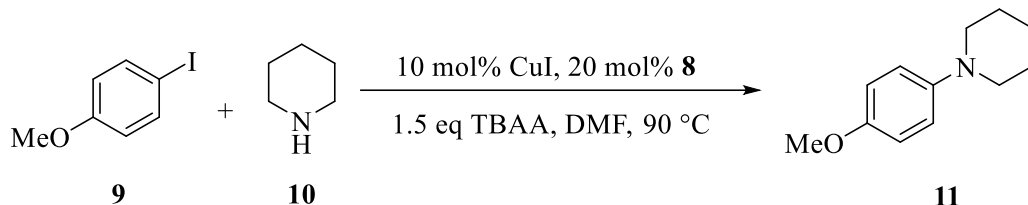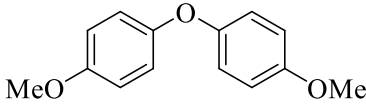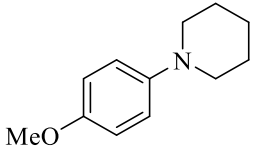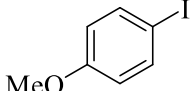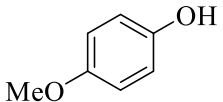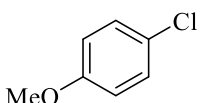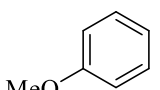

The GC/MS data for the reaction is shown in Table 2.2 below, in which 5 side products were seen and characterised from the m/z and referencing with GC/MS data for the pure compounds. The side products seen in this reaction includes anisole **18**, formed from the hydrodehalogenation reaction which is known to occur. It is possible here that as the reaction proceeds, the protonated adipate base may be able to act as a proton source for this reaction, or the acidic proton of the ligand, **8** may also be involved. **14** is formed as in previous reactions, however in smaller quantities. A *bis*-arylether product **16** is also observed, likely from **14** coupling with **9,** in a typical copper-catalysed etherification reaction. 4-Chloroanisole **17** was also seen to be present in the reaction mixture in small quantities, this is likely to be due to a similar situation as in **15,** as previously discussed, whereby the TBAH may have been prepared from the chloride salt.
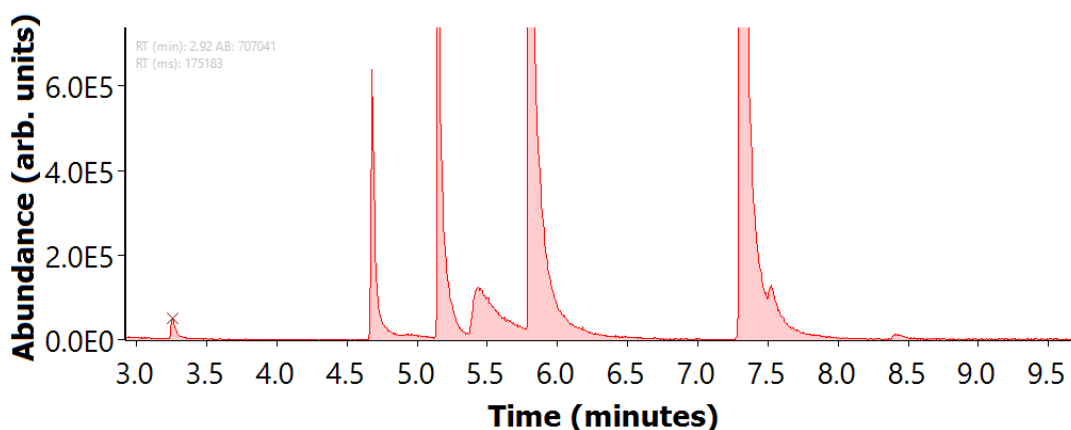

Figure 2.4 - GC/MS data of the crude reaction mixture for the *N*-arylation reaction shown in Scheme 2.4.

Table 2.2 - GC/MS assignments for the chromatogram shown in Figure 2.4.

| Retention time (min)	m/z	Fragmentation	Compound
8.34	230	215 Fragment (-CH$_3$)	**16**
7.30	191	176 Fragment (-CH$_3$)	**11**
5.80	234	219 Fragment (-CH$_3$)	**9**
5.40	124	109 Fragment (-CH$_3$)	**14**
4.67	142	127 Fragment (-CH$_3$) Cl splitting pattern	**17**
3.23	108	93 Fragment (-CH$_3$)	**18**

In separate experiments on the reaction in Scheme 2.4, another peak was seen in the NMR analysis of the crude mixture. GC-MS analysis shows the presence of an impurity which appears on the chromatogram at 5.8 minutes with a mass of 151 (136 –CH$_3$), overlaps with **9** (Figure 2.5).
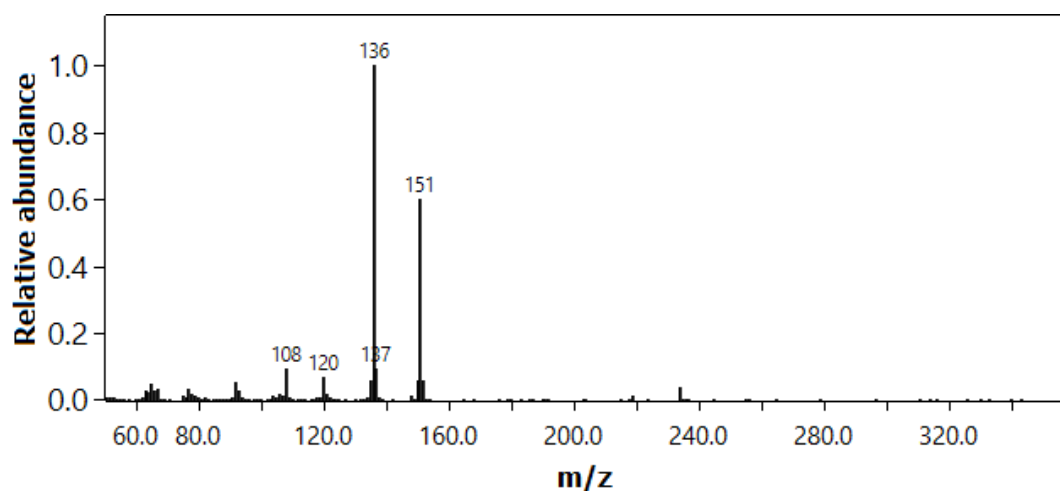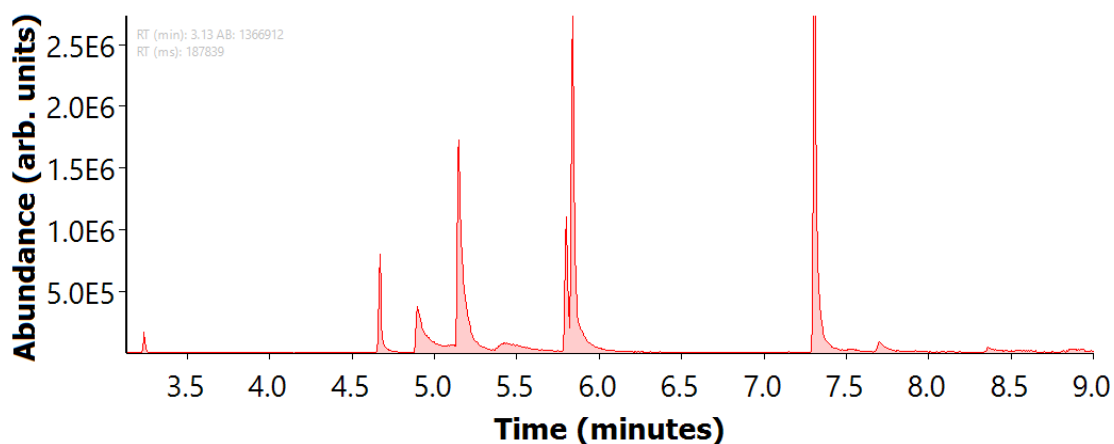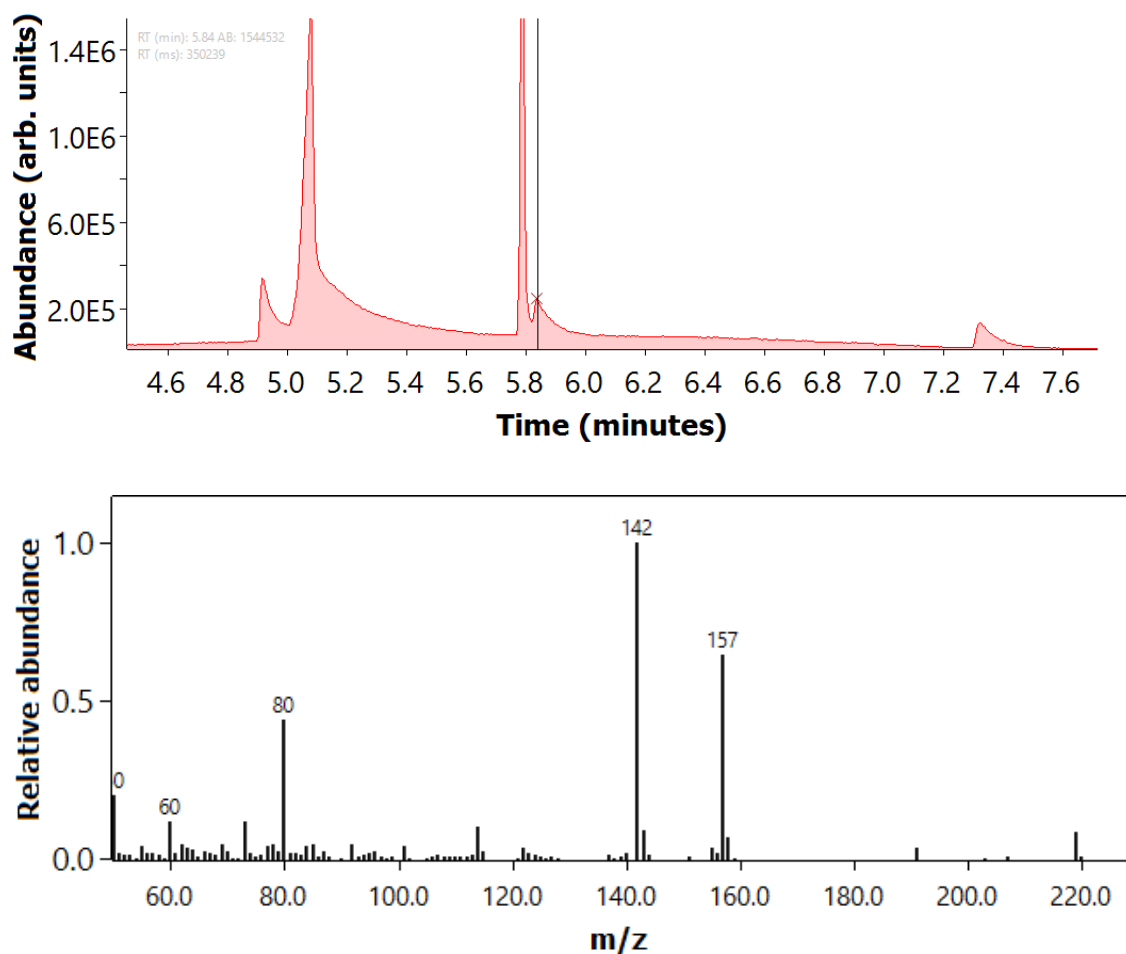
Figure 2.5 - GC profile of the reaction mixture and MS data for the peak at 5.8 minutes in reaction using DMF.

Based on the mass and splitting pattern, this was hypothesised to be *N,N*-dimethylanisidine **(19)**. Comparison of the GC trace with the GC/MS of pure **19** was used to determine whether this was the case. The trace, shown in Figure 2.6 is evidence that this is a species which is formed in the *N*-arylation reaction, as appears on the chromatogram at 5.8 minutes with the same mass splitting of 151 (136) m/z.
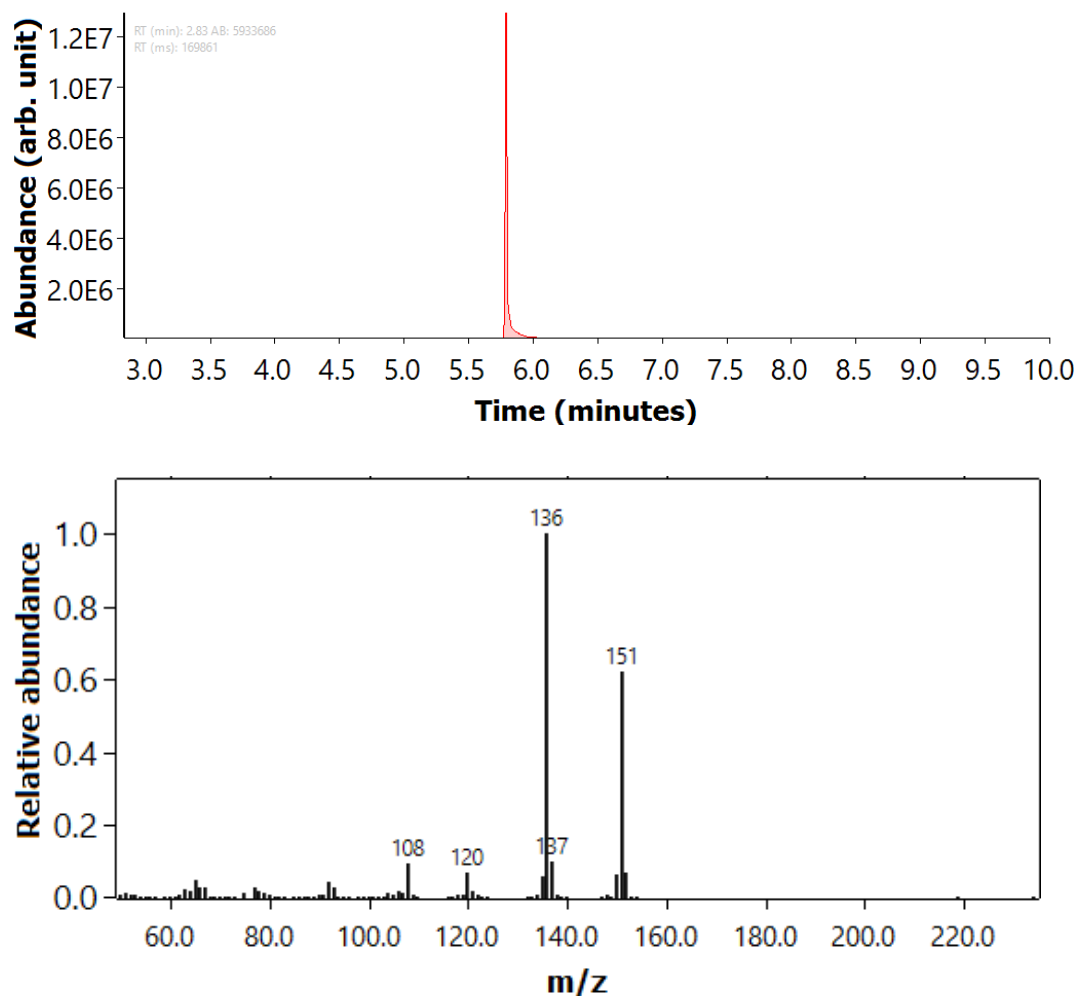
Figure 2.6 - GC/MS data for commercially sourced **19**. (Top) GC trace. (Bottom) Mass spectrum.

The most predictable source of the dimethyl functionality is from either the DMF used as solvent, or *N,N*-dimethylglycine **(8),** used as the ligand. To determine which of these the source is, the same reaction was performed with *d₇*-DMF as solvent. The peak which appears at 5.8 minutes now was found to have a mass of 157 (142 –CH₃), showing that the origin of this impurity is reaction with the DMF solvent used in the reaction. The GC/MS data is given in Figure 2.7.

Figure 2.7 - GC profile of the reaction mixture and MS data for the peak at 5.8 minutes in reaction using d_7-DMF.

19

m/z = 151.2

20

m/z = 157.2
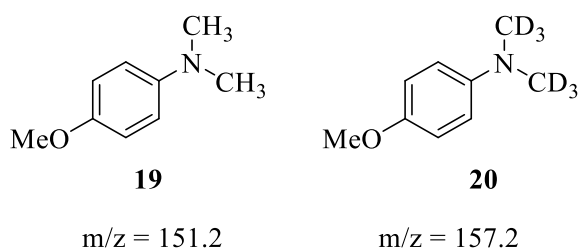
Figure 2.8 - *N,N*-Dimethylanisidine (**19**) and *N,N*-(d_6-dimethyl)-anisidine (**20**).

From ^{1}H NMR of the crude mixture, there was still some unknown entities in the reaction mixture, albeit in small quantities that were not necessarily aryl species. Figure 2.9 shows a reaction mixture from an experiment which was performed in the same manner as that outlined in Scheme 2.4, in which a peak at m/z 113 was found. Together with NMR analysis, showing conformation with literature values, this was assigned as 1-formylpiperidine (**21**).[10] Similarly to the formation of (**19**), reactions with deuterated

50

DMF showed a shift in the mass spectrum data, where a shift from 113 to 114 m/z was observed, as well as loss of the formyl proton in ^{1}H NMR.
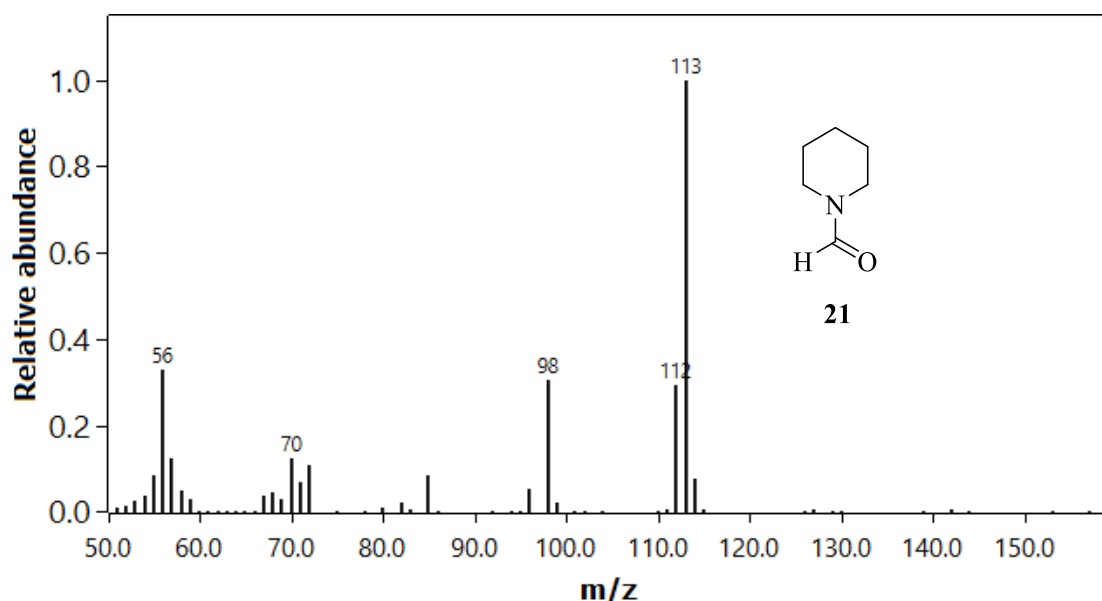

Figure 2.9 - GC/MS data for 1-formylpiperidine **21**.

There are examples, such as the Vilsmeier-Haack reaction, where DMF is used as the formylation agent of aryl rings in the presence of phosphorus oxychloride. The byproduct of this reaction is $HNMe_2$, which in turn, could explain the formation of **19**, as the dimethylamine may then act as the nucleophile in an *N*-arylation reaction.

2.5. Kinetic Monitoring of Reactions

To further understand the rate of the product and side product formation, kinetics of the reaction were sought. The work done prior to this had shown that this reaction could not be performed under aerobic conditions, which is unsurprising given the instability of many Cu(I) complexes in solution. As such, the reaction shown in Scheme 2.4 was performed in a Schlenk flask under a flow of nitrogen. The needles/syringes used for sampling were flushed >3 times with nitrogen before sampling through the SubaSeal of the Schlenk flask. The results of this experiment can be seen in Figure 2.10.
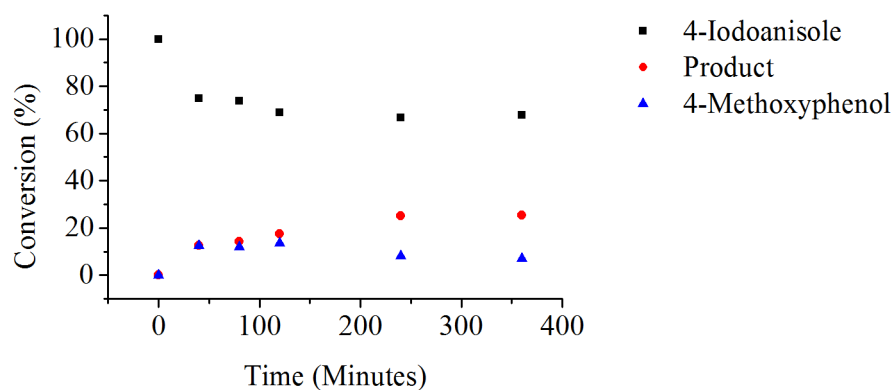
Figure 2.10 - Kinetic profile of *N*-arylation reaction, sampled and monitored by GC.

It is clear from these results that this method was not adequate for preventing the oxidation of the reaction. This technique also made full monitoring of side products more difficult as a large number of calibrations would be necessary and peaks were very small at the concentrations needed. As the reactions using TBAA are fully homogeneous due to the high solubility of TBAA in polar aprotic solvents such as DMF and MeCN, an *in situ* method of monitoring was explored. The aryl starting material and products in this reaction lend themselves well to ^{1}H NMR spectroscopy, due to the 1,4-substitution giving two sets of doublets, and the –methoxy functionality may also be visible.

An initial assessment of ^{1}H NMR as a monitoring technique showed promise, no more product was being formed after 5 hours and there was near full conversion of the 4-iodoanisole. Characterisation of the complex aryl region was necessary to get accurate data, so a combination of 2D techniques and doping experiments were used to fully understand the species visible. It should be noted that the formation of side products in >5 % of the aryl halide will not be monitored using more common *in situ* techniques such as calorimetry or IR. As such, very little information is previously reported on the source of side products and the possible influence they may have on the kinetics of the main *N*-arylation reaction.

2.5.1. Integration of ^{1}H NMR Kinetics

Figure 2.11 shows the ^{1}H COSY spectrum for a post-reaction mixture for the coupling of 4-iodoanisole with piperidine. The spectrum is zoomed into observe the side product peaks, to understand which peaks should be integrated together for accurate data. It is clear that there are numerous overlapping peaks which need to be accounted for.
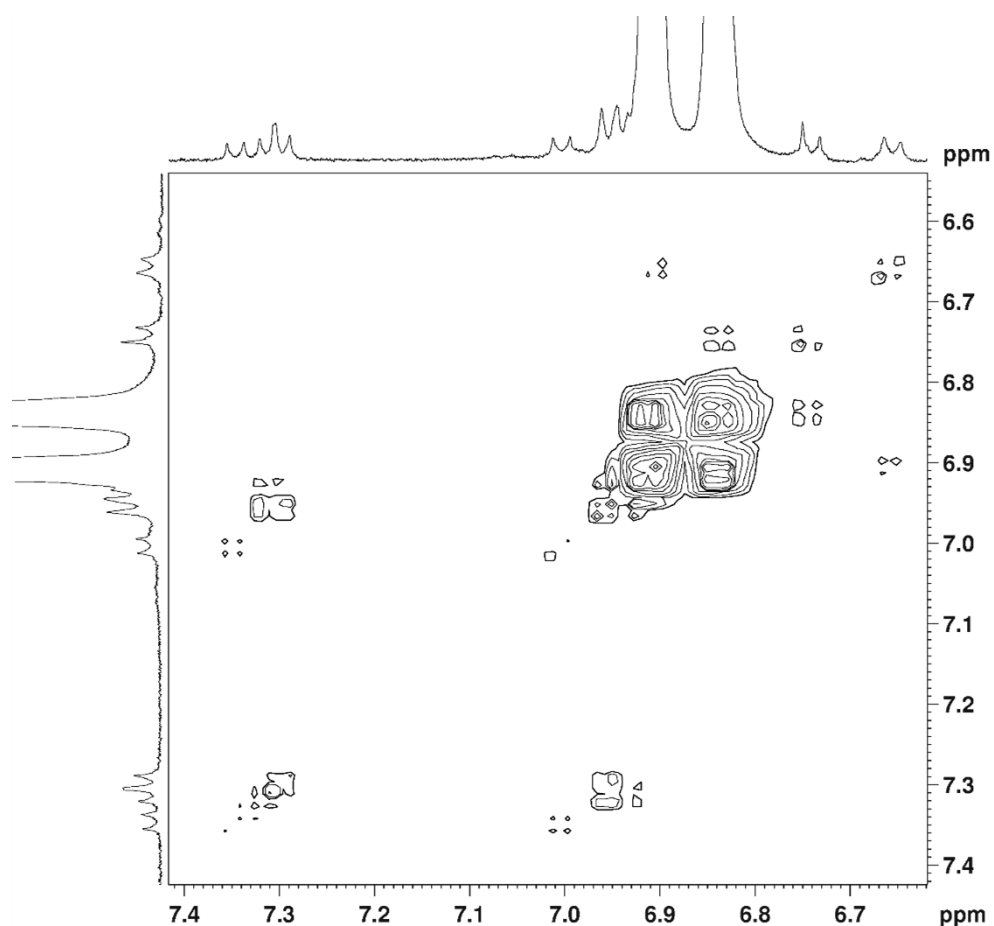
Figure 2.11 - 1H COSY (500 MHz, d_7-DMF, 25 °C) spectrum of reaction mixture post-reaction (*ortho* protons of **9** out of image).

From the COSY spectrum, it is clear that the large doublets which appear between 6.8 and 6.9 ppm belong to **11**. Figure 2.12 depicts a doping experiment to determine which protons belong to the anisole side product. Despite the broadness of the peaks, which occurs due to paramagnetic influence of Cu(II) when the NMR tube was exposed to air, this experiment can be correlated with the COSY data to expose the peaks which arise from the presence of anisole.
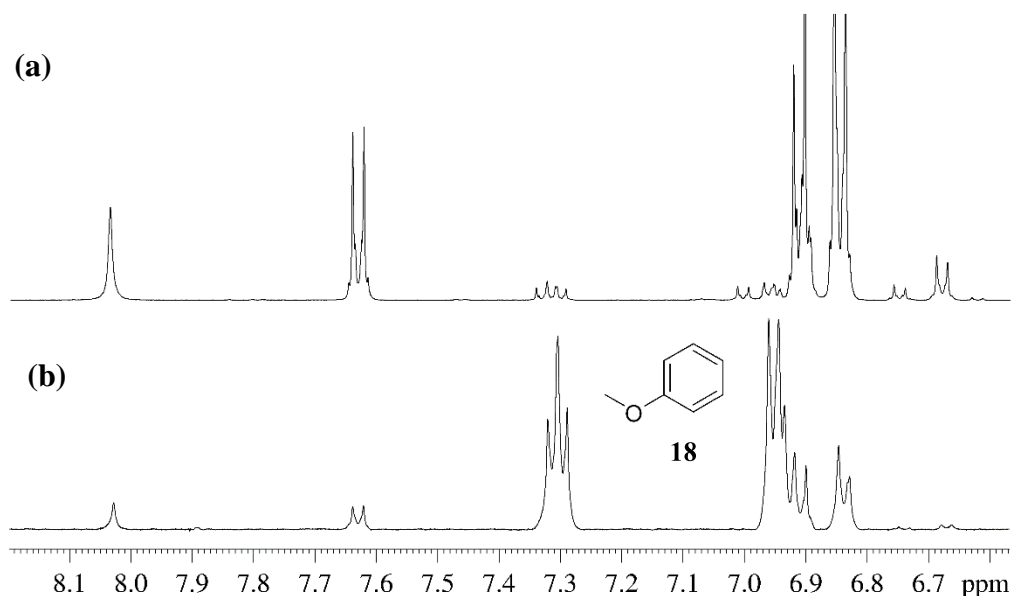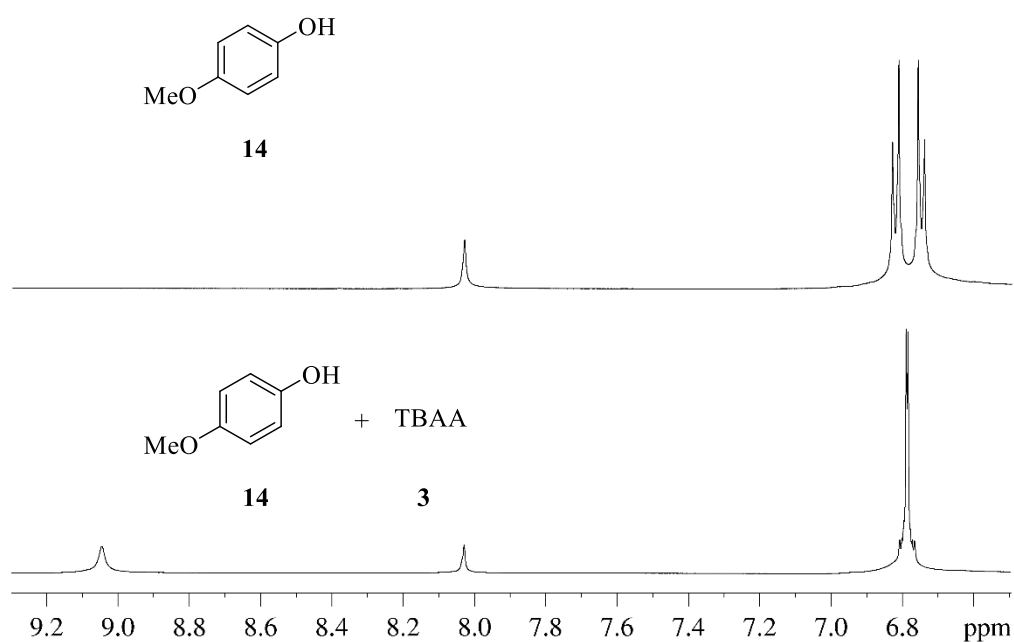
Figure 2.12 - ^{1}H NMR spectra (500 MHz, d_7-DMF, 25 °C) of (a) an in situ reaction mixture; and (b) the same reaction mixture spiked with **18** after exposure to air.

NMR data in d_7-DMF for **17** and for **19** shown in Figure 2.13 shows clearly the peaks found in the *in situ* experiment. It is somewhat fortunate that all compounds found in the aryl region of the ^{1}H NMR spectra provide at least one set of peaks which do not overlap with other signals, allowing accurate integration for the kinetic monitoring experiment.
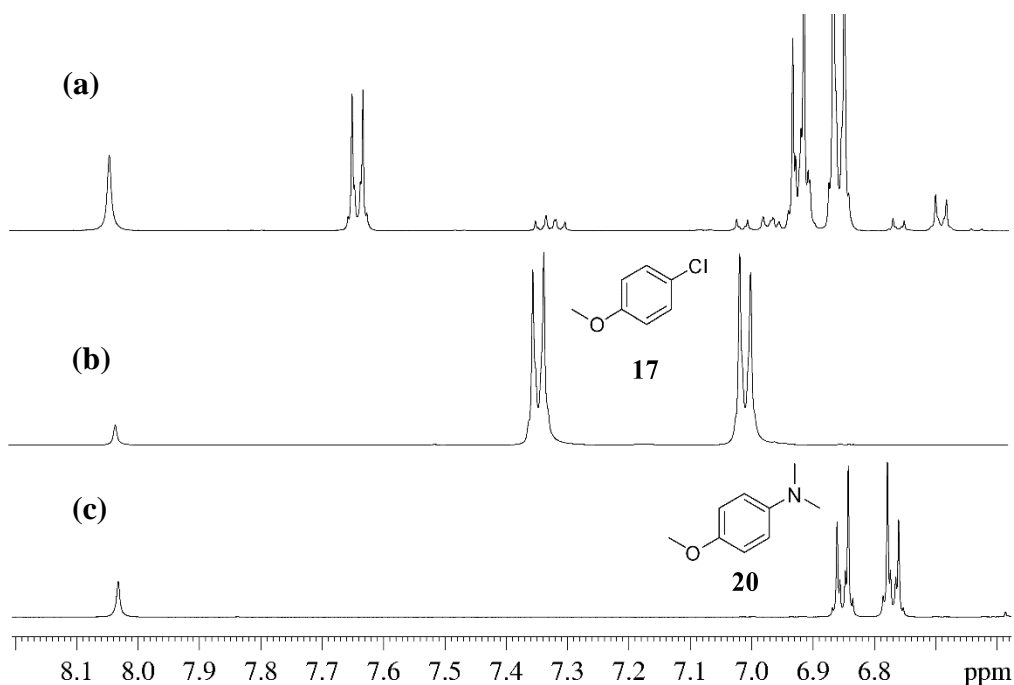
Figure 2.13 - ^{1}H NMR (500 MHz, d_7-DMF, 25 °C) spectra of (a) an in situ reaction mixture, (b) 4-chloroanisole (**17**) (c) N,N-dimethylanisidine (**20**).

The final compound seen to form as a side product of this reaction is **14**. This appears to exist as 4-methoxyphenolate in the *in situ* NMR studies. Figure 2.14 shows how when a reference spectrum of **14** is taken in d_7-DMF, only one multiplet is seen in the aromatic region at 6.8 ppm, with the –OH peak seen at 9.1 ppm. When base is added, loss of the –OH signal is seen and splitting of the aromatic peaks is noted, giving the doublets seen in the *in situ* studies. The presence of the phenolate in the reaction is something which needs to be considered due to its ability to coordinate copper as well as undergo the etherification reaction with another molecule of **9**.


Figure 2.14 - ^{1}H NMR spectra (500 MHz, d_7-DMF, 25 °C) of **14** with and without TBAA.

Scheme 2.5 and Figure 2.15 detail the full list of products and side products seen in the ^{1}H NMR monitoring the the *N*-arylation reaction being studied and the characterisation used in the integration of the NMR spectrum to gather kinetic data for these compounds.
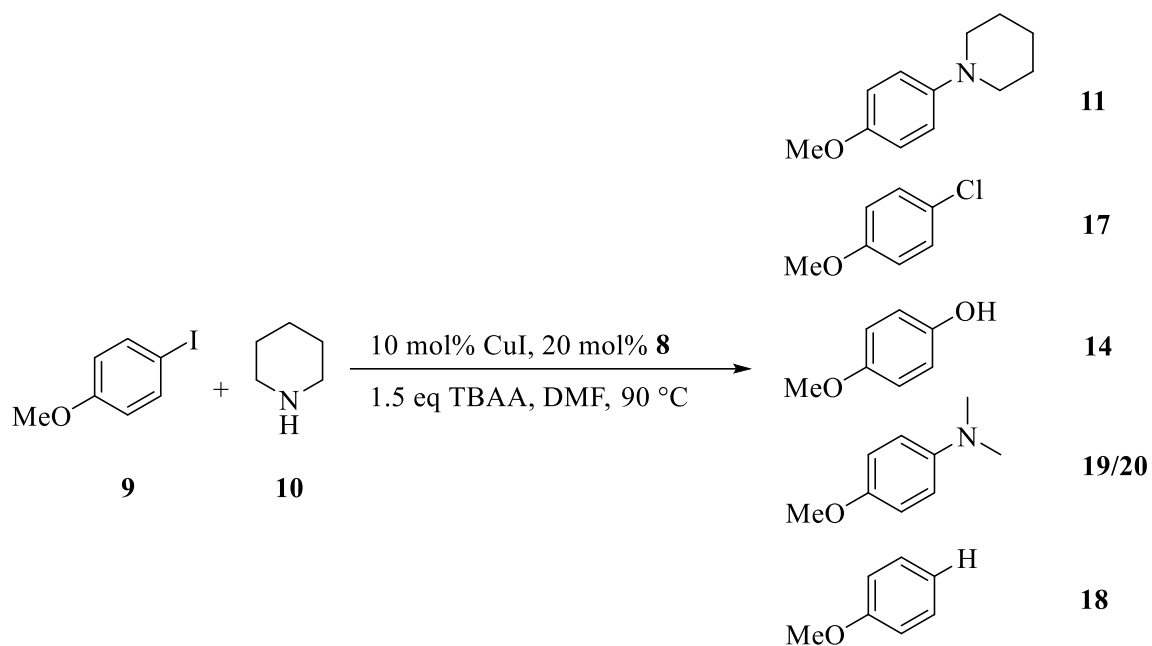
Scheme 2.5 - Full scheme for compounds seen in ^{1}H NMR spectroscopy kinetic experiments.
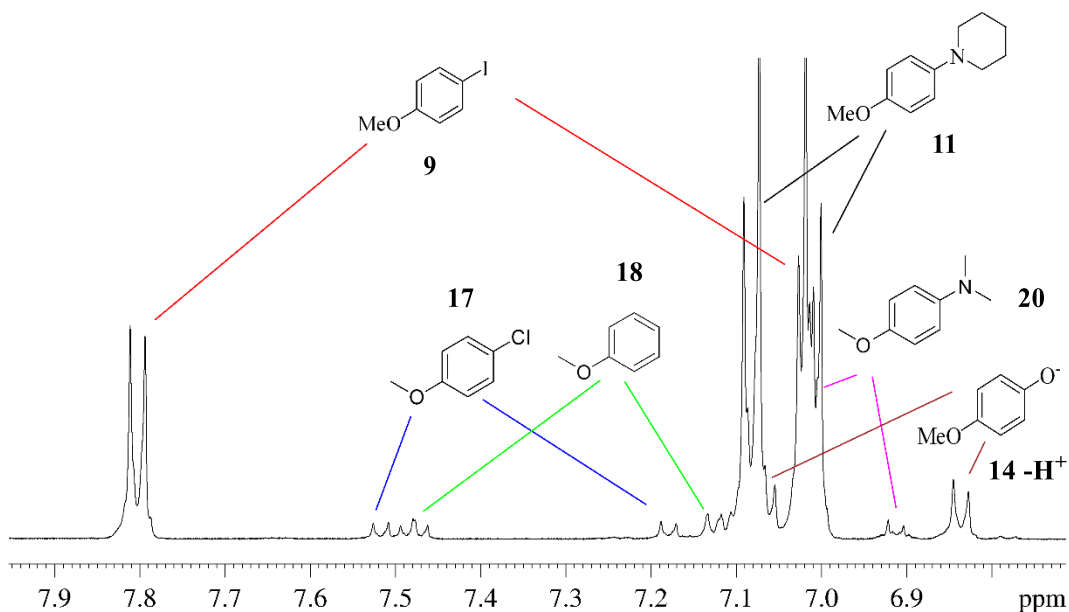

Figure 2.15 – Full characterisation of the aromatic region seen in ^{1}H NMR kinetic experiments (500 MHz, d_7-DMF, 25 °C).

2.6. *In Situ* ^{1}H NMR Development

Due to the air sensitivity of the chosen system, it is necessary to develop a reliable and reproducible technique for preparing and running the kinetic experiments. An initial run

involved using a screw-cap NMR tube, fitted with a SubaSeal, in which all solids were loaded prior to being flushed with nitrogen. The 0.5 mL d_7-DMF was added, followed by the desired amount of **10** *via* a micro syringe. The SubaSeal was quickly replaced with the screw cap whilst a flow of nitrogen from a needle protected the sample from oxidation. The sample was taken to a 500 MHz Bruken NMR spectrometer and loaded directly. Two room temperature readings were taken before the heating coil was set to 90 °C and spectra were taken every 10 minutes for four hours (Figure 2.16).
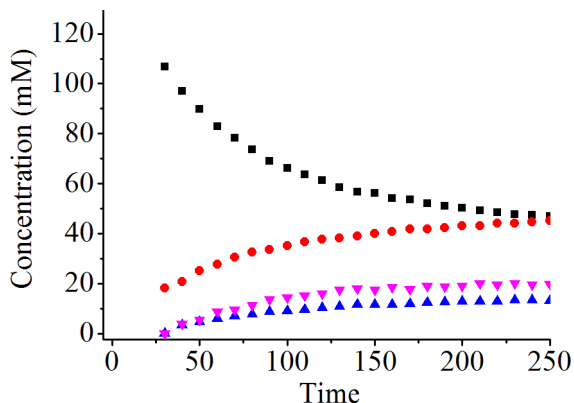
Figure 2.16 - ^{1}H NMR monitoring of reaction from Scheme 2.5. ■ = **9**, ● = **11**, ▲ = **14**, ▼ = Other products. Initial concentrations; $[9]_0$ = 125.0 mM, $[10]_0$ = 187.5 mM, $[CuI]_0$ = 12.4 mM, $[8]_0$ = 25.0 mM, $[TBAA]_0$ = 187.5 mM in 0.5 mL d_7-DMF.

The smoothness and trend of data from this run was much greater than that seen in the sampling experiments, however the conversion to product is significantly lower than that which was obtained when running the same reaction under standard Schlenk conditions on a 5x scale. This was reasoned to be a result of the difficulty in keeping the reaction anaerobic during the set up. The high amounts of side products seen is also an indication that some of background reactions are possible or even favoured under aerobic conditions. For these reasons, a repeat of the experiment was performed, with the sample prepared in a glovebox with a nitrogen atmosphere.

One issue involved with this method of kinetic monitoring is that the reaction was found to proceed at room temperature, meaning that the time which is taken to mount the sample and for the NMR to take a room temperature spectrum and the magnet to shim at 70 °C is non-trivial. Approximately 5 – 10% conversion has occurred by the first 70 °C sample and for this reason, the room temperature spectrum is considered the t_0 for this data.

## 2.7. Kinetic Analysis of the *N*-arylation of piperidine

According to the most common mechanism,[11] the rate law for the reaction in Scheme 2.5 may be simplified to be:

$$Rate \approx k[\mathbf{9}][\mathbf{10}][CuI]$$

Due to the complex interactions involved between substrate, solvent, catalysts etc. and the alternative pathways to side products, actual kinetic data may not fully comply with the rate law. A thorough study using ^1H was therefore used to probe the reaction and understand better the behaviour of the reaction in a non-perfect system. A number of reactions were prepared in which the initial concentration of substrates, base, ligand and other components of the reaction were varied, with the *in situ* NMR method used to follow the main reaction and the side reactions.

The data visualised by the kinetic profiles shown in Figure 2.17 explains a number of aspects of this reaction. With regards to the *N*-arylation reaction it can be seen from **A** the reaction does not go to completion in the time scale of monitoring, this appears to be due to significant slowing of the reaction after the first 50 – 60 minutes at 70 °C. Profile **B** indicates that the concentration of **10** influences the rate of reaction, with an increase in the initial rate clearly observed. Profile **C** shows a negative effect of increasing the TBAA concentration as the initial rate and the overall conversion to product is seen to be lower than in profile **A**.

2.7.1. Kinetic Study in d_7-DMF
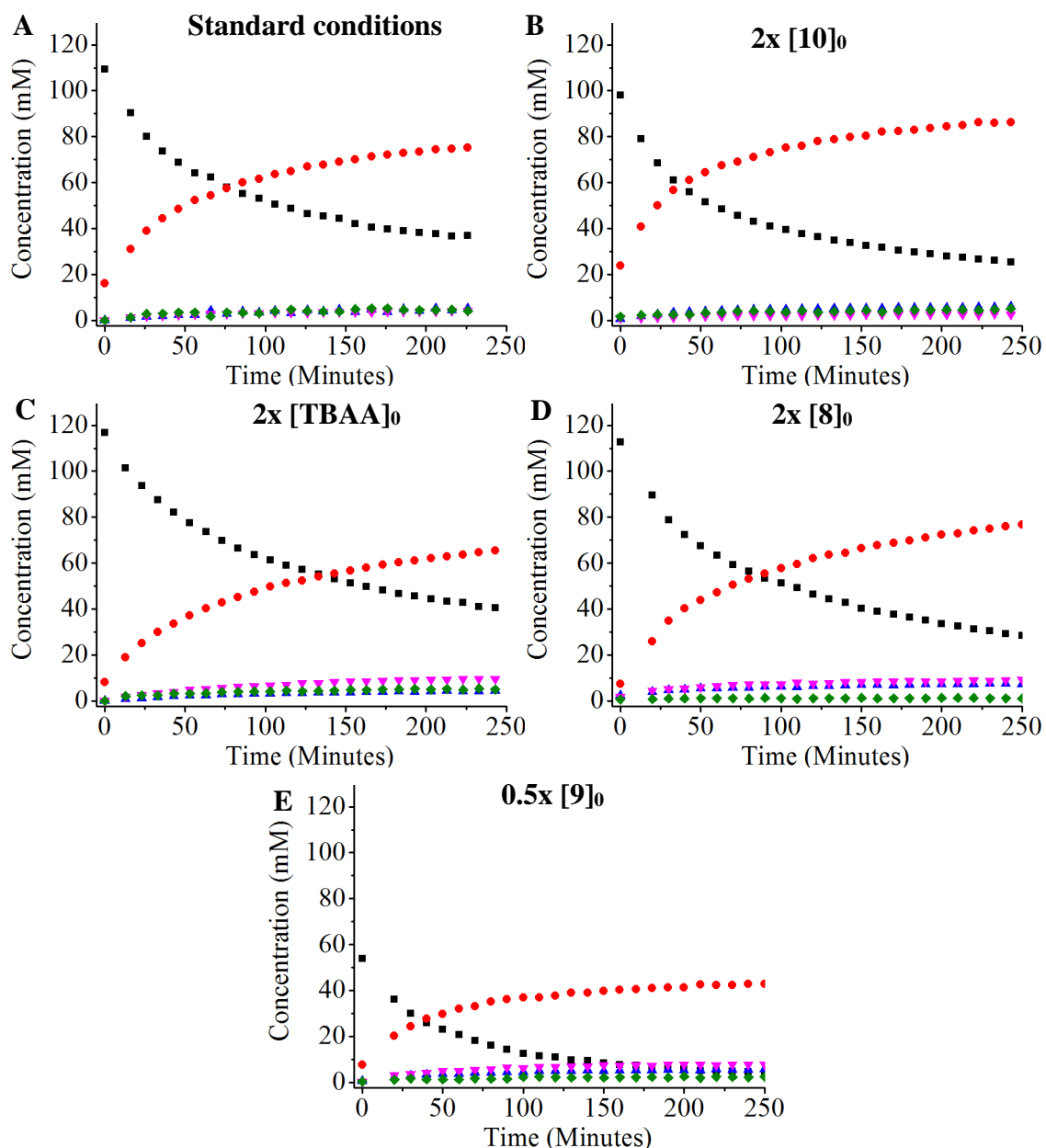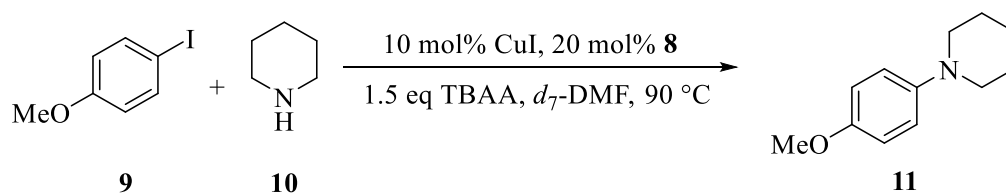
Figure 2.17 - ■ = **9**, ● = **11**, ▲ = **18**, ▼ = **14**, ◆ = Other products. First room temperature used as t_0 for kinetic profiles. Concentrations in 0.5 mL d_7-DMF   **A)** Initial concentrations; $[9]_0 = 125.0$ mM, $[10]_0 = 187.5$ mM, $[CuI]_0 = 12.5$ mM, $[8]_0 = 25.0$ mM, $[TBAA]_0 = 187.5$ mM **B)** $[10]_0 = 375.0$ mM **C)** $[TBAA]_0 = 375.0$ mM **D)** $[8]_0 = 50.0$ mM **E)** $[9]_0 = 62.5$ mM.

The effect of increasing the ligand concentration is seen in profile (**D**) however the subtle differences in the rate of formation of the product are better observed by plotting the rate of product formation against the concentration of **9** (Figure 2.18A). This plot shows very similar initial rates and this continues throughout the course of the reaction, however toward the end of the data, the 0.050 M **8** rate does not decrease as fast as the 0.025 M **8** rate. This indicates that the ligand plays a part in protecting the active catalyst from deactivation pathways. To interpret plot **E** more accurately, a plot of rate of product formation against time is helpful (Figure 2.18B). The data in this plot shows a significant decrease in the initial rate of reaction, expected based on the predicted rate equation, although the rates do eventually decrease to a similarly low point at the end of the dataset.
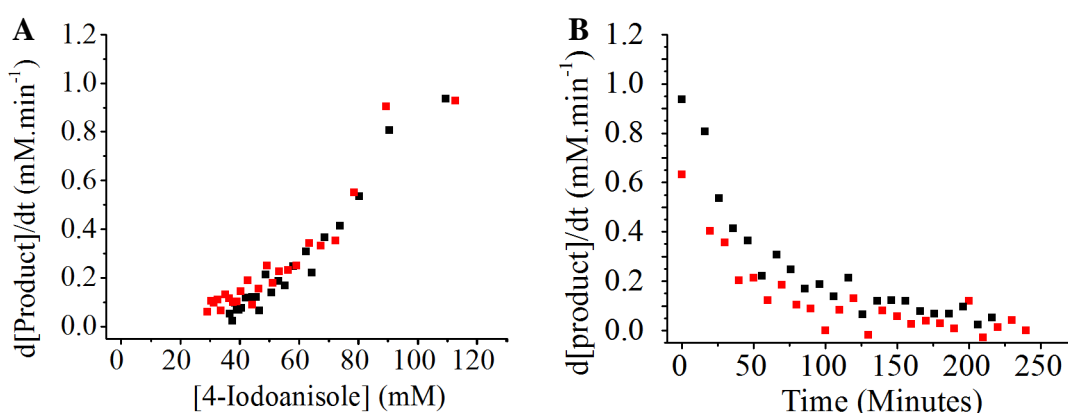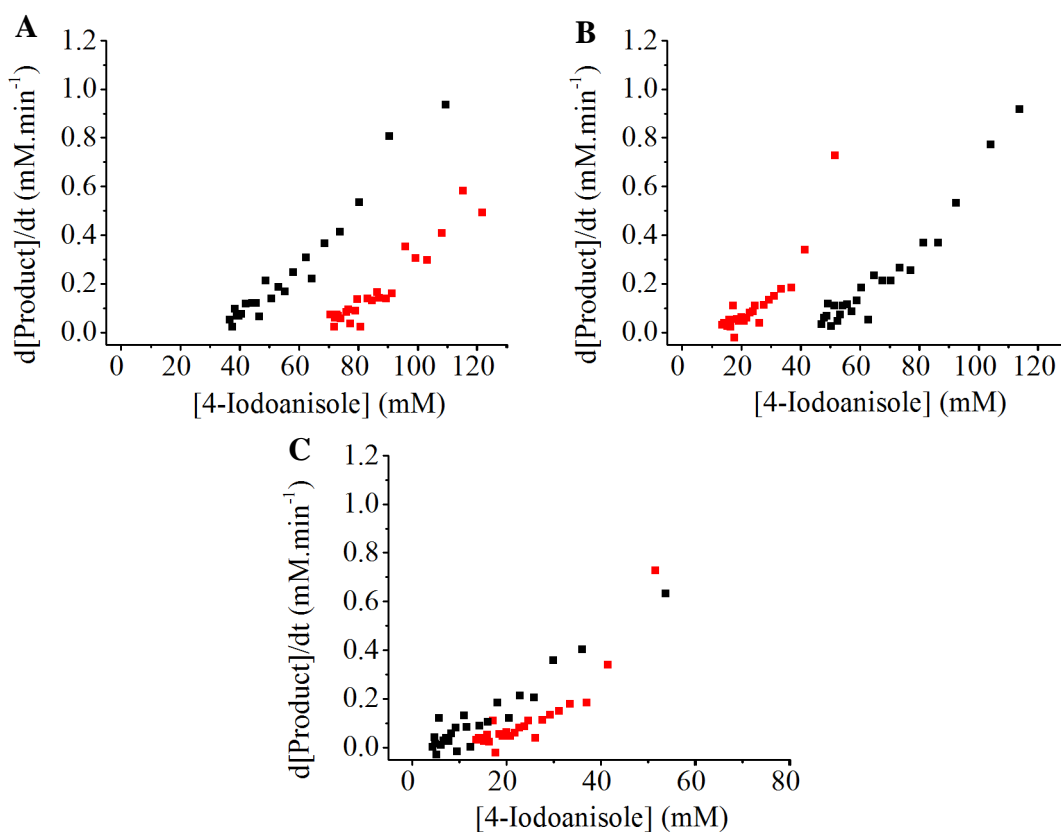
Figure 2.18 – A) ■ Initial concentrations; $[9]_0 = 125.0$ mM, $[10]_0 = 187.5$ mM, $[CuI]_0 = 12.5$ mM, $[8]_0 = 25.0$ mM, $[TBAA]_0 = 187.5$ mM in 0.5 mL d_7-DMF. ■ $[8]_0 = 50.0$ mM. **B)** ■ Initial concentrations; $[9]_0 = 125.0$ mM, $[10]_0 = 187.5$ mM, $[CuI]_0 = 12.5$ mM, $[8]_0 = 25.0$ mM, $[TBAA]_0 = 187.5$ M in 0.5 mL d_7-DMF. ■ $= [9]_0 = 75.0$ mM.

What is apparent from the data gathered from this study is that the rate law does not fully explain the reaction used in this system. Though the rate is proportionate to the [**9**] and [**10**], the extent of this indicates a number of other influential factors. The ligand is seen to have a stabilising effect on the reaction, causing as slower drop in the rate of reaction at low concentration of **9**. The concentration of TBAA was also found to have a marginal effect on the rate of the reaction, slowing it down, albeit only to a small extent.

The reaction profiles all show a similar pattern, with a somewhat fast initial rate of reaction, followed by a sharp drop, illustrated well by the first hour of the data shown in Figure 2.18B. This combined with the rate against the concentration data in Figure 2.18A not going through the [0,0] axis is a strong indication that either reversible or irreversible catalyst deactivation is occurring on the reaction time scale.

The reaction was subsequently probed for catalyst deactivation using the same "[excess]" techniques outlined by Blackmond.[4] The purpose of these experiments is to expose catalyst deactivation over the course of a reaction and to give information as to the source of it in the fewest amount of reactions possible. The same "[excess]" experiment allows the analysis of the catalytic system at different concentrations, as long as the stoichiometry of the reaction remains the same under the varying conditions. Figure 2.19 contains the data from a reduced catalyst loading (A), same "[excess]" experiments (B) and compares the same "[excess]" data against a reduced $[2.1]_0$.

The data found in these experiments confirms the hypothesis of catalyst deactivation occurring on the reaction timescale. From Figure 2.19A, the effect of halving the copper and ligand loading in the reaction is seen, where the initial rate is seen to reduce by approximately 40 %. This drop is expected given the expected first order dependency on the catalyst and that the drop is not exactly 50 % indicates a possible shift in the equilibria as a result of increasing the amine concentration relative the both the ligand and copper. Figure 2.19B shows the same ["excess"] result, in which the "[excess]" was 0.0625 M and applied to $[\mathbf{9}]_0$, $[\mathbf{10}]_0$ and [TBAA], which simulates the half-way point of the reaction. The two plots shown in this figure have significantly different plots, with the same "[excess]" rate much higher than the standard reaction. It may be interesting to compare the same "[excess]" data with the plot where only $[\mathbf{9}]_0$ was halved (Figure 2.19C). Although the initial rates are similar, the reaction with only reduced $[\mathbf{9}]_0$ proceeds faster as the reaction advances, likely to be a result of the greater $[\mathbf{10}]_0$ in this reaction relative to the same ["excess"] experiment.

Figure 2.19 – Deactivation investigation using ^{1}H NMR kinetics. Rate vs [**9**] **A)** Effect of halving catalyst ■ 10 mol% CuI and 20 mol% **8** ■ 5 mol% CuI and 10 mol% **8**. **B)** Same "[excess]" experiment ■ Initial concentrations; [**9**] = 125.0 mM, [**10**] = 187.5 mM, [CuI] = 12.5 mM, [**8**] = 25.0 mM, [TBAA] = 187.5 mM in 0.5 mL d_7-DMF. ■ [**9**] = 62.5 M, [**10**] = 125.0 mM, [CuI] = 12.5 mM, [**8**] = 25.0 mM, [TBAA] = 125.0 mM in 0.5 mL d_7-DMF. **C)** Same "[excess]" compared with half 4-iodoansiole **9** ■ 0.5x [**9**]$_0$ ■ Same "[excess]" conditions.

To probe a likely deactivation pathway, a product inhibition experiment was performed (Figure 2.20), in which 0.62 eq of the authentic product, **11** was included in the starting conditions. The quantity was determined by taking a reference NMR spectrum of the sample prior to [**10**] being added to the NMR tube, this was used as the start point of the reaction. The profile in Figure 2.20A clearly shows a decrease in the catalyst activity, giving poor conversions whilst Figure 2.20B shows how the rate of product formation has been reduced significantly by the addition of **11**.
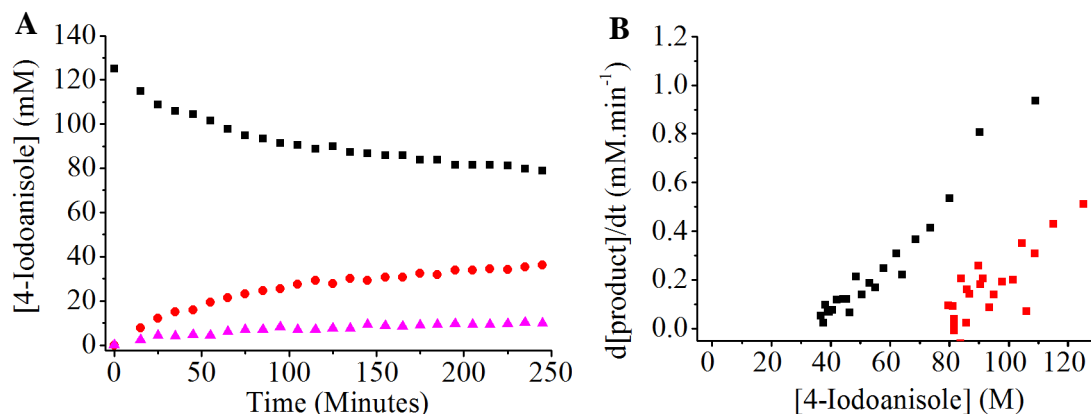
Figure 2.20 – Product inhibition experiments with $[11]_0 = 78.0$ mM. **A)** Kinetic profile of product inhibition reaction: ■ = **9**, ● = **11** and ▲ = all side products. **B)** Rate vs [**9**] profile: ■ = $[11]_0 = 0.0$ mM. ■ = $[11]_0 = 78.0$ mM.
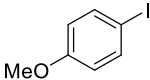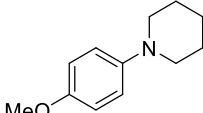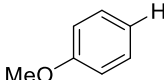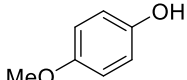
Product inhibition in this manner may be expected given the availability of the nitrogen lone pairs in tertiary amines and the subsequent coordination of to the product. Whilst this may be classed as a reversible catalyst deactivation pathway, the increase in product formation over the course of the reaction is seemingly having a hugely inhibitory effect and preventing the reaction from going to completion. Primary and secondary diamine ligands are widely reported to be excellent ligands in copper-catalysed reactions however tertiary amines are not usually efficient.[12] This may help explain the product inhibition, their strong ligation in increasingly high concentrations through the reaction will block the nucleophile coordination/deprotonation and the oxidative addition.

2.7.2. Side Product Analysis – *d₇*-DMF

To analyse the effect that changing conditions has on the side product formation for this reaction, the product distribution is of use (Table 2.3). The side two most prominent side products, anisole **18** and 4-methoxyphenol **14** are the only compounds with enough variation to make comparisons between experiments worthwhile.

**Table 2.3** - Product distributions for various d_7-DMF kinetic experiments after 4 hours at 90 °C. Values rounded to the nearest integer.

Conditions	9	11	18	14	Other (17 + 20)
Standard	27	63	4	3	2
2 x [10]$_0$	20	69	5	2	2
2 x [TBAA]$_0$	32	54	3	8	2
2 x [8]$_0$	23	62	7	8	1
0.5x [CuI/8]$_0$	56	35	1	5	2

This data is displayed in Figure 2.21 for visual comparison. As would be expected from the hypothesised pathways to these side products, increasing the concentration of **9** does not have a noticeable effect on side product formation. Increasing the TBAA concentration is found to cause a significant increase in **14**, giving further evidence that its formation is linked with residual H_2O from the hygroscopic base. Increasing the ligand concentration is found to have a substantial effect on the side products, causing an increase in **14** and the hydrohalogenation product **18**.

In palladium and nickel catalysed cross-coupling reactions, hydrodehalogenation is often a result of β-hydride elimination from an alkoxide or amine, giving the corresponding aldehyde or imine partner.[13] As 2,3,4,5-tetrahydropyridine is not observed in any of the reactions, it is unlikely that a similar pathway is occurring with the piperidine substrate. The link between ligand concentration and hydrodehalogenation may also be observed when lowing the CuI/**8** loading, causing only a small amount of **18** product to be formed (1 %).
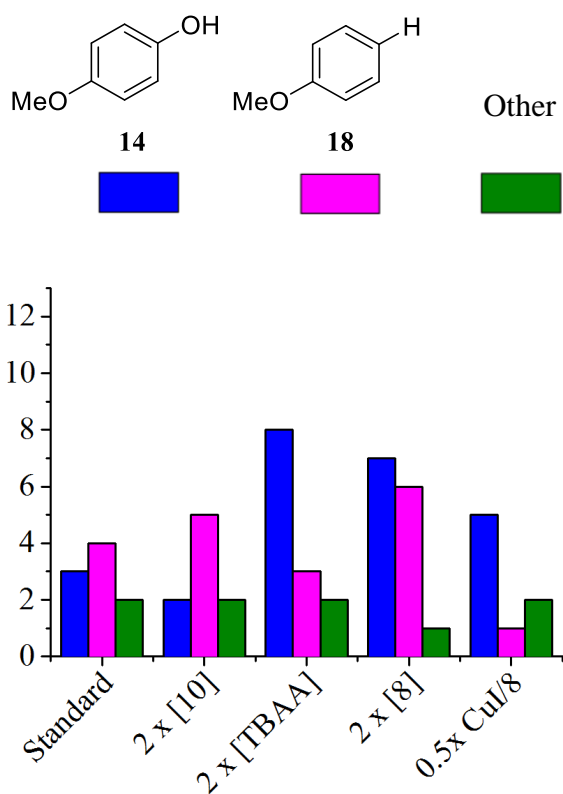
Figure 2.21 - Bar chart graphic of the data in Table 2.3 focusing on side product formation.

2.7.3. Solvent Effects – Kinetic Study in d_3-MeCN

As DMF is not a desirable solvent for industrial processes, it was decided to perform a similar kinetic experiment using d_3-MeCN as an alternative solvent. Acetonitrile is widely used as a solvent for copper-catalysed reactions and is considered much more desirable from an industrial standpoint, whilst still being a polar aprotic solvent and retaining the coordinating properties of DMF. From the initial reaction screening shown in Table 2.1, it was seen that MeCN is a good solvent for this reaction system and the reaction even proceeded with lower side products as the hydrolysis products formylpiperidine (**21**) and *N,N*-dimethylanisidine (**19/20**) are avoided. The results of the kinetic study in d_3-MeCN are displayed in Figure 2.22.
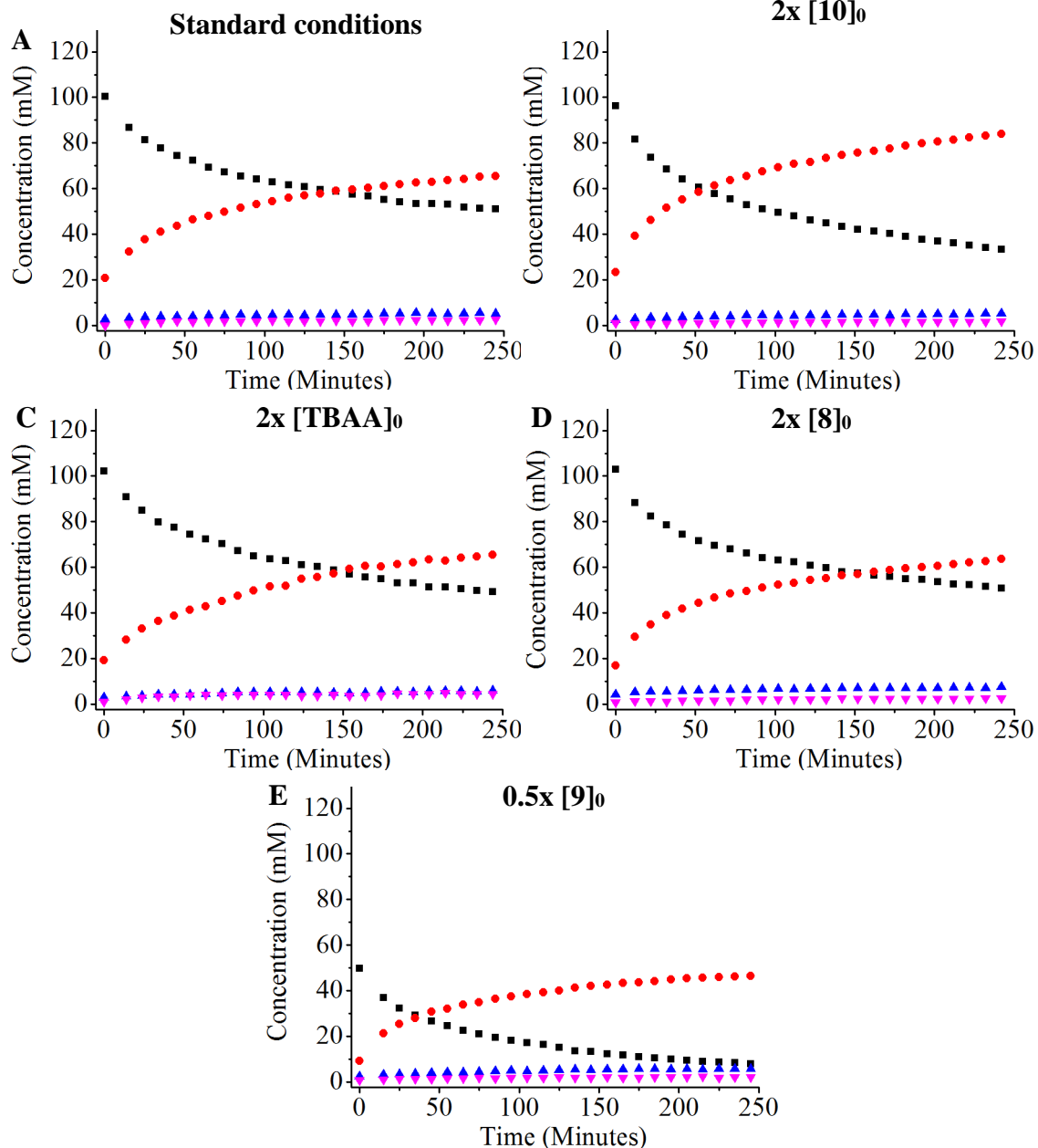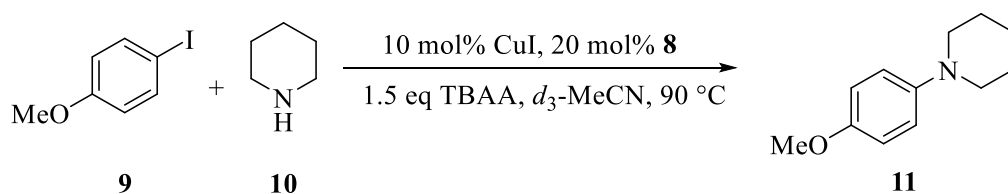
Figure 2.22 - ■ = **9**, ● = **11**, ▲ = **18**, ▼ = **14**. First room temperature used as t_0 for kinetic profiles. Concentrations in 0.5 mL d_3-MeCN. **A)** Initial concentrations; [**9**] = 0.125 mM, [**10**] = 0.1875 mM, [CuI] = 125.0 mM, [**8**] = 25.0 mM, [TBAA] = 187.5 mM. **B)** [**10**] = 375.0 mM **C)** [TBAA] = 375.0 mM **D)** **8** = 50.0 mM **E)** **9** = 62.5 mM.

The kinetic profiles obtained from the study in d_3-MeCN show very similar behaviour to the data obtained in d_7-DMF. The profile when the reaction is submitted to the standard reaction conditions (Figure 2.22A) shows that the reaction generally proceeds slowly after the initial 20 – 30 % conversion to product, indicating similar deactivation behaviour as in DMF. The biggest influence is seen when the initial concentration of the amine, **10** is doubled (Figure 2.22B), resulting in a faster reaction and greater conversion over the course of 4 hours. The data displayed in Figure 2.22C and Figure 2.22D show very little influence of increasing the ligand and base concentration on the kinetic profiles.

A more detailed look into the rates of reaction is given in Figure 2.23. Representing the data in this manner shows that there is a marginal increase in the initial rate of the reaction when using 40 mol% ligand compared to 20 mol% (Figure 2.23A). This effect could be linked with improving the solubility of the copper species initially however the influence is seen to diminish as the reaction goes on with almost perfect overlap of the rates after approximately 30 % conversion to product. The positive effect that increasing $[10]_0$ has on reaction rate and catalyst stability is displayed in Figure 2.23B, where the initial rate is almost doubled and remains higher than when a lower concentration of **10** is present. This may be attributed to the multiple roles the substrate may play in the reaction, acting as substrate and a ligand in its protonated form, which may block product inhibition. A small influence of the $[TBAA]_0$ on rate is seen with a lower initial rate, though this may not be considered significant.
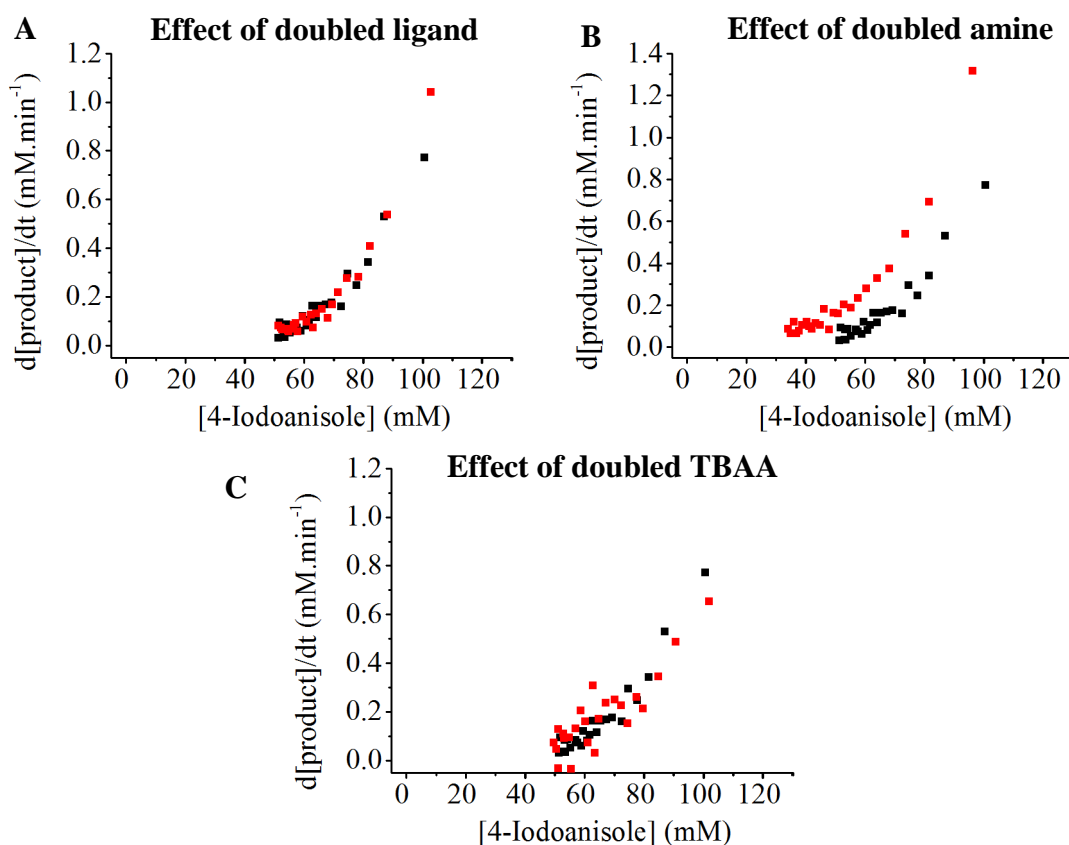
Figure 2.23 – Rate vs [**9**] profiles. **A) -** ■ 10 mol% CuI and 20 mol% **8** ■ 10 mol% CuI and 40 mol% **8**. **B) -** ■ $[10]_0 = 187.5$ mM ■ $[10]_0 = 375.0$ mM. **C) -** ■ $[TBAA]_0 = 187.5$ mM ■ $[TBAA]_0 = 375.0$ mM.

To analyse the effect of reducing the concentration of aryl iodide, the rate vs time plot in Figure 2.24 was used. This shows little to no effect on the rate of the reaction over the course of the kinetic data, this implies a zero-order dependence of the rate on [**9**] and is somewhat contradictory to the current mechanism. The accepted theory that oxidative addition of the aryl halide is the rate limiting step means that varying the concentration of **9** should have an effect on the rate of reaction.
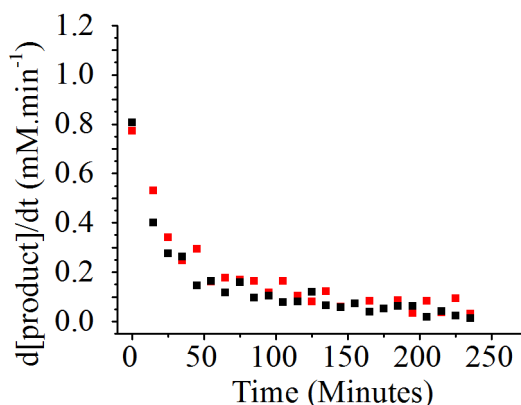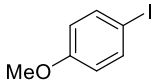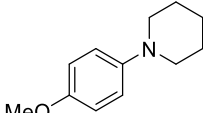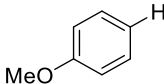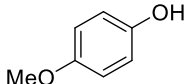

Figure 2.24 – Rate vs time plot. ■ $[9]_0 = 125.0$ mM ■ $[9]_0 = 62.5$ mM.

2.7.4. Side Product Analysis – d_3-MeCN

As was expected in the MeCN system, the side products were fewer than in DMF as it cannot decompose into reactive species in the same manner as DMF. Nevertheless, the phenol (**14**) and hydrodehalogenation (**18**) products are still formed under these reaction conditions (Table 2.4). A comparison of the extent of side product formation shows that under the standard conditions 7 % of the aryl species are side products after 4 hours opposed to 9 % in DMF, where *N,N*-dimethylanisidine (**19/20**) is the main contributor to the difference.

Table 2.4 - Product distributions for various d_3-MeCN kinetic experiments after 4 hours at 90 °C. Values rounded to the nearest integer.

Conditions	9	11	18	14	Other
Standard	41	52	4	2	1
2 x [10]$_0$	27	67	4	1	1
2 x [TBAA]0	39	52	5	4	1
2 x [8]$_0$	41	51	6	2	1

The trends seen agree with the previous hypotheses, that **14** is a result of excess moisture and so is formed in greater quantities with increased [TBAA]$_0$, and **18** is more prevalent with increased [**8**]$_0$ (visualised in Figure 2.25). The differences in values are small due to the low levels of conversions which limits definitive conclusions somewhat.
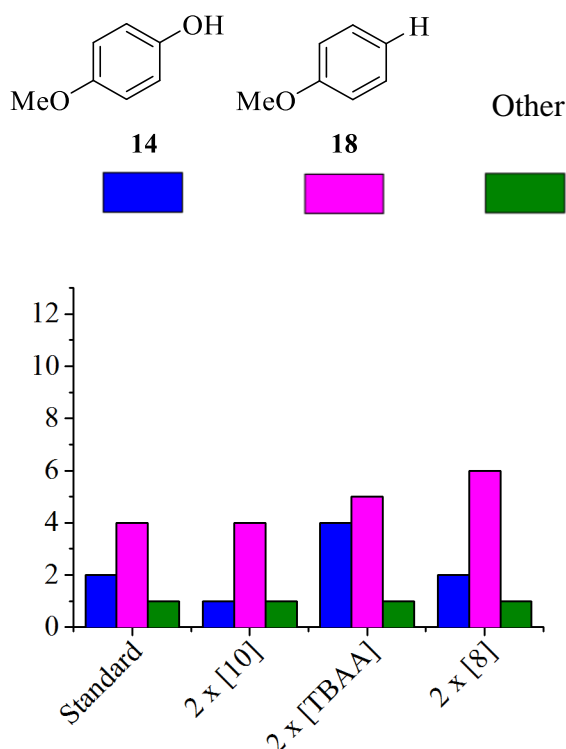
Figure 2.25 - Bar chart graphic of the data in Table 2.4 focusing on side product formation

2.7.5. Comparison of d_7-DMF and d_3-MeCN data

The behaviour of this *N*-arylation reaction in DMF and MeCN is not seen to differ greatly from the study that has been performed. The effects seen from varying the substrates, ligand and base were mostly identical, where only minor effects were seen when $[8]_0$ and $[TBAA]_0$ were increased. The small differences that were seen when increasing $[TBAA]_0$ are likely to be a result of the resultant increase in the phenol side product, which exists as the phenolate and is believed to contribute to the inhibition of the reaction due to coordination to the catalyst. A positive order in the amine was seen in both solvent systems and the role of **10** in this reaction may be to prevent the coordination of the product to stabilise the catalytic species. Interestingly, the behaviour of the reduced $[9]_0$ reactions differed between the solvents, where the rate of reaction was seen to slow somewhat in DMF, but no effect was seen in MeCN. This data could require repeating to ensure that this is true behaviour, but the slower reaction of the MeCN system may be a result of a shift in the pre-reaction equilibria.

Although the same ["excess"] and lowered catalyst loading experiments haven't been performed on the MeCN system, the non-linear rate behaviour over the course of the reaction implies that like DMF, significant deactivation is occurring. Product inhibition is likely to be prevalent in MeCN, as it is in DMF, however other deactivation or inhibition pathways may also be occurring.

A direct comparison of the d_7-DMF and d_3-MeCN data is shown in Figure 2.26, showing the difference in conversion of [**9**] to product (Figure 2.26A) and the different rate of the reaction (Figure 2.26B). The data appears to show greater deactivation in the MeCN system, in which the room temperature turnover prior to the first data point is actually greater than in DMF, however after this the reaction rate is considerably slower. This may be somewhat counterintuitive given the greater number of side products and quantity in which they are formed in DMF. The differences in the rate of catalyst deactivation implies that different pathways are viable in the different solvents, or shifts in the equilibria are occurring. Whilst both solvents investigated are polar aprotics with very similar dielectric constants, different densities, molar volumes, molecular shape and dipoles can all result in different reactivity.
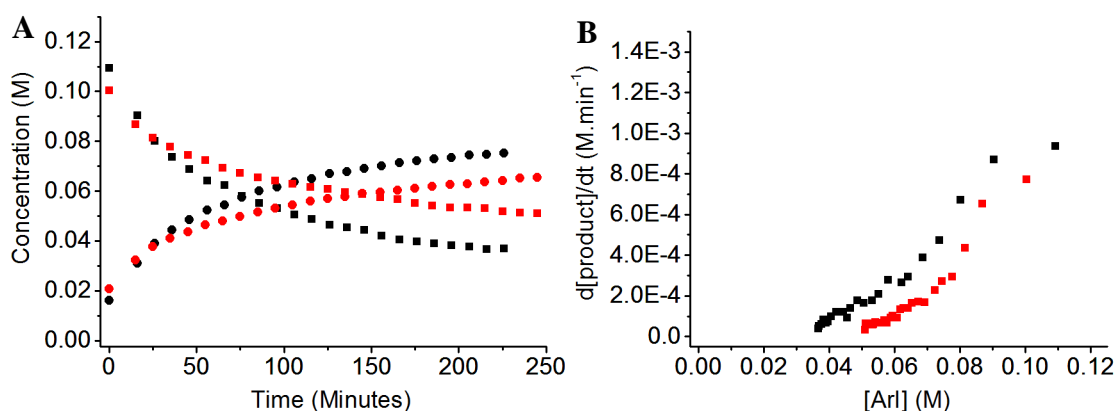

Figure 2.26 – Comparison of d_7-DMF and d_3-MeCN data from ^{1}H NMR kinetic monitoring experiments. **A)** Concentration vs time data for loss of **9** and increase of **11**: ■ = d_7-DMF ■ = d_3-MeCN. **B)** Rate vs [**9**]: ■ = d_7-DMF ■ = d_3-MeCN.

2.8. Mechanistic Insights

The kinetic study performed may be useful in providing insight into the mechanism of the copper-catalysed *N*-arylation reaction. One of the key considerations in the mechanistic discussion of this reaction is the ligand, which is often neutral (phenanthrolines, diamines) or anionic (1,3-diketones, amino acids). The widely cited investigations from Buchwald[1, 2] and Hartwig[14, 15] all utilise neutral N,N-type chelating ligands, whilst consideration of anionic ligands is slightly less prominent and are mostly computational.[16, 17] Within these studies, Buchwald reports that the electron rich *β*-diketone ligand promotes a SET mode of activation of the aryl halide.[17] Liu *et al* reported their alternative explanations based on their own computational study, in which they propose that the use of anionic ligands promotes a facile oxidative addition of the aryl halide, prior to the rate determining coordination of the *N*-nucleophile.[16] The oxidation addition pathway also accounts better for the I > Br >> Cl reactivity order which is observed in these reactions, where the calculated energy difference between oxidative addition of PhCl is +4.3 kcal/mol higher than PhBr, accounting for a 10^3 fold decrease in reactivity from Br to Cl.

The results reported from this kinetic study agree mostly with the work by Liu, in which the rate determining step is likely to be the coordination of **10** to species **24** (Scheme 2.6), following the oxidative addition of the aryl halide to the Cu(I)-ligand species **23**. The subsequent deprotonation and halide abstraction of **25** to give the intermediate **26** precedes the reductive elimination of the product and regeneration of **23**. This mechanism explains the positive order seen with respect to the amine [**10**] and the marginal dependence of the rate on [**9**]$_0$. Intermediate **25** also provides a feasible pathway to the hydrodehalogenation product [**18**], though a separate catalytic cycle is probably occurring for the formation of the phenol product [**14**]. Watson has recently reported a thorough study of the Chan-Lam reaction, in which the formation of a phenol by-product is said to occur *via* a Cu(I) species in a separate catalyst cycle.[18] Given the facile oxidation which is proposed, a reductive elimination step could occur following a halogen exchange reaction of intermediate **24**, with the trace chloride and bromide anions remaining from TBAH and TBPH.
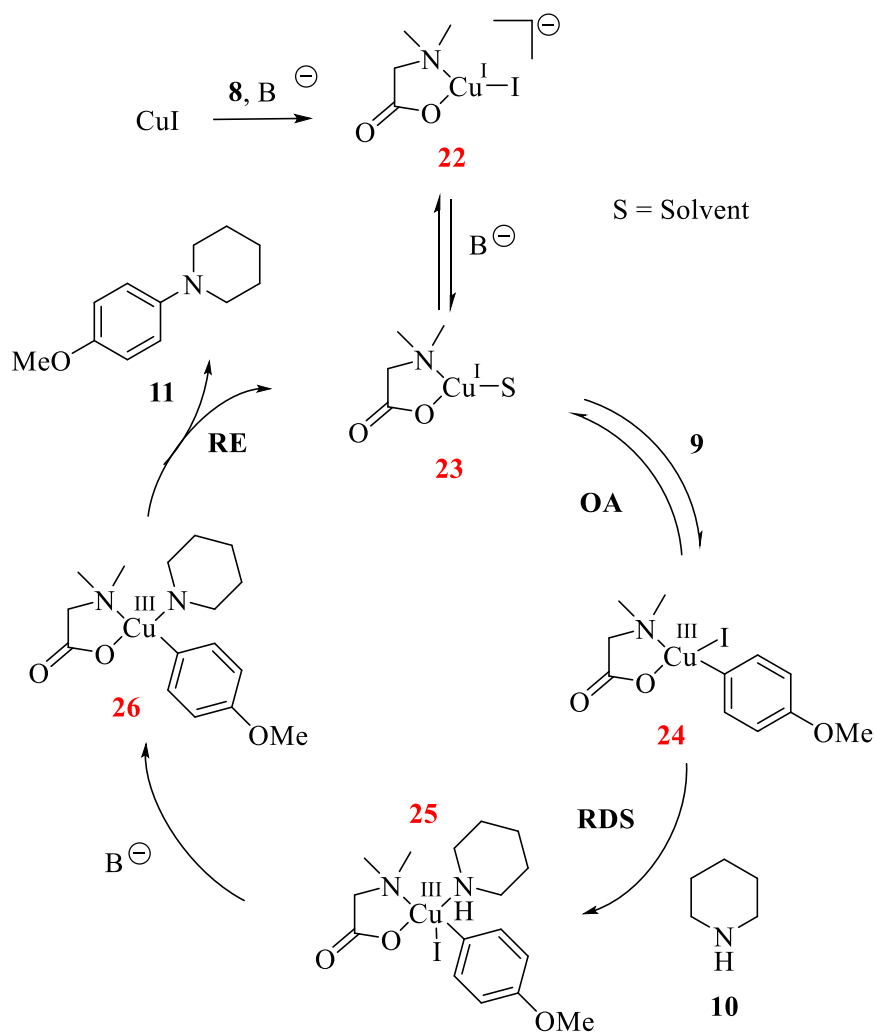
Scheme 2.6 - Proposed mechanism for the copper-catalysed coupling reaction between 4-iodoanisole and piperidine in the presence of **8**.

Kinetic modelling of this system could be used to help provide further insight into the plausibility of this mechanism and some of the steps involved. Attempts to model the system using DynoChem software proved difficult however due to the complex nature of the system, significant side product pathways and the multiple roles assumed by numerous reaction components in reality. The expected instability of the proposed intermediates makes synthesis and observation of the species very difficult, with few Cu(III) compounds reported and none of this nature, where dynamic equilibria and ligand exchange will likely be occurring.

2.9. Summary and Conclusions

The use of organic bases in the copper-catalysed *N*-arylation reaction between 4-iodoanisole and piperidine was found to provide novel insight into the *N*-arylation reaction as well as side reactions which occur in this system. Reactions with TBAA as the base were found to proceed under relatively mild conditions (70 °C) in DMF and MeCN with a fully homogeneous system. The use of ^{1}H NMR spectroscopy as a reaction monitoring tool was found to be powerful in gathering a large amount of kinetic data in d_7-DMF and d_3-MeCN. A study of the catalyst deactivation using same ["excess"] and product inhibition experiments showed a significant influence of catalyst deactivation on the reaction rate. Considerable product inhibition was observed and is expected to occur *via* coordination of the tertiary amine which is formed to the copper centre, blocking coordination sites of the catalyst.

The study covers the area of anionic ligands in the amination reaction, where experimental mechanistic studies have previously focussed on neutral ligands, which have been shown to possess different reactivity. The behaviour of the reaction kinetics under the conditions covered appears to give further experimental data to the proposal of Liu that the rate determining step of the reaction may be the coordination of the *N*-nucleophile, occurring after oxidative addition of the aryl iodide. This mechanism differs somewhat from the most commonly used mechanism proposed by Buchwald and Hartwig previously, in which oxidative addition is the rate determining step and follows the nucleophile coordination.

2.10. References

1.   E.R. Strieter, D.G. Blackmond and S.L. Buchwald, *J. Am. Chem. Soc.*, 2005, **127**, 4120-4121.

2.   E.R. Strieter, B. Bhayana and S.L. Buchwald, *J. Am. Chem. Soc.*, 2009, **131**, 78-88.

3.   S. Sung, D. Sale, D.C. Braddock, A. Armstrong, C. Brennan and R.P. Davies, *ACS Catal.*, 2016, **6**, 3965-3974.

4.   D.G. Blackmond, *Angew. Chem. Int. Ed.*, 2005, **44**, 4302-4320.

5.   C.T. Yang, Y. Fu, Y.B. Huang, J. Yi, Q.X. Guo and L. Liu, *Angew. Chem. Int. Ed.*, 2009, **48**, 7398-7401.

6.   D.B. Zhao, N.J. Wu, S.A. Zhang, P.H. Xi, X.Y. Su, J.B. Lan and J.S. You, *Angew. Chem. Int. Ed.*, 2009, **48**, 8729-8732.

7.   P.Y.S. Lam, D. Bonne, G. Vincent, C.G. Clark and A.P. Combs, *Tetrahedron Lett.*, 2003, **44**, 1691-1694.

8.   Y. Imazaki, E. Shirakawa, R. Ueno and T. Hayashi, *J. Am. Chem. Soc.*, 2012, **134**, 14760-14763.

9.   J. Kagimoto, S. Taguchi, K. Fukumoto and H. Ohno, *J. Mol. Liq.*, 2010, **153**, 133-138.

10.   T.V.Q. Nguyen, W.J. Yoo and S. Kobayashi, *Angew. Chem. Int. Ed.*, 2015, **54**, 9209-9212.

11.   E. Sperotto, G.P.M. van Klink, G. van Koten and J.G. de Vries, *Dalton Trans.*, 2010, **39**, 10338-10351.

12.   D.S. Surry and S.L. Buchwald, *Chem. Sci.*, 2010, **1**, 13-31.

13.   Z. Ahmadi and J.S. McIndoe, *Chem. Commun.*, 2013, **49**, 11488-11490.

14.   J.W. Tye, Z. Weng, A.M. Johns, C.D. Incarvito and J.F. Hartwig, *J. Am. Chem. Soc.*, 2008, **130**, 9971-9983.

15.   R. Giri and J.F. Hartwig, *J. Am. Chem. Soc.*, 2010, **132**, 15860-15863.

16.   H.Z. Yu, Y.Y. Jiang, Y. Fu and L. Liu, *J. Am. Chem. Soc.*, 2010, **132**, 18078-18091.

17.   G.O. Jones, P. Liu, K.N. Houk and S.L. Buchwald, *J. Am. Chem. Soc.*, 2010, **132**, 6205-6213.

18.   J.C. Vantourout, H.N. Miras, A. Isidro-Llobet, S. Sproules and A.J.B. Watson, *J. Am. Chem. Soc.*, 2017, **139**, 4769-4779.

Chapter 3

Partially-soluble Bases in the Copper-Catalysed Amidation of Aryl Halides

3.1. Introduction

The use of inorganic salts such as K_2CO_3, K_3PO_4 and Cs_2CO_3 in transition metal catalysis is widespread.[1-4] These compounds benefit from being easy to handle, commercially available and versatile. The choice of which base will perform best in any given reaction is however difficult to predict, and base screens are commonly employed in catalysis to find the best option. The limited solubility of the inorganic salts in the organic solvents which are most common in catalysis, such as MeCN, Toluene, EtOH or acetone, means that the rate of solubility often has a significant effect on the rate of reaction.

Various examples of highly efficient Ullmann-type *N*-arylation reactions which utilise the carbonate and phosphate salts have been reported in the literature, however finding consistent trends in the which bases are more efficient is difficult. Scheme 3.1 contains an example in which K_2CO_3 was shown to be useful in the amidation of aryl halides with the 1,2-diamine ligand **29**.[5]
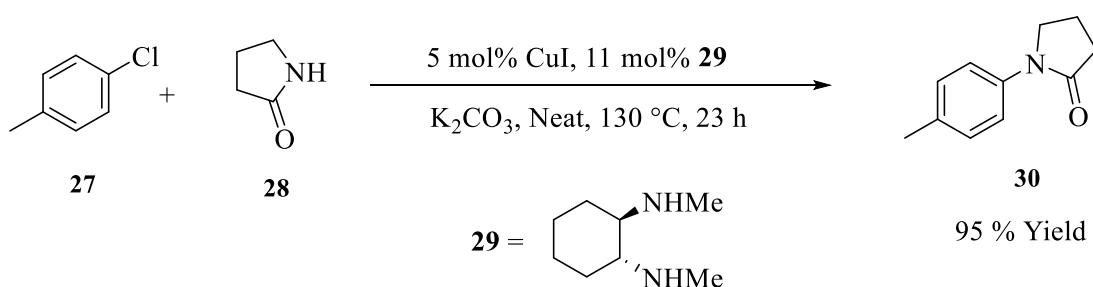
Scheme 3.1 – K_2CO_3 in the amidation of aryl chlorides.[5]

Although Cs_2CO_3 and K_2CO_3 share the same anion, they are not analogous in the copper-catalysed systems, often displaying contrasting reactivity. This demonstrates that pKa values are not the only drive for reactivity and it is likely that the cation also plays a role. Cs_2CO_3 is more commonly employed than K_2CO_3 and was used in the preliminary work on forming aryl ethers by Buchwald.[6] Since then, Cs_2CO_3 has been reported to promote

the amination of aryl chlorides at low catalyst loadings (Scheme 3.2),[7] and rapid room-temperature aminations of aryl iodides.[8]
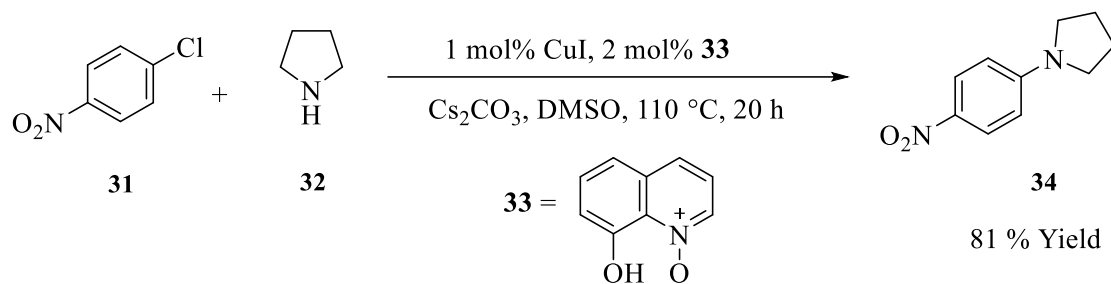
Scheme 3.2 – Amination of aryl chlorides using Cs_2CO_3 and an 8-hydroxyquinolin-*N*-oxide ligand **33**.[8]

K_3PO_4 is the most effective base in some reported reactions, possibly due to its increased solubility and higher pKa than K_2CO_3.[9] Buchwald demonstrated its use when reporting the application of ligand *N,N*-diethylsalicylamide (**37**) in the *N*-arylation of primary alkylamines (Scheme 3.3).[10] It has also found use as a base in the formation of primary arylamines from aryl halides and aqueous ammonia,[11] and in the *N*-arylation of acyclic amides.[12]
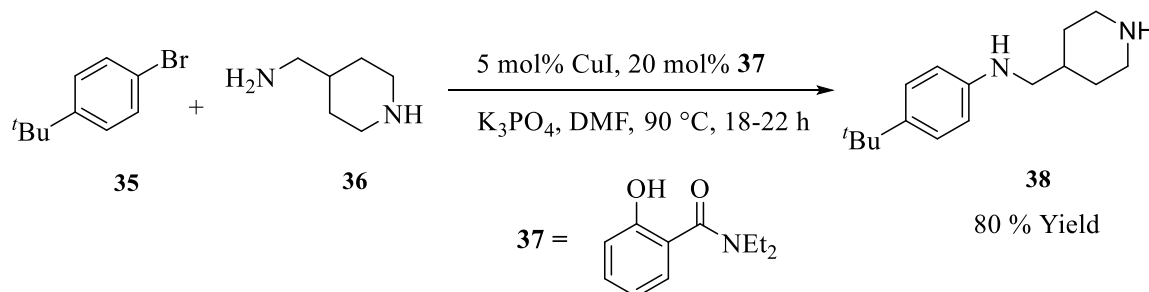
Scheme 3.3 – K_3PO_4 as a base in the competitive selective *N*-arylation of primary amines.[10]

In some specific cases, stronger bases have been found to be effective in copper-catalysed amination reactions. Buchwald showed that the strong base KHMDS is inefficient for aryl amidations when added in one portion, but can give good conversions when added slowly to the reaction.[5] Hydroxide salts such as NaOH or KOH have been used as a hydroxide source in the formation of phenols from aryl halides in the presence of copper, and thus are generally not a good choice of base as this will act as a competitive reaction.[13-15] Some examples can be found using KOH under specialised conditions

however,[16] and Scheme 3.4 shows a system reported by Chan *et al.* which works using NaOH under ligand-free conditions in the presence of the phase-transfer catalyst tetrabutylammonium bromide (TBAB).[17]
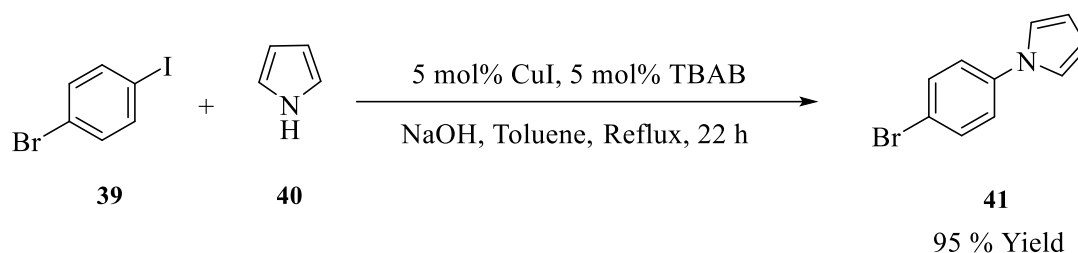
Scheme 3.4 – NaOH as an efficient base for the *N*-arylation of nitrogen heterocycles

The use of *tert*-butoxide bases is commonly reported in palladium-catalysed amination reactions,[1] but fewer examples can be found in similar copper-catalysed systems. In the handful of examples that are available, such as the ligand-free amination of aryl iodides, KO^tBu is shown to be capable of promoting the more difficult double-amination to give the tertiary arylamine (**44**) as a major product (Scheme 3.5).[18]
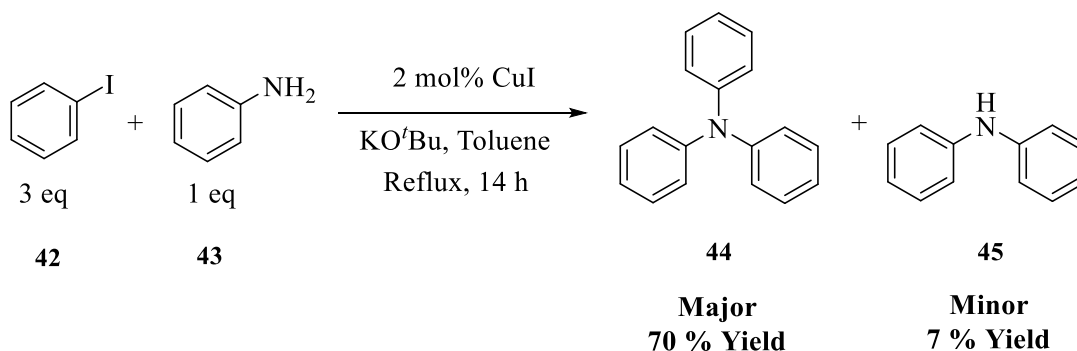
Scheme 3.5 – KO^tBu in the selective formation of triarylamines.

Buchwald has previously stated that the key to choosing an appropriate base in Ullmann-type reactions is to match the rate of deprotonation of the substrate with the rate of dissolution. The examples of strong bases described above are performed with toluene as the solvent, and the poor solubility of these bases in this solvent may limit deprotonation, allowing these specific examples to work. Alternatively, the work reported by Liu on fully-soluble bases,[19] and that discussed in Chapter 2 means that this may not hold true for all systems, and reactivity is dependent on more than just solubility.

3.2. Initial screening of conditions

Various substrates and conditions were screened to build on the literature understanding of scope and reactivity for inorganic bases in the Ullmann-Goldberg reaction. Poor initial results compared with literature reports indicated a complexity to Ullmann-Goldberg coupling, which are often referred to as unreliable.[20] One of the immediately apparent sources of irreproducibility was the reaction set-up and reactor type. Literature procedures vary greatly in terms of the set-up used for copper-catalysed amidation reactions, with most being performed under inert conditions with septum seal vials,[21] Schlenk flasks[22] or round-bottom flasks,[23] though some procedures do tolerate aerobic conditions.[24] If the reaction is to proceed *via* a Cu(I)/Cu(III) mechanism, as was discussed in Chapter 1, the Cu(I) resting state must be stable to oxidation to Cu(II), or a facile reduction from Cu(II) to Cu(I) must be possible for aerobic conditions to be viable.

The C-N coupling reaction shown in Scheme 3.6 was used to determine the reproducibility of various reaction apparatus. This reaction was shown to proceed efficiently at 110 °C using K_3PO_4 as the base and a protic ligand, glycine,[23] indicating that it would be a good choice for a model reaction. Initial results did however show that the ligand 2-isobutyrylcyclohexanone (**13**) was a more effective alternative and so this was the ligand used.
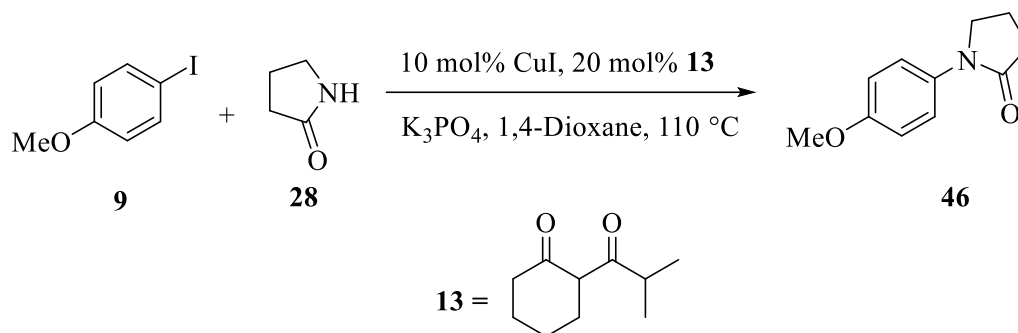
Scheme 3.6 - Ullmann-Goldberg coupling between 4-iodoanisole and 2-pyrrolidinone

Table 3.1 – Screening results for the C-N coupling shown in Scheme 3.6. Conversions determined by ^{1}H NMR analysis.

Entry	Reactor	Inert Gas	Time (hours)	Conversion %
1	RB flask/ condenser	N_2	48	98
2	RB flask/ Condenser (repeat)	N_2	48	26
3	Sealed tube	N_2	19	9
4	Septum-sealed vial	N_2	24	Trace
5	Schlenk flask	N_2	18	> 99
6	Schlenk flask	N/A	18	Trace
7	Carousel reactor	N_2	18	Trace

Although Entry 1 indicated that a simple round-bottom flask fitted with a condenser can provide good conversions, further repeats using this setup indicated that this was not reproducible (Entry 2). Having a constant flow of nitrogen was found to be important to reactivity in this system, where a sealed tube and vial were found to be inadequate (Entries 3 and 4). The ability to fully evacuate and backfill a Schlenk flask allowed for the greatest reproducibility, and unless otherwise stated, all reactions were performed using this setup (Entry 5). From the results of this study, it was clear that this amidation reaction had a considerable sensitivity to air, particularly noticeable from the reaction detailed in Entry 6, with aerobic conditions, and Entry 7, in which the reaction was performed under a nitrogen atmosphere but the imperfect seal of the carousel reactor tubes prevented significant turnover of all reactions performed with this setup.

3.2.1. Base Scope

The coupling between 4-iodoanisole (**9**) and 2-pyrrolidinone (**28**) was also used to provide insight into the tolerance of the base in the Ulmann-Goldberg amidation. Alhough the solubility of the various inorganic bases are not known under these conditions, it is expected that this, along with the pKa of the conjugate acid, will be influential factors which govern reactivity. The data in Table 3.2 shows that the most effective base is Cs_2CO_3, and whilst K_3PO_4 and K_2CO_3 are also able to promote some

reactivity, the cesium cation may be important in giving good conversions (Entries 1-3). Entries 4 and 5 test more unconventional bases but show no significant reactivity, perhaps unsurprising given that Na-*L*-ascorbate (**47**) is a weak base (pK_a = 4.2) and the limited solubility of **48** observed in the reaction solvent. The highly soluble CsOAc in Entry 6 was found to be similarly active too, showing that both the anion and cation are important to the performance of the base.

Table 3.2 – Reaction conditions for base screening. Conversions determined by ^{1}H NMR analysis.

Entry	Base	Solvent	Time (hours)	Temperature ° C	Conversion %
1	K₃PO₄	DMF	17	90	30
2	K₂CO₃	DMF	17	90	35
3	Cs₂CO₃	DMF	20	90	83
4	**47**	DMF	18	90	Trace
5	**48**	DMF	18	90	Trace
6	CsOAc	DMF	16	90	30

Due to the considerable p*K*a difference between cyclic amides such as **28** (p*K*a = 24), and secondary amines (p*K*a > 40), an evaluation of bases in a coupling reaction between **9** and piperidine (**10**) (Table 3.3) may show a different reactivity trend. The deprotonation of the nucleophile in palladium- and copper-catalysed aminations is widely accepted to occur following coordination of the nucleophile.[2, 25] The poor understanding of how facile this step is for different nucleophiles and metals can mean that prediction of reactivity is difficult.

The study detailed in Table 3.3 shows that the efficiency of the inorganic base systems is lower when using a secondary amines compared to amides. Generally, poor reactivity was obtained under the conditions applied, although it should be noted that they represent some of the more mild conditions (< 100 °C/< 24 hours) seen until specifically designed ligands are used.[26] Of the conditions screened, Entry 2, with Cs_2CO_3 provided the highest conversion to products, whilst similar conditions with K_3PO_4 in Entry 1 gave considerably lower conversion. Similarly to the amidation reaction, **48** (Entry 3) showed limited reactivity, despite its high observed solubility. When comparing potassium and cesium salts in Entries 6 and 7, CsOAc was able to give some conversion, contrasting the lack of any product formation when using KOAc.

Table 3.3 – Base screening when using **10** as the *N*-nucleophile.
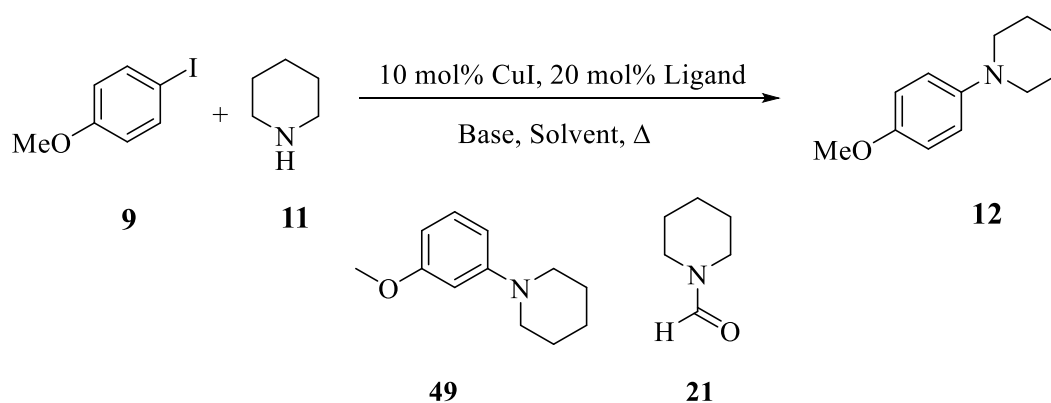
Entry	Base	Solvent	Time (hours)	Temp ° C	Conversion %
1[a]	K_3PO_4	DMF	19	100	36
2[a]	Cs_2CO_3	DMF	21	90	60
3	**48**	DMF	18	90	25
4[a,b]	KO^{t}Bu	DMF	20	110	30* (30 % **49**)
5[a]	KO^{t}Bu	1,4-Dioxane	19	110	15* (12 % **49**)
6	KOAc	DMF	18	90	20* (0.8 eq **21**)
7	CsOAc	DMF	15	90	36* (1.2 eq **21**)
8[c]	CsOAc	DMF	17	90	17* (0.4 eq **21**)

*Indicates that side products were found post-reaction. Conversions determined by ^{1}H NMR analysis relative to 9. [a]Ligand = 13, [b]4-bromoanisole (15), [c]no ligand.

Along with the poorer conversions obtained, the reactions with **10** showed other contrasting behaviour in the greater formation of side products. This may be because the conjugate acids of the carbonate and phosphate bases are insoluble solids of bicarbonate and hydrogenphosphate, whilst the conjugate acids of the salts in Entries 4 – 8 are expected to be fully soluble in the reaction solvent.

When using KO^{t}Bu, roughly 1 : 1 ratio of para : meta substituted *N*-arylation product in Entries 4 and 5 was observed, indicative of a benzyne intermediate, which can then undergo nucleophilic attack.[27] This reactivity has been reported previously as a metal and ligand free Ullmann-coupling,[28] in which the authors found the reactivity trend followed Br > I, explaining the higher conversion of Entry 4 than Entry 5.

When using the acetate salts (Entry 6 - 8), *N*-formylpiperidine **(21)** was formed as a byproduct. The *N*-formylation of secondary amines through transamidation of DMF has been previously reported as a side reaction in the palladium-catalysed nucleophilic substitution of napthylmethyl and allyl acetates, using morpholine as the nucleophile.[29] In this work the authors propose that this is the result of an uncatalysed transfer of the formyl group from DMF to morpholine, leaving *N,N*-dimethylamine as the byproduct (Scheme 3.7). Utilisation of transamidation to promote *N*-formylation of amines was also reported in an Fe(III)-catalysed system, in which the formylation of **10** was demonstrated using 5 mol% $Fe(NO_3)_3.9H_2O$ at reflux with formamide in toluene for 18 hours.[30]
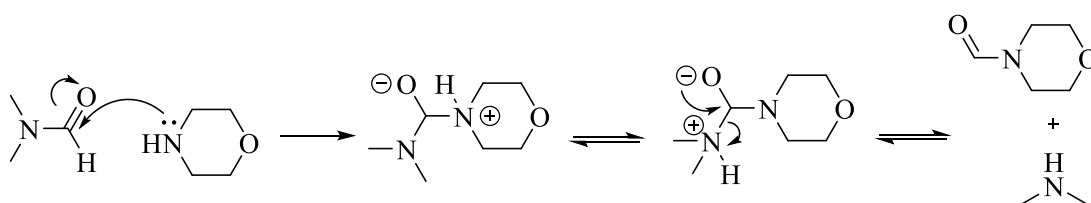
Scheme 3.7 –Mechanism of *N*-formylation to give **21** and *N,N*-dimethylamine through transamidation of DMF, as reported by Fiaud.[29]

Further reactions were able to shed light on the nature of the formylation reaction under Ullmann-Goldberg conditions (Table 3.4). It was found that the reaction does not convert well under copper/ligand-free conditions (7 %), and the ligand **8** cannot be replaced by **50**, which gave only trace amounts of product. A ligand-free reaction using CsOAc did result in 25 % conversion to the product, presumably due to the ability of

acetate to act as a ligand. Lastly, the reaction converted well under aerobic conditions (75 %) and the copper source was found to be interchangeable, as Cu(OAc)$_2$ gave similar conversions under aerobic conditions (80 %). These results indicate that the copper catalyst acts as a Lewis acid in the reaction, necessary to activate the DMF. It is unsure as to why the acetate salts promote the reaction yet the carbonates do not, however the *N*-formylation will compete with the cross-coupling reaction if these conditions are used in the presence of an aryl halide.

Table 3.4 – *N*-formylation of piperidine under Ullmann-Goldberg conditions. [a]Aerobic conditions. Conversions determined by ^{1}H NMR analysis.
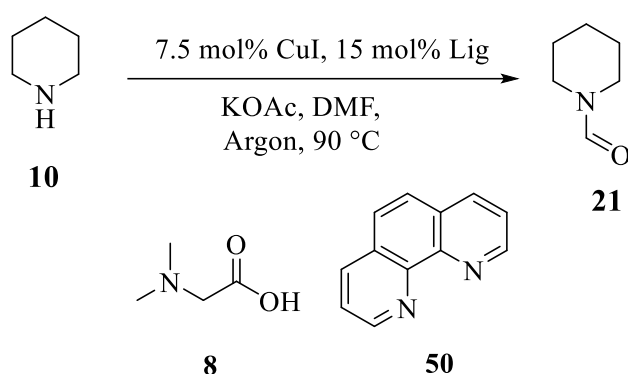
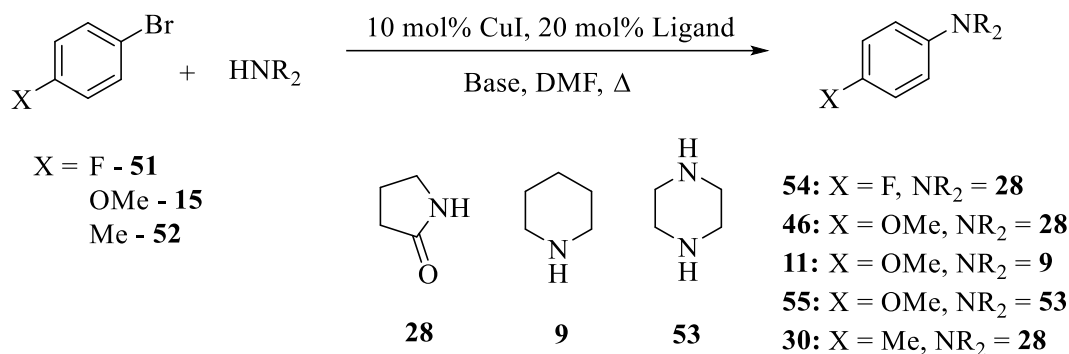| Entry	Base	Copper source	Ligand	Time (hours)	Conversion %
1	KOAc	CuI	**8**	17	53
2[a]	KOAc	CuI	**8**	17	75
3[a]	KOAc	CuOAc	**8**	17	80
4	KOAc	None	None	17	7
5	KOAc	CuI	**50**	17	Trace
6	CsOAc	CuI	**8**	22	79
7	CsOAc	CuI	None	22	25

3.2.2. Aryl Bromide Reactivity

The reactivity of aryl bromide reagents are reported in the literature to be much lower than those of aryl iodides, requiring longer reaction times and higher temperature to go to completion. The conditions detailed in Table 3.5 show how applicable the relatively mild conditions used for aryl iodides are for aryl bromides.

Results with aryl bromides showed lower conversions than with aryl iodides, as would be expected. The conditions in Table 3.2, Entry 3 were used due to the good conversion seen with the aryl iodide **9,** but as the Entries 1 and 8 in Table 3.5 show, very poor conversion was observed after 17 hours. This demonstrated the stark difference in reactivity of the aryl bromides over the aryl iodides. It was found that the reaction could go to greater conversion when much longer reaction times were used (Entry 2). This is significant as the prolonged stability of the catalyst indicates that catalyst deactivation is not as apparent in this system as it was with the organic bases discussed in Chapter 2.

The use of K_2CO_3 was included to explore the statement of Buchwald that K_2CO_3 is the base of choice with aryl bromides due to the slow rate of dissolution matching the rate of product formation.[31] In this case, conversion was not improved by the use of K_2CO_3 (Entry 4). Use of K_3PO_4 also showed poor reactivity with **28** (Entry 5), and with secondary amines (Entries 6 and 7), which were similarly found to give limited reactivity with aryl iodides.

Table 3.5 – Screening conditions for *N*-arylation of aryl bromides.   [a]1,4-Dioxane as solvent. Conversions determined by ^{1}H NMR analysis.

X = F **- 51**
OMe **- 15**
Me **- 52**

28   **9**   **53**

54: X = F, NR$_2$ = **28**
46: X = OMe, NR$_2$ = **28**
11: X = OMe, NR$_2$ = **9**
55: X = OMe, NR$_2$ = **53**
30: X = Me, NR$_2$ = **28**

	Base	Ligand	X-	HNR$_2$	Time (hours)	Temp ° C	Conversion %
1	Cs$_2$CO$_3$	**8**	F	**28**	17	90	8
2^a	Cs$_2$CO$_3$	**13**	F	**28**	50	110	44
3^a	K$_3$PO$_4$	**13**	F	**28**	18	100	2
4	K$_2$CO$_3$	**13**	F	**28**	72	110	Trace
5	K$_3$PO$_4$	**8**	OMe	**28**	20	110	Trace
6	K$_3$PO$_4$	**13**	OMe	**10**	19	100	16
7	K$_3$PO$_4$	**13**	OMe	**53**	18	100	Trace
8	Cs$_2$CO$_3$	**8**	Me	**28**	17	90	7

3.2.3. Implications of Screening Studies

The preliminary studies performed highlight the need to consider many aspects of the reaction setup and conditions in order to achieve significant reactivity and reproducible results. The air sensitivity of the reaction means that an inert environment (N$_2$ or Ar) is necessary for the turnover and can also impede sampling, as this can introduce air. The base scope was found to be relatively limited with regards to the inorganic salts, with Cs$_2$CO$_3$ and K$_3$PO$_4$ being the only effective bases. Side products observed when using acetate salts and KO^{t}Bu explain why these are not commonly used, although the acetate salts may be more efficient when working with phenol substrates and avoiding DMF as a solvent. The reactivity of a cyclic amide was found to be higher than that of secondary

amines, which may be correlated with the greater difficulty in deprotonation of the amines. Lastly, aryl bromides were found to be unreactive under the conditions screened; they most likely require longer reaction times and higher reaction temperatures to overcome the heightened barrier for C-X bond cleavage.

3.3. Cs_2CO_3 Drying

The reactions discussed prior to this point using Cs_2CO_3, K_3PO_4 and K_2CO_3 all used solids kept in a 75 °C oven prior to use. Attempts to translate the previous work to AstraZeneca's Macclesfield laboratories, using the compounds available at this lab resulted in a sudden loss of reactivity in systems which were previously found to convert well. This was narrowed down to the storage of the bases being used in the reaction, summarised in Table 3.6.

Table 3.6 – Evaluation of drying procedure for Cs_2CO_3 on the reactivity in an *N*-arylation reaction. Drying refers to 24 hours in a 60 °C vacuum oven. [a]4 Å molecular sieves were added to the reaction.
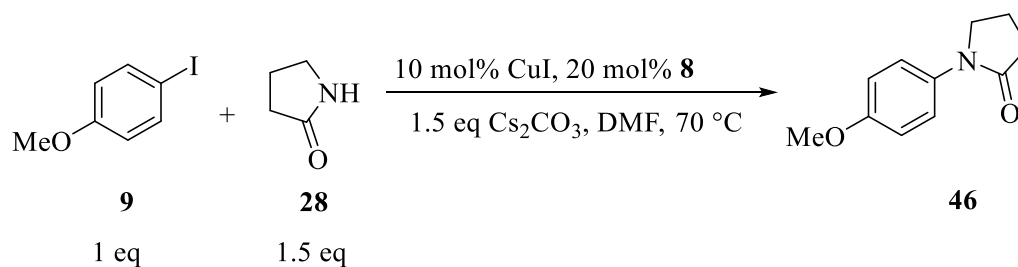
Entry	Supplier	Drying	Time (hours)	Conversion %
1	Sigma-Adrich	No	16	Trace
2	Chemetall	No	17	15
3	Chemetall	Yes	22	93
4[a]	Chemetall	Yes	22	73

3.3.1. Irreproducibility from base storage

By comparing "fresh" Cs_2CO_3 with that which had undergone drying, weight can be added to the anecdotal discussions of unreliability.[20] Whilst it is common procedure for synthetic chemists to store hygroscopic materials in ovens, it is unlikely that all are aware

that failure to handle the base correctly may completely shut-down reactivity. This could be a key cause for the poor reproducibility of the Ullmann-type reactions, particularly on a large scale, where drying the materials in this manner is difficult.

3.4. Kinetic monitoring experiments

The importance of furthering the understanding of the *N*-arylation reaction kinetics and mechanism led to the development of a number of kinetic experiments. Two reaction systems were noted as possible systems for kinetic monitoring, covering both Cs_2CO_3 and K_3PO_4 bases (Table 3.7), with amino acid derivative **8** and *N,N*-diethylsalicylamide (**37**) as ligands. The less efficient bromide substrate was not used to ensure shorter reaction times. The amide **28** has been used in previously reported mechanistic studies and so was chosen to provide some comparison between this work and those in the literature.[32-34]

Table 3.7 – Reaction conditions assessed for kinetic profiling. All reactions prepared in a N_2 filled glovebox before sealing and heating.
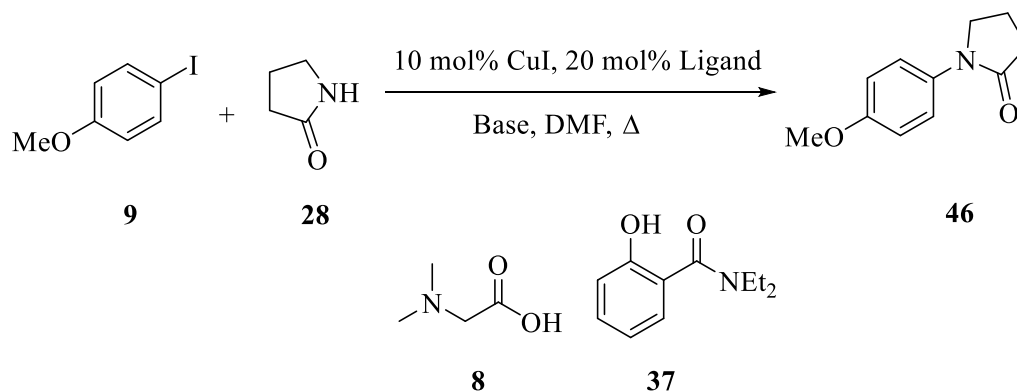
Entry	Base	Ligand	Time (hours)	Temperature ° C	Conversion %
1	Cs_2CO_3	**8**	22	85	93
2	Cs_2CO_3	**8**	3	90	90
3	Cs_2CO_3	**37**	22	70	31
4	K_3PO_4	**37**	20	90	99
5	K_3PO_4	**37**	3	90	35

After finding that the conditions in Entries 1 and 4 gave good conversion after 22 hours, the reaction times were reduced to three hours, as shown in Entries 2 and 5. The Cs_2CO_3 reaction was found to be faster than K_3PO_4 and it was predicted that reaction monitoring over the course of 8 - 10 hours may be necessary to cover the full course of both reaction systems. Exploration of a lower temperature reaction (70 °C) did not yield sufficient reactivity, with conditions in Entry 3 giving only 31 % conversion after 22 hours.

3.4.1. Automation set-up and test reactions

With two suitable conditions for the coupling of **9** and **28** found, kinetic evaluation of the reaction could be used to provide insight into the rate and influence of substrates on the reaction. Using Freeslate automation equipment, contained within a N_2-filled glovebox, 18 samples were programmed over 10 hours for the two reactions shown in Scheme 3.8. To get an accurate t_0 value, the reaction procedure required pre-mixing of CuI, ligand, **28** and the base in DMF at 90 °C in vial 1 for 20 minutes, **9** and the internal standard, biphenyl mixed in DMF at 90 °C in vial 2, before adding vial 2 to vial 1 to initiate the reaction.
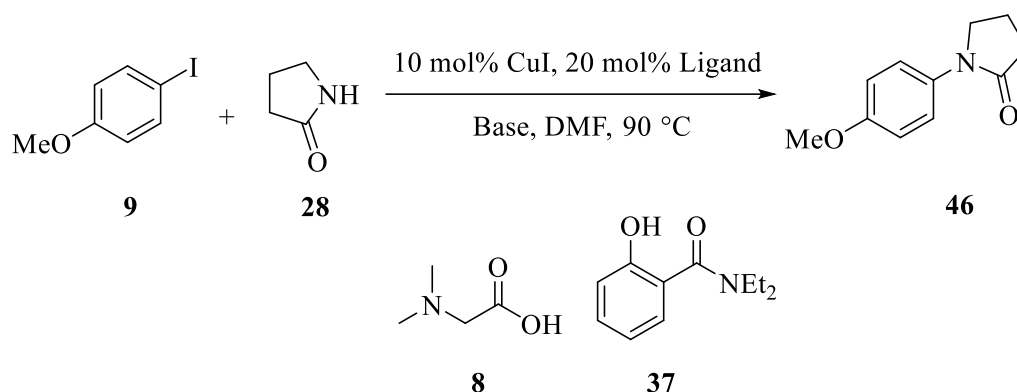
Scheme 3.8 - Reaction systems used for kinetic studies. 1) **8**, Cs_2CO_3. 2) **37**, K_3PO_4.
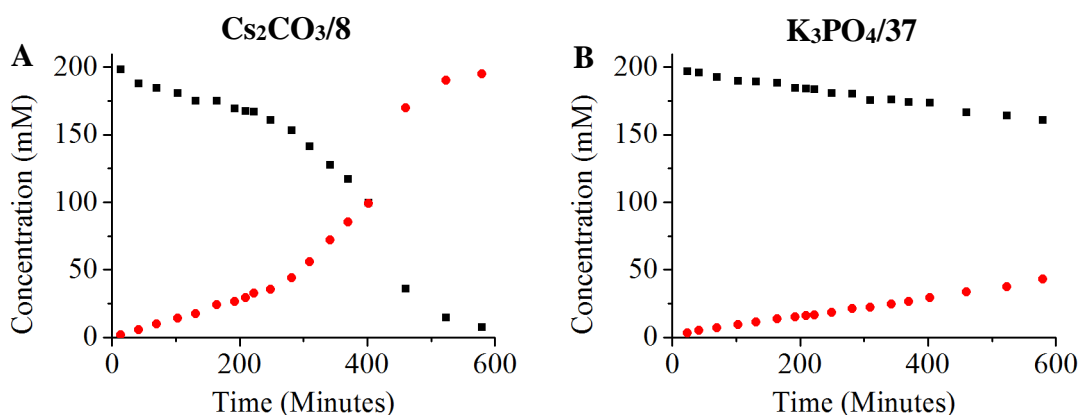
Figure 3.1 – Initial kinetic profiles when using Cs_2CO_3/**8** and K_3PO_4/**37** with of ■ **9** and ● **46**: **A** – [CuI] (20 mM), [**8**] (40 mM), Cs_2CO_3 (0.75 mmol), [**9**] (200 mM), [**28**] (300 mM) and DMF (2.5 mL). **B** – [CuI] (20 mM), [**37**] (40 mM), K_3PO_4 (0.75 mmol), [**9**] (200 mM), [**28**] (300 mM) and DMF (2.5 mL).

Due to the low solubility of both Cs_2CO_3 and K_3PO_4 in DMF, the initial values for these are given as the milimoles weighed out, rather than concentration. The two profiles obtained in these experiments, shown above in Figure 3.1 displayed interesting slow turnover behaviour, which was not apparent in previous results. The Cs_2CO_3 profile (Figure 3.1A) appears to exhibit three distinct phases, slow between 0 – 200 minutes, increased between 200 – 400 minutes, before reaching its fastest rate at ~ 400 minutes. The K_3PO_4 reaction profile on the other hand shows linear conversion over the course of 10 hours.

Previous work by Buchwald on the *N*-arylation of amides discusses the presence of a "time-lapse" during the first 5 – 15 % of conversion.[34] They report that the duration of the time lapse was irreproducible, but the method of drying and storage of the K_3PO_4 base used had a clear effect on the duration. The conclusion from the reported study is that the effect observed is not mechanistically relevant, in terms of the active catalytic cycle and intermediates. Due to these observations, the kinetic study of the two systems outlined was performed using Cs_2CO_3 and K_3PO_4 dried at 60 °C in a vacuum oven for 24 hours, before storage in a N_2-filled glovebox.

3.4.2. Reactions with Cs_2CO_3

The kinetic study was designed to investigate the effects of base, aryl halide, catalyst and ligand by varying the initial concentrations and monitoring the reactions. The induction-type behaviour seen in Figure 3.1A led to the decision to automate sampling to occur more frequently around 400 minutes, in an attempt to record the fastest phase of the

reaction, under the assumption that a similar profile would be obtained under the standard conditions detailed in Scheme 3.9.
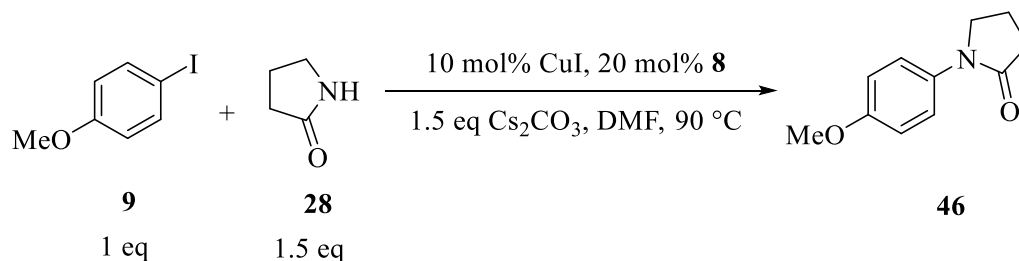

Scheme 3.9 – *N*-arylation system used to gather kinetic data under various conditions

3.4.2.1. Experiment 1

The results of kinetic monitoring under standard conditions, analysed by HPLC, are shown in Figure 3.2. A repeat was performed to assess the reproducibility of the techniques used. The same pre-mixing procedure discussed in Section 3.4.2.1. was used, to ensure full solubility of the CuI prior to t_0.

It is apparent from kinetic profiles obtained under these conditions that the initiation-type behaviour was not present in this experiment, with the reaction proceeding extremely fast over the initial ~ 200 minutes. This was not predicted given that the same procedure, materials and storage of chemicals was used as in Figure 3.1A. A possible explanation for this is that the reactions discussed in this experiment were performed using two magnetic stirring disks, with the intention of this giving more efficient agitation of the heavy Cs_2CO_3 which tends to settle at the bottom of the reaction vial.[35] This was unsuccessful however due to interaction between the two disks providing uneven stirring. Analysis and comparison of the data in this experiment should still be possible however, due to them all being performed in the same manner, in parallel.
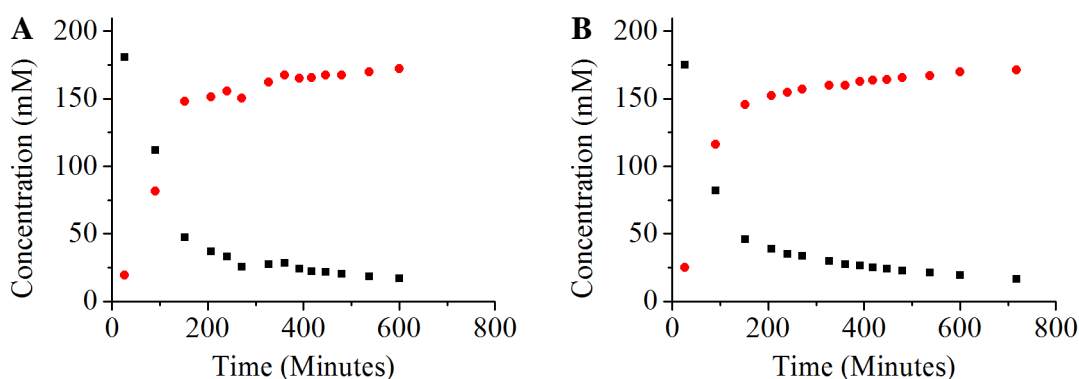
Figure 3.2 – Kinetic profile for the reaction shown in Scheme 3.9 and a repeat of the same conditions. ■ **9** and ● **46**: [CuI] (20 mM), [**8**] (40 mM), Cs₂CO₃ (0.75 mmol), [**9**] (200 mM), [**28**] (300 mM) and DMF (2.5 mL).

By comparing ligand concentration at 20 mol % (Figure 3.2) with 10 mol% and 40 mol% (Figure 3.3A and B respectively), it is seen that this impacts on the first data point significantly. Whilst one data point between 0 and 80 minutes is not sufficient to discuss the initial rate, it is seen that with 40 mol% ligand, the conversion in 30 minutes is more than twice that of 20 mol%. Conversely, halving the ligand loading to 10 mol% reduced the initial conversion in this time to almost half that in Figure 3.2B.

Interestingly however, the initial turnover is not indicative of the rate and conversion after this, as Figure 3.3B actually shows the marginally lower conversion (81 % after 600 minutes) relative to the other three profiles (85 – 86 % after 600 minutes). This effect may be related to the solubility of the active catalyst, although having allowed pre-quilibration time prior to addition of **9** may mean that the behaviour is an effect related to Buchwald's proposed equilibrium, shown in Scheme 3.10.[32] The consequence of this could be that the 4 : 1 ratio of ligand to copper protects the *bis*-coordination of the amide, to prevent the equilibrium from favouring **56c**, but as the reaction proceeds and the amide concentration lowers, coordination and deprotonation of any amide is unfavourable.
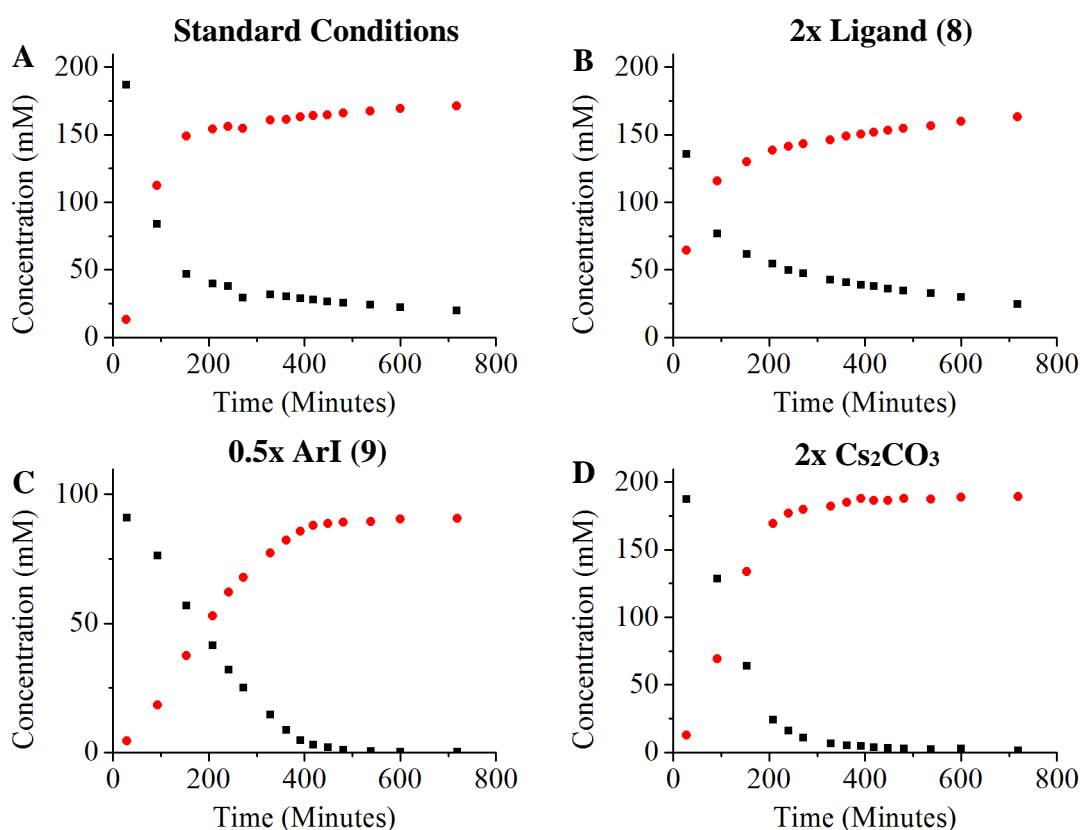
Figure 3.3 – ■ **9** and ● **46: A)** 0.5x [**8**]₀ – [CuI] (20 mM), [**8**] (20 mM), Cs₂CO₃ (0.75 mmol), [**9**] (200 mM), [**28**] (300 mM) and DMF (2.5 mL). **B)** 2x [**8**]₀ – [**8**] (80 mM). **C)** 0.5x [**9**]₀ – [**9**] (100 mM). **D)** 2x Cs₂CO₃ – Cs₂CO₃ (1.5 mmol).
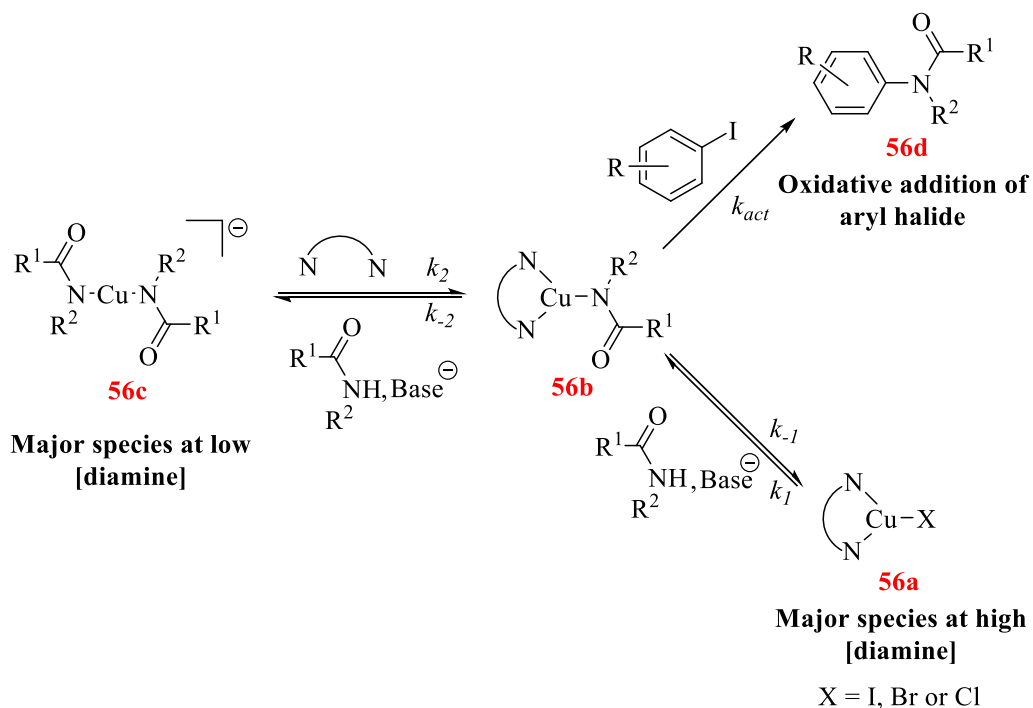
Scheme 3.10 – Equilibrium between Cu, ligand and nucleophile, believed to drive the activation of the aryl halide.

Figure 3.3C shows the effect of performing the reaction at half concentration (0.1 M) of **9** on the kinetic profile, where a much lower rate of reaction is observed. This is displayed as a rate vs time graph in Figure 3.4A and shows that the rate decreases by greater than 50 % versus the reaction performed with 0.2 M **9**, although there is little variation in the rate of the reaction over the first 250 minutes. The drastic drop in reaction rate from $[9]_0 = 0.2$ M to $[9]_0 = 0.1$ M strongly indicates a positive order with regards to $[9]$, whilst other changes to the reaction equilibria may also influence the reaction rate.

The final kinetic profile obtained from this experiment shows the influence of increasing the solid Cs_2CO_3 in the reaction (Figure 3.3D). Here it is actually seen that increasing the base has a marginally positive effect on the reaction performance, resulting in the rate remaining consistent for a longer period and the reaction going to completion (Figure 3.4B). This could be a result of the competitive solubility between active Cs_2CO_3 and inactive $CsHCO_3/CsI$ as the reaction progresses, whereby a higher amount of Cs_2CO_3 available for dissolution at the end of the reaction prolongs the reactivity. It is likely that the increase in rate from the first to the second data point in these rate graphs is an artefact of the mass transfer directly after the adding the substrate to the catalyst mixture.
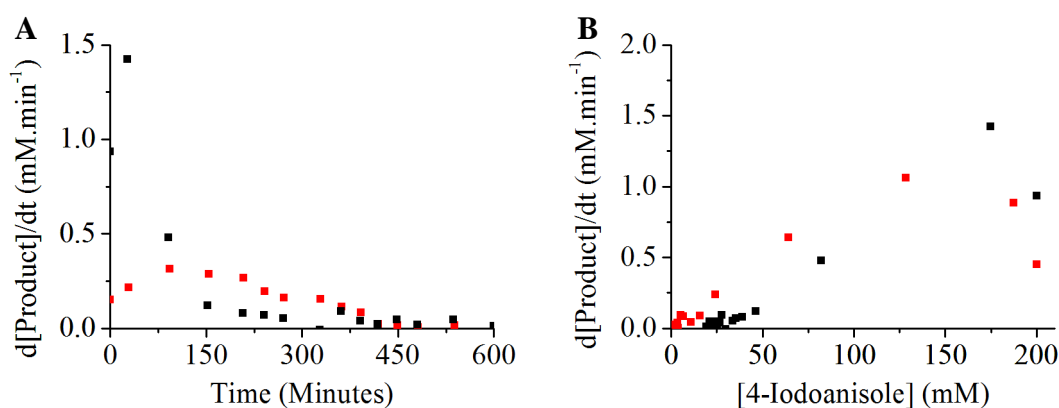
Figure 3.4 – A) Rate of product formation vs time plot. ■ $[9]_0 = 0.2$ M. ■ $[9]_0 = 0.1$ M. **A)** Rate of product formation vs $[9]$. ■ $Cs_2CO_3 = 0.75$ mmol. ■ $Cs_2CO_3 = 1.50$ mmol.

3.4.2.2. Experiment 2

A second set of conditions was run to address the role of the copper catalyst and explore inhibition/deactivation pathways. In this experiment the same sampling method and set-up was used, except that the pre-mixing lasted 30 minutes (20 minutes previously) and the stirring method changed to a single stirrer disk, which gave uniform stirring and a vortex in the solvent. Surprisingly, the kinetic behaviour in these experiments was

different to the previous experiment, despite the identical conditions. The standard conditions, analogous to those displayed in Figure 3.2 are shown below (Figure 3.5), exhibiting induction-type kinetics at the beginning of the reaction, which were seen in Figure 3.1A.

The reproducibility of the two profiles is good, although the induction time of the repeat reaction (Figure 3.5B) does last for approximately 60 minutes longer than that in Figure 3.5A. This difference could be a result of the error associated with manually weighing these materials inside a glovebox, particularly CuI (9.5 mg $\pm$ 0.5 mg) and **8** (10.3 mg $\pm$ 0.5 mg). It would seem unlikely that the drastic change in the nature of the kinetic profiles will occur due to extension of the pre-mixing time, however, this may be possible. Buchwald has previously reported a variable induction time which is affected by pre-mixing of the catalyst, ligand, amine and base in Pd-catalysed amination of aryl bromides,[36] although in this case pre-mixing is necessary to compensate for the slow formation of the active catalyst.
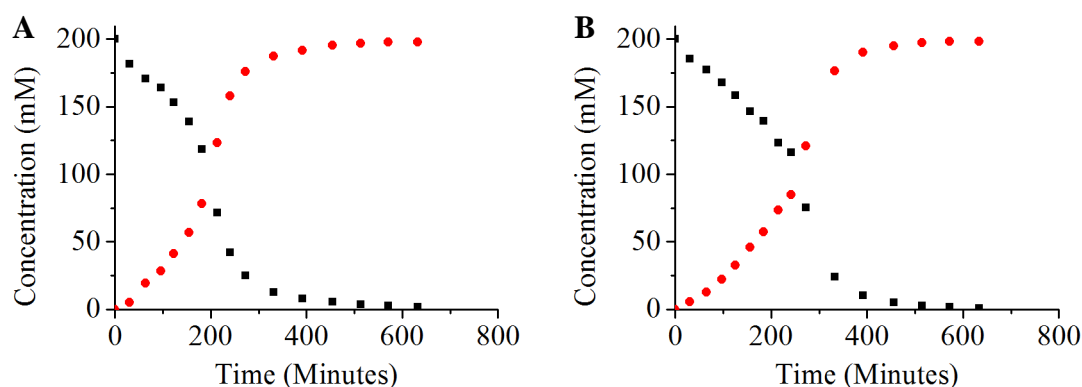
Figure 3.5 – Experiment 2. Standard condition profiles for the reaction in Scheme 3.9 and a repeat of the same conditions. ■ **9** and ● **46**: [CuI] (20 mM), [**8**] (40 mM), Cs_2CO_3 (0.75 mmol), [**9**] (200 mM), [**28**] (300 mM) and DMF (2.5 mL).

The reduced [catalyst] experiments shown in Figure 3.6 demonstrate the sensitivity of this system to catalyst loading, as the reaction times are greatly increased by halving the copper and ligand loading. Figure 3.6A represents the reaction conversion when only the CuI is decreased from 10 mol% to 5 mol%, causing the induction behaviour to last for approximately twice as long. The rate after the induction behaviour ends is also lower than that of the 10 mol% reaction discussed previously (Figure 3.5), which is expected given the presumed dependence of rate on [CuI]. When decreasing both CuI and **8** to 5

mol% and 10 mol% respectively, the increase in induction time is even more pronounced (Figure 3.6B). In this case, the induction time lasts for between 700 and 800 minutes, before a rapid rise in product formation. Unfortunately, further data points were not gathered due to the sampling procedure ending, however, no starting material was detected by HPLC analysis when the reaction was stopped at 18 hours.
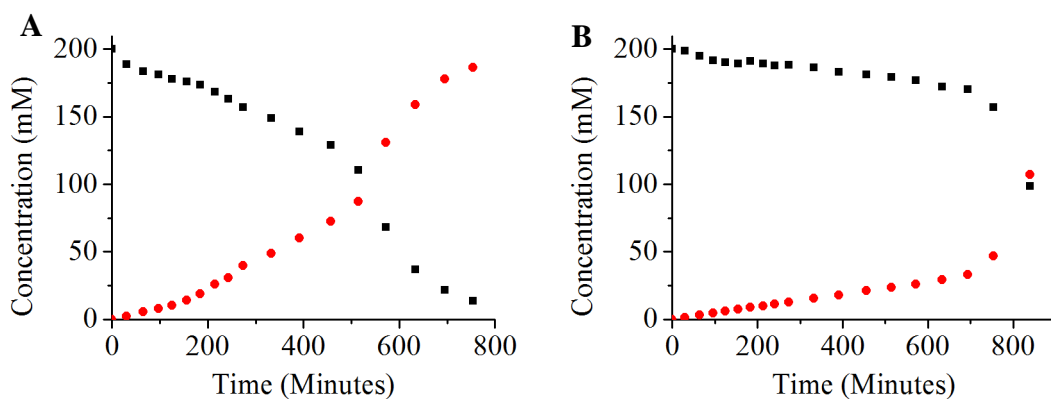
**Figure 3.6** – Reduced catalyst loadings. ■ **9** and ● **46**: **A)** 0.5x $[CuI]_0$ – [CuI] (10 mM), [**8**] (40 mM), Cs_2CO_3 (0.75 mmol), [**9**] (200 mM), [**28**] (300 mM) and DMF (2.5 mL). **B)** 0.5x $CuI/[8]_0$ – [CuI] (10 mM), [**8**] (20 mM).

The effect that lowering the catalyst loading has on this reaction has big implications on the prospective use of this system, as lowering the catalyst loading is a crucial goal. Returning to the work by Buchwald which discusses a mechanistically irrelevant "time-lapse",[34] it is apparent from this experiment that the copper and ligand concentration both have a significant effect on the duration of the induction behaviour. As such, we cannot rule out the mechanistic implications of the observations, though the kinetic profile at increased [**28**] (Figure 3.7A) provides further discussion.

The increased $[28]_0$ resulted in an increased duration of the slow turnover, lasting until 400 minutes, where a transition to fast turnover occurs. Interestingly, there is a clear zero-order dependence of rate on the concentration of [**9**] for the first one-third of the reaction under the increased amide conditions, as seen by the constant rate during this period in Figure 3.7B. Following the sharp rise in reaction rate, which happens at around 125 mM of the aryl halide under both conditions, the 300 mM and 600 mM **28** have very similar behaviour, indicating a shift in the rate-limiting process. This may indicate that the induction behaviour is linked with Buchwalds proposed equilibrium (Scheme 3.10),

whereby the high concentration of [28] shifts the equilibrium to the inactive *bis*-amido cuprate.
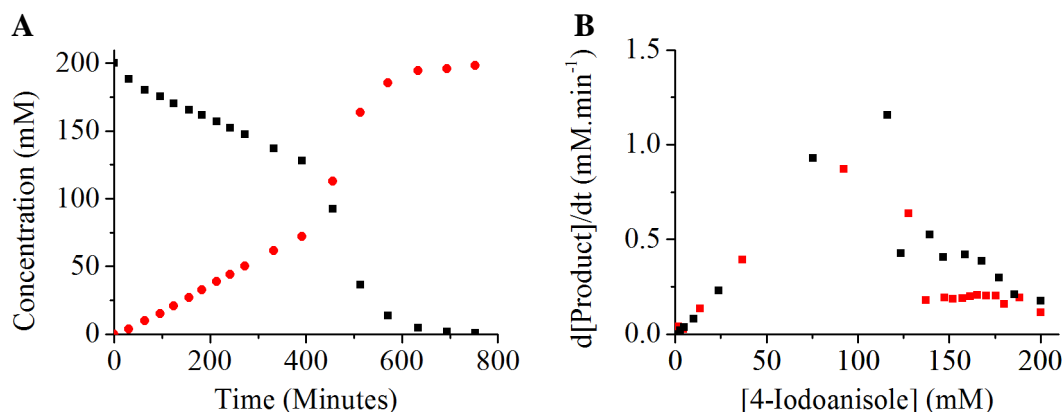
Figure 3.7 – A) ■ **9** and ● **46**: 2x [28]$_0$ - [CuI] (20 mM), [8] (40 mM), Cs$_2$CO$_3$ (0.75 mmol), [9] (200 mM), [28] (600 mM) and DMF (2.5 mL). **B)** ■ [28]$_0$ = 300 mM. ● [28]$_0$ = 600 mM.

Deactivation and inhibition was explored in this system through product inhibition (Figure 3.8A), through the addition of 1 eq H$_2$O to the reaction mixture (Figure 3.8B). Unlike the organic base system discussed in Chapter 2, it is clear that product inhibition is not an issue in this system, which is likely a result of the poor coordination ability of the tertiary amide product. It may be considered surprising that there is very little induction seen in this reaction. Conclusive reasoning for this is not possible from this data alone, though it raises the question of autocatalysis. Hartwig has previously shown that stoichiometric reactions of copper(I)-amido with iodoarenes are autocatalytic due to free CuI formed following reductive elimination.[37] It is difficult to envisage a mechanism in which autocatalysis will be caused by the product being formed, and so without further understanding the reduced induction time is explained by either weighing error or labile coordination of the product to copper.
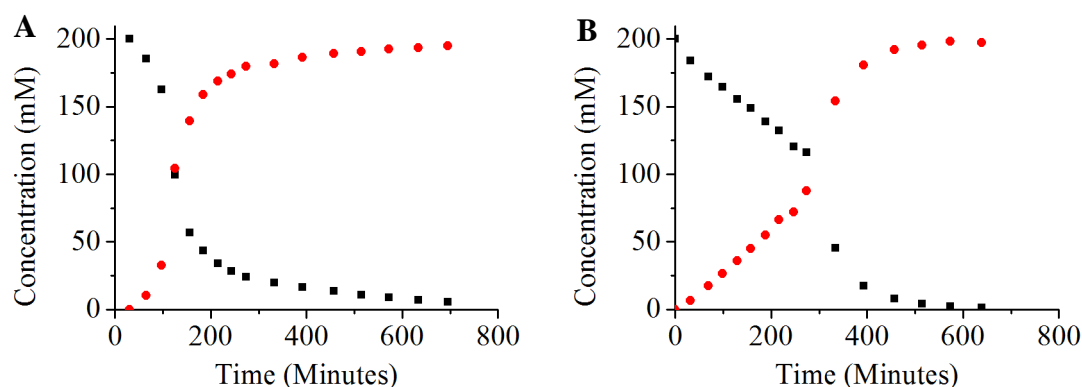
Figure 3.8 - **A)** ■ **9** and ● **46**: Product Inhibition - [CuI] (20 mM), [**8**] (40 mM), Cs$_2$CO$_3$ (0.75 mmol), [**9**] (200 mM), [**28**] (300 mM), [**46**] = 100 mM and DMF (2.5 mL). **B)** ■ [**28**]$_0$ = 300 mM. ● [H$_2$O]$_0$ = 200 mM.

Analysis of the reaction with 1 eq H$_2$O added to the reaction mixture shows little effect on the reaction performance. Figure 3.9 shows a comparison of the H$_2$O inhibition with the standard conditions, showing that there is no significant lengthening of the induction time when overlaid with the standard conditions plot (Figure 3.5B), although both of these are somewhat longer than the other plot for standard conditions (Figure 3.5A). Nevertheless, 1 eq was considered an "extreme" scenario given that the copper is in the reaction at 10 mol%, and so it appears solubilised H$_2$O does not greatly inhibit or slow the reaction.
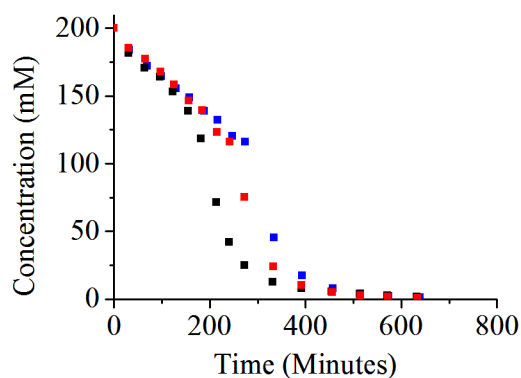
Figure 3.9 – Overlay of [**9**] vs time plots for ■ [CuI] (20 mM), [**8**] (40 mM), Cs$_2$CO$_3$ (0.75 mmol), [**9**] (200 mM), [**28**] (300 mM) and DMF (2.5 mL). ■ Repeat ■ Added H$_2$O (100 mM).

3.4.3. Reactions with K$_3$PO$_4$

It was believed that performing a similar set of reactions to those detailed in 3.4.2.1. with K$_3$PO$_4$ as the base and **37** as the ligand would explore the generality of the results (Scheme 3.11). Buchwald previously reported the use of a similar reaction system with K$_3$PO$_4$/**37** for the coupling of aryl bromides with primary alkylamines,[10] however there is limited understanding of **37** as it is not a commonly used ligand in mechanistic studies.
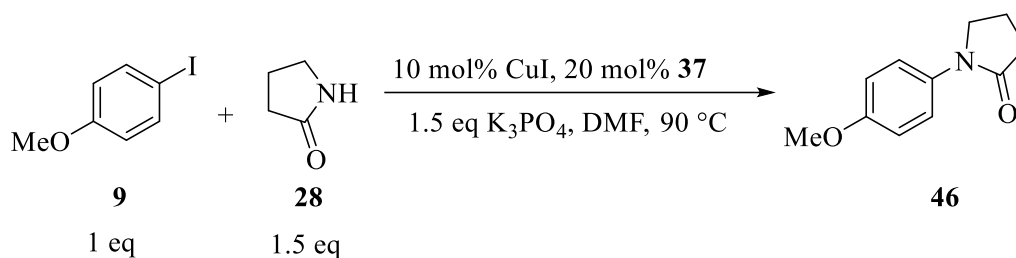
Scheme 3.11 – Reaction used for kinetic profiling; conditions detailed refer to the "standard" conditions.

3.4.3.1. Experiment 1

This experiment was run concurrently with the experiment detailed in Section 3.4.2.1. Resultantly, direct comparison of rates and conversions can only be made against the results discussed in that experiment, although similar trends may be seen which were reported in Section 3.4.2.2. A small amount of ligand-coupling product is seen in the post-reaction mixture, however HPLC peak areas of post-reaction mixtures indicate that this is approximately 5 % relative to **37**, which equates to 1 % of the total substrate and should not affect kinetics significantly.

The repeat conditions in Figure 3.10 indicate good reproducibility in this system, with near identical kinetic profiles given. It is noticeable that there is no induction period under these reaction conditions, contrasting the reaction behaviour seen in the preliminary reaction (Figure 3.1B). Good conversion is observed on the timescale of sampling (~ 80 %), although the same conditions using Cs$_2$CO$_3$ were slightly more efficient (~ 90 %). The reaction shows a slower reaction rate than that of Cs$_2$CO$_3$, this may be linked to the lower expected solubility of the potassium base than cesium, which may benefit from a "cesium effect".[38]
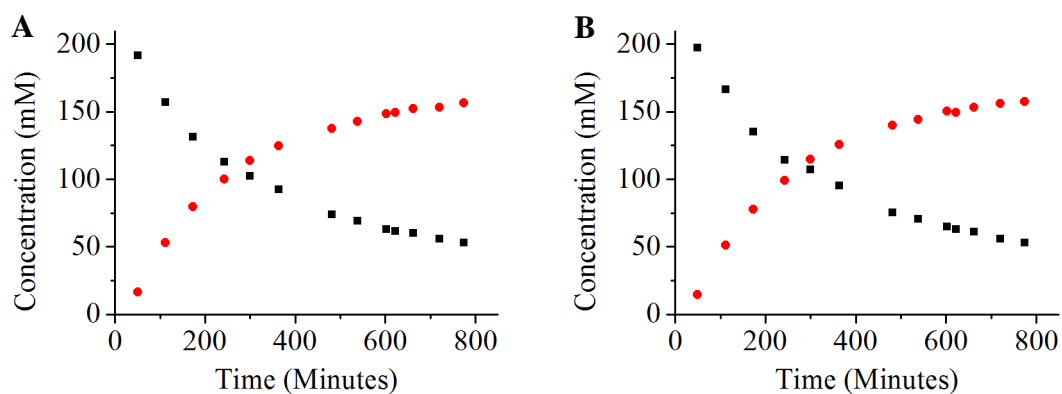
Figure 3.10 - Standard condition profiles for the reaction in Scheme 3.11 and a repeat of the same conditions. ■ **9** and ● **46**: [CuI] (20 mM), [**37**] (40 mM), K₃PO₄ (0.75 mmol), [**9**] (200 mM), [**28**] (300 mM) and DMF (2.5 mL).

A comparison of the reaction rates for the Cs₂CO₃ and K₃PO₄ systems is shown in Figure 3.11, in which the Cs₂CO₃ reaction has approximately 3x faster rate when the reaction has reached steady state.
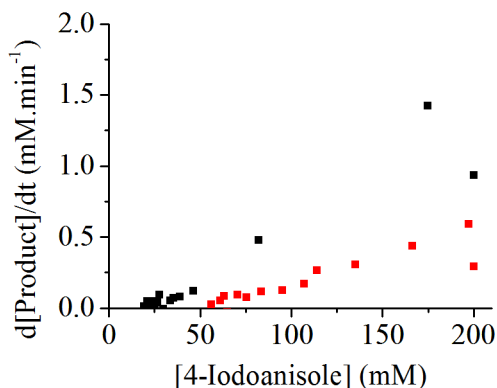
Figure 3.11 - Rate vs [**9**] plot. [CuI] (20 mM), [**8**] (40 mM), Base (0.75 mmol), [**9**] (200 mM), [**28**] (300 mM) and DMF (2.5 mL). ■ Cs₂CO3 ● K₃PO₄.

Figure 3.12 demonstrates the effect of ligand concentration on the reaction. Unsurprisingly, it was seen that increasing the initial ligand concentration increases the initial rate of the reaction, but leads to no increased reactivity overall (Figure 3.12A). This is the same behaviour as was seen with Cs₂CO₃/**8**. Figure 3.12B depicts the kinetic behaviour when halving the initial ligand concentration, which results in a small initiation period, prior to similar reaction rate to Figure 3.12A. This dependence of initial rate on ligand concentration is observed in all of the experiments run with the inorganic bases and highlights the importance of the concentration of ligand in forming the active catalyst.
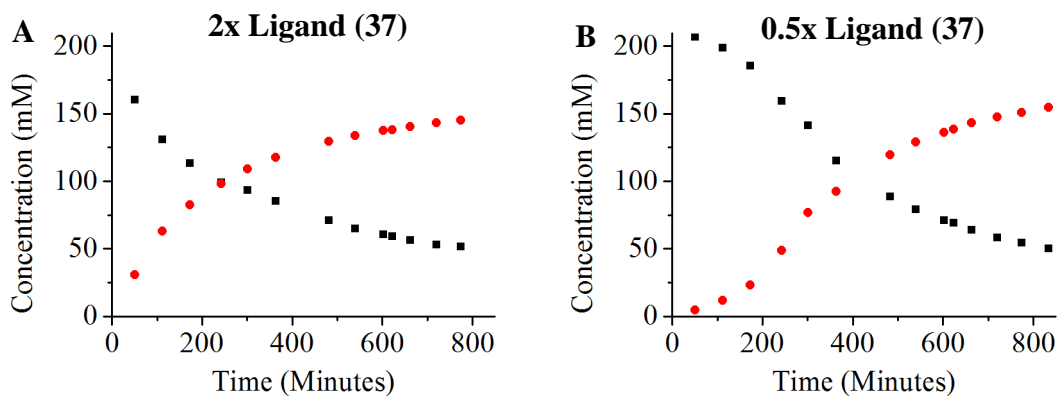
Figure 3.12 - ■ **9** and ● **46**: Conditions adjusted from standard conditions detailed in Figure 3.10. A) 2x $[37]_0$ - (80 mM), B) 0.5x $[37]_0$ - (20 mM).

It was seen with the Cs_2CO_3 system that increasing $[Pyrr]_0$ increased the duration of the induction time of the reaction. Figure 3.13A shows that although turnover is fast at [**28**] = 300 mM, when this is increased to 600 mM, an induction time is seen to last for 300 minutes, before an increase in turnover. A major effect of increasing the initial base loading is seen in Figure 3.13B, in which slow kinetics are observed through the whole timescale of sampling. This behaviour contrasts that seen in the Cs_2CO_3 system (Figure 3.3D), in which the increased base loading led to a faster initial rate and full conversion to product. The same, prolonged induction time is also seen when the CuI/**37** concentration is reduced by half (Figure 3.13C), resulting in a very slow reaction (< 20 % conversion after 13 hours).
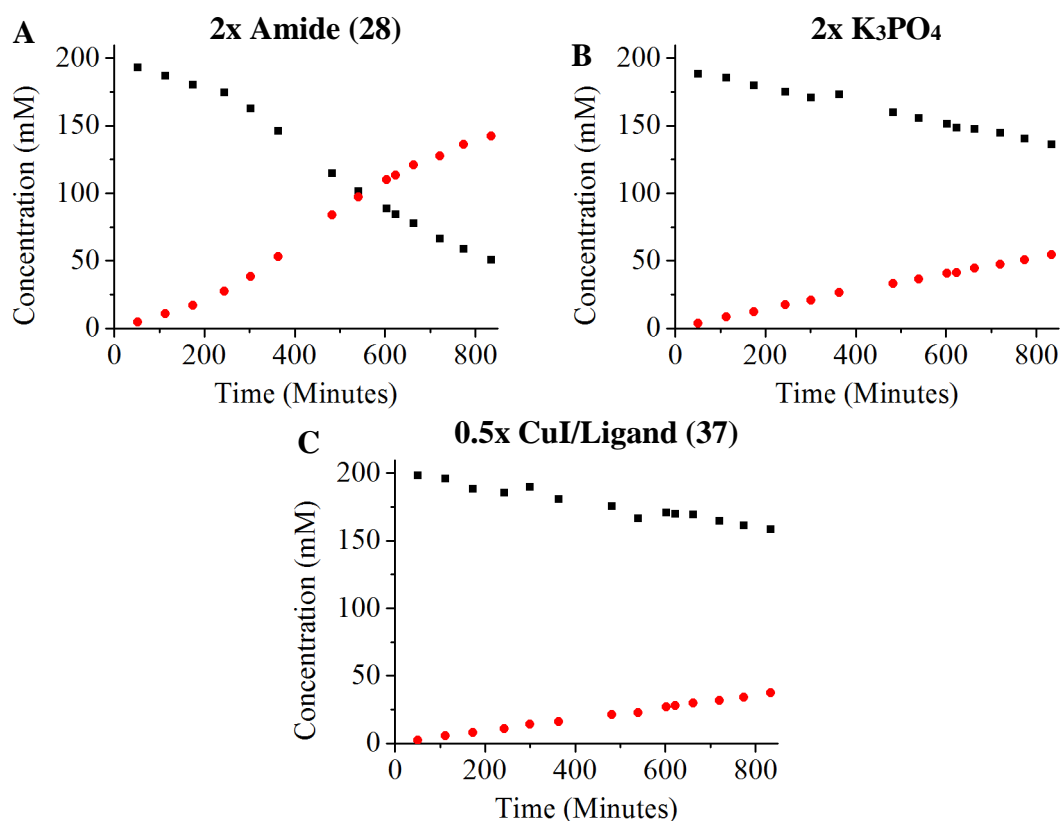
Figure 3.13 - ■ **9** and ● **46**: Conditions derived from those detailed in Figure 3.10. A) 2x [**28**] - (600 mM), B) 2x K₃PO₄ - (1.50 mmoles), C) 0.5x [CuI]₀ – (10 mM) and [**37**]₀ – (20 mM).

Overall, the behaviour of this reaction system, utilising K_3PO_4 and **37**, shows many similarities with the Cs_2CO_3/**8** system which was previously analysed. It was found that both reaction systems show induction periods under certain conditions. The role of the ligand is strongly linked to the initial turnover of the catalyst, despite not playing a part in the overall rate of the reaction. To compare the conversions at the end of sampling, the Cs_2CO_3 system does appear to be more efficient than K_3PO_4, which may be linked to the small amount of ligand which is lost through ligand coupling when using **37**, however this is unlikely as increasing the concentration of [**37**] does not improve conversions.

3.5. Nature of the Induction Behaviour

Induction periods in homogeneous catalytic systems are often a result of slow formation of the active catalyst.[36] This may be due to a high energy barrier associated with the activation of the catalyst, or limitation of one of the components needed for turnover of the catalytic cycle. Induction periods are noted in various homogeneous organometallic reactions, such as Grignard reactions, which require time to wear away the oxide layer of the magnesium turnings.[39] Various reports on palladium-catalysed amination

reactions discuss induction periods, due to the slow dissociation of ligands from Pd(0) complexes.[36, 40] It is believed in the palladium system reported that two catalyst cycles are involved, turning over at different rates, with multiple "entry points" from the pre-catalyst (Scheme 3.12).
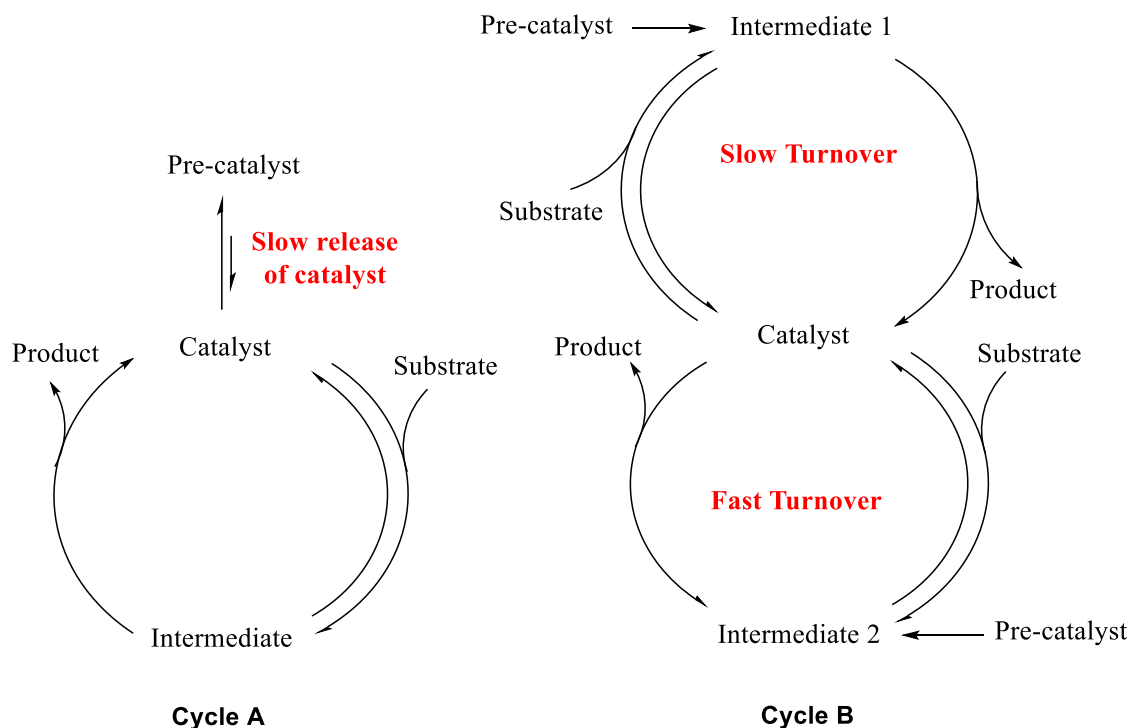
Scheme 3.12 – Schematic catalyst cycles depicting two systems which may exhibit induction periods. Cycle A – Slow release of the pre-catalyst into the catalytic cycle, *e.g.* Grignard reaction. Cycle B – Multiple catalytic pathways require time for system to reach steady-state.

Buchwald's assertion that the "time-lapse" seen in his similar reaction system is a relic of surface-adsorbed H_2O, and thus mechanistically irrelevant, is difficult to disprove. This work does however show that, whilst difficult to control, the slow kinetic behaviour is influenced by ligand, copper, amide and base concentration. Given this, it is likely that it is mechanistically relevant in this particular system, whether it be a result of off-cycle processes or reaction equilibria.

To consider the idea that the specifications and storage of the Cs_2CO_3 and K_3PO_4 used in the reactions influences the kinetic behaviour, the method of storage used prior to performing the experiments in this research must be evaluated. Cs_2CO_3 is well known to be hygroscopic and as such, many laboratories partake in the practice of storing it in high-temperature ovens (> 100 °C) to prevent adsorption of water and the clumping of

particles which occurs as a result. The need to perform some method of drying was observed in the preparation of experiments for the kinetic monitoring, in which Cs_2CO_3 directly from the bottle did not work well in the reaction. Alternatively, Chang reported in 2007 that the coupling of iodobenzene with pyrrole was inhibited when the K_2CO_3 used was dried excessively.[17] In both the Cs_2CO_3 experiments discussed in 3.4.2. the base was kept in a 60 °C vacuum oven for 24 hours, then stored in a sealed vial within a N_2-filled glovebox until used. The same batch of milled Cs_2CO_3 from Chemetall was used for all of the experiments, yet the induction time was only observed in the second experiment.

If Cs_2CO_3 is to adsorb water, it is possible that a reaction could result in the presence of $CsHCO_3$/$CsOH$, which are too weak and too strong respectively to act as adequate bases in the reaction, respectively. This may be a surface reaction, which would result in an outside "shell" of unreactive species, and limited availability of Cs_2CO_3 at the centre of the particle and thus, slow deprotonation of the amide. This theory would go some way to explain the slow reactivity but not the dependence of the length of induction on the loading of the copper.

The theory which fits the experimental data best relates back to Buchwald's equilibrium (Scheme 3.10). The formation of the catalytically inactive **59** may be favoured at high concentrations of base, limiting the active copper species which can undergo oxidative addition and subsequent reductive elimination to product.[33] If this equilibrium is driving the rate of turnover, it would be expected that the solubility of base in the reaction solvent will shift the position of equilibrium. The idea of base solubility may provide insight into the variation in induction kinetics between the experiments in Sections 3.4.2.1. and 3.4.2.2. as the more efficient stirring in the second experiment could result in greater solubility of Cs_2CO_3.
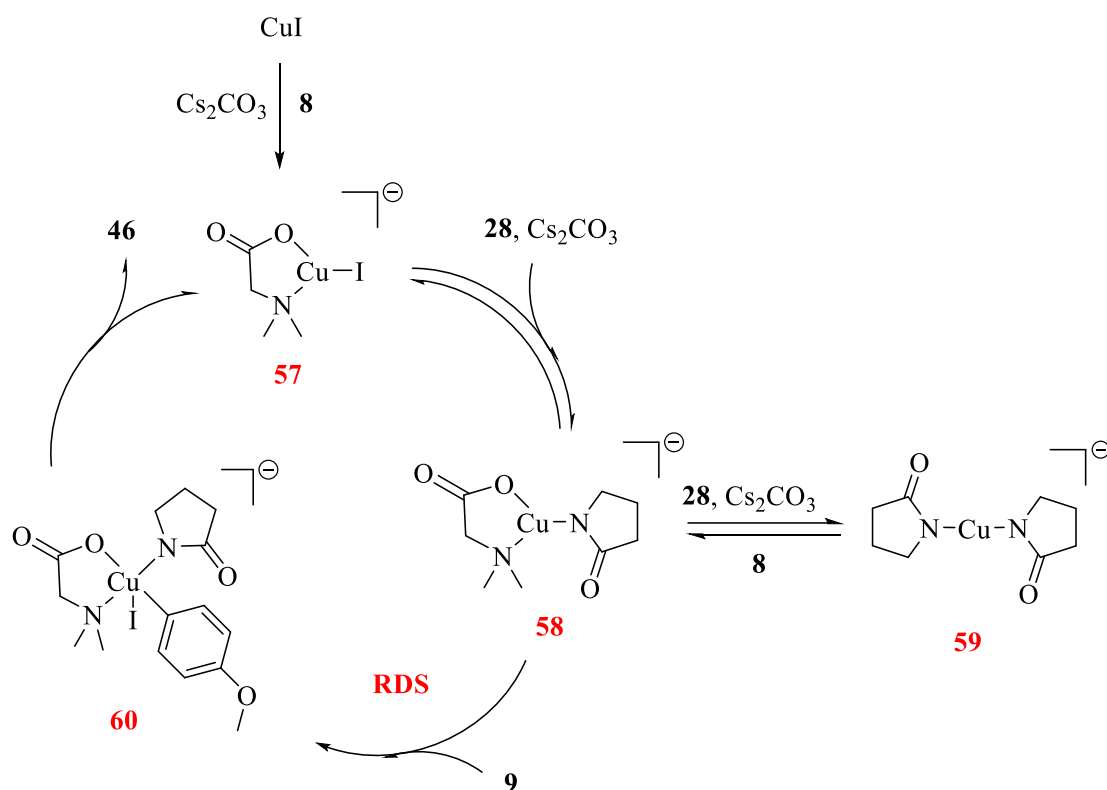
Scheme 3.13 - Expected mechanism for *N*-arlyation reaction between **28** and **9,** using **8** as a ligand and Cs₂CO₃ as a base.

Using the mechanism depicted in Scheme 3.13, it is possible to rationalise the kinetics obtained when using Cs_2CO_3. The dependence of initial turnover on [**8**], but not the overall rate, implies that coordination of the ligand is the entry point to the catalytic cycle, with no dissociation of the ligand in the main cycle. It would be expected from the mechanism that an increase in [**28**] would drive the equilibrium towards the inactive species, causing the increased induction time that was observed. Zero-order behaviour with respect to [**9**] was observed at high [**28**], indicating that the oxidative addition is not the rate limiting step under these conditions. The same zero-order dependence is seen when analysing the reaction at 0.5 x [CuI/**8**]₀, (Figure 3.14) which has the same relative ratio of [CuI]₀ : [**28**].

Analysis of the data in Figure 3.14 appears to give the conclusion that the length of induction time is related to the relative concentrations of [**28**] and [**8**] but not the copper loading in the reaction. The rate of the turnover during the induction period is still influenced by the copper loading in the reaction however, giving a lower rate of reaction in this phase of the reaction. One area of interest is that the induction period is present

until ~ 25 – 30 % of the [**9**] has converted in both the 2 x [**28**]$_0$ and 0.5 x [CuI]$_0$ reactions, which may be linked with the stoichiometry of CuI : **28**, which in both cases works out to be 1 : 30. The reduced ligand concentration in the 0.5 x [CuI/**8**] reaction could then be the reason for the differences between the three sets of data.
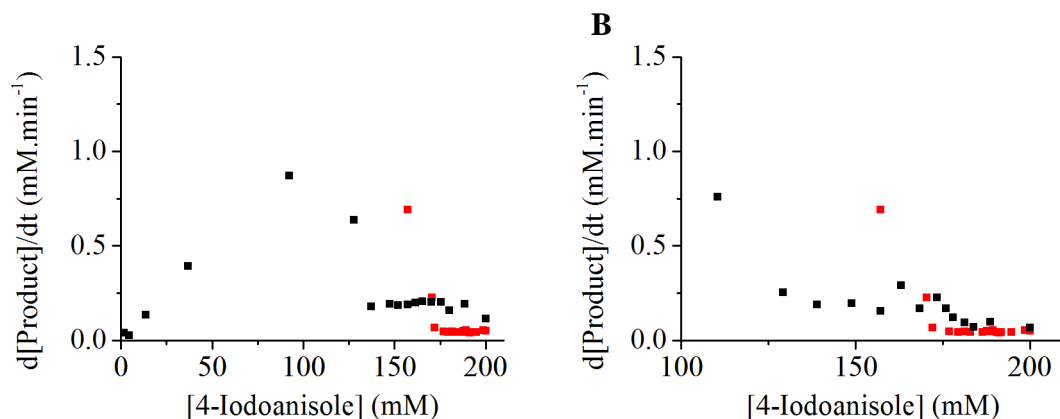
Figure 3.14 – Rate vs [**9**] plots for: A) ■ [**28**]$_0$ = 600 mM, [CuI]$_0$ = 20 mM, [**8**]$_0$ = 40 mM ● [**28**]$_0$ = 300 mM, [CuI]$_0$ = 10 mM, [**8**]$_0$ = 20 mM. B) ■ [CuI]$_0$ = 10 mM, [**8**]$_0$ = 40 mM ● [CuI]$_0$ = 10 mM, [**8**]$_0$ = 20 mM.

Ultimately, it is difficult to come to a definitive conclusion based on these profiles alone, however it does appear that the deprotonation of [**28**] is involved, as is the ligand in the reaction, which due to its pKa value (~ 3) is deprotonated in solution and is able to bind to the copper catalyst prior to the substrate. This draws attention to the need to understand the base solubility in the reaction as at high concentrations of carbonate/phosphate, the kinetics of the reaction can change drastically.

3.5.1. Order of Addition

To understand the initial rate of reaction better an experiment was performed looking at the effect of the order of addition and equilibration allowed in the system. This was prepared under standard reaction conditions with Cs_2CO_3, as detailed in Section 3.4.2. along with a reaction with increased [**28**]$_0$, which was expected to give a greater amount of induction based on previous results.

Table 3.8 – Conditions used in 'Order of Addition' experiment. Standard conditions refers to [CuI] (20 mM), [**8**] (40 mM), Cs_2CO_3 (0.75 mmol), [**9**] (200 mM), [**28**] (300 mM), biphenyl (internal standard, 20 mM) and DMF (2.5 mL).

Entry	Description	Vial 1 (1.7 mL DMF)	Vial 2 (0.8 mL DMF)
1	Standard conditions/ **9** added last	CuI, **8**, **28**, Cs_2CO_3	**9**, biphenyl
2	2x [**28**]$_0$/ **9** added last	CuI, **8**, **28**, Cs_2CO_3	**9**, biphenyl
3	Standard conditions/ **28** added last	CuI, **8**, **9**, Cs_2CO_3	**28**, biphenyl
4	2x [**28**]$_0$/ **28** added last	CuI, **8**, **9**, Cs_2CO_3	**28**, biphenyl

The experiment was monitored following 30 minutes pre-mixing at 90 °C in the necessary vial, with three samples at 30, 60 and 90 minutes. Previously, it was seen that by increasing the concentration of **28**, the rate of turnover was slowed, due to the induction-type kinetics. An interesting question was posed as to whether the pre-mixing allowed the formation of an active species, or drove the reaction to an inactive resting state.

The results shown in Figure 3.15 indicate that the rate of turnover during induction can be affected substantially by the order of addition used. The conversions seen when adding **9** last matches those seen in Section 3.4.2.2. within 2 % at each data point, showing some reproducibility here. The other reactions in the experiment all have a similar gradient over this time period, though Entry 2 (●) may be marginally faster. Comparison of Entries 1 (■) and 3 (▲) indicate that allowing pre-mixing with the amide substrate has an effect on the initial rate of the reaction. The presence of relatively slow, induction kinetics in all four reactions does however indicate that the induction period found is not an artefact of the pre-mixing of the reaction.
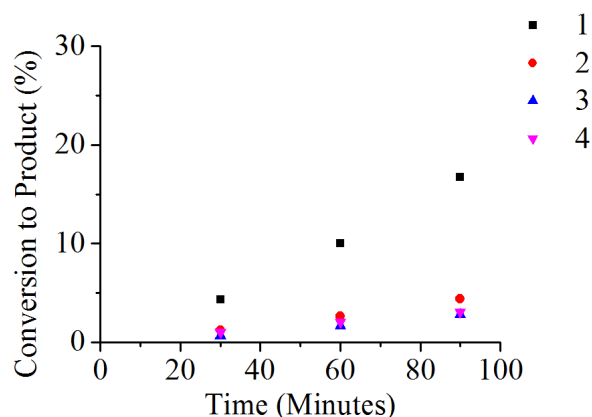
Figure 3.15 – Conversion data for Entries 1 - 4 described in Table 3.8. Legend numbers relate to the Entry number.

3.5.2. Effect of particle size on rate kinetics

All of the kinetic experiments that were discussed in Section 3.4.2. were performed with the same source of Cs_2CO_3, obtained from Chemetall. The use of Sigma Aldrich Cs_2CO_3 initially gave poor results (Table 3.6), however this may have been a consequence of using it without further drying. Given that the kinetic monitoring experiments show an important role of the dissolution of Cs_2CO_3 on the kinetic profiles, an experiment exploring how particle size affects the kinetics was performed.

The three sources of Cs_2CO_3 were obtained from Sigma Alrich, Acros Organics and Chemetall, where the Chemetall Cs_2CO_3 was milled to a particle size of $D_{50} = 20$ µm, $D_{90} = 50$ µm, meaning 50 % of the particles are under 20 µm and 90 % under 50 µm. To get some form of characterisation on the particle size, scanning electron microscopy (SEM) was used. Whilst this does not provide quantitative analysis of particle size, it offers insight into the homogeneity of size in each sample, morphology and relative size comparisons between the three suppliers. The SEM images at a low zoom and a higher zoom are shown in Figure 3.16 and Figure 3.17 respectively.
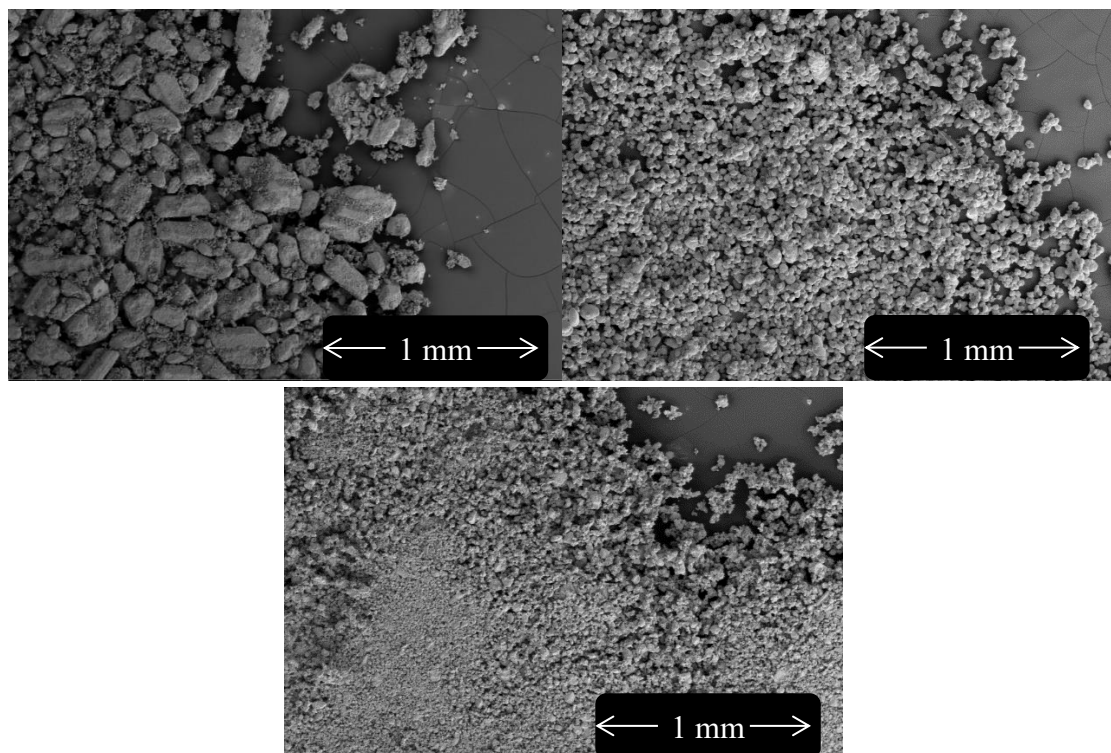
Figure 3.16 – SEM images of the three source of Cs_2CO_3 used in particle size experiments at low zoom. **Top left** – Sigma Aldrich. **Top right** – Acros Organics. **Bottom** – Chemetall.
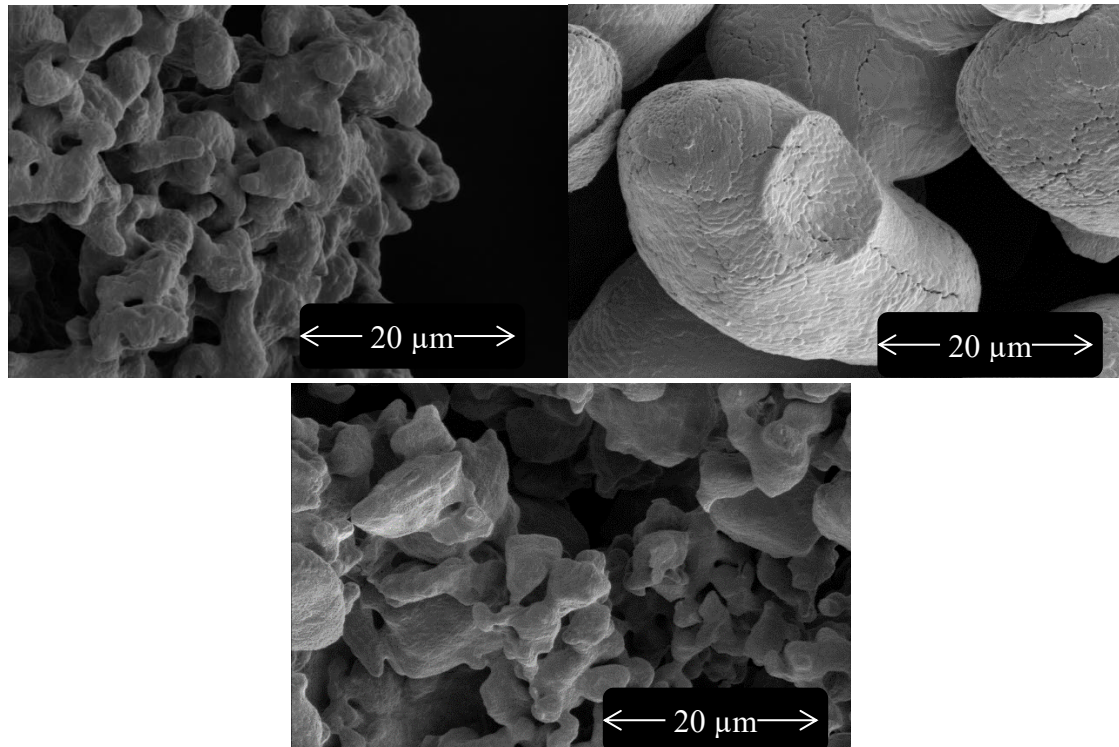
Figure 3.17 - SEM images of the three source of Cs_2CO_3 used in particle size experiments at high zoom. **Top left** – Sigma Aldrich. **Top right** – Acros Organics. **Bottom** – Chemetall.

The SEM images indicate that the three different sources of Cs_2CO_3 all have noticeably different particle sizes and morphology. Figure 3.16 shows that the Sigma Aldrich Cs_2CO_3 has poor regularity to the particle sizes, with some being 200 – 300 µm, and some being very small. The Acros Cs_2CO_3 was found to have very good regularity to the particle size, whilst the Chemetall shows some variation, but the overall particle size does appear to be small. Further magnification, shown in Figure 3.17 confirms these observations, where particularly the Acros Cs_2CO_3 was seen to have very well defined, uniform pebble shapes of ~ 50 µm. The Sigma Aldrich particles were found to have a very different, porous structure and the Chemetall particles were in general much smaller, however some of the small particles had coalesced, possibly as a result of exposure to air.

It is expected that the different particle sizes and morphologies of the Cs_2CO_3 sources would result in different rates of solubility in the reaction solvent. As such, the performance of each source of Cs_2CO_3 was assessed by kinetic monitoring, as shown in Figure 3.18). The kinetic behaviour over the first 250 minutes for these 3 samples of Cs_2CO_3 are all notably different, where the Acros and Sigma sourced bases give much higher conversion over this time period. As was seen in 3.4.2.2. the milled base can give slow kinetics at the beginning of the reaction. These results have important implications on the considerations needed for chemists when performing copper-catalysed *N*-arylation reactions, as well as many other transition metal-catalysed reactions, as improved solubility may not always be desirable.
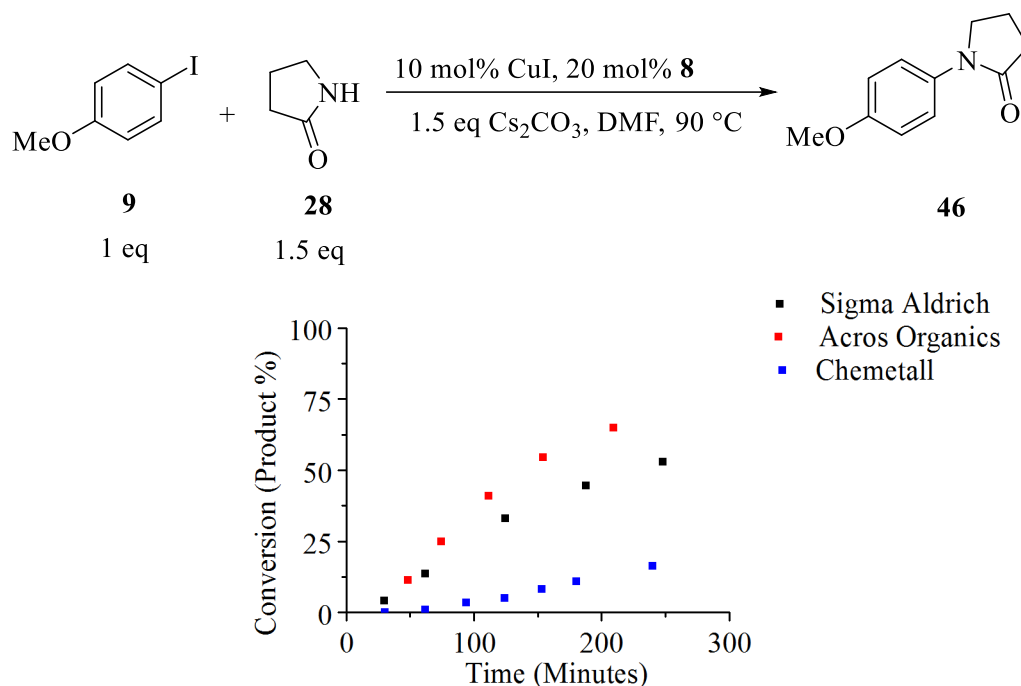
Figure 3.18 – Kinetic competence of the three sources of Cs_2CO_3 with various particle sizes in the copper-catalysed C-N cross-coupling reaction.

3.5.3. Investigation into Amide Deprotonation

Given that deprotonation of the *N*-nucleophile appears to have an important role to play in rate-determining equilibria, the effects of removing the deprotonation step was explored. The Na-salt of 2-pyrrolidinone (**28**) was prepared by reacting this with sodium hydride, chosen to avoid further purification of the product (Scheme 3.14).
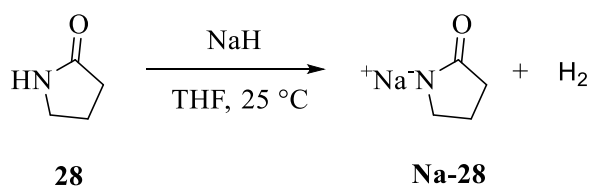
Scheme 3.14 - Deprotonation of **28** with NaH to give the Na-salt **Na-28.**

After allowing the reaction to proceed until the evolution of H_2 gas ceased, the solvent was evaporated, yielding a free-flowing white powder. Characterisation of the resulting salt proved difficult, as IR analysis was inconclusive. Previous studies using phenoxide salts performed by Hartwig use the white powders without further characterisation,[41] and Buchwald determines conversion to copper-pyrrolidinoate through the loss of 2-pyrrolidinone.[34]
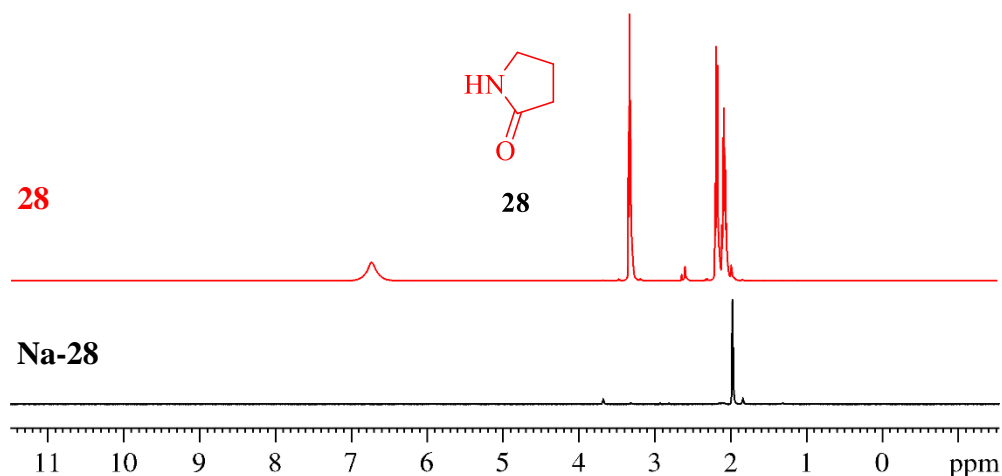
Figure 3.19 – ^1H NMR spectrum (500 MHz, d_3-MeCN) showing full conversion of 2-pyrrolidinone following deprotonation with NaH.

The ^1H NMR analysis shown in Figure 3.19 was used to confirm that there was no **28** remaining with the white solid of the salt, which itself is insoluble in MeCN. Other than the residual solvent peak (d_3-MeCN – 1.94 ppm), two small peaks in the **Na-28** spectrum are present due to a small amount of THF (1.80 and 3.64 ppm), otherwise no soluble impurities were found. Based on the analysis, it was decided that the salt was likely sufficiently pure to use in further reactions (Scheme 3.15).
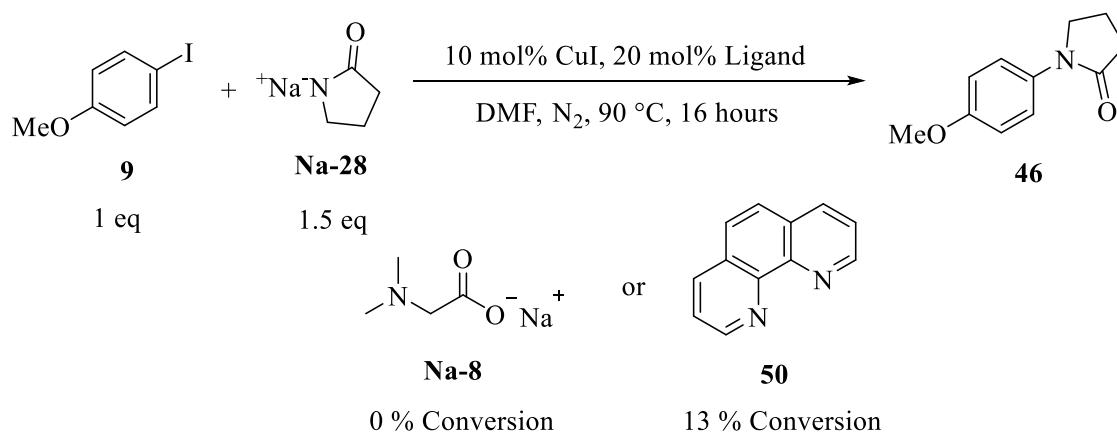
Scheme 3.15 - One-pot "base-free" *N*-arylation reaction between **9** and **Na-28**.

The sodium salt of **8** was also prepared using the same method as **Na-28** for use in this reaction, as well as the neutral ligand 1,10-phenanthroline (**50**) being used. Performing these reactions using a one-pot procedure under an N_2 atmosphere gave no conversion when the ligand was **Na-8** and just 13 % conversion when using **50**. These can be compared with the conversions obtained when using **28** and Cs_2CO_3, with **8** (full

conversion) and **50** (85 %). The limited turnover of the catalyst is thought to be a result of the strong coordination of the amidate to copper, which is favoured over ligand coordination due to the excess of amidate relative to ligand.

The reactions add weight to the idea that it is necessary to control the rate of deprotonation to prevent the formation of a *bis*-amidate species. It was notable during the reaction using **50**, that the typical deep red colour was replaced with a colourless/pale yellow solution. The colourless solution remained for at least 8 hours of the reaction, then after 16 hours, the colour had changed to dark red. A deep red colour is usually seen in reactions with **50** as a result of $[Cu^{I}(50)]_2$ or similar species,[42] whilst a colourless solution may be expected based on the solid state colour of various Cu(I)-amido complexes.[41, 43] The displacement of a Cu-pyrrolidinoate species for a ligand-bound complex was explored through a 'portioned addition' experiment (Figure 3.20).

This experiment displayed intriguing equilibrium behaviour, as depicted in Figure 3.20. Addition of 0.5 eq of **Na-28** was performed over the course of 5 minutes, as indicated by the thick blue lines, causing the deep-red solution to subside to a colourless solution. The sample a was taken following addition of this first 0.5 eq and provided a start-point for the reaction. By the time of sample b (20 minutes after addition), the colour change reverted back to deep-red and a plateau in conversion between samples b and c. This is visualised by the diluted samples at each of these time points (oxidation of samples a, c and e give a pale green colour), and across the course of the reaction, this equilibrium shifts depending on the addition of **Na-28**. The final data point, f, following the third 0.5 eq addition of **Na-28** showed little turnover and a much less drastic change in colour, as the equilibrium favours a Cu(I)-pyrrolidinoate species at high [**Na-28**].
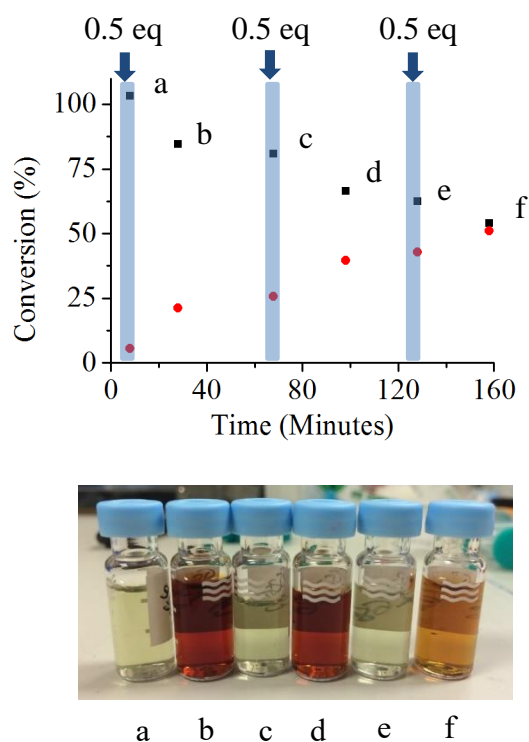
Figure 3.20 – Portioned addition of **Na-28** by a two-pot reaction. ■ **9** and ● **46**: Flask 1 – **9** (1.0 mmol), CuI (0.1 mmol), **50** (0.2 mmol) and biphenyl (0.1 mmol) in 3.5 mL DMF. Flask 2 – **Na-28** (1.5 mmol) in 1.5 mL DMF.

This experiment indicates that competitive binding of ligand and substrate can "turn on" and "turn off" catalyst turnover, depending on concentration. Although conversion did not reach 100 %, the ~ 50 % conversion seen after 160 minutes is significantly higher than 13 % after 16 hours. The plateau in conversion that is observed following the shift in colour indicates that $[Cu^I(50)]_2$ (**61**) may be the catalyst resting state and an excess of substrate is necessary for turnover. The equilibrium which is present under these conditions is summarised in Scheme 3.16, agreeing well with the work by Buchwald.[32]
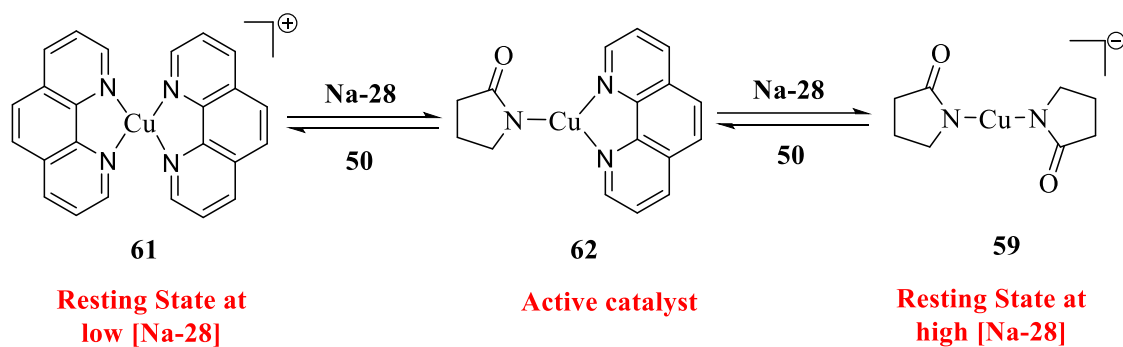
Scheme 3.16 - Summary of equilibrium observed in portioned addition experiment

Work was performed to explore this potential equilibrium through the use of UV-vis. Due to the significant colour change and well defined nature of the **61**, monitoring this reaction by UV-*vis* may assist in finding a "sweet spot" of deprotonated amide/ligand concentrations. Unfortunately, under the conditions used for this experiment, concentrations were too high and spectra were poor. Further development of this method by addition of a sample loop and dilution could however prove useful in understanding the behaviour discussed here.

3.6. Summary and Conclusions

The use of different inorganic bases in Ullmann-Goldberg amination reactions has been found to promote varied reactivity, selectivity and kinetics. In reactions between iodoarenes and cyclic amides, salts of cesium and potassium can lead to fast turnover, but are less efficient when the nucleophile is a secondary amine. Although the reactions are generally clean, with few side products, the use of strong bases such as KO^tBu have been found to promote the formation of regioisomers through reduction of the aryl halide to a benzyne. This reaction is most prominent with reactions of aryl bromides, explaining why some examples of KO^tBu have been reported when using aryl iodides. Soluble acetate bases such as KOAc promote the formylation of secondary amines *via* a transamination reaction when the solvent used is DMF. Use of these acetate salts with DMF should therefore be avoided, as the competitive reaction is faster than the *N*-arylation reaction.

Mechanistic study through kinetic experiments of reactions using Cs_2CO_3 and K_3PO_4 show complicated behaviour, with induction-type behaviour which could last up to 50 % conversion of the aryl halide. Despite this, the kinetic experiments were able to indicate that the reaction systems studied follow a Cu(I)/Cu(III) kinetic cycle, when using two different anionic ligands commonly employed in Ullmann-Goldberg reactions. Coordination of the ligand to CuI is expected to be the entry point into the catalytic cycle. Order of addition experiments were used to demonstrate that the reaction mechanism is likely to involve coordination and deprotonation of the *N*-nucleophile prior to the oxidative addition of aryl iodide.

If it is considered that an induction period should be caused by the slow formation of catalytically active species, it is incorrect to describe the slow-kinetic behaviour seen at the beginning of many reactions as an induction period. Instead, the kinetic dependence of this slow turnover on $[Amide]_0$, $[Ligand]_0$ and $[CuI]_0$ found from this work shows the "time-lapse" is likely caused by an off-cycle equilibrium. The solubilised [Base] is expected to be a driving force of this equilibrium, promoting coordination and deprotonation of further nucleophile species. The ligand used in the reaction is likely to play a big part in this equilibrium, and the portioned addition of an anionic amide salt with the neutral 1,10-phenanthroline ligand has been used to demonstrate that dissociation of ligands may cause the loss of activity. Product inhibition is not an issue

when using cyclic amides and the catalyst is shown to be stable for long periods, still able to give fast conversion to product when turnover accelerates after 14 hours of slow kinetics when using 5 mol% catalyst.

The results discussed in this work are also important from a process chemistry perspective, and provide a number of answers as to why the copper-based systems are seen as unreliable. Reactivity could be shut-off by air-sensitivity, side reactions, incorrectly stored bases and low copper loadings. The reaction can also show drastically different behaviour with different sources of base, where particle size or morphology may have large effects on dissolution rates. These considerations can cause drastic changes in reaction kinetics and represent a fine balance between fast, efficient reactions, and insufficient turnover. As a result, solvent, base, aryl halide (I, Br or Cl), *N*-nucleophile and ligand are all interlinked, and an understanding of what effects altering one of these will have is vital when changing reaction systems.

3.7. References

1.   I.P. Beletskaya and A.V. Cheprakov, *Organometallics*, 2012, **31**, 7753-7808.

2.   Y. Sunesson, E. Lime, S.O.N. Lill, R.E. Meadows and P.O. Norrby, *J. Org. Chem.*, 2014, **79**, 11961-11969.

3.   A.F. Littke and G.C. Fu, *J. Org. Chem.*, 1999, **64**, 10-11.

4.   D.S. Surry and S.L. Buchwald, *Chem. Sci.*, 2010, **1**, 13-31.

5.   A. Klapars, X.H. Huang and S.L. Buchwald, *J. Am. Chem. Soc.*, 2002, **124**, 7421-7428.

6.   J.F. Marcoux, S. Doye and S.L. Buchwald, *J. Am. Chem. Soc.*, 1997, **119**, 10539-10540.

7.   K. Yang, Y.T. Qiu, Z. Li, Z.Y. Wang and S. Jiang, *J. Org. Chem.*, 2011, **76**, 3151-3159.

8.   A. Shafir and S.L. Buchwald, *J. Am. Chem. Soc.*, 2006, **128**, 8742-8743.

9.   A. Seidell, '*Solubilities of inorganic and metal organic compounds: a compilation of quantitative solubility data from the periodical literature*' Van Nostrand, New York, 3rd edition, 1940, vol. 2.

10.   F.Y. Kwong and S.L. Buchwald, *Org. Lett.*, 2003, **5**, 793-796.

11.   C.Z. Tao, W.W. Liu, A.F. Lv, M.M. Sun, Y. Tian, Q. Wang and J. Zhao, *Synlett*, 2010, 1355-1358.

12.   E. Racine, F. Monnier, J.P. Vors and M. Taillefer, *Org. Lett.*, 2011, **13**, 2818-2821.

13.   A. Tlili, N. Xia, F. Monnier and M. Taillefer, *Angew. Chem. Int. Ed.*, 2009, **48**, 8725-8728.

14.   D.B. Zhao, N.J. Wu, S.A. Zhang, P.H. Xi, X.Y. Su, J.B. Lan and J.S. You, *Angew. Chem. Int. Ed.*, 2009, **48**, 8729-8732.

15.   Y. Xiao, Y.N. Xu, H.S. Cheon and J. Chae, *J. Org. Chem.*, 2013, **78**, 5804-5809.

16.   H.B. Goodbrand and N.X. Hu, *J. Org. Chem.*, 1999, **64**, 670-674.

17.   J.W.W. Chang, X.H. Xu and P.W.H. Chan, *Tetrahedron Lett.*, 2007, **48**, 245-248.

18.   A.A. Kelkar, N.M. Patil and R.V. Chaudhari, *Tetrahedron Lett.*, 2002, **43**, 7143-7146.

19.   C.T. Yang, Y. Fu, Y.B. Huang, J. Yi, Q.X. Guo and L. Liu, *Angew. Chem. Int. Ed.*, 2009, **48**, 7398-7401.

20.   P.E. Maligres, S.W. Krska and P.G. Dormer, *J. Org. Chem.*, 2012, **77**, 7646-7651.

21.   R.A. Altman and S.L. Buchwald, *Nat. Protoc.*, 2007, **2**, 2474-2479.

22.   X. Lv and W.L. Bao, *J. Org. Chem.*, 2007, **72**, 3863-3867.

23.   W. Deng, Y.F. Wang, W. Zou, L. Liu and Q.X. Guo, *Tetrahedron Lett.*, 2004, **45**, 2311-2315.

24.   C. Sambiagio, R.H. Munday, A.J. Blacker, S.P. Marsden and P.C. McGowan, *RSC Adv.*, 2016, **6**, 70025-70032.

25.   H.Z. Yu, Y.Y. Jiang, Y. Fu and L. Liu, *J. Am. Chem. Soc.*, 2010, **132**, 18078-18091.

26.   Y.B. Wang, J. Ling, Y. Zhang, A. Zhang and Q.Z. Yao, *Eur. J. Org. Chem.*, 2015, 4153-4161.

27.   G.B. Bajracharya and O. Daugulis, *Org. Lett.*, 2008, **10**, 4625-4628.

28.   S.L. Yang, C.Q. Wu, M.B. Ruan, Y.Q. Yang, Y.X. Zhao, J.J. Niu, W. Yang and J.W. Xu, *Tetrahedron Lett.*, 2012, **53**, 4288-4292.

29.   M. Toffano, J.Y. Legros and J.C. Fiaud, *Tetrahedron Lett.*, 1997, **38**, 77-80.

30.   L. Becerra-Figueroa, A. Ojeda-Porras and D. Gamba-Sanchez, *J. Org. Chem.*, 2014, **79**, 4544-4552.

31.   A.D. Averin, K.S. Tyutenov, A.V. Shukhaev, S.M. Kobelev, A.K. Buryak, F. Denat, R. Guilard and I.P. Beletskaya, *Heterocycles*, 2012, **86**, 1341-1366.

32.   E.R. Strieter, D.G. Blackmond and S.L. Buchwald, *J. Am. Chem. Soc.*, 2005, **127**, 4120-4121.

33.   J.W. Tye, Z. Weng, A.M. Johns, C.D. Incarvito and J.F. Hartwig, *J. Am. Chem. Soc.*, 2008, **130**, 9971-9983.

34.   E.R. Strieter, B. Bhayana and S.L. Buchwald, *J. Am. Chem. Soc.*, 2009, **131**, 78-88.

35.   D.B. Damon, R.W. Dugger, S.E. Hubbs, J.M. Scott and R.W. Scott, *Org. Process Res. Dev.*, 2006, **10**, 472-480.

36.   U.K. Singh, E.R. Strieter, D.G. Blackmond and S.L. Buchwald, *J. Am. Chem. Soc.*, 2002, **124**, 14104-14114.

37.   R. Giri and J.F. Hartwig, *J. Am. Chem. Soc.*, 2010, **132**, 15860-15863.

38.   G. Dijkstra, W.H. Kruizinga and R.M. Kellogg, *J. Org. Chem.*, 1987, **52**, 4230-4234.

39.   G.S. Silverman and P.E. Rakita, '*Handbook of grignard reagents*' Marcel Dekker, New York, 1996.

40. C. Amatore, A. Jutand, F. Khalil, M.A. Mbarki and L. Mottier, *Organometallics*, 1993, **12**, 3168-3178.

41. J.W. Tye, Z.Q. Weng, R. Giri and J.F. Hartwig, *Angew. Chem. Int. Ed.*, 2010, **49**, 2185-2189.

42. G. Franc and A. Jutand, *Dalton Trans.*, 2010, **39**, 7873-7875.

43. S. Sung, D.C. Braddock, A. Armstrong, C. Brennan, D. Sale, A.J.P. White and R.P. Davies, *Chem. Eur. J.*, 2015, **21**, 7179-7192

Chapter 4

Investigating deactivation pathways in Ullmann-Goldberg reactions

4.1. Introduction

#### 4.1.1. Catalyst deactivation studies in the Ullmann-Goldberg reaction

Deactivation studies in the literature of the Ullmann-Goldberg C-N coupling reaction are limited, despite the often discussed poor turnover numbers and reproducibility associated with the reaction. A study in 2016 by Davies did discuss the deactivation of the copper catalyst for the reaction shown in Scheme 4.1.[1] By monitoring the heat flow of the reaction in three subsequent additions of substrates, it was seen that the rate of reaction decreased upon each reaction. A negative rate dependence on the tetrabutylphosphonium malonate (TBPM) **(64)** base led to the conclusion that, whilst able to act as ligand and base, **64** also provided a pathway for disproportionation to Cu(0)/Cu(II).
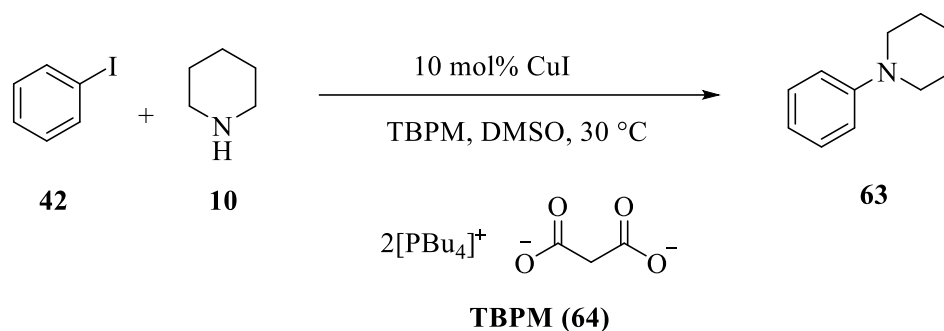
Scheme 4.1 - C-N coupling between iodobenzene (**42**) and piperidine (**10**), mediated by **64**, studied by Davies.[1]

Previous work on the use of anionic picolinamide ligands in the copper-catalysed etherification reaction reported the isolation of Cu(II) complexes from the post-reaction mixture.[2] These complexes often were mostly observed as [CuL$_2$] species, although some examples bearing a H$_2$O ligand were also isolated. A disproportionation pathway was again believed to be the source of the Cu(II) complexes. These deactivation pathways proposed agree well with an investigation into the mechanism of the Hurtley

C-C formation, utilising *in situ* IR and XANES/EXAFS performe d by Liu *et al.*[3]. In this study, the acetylacetone **(65)** acts as both ligand, substrate and is shown to be involved with an off-cycle disproportionation to **68** (Scheme 4.2).
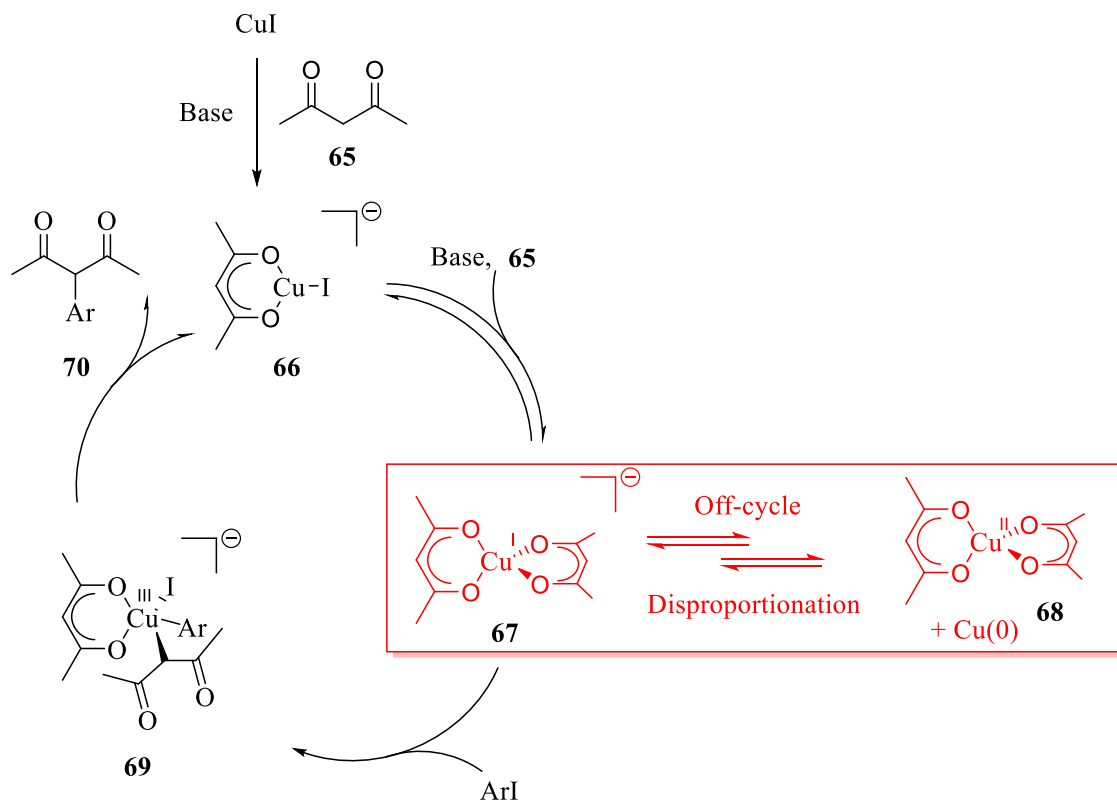
Scheme 4.2 - Off-cycle disproportion of Cu(I) species studied by Lei.[3]

These studies provide solid evidence that the formation of Cu(II) complexes through the disproportionation of Cu(I) is a possible deactivation pathway in Cu(I)-catalysed reactions. It is still unknown what conditions favour disproportionation, Davies hypothesised that the coordination of **10** stabilised the Cu(I) species, whilst neutral ligands such as 1,10-phenanthroline **(50)** may also provide a similar role. The reversibility of Cu(II) formation is also still under scrutiny, where work in the 1980's by Weingarten showed that Cu(II) salts could act as a precursor to the catalyst due to *in situ* reduction to Cu(I).[4]

4.1.2. Homogeneous vs heterogeneous catalysis

Formation of aggregates such as palladium black from homogeneous complexes and leaching of solid-supported metal catalysts are often considered to be deactivation pathways, however many catalytic systems still suffer from ambiguity of the active catalytic state. It is not always trivial to distinguish between homogeneous and heterogeneous catalysis, and cases of *quasi*-heterogeneous or hybrid homogeneous-heterogeneous catalysis have been studied widely in coupling reactions.[5-10]

Modern focus on nanoparticle and nanocluster catalysis has helped blur the lines of homogeneity and heterogeneity in catalysis, and the use of soluble "homogeneous" precursors to these materials lead to the question of where the phase-boundary exists.[10] The issue also extends to catalysts considered to be heterogeneous, but in which leaching of the supported metal is required for catalysis. This area is of significant interest in industry, where heterogeneous catalysts are considered ideal due to the low levels of residual metals required in products such as pharmaceuticals, as well as for catalyst recovery or recycling.

Many studies in the literature address this ambiguity, particularly in the case of palladium catalysis. For example, in the investigation of a "heterogeneous" Pd/C-catalysed Suzuki-Miyaura reaction, it was found that the levels of palladium increased throughout the reaction in conjunction with the oxidative addition of an aryl bromide to the palladium catalyst (Scheme 4.3).[6] The dissolution and precipitation of palladium was found to vary with base and the nature of the carbon support, where the solubilised palladium was concluded to be the active catalyst. Fagnou reported a direct arylation mediated by Pearlman's catalyst ($Pd(OH)_2$/C) in which turnover of an aryl halide supported on Wang resin indicated leaching of the palladium catalyst. Inhibition of the reaction by a heterogeneous metal scavenger also provided evidence that leached palladium is necessary for catalysis.[11]

Pd/C **Heterogeneous precursor**

Ar-Br

KX   X = OH or F

Ar-Pd-Br

Homogeneous intermediates

KBr

Ar'B(OH)$_2$

Ar-Br

Pd(0)

Ar-Pd-X

KX   X = OH or F

Ar-Ar'

Ar'BX(OH)$_2$K

Ar-Pd-Ar'

KBX$_2$(OH)$_2$
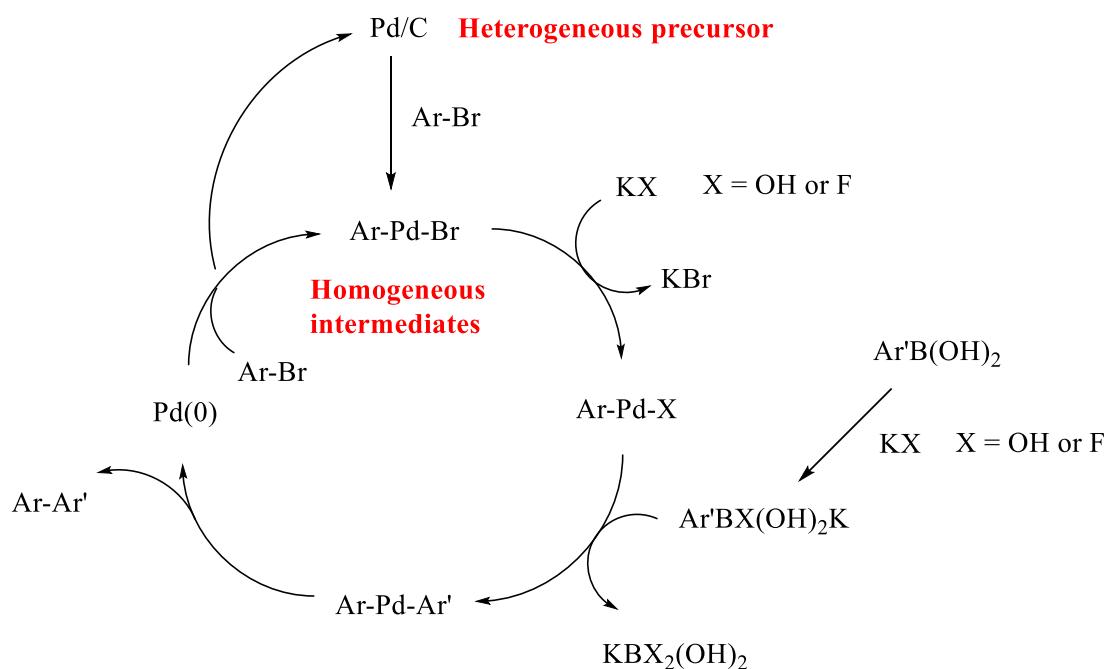
Scheme 4.3 – Proposed catalytic cycle for the Pd/C mediated Suzuki-Miyaura cross-coupling by Conlon. Leaching of the palladium following oxidative addition to the Pd/C results in a homogeneous catalyst.[6]

Alternatively, there is substantial evidence that the use of soluble palladium precursors, such as Pd(OAc)$_2$ in Mizoroki-Heck and Suzuki-Miyaura cross-coupling reactions results in the formation of palladium aggregates and nanoparticles.[8] Much discussion has been made of the catalytic cycle and whether formation of palladium aggregates and nanoparticles can act as a reservoir of active palladium for homogeneous catalysis, or as a quasi-heterogeneous catalyst in the cross-coupling reaction, though clear distinction remains difficult still.

4.2. Recovery of base and catalyst post-reaction

One of the notable features of copper-catalysed reactions using partially soluble bases such as Cs_2CO_3 and K_2CO_3 is the observation of a colour change to the white solid of the base. Anecdotal evidence of this has been noted under both aerobic and anaerobic conditions for copper-catalysed coupling reactions.[2] This was observed consistently in substrate screening reactions in this study, for example, the reaction between 4-iodoanisole (9) and 2-pyrrolidinone (28), which gives full conversion to (46) overnight, as shown in Figure 4.1. The images show the dissolution of the copper catalyst to give a white/grey solid and dark blue solution, eventually producing a colourless solution with blue solid. It is noted that exposure of the solution to aerobic conditions at the 1 hour point causes oxidation of the colourless solution, but at 16 hours, oxidation was not always observed.
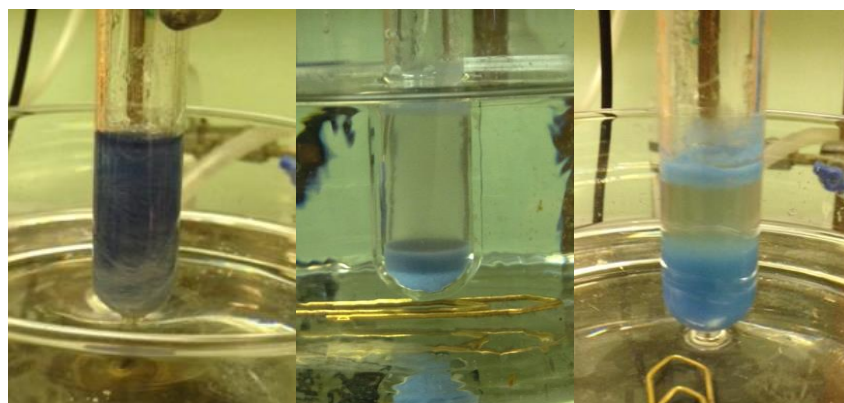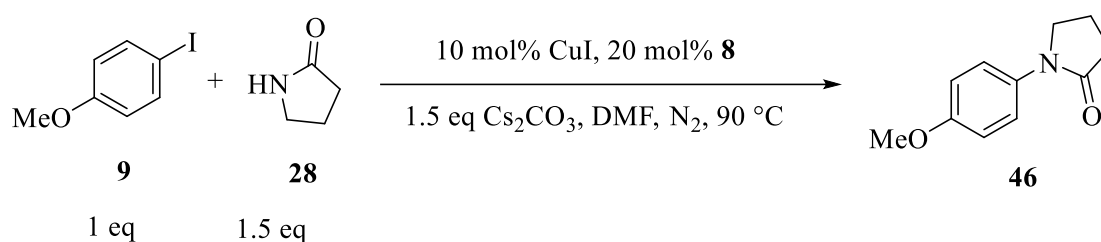
Figure 4.1 – Images of a Cu-catalysed *N*-arylation reaction at 5 minutes (left), 1 hour (centre) and 16 hours (right).

The remaining solid seen at the end of the reaction is insoluble in most organic solvents, including polar solvents such as DMSO, DMF, ethanol and acetone. An investigation into the nature of the copper species at the end-point of the reaction was desired, however due to the insolubility of the suspended solid in organic solvents, the solution-based copper was investigated first.

4.2.1. Cu(II) formation

The work-up for the copper-catalysed reaction between **9** and **28** shown in Scheme 4.4 involved filtration of the crude reaction mixture through silica with ethyl acetate, to yield the organic compounds. Flushing the silica with ethanol following this eluted a blue solution, which was evaporated to give a blue solid. This blue solid was characterised by single crystal x-ray diffraction following vapour diffusion (MeOH/EtOH), and found be the *bis*-(*N,N*-dimethylglycinato)copper(II) monohydrate complex **71**.
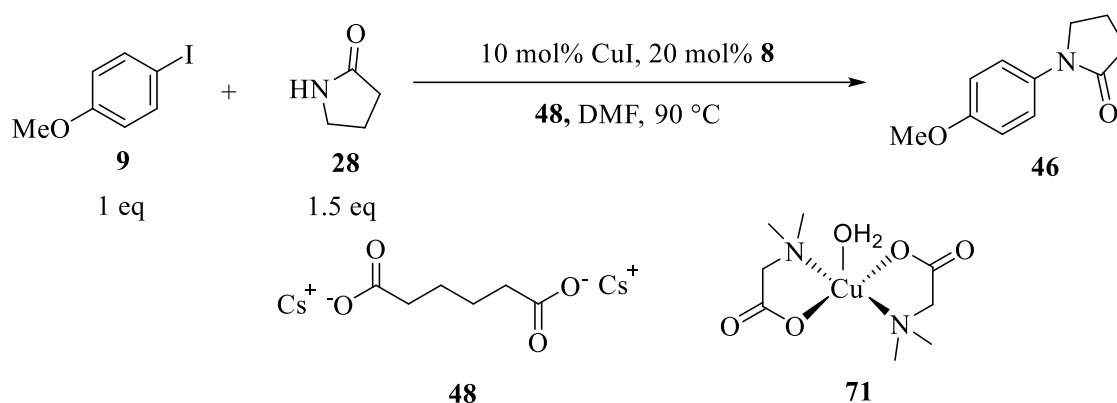
Scheme 4.4 – *N*-Arylation reaction from which a complex **71** was recovered.
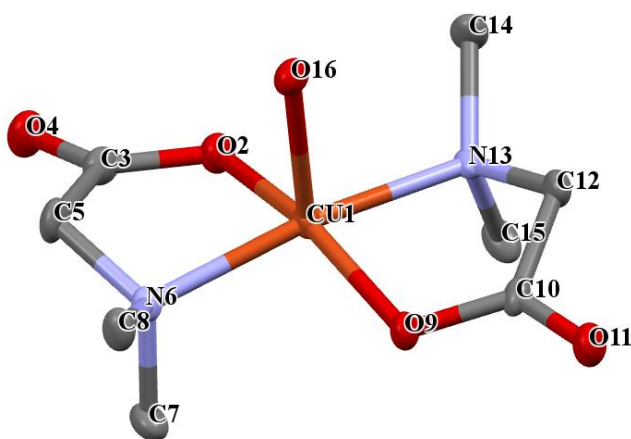
Figure 4.2 – Crystal structure of **71**. Atomic displacement parameters are drawn at the 50 % level, hydrogen atoms have been omitted for clarity.

This complex exists in a five-coordinate, distorted square-based pyramidal geometry, with one water molecule occupying the axial position at a bond distance of 2.270(3) Å (Cu(1)-O(16)). This bond length is very similar to that which has been reported in various other Cu(II) complexes with an axial H$_2$O coordinated.[2, 12, 13] It is most likely

that the water molecule was introduced in the work-up procedure, rather than being formed in the anhydrous conditions of the coupling reaction. Whether this complex is formed through a disproportion reaction cannot be reliably said, however, it may represent a possible deactivation pathway for the Cu(I) catalytic cycle.

4.2.2. Investigation of Cu(II) formation in solution

To explore a Cu(I) → ½ Cu(II) + ½ Cu(0) disproportionation pathway further, analysis of how Cu(II) concentrations affect NMR signal was performed. Cu(II) compounds such as $Cu(OAc)_2$ are paramagnetic,[14] which extends relaxation times and causes peak broadening in NMR spectroscopy.[15] By spiking a reaction mixture with various levels of $Cu(OAc)_2$, a visual assessment of the broadening in the system shown in Figure 4.3 and Figure 4.4.

$$10 \text{ mol\% CuI, 20 mol\% } \mathbf{8}$$
$$1.5 \text{ eq TBAA, } d_7\text{-DMF, 70 °C}$$

9   **10**   **11**

A - 0 eq **10**, 10 mol % $Cu(OAc)_2$
B - 0 eq **10**, 1 mol % $Cu(OAc)_2$
C - 1.5 eq **10**, 0 mol % $Cu(OAc)_2$, 10 minutes
D - 1.5 eq **10**, 0 mol % $Cu(OAc)_2$, 240 minutes
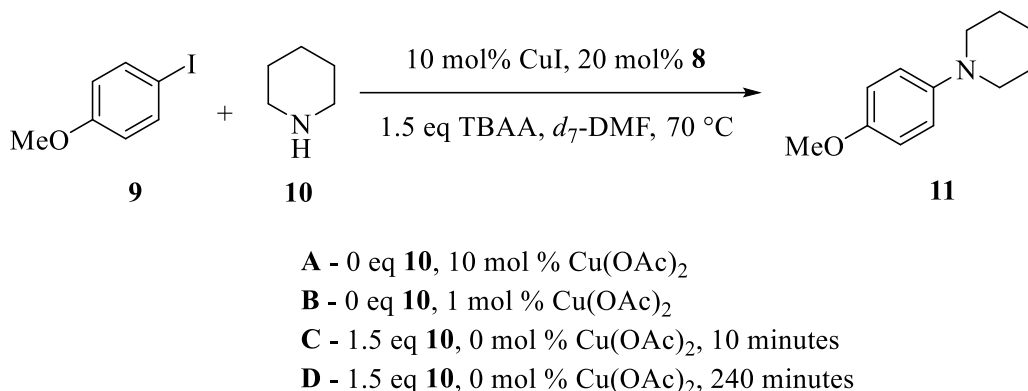
Scheme 4.5 – Conditions assessed in Cu(II) ^{1}H NMR broadening experiment (500 MHz). Reactions performed in 0.5 mL solvent and 0.125 M **9**.

The low-field region relating to the aromatic peaks were found not to be significantly broadened or changed in any way, even at 10 mol% loading of $Cu(OAc)_2$. Alternatively, the high-field region shows clear loss of peak definition in going from 1 mol% to 10 mol% $Cu(OAc)_2$. If one compares the *in situ* NMR experiment at different time periods (Figure 4.4C and D), a small change is noted in the splitting pattern sharpness of the peaks at 1.4 ppm and 3.5 ppm. This indicates that formation of Cu^{2+} may be occurring in solution over the 4 hours of the coupling reaction, however the results are not conclusive. Magnetic susceptibility would provide a method of gaining a more definitive answer, however *in situ* measurements of this reaction system would pose difficulty.
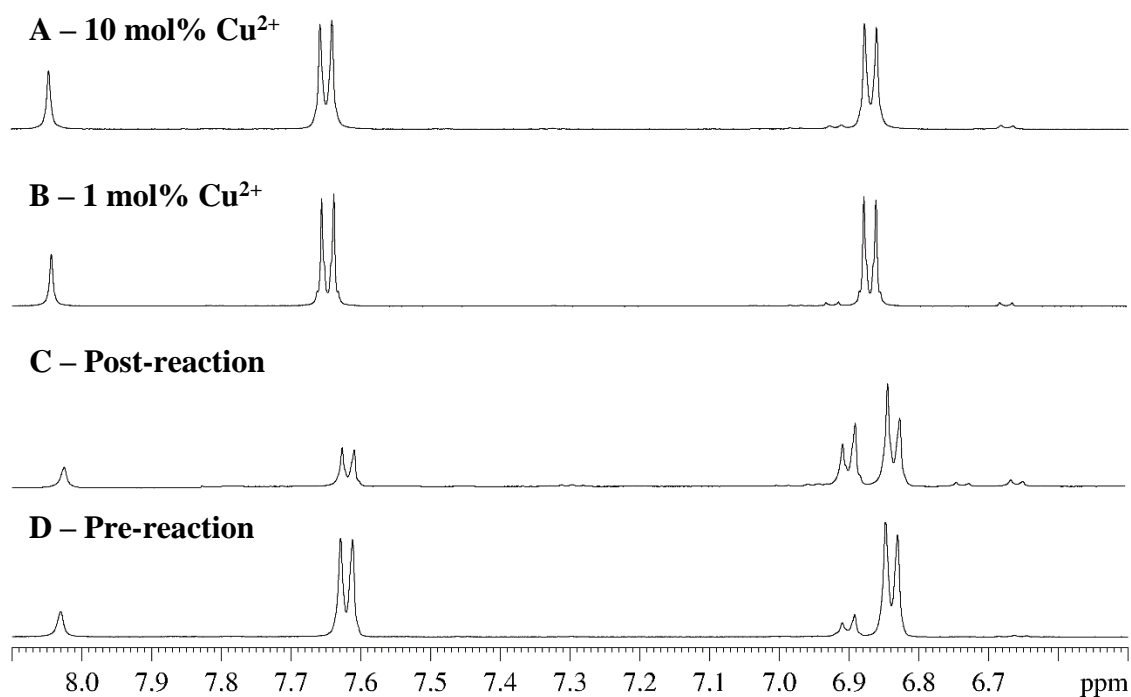
Figure 4.3 – Low-field region of ^{1}H NMR displayed for conditions A – D (Scheme 4.5).
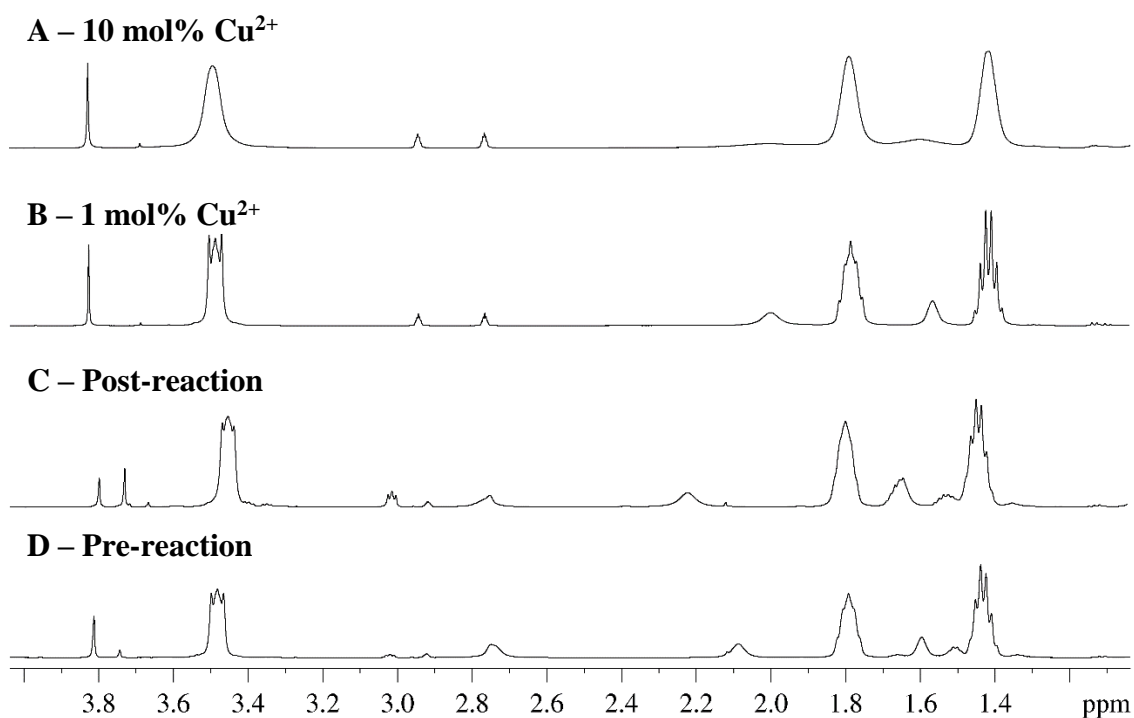

Figure 4.4 – High-field region of ^{1}H NMR displayed for conditions A – D (Scheme 4.5).
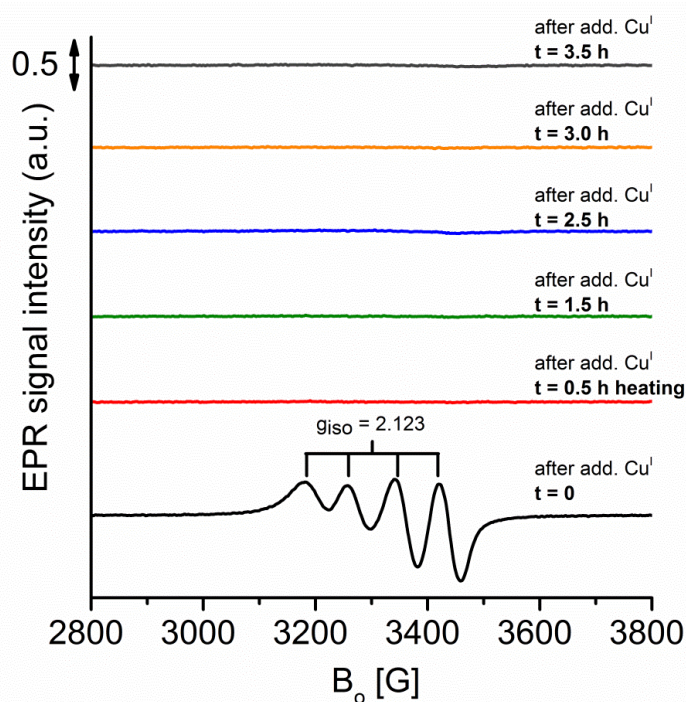
4.2.3. EPR measurements

The reaction with amide coupling partner **28** was also studied, however due to the poor solubility of the Cs_2CO_3 used in this reaction, electron paramagnetic resonance (EPR)

was used. Weingarten used EPR to show the reduction of Cu(II) to Cu(I) *in situ* when performing early mechanistic studies of the Ullmann etherification.[4] The EPR measurements were performed under anhydrous conditions in an inert argon atmosphere by Dr Bao Nguyen with assistance from Mr. Sven Adomeit of the Leibniz Institute for Catalysis.
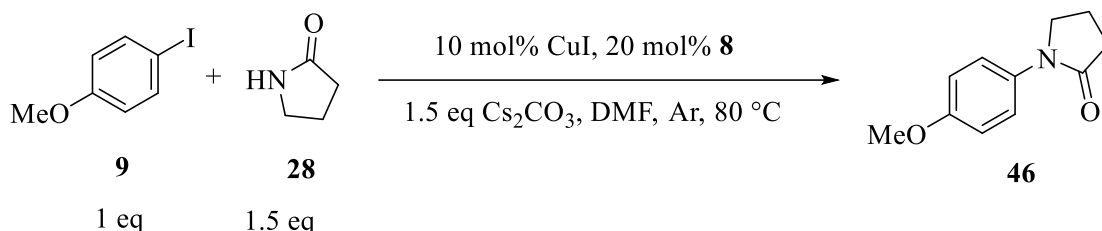
Scheme 4.6 - C-N coupling reaction used in EPR study. Reaction scaled up to 2.5 g **9** using 53 mL of DMF.

Figure 4.5 - *In situ* EPR measurements over the course of the experiment. Reaction was initiated with the addition of CuI after all other reaction components.

The *in situ* EPR data gathered during the reaction displayed in Scheme 4.6 shows an initial formation of Cu^{2+} following the addition of CuI, giving rise to an EPR signal (Figure 4.5). This then subsides in the first 30 minutes of the reaction, with little to no EPR signal observed. The EPR data indicates that any paramagnetic Cu(II) formed is

quickly reduced to the EPR inactive Cu(I). Quantification of the Cu(II) directly after t_0, cannot be given without further work, thus it is unknown how much of the CuI is oxidised.

The initial oxidation of CuI is interesting however, and was explored further with an experiment combining just CuI and two equivalents of **8** in DMF (Figure 4.6). The similarity of the EPR signal obtained under these conditions to that which was seen under reaction conditions provides a strong indication that the same Cu^{2+} species is formed. Further experiments on this system would be useful to uncover the reducing agent or process in which the Cu^{2+} is removed from the system. Weingarten concluded that phenoxide ions were responsible for the reduction of $CuBr_2$ to a Cu(I) species, and in this system, the deprotonated ligand or the carbonate base may perform a similar role.
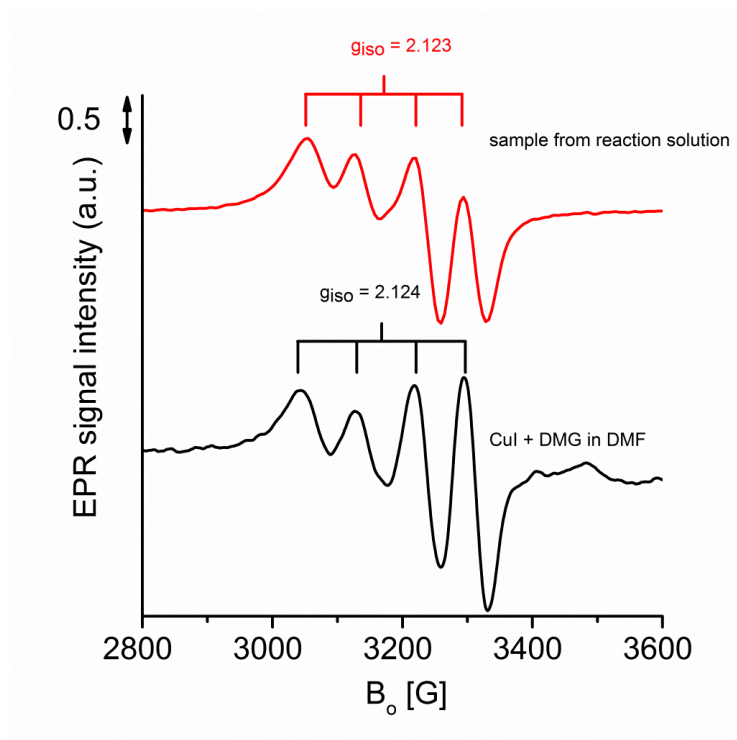
Figure 4.6 - Normalized EPR spectra of Cu(II) signal observed during reaction (red) and Cu(II) signal observed when CuI is added to a solution of 2.0 equivs of **8** in DMF in Glovebox (black).

4.2.4. SEM/EDX

An alternative explanation for the loss of Cu(II) from the solution is that it is linked with the observation of the blue precipitate discussed in Section 4.2. Due to the insolubility of this solid, and the large concentration of cesium species relative to the copper in the system, many forms of analysis proved insufficient in confirming the presence of copper. Energy dispersive X-ray spectroscopy (EDX) did however provide a possible method of analysing the solid, and its combination with SEM could prove useful in understanding the shift in base species throughout a reaction.

A - Fresh Cs_2CO_3
B - Solid precipitate after 2.5 hours reaction
C - Solid precipitate after 5 hours reaction
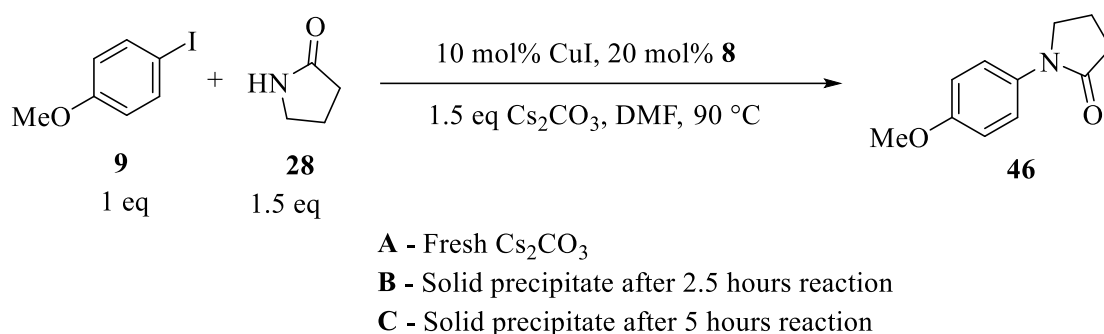
Scheme 4.7 - Conditions for coupling reaction before isolation of solids for SEM/EDX analysis.

Two different sources of Cs_2CO_3 were analysed to explore any differences which may occur due to particle size, these were the Chemmetal and Acros Organics discussed in Chapter 3. The fresh samples and two points in the reaction outlined in Scheme 4.7 were used to observe any changes from $0 \rightarrow 2.5$ hours $\rightarrow 5$ hours of the reaction. The SEM images and elemental composition data was obtained by Dr Robert Menzel at the University of Leeds.

Table 4.1 – Conversion data for the four reactions used in SEM/EDX study.

Base Supplier	Reaction Time (minutes)	Conversion (% product)
Chemmetal	150	37
Chemmetal	300	66
Acros	150	29
Acros	300	56

4.2.4.1. Milled Cs₂CO₃ Local Elemental Composition
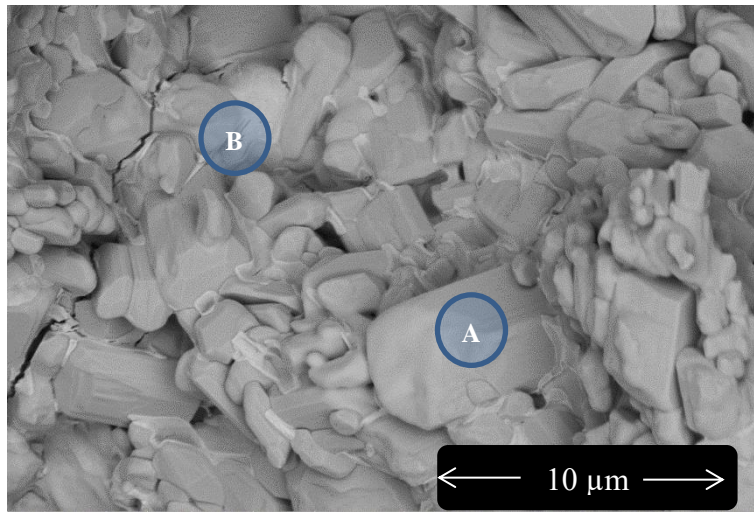
	Cs	O	I	Cu
A	32	68	0	0
B	26	74	0	0
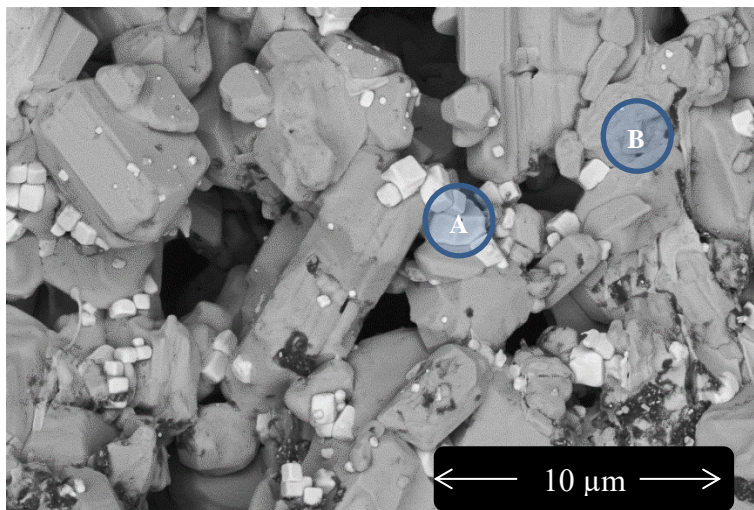
	Cs	O	I	Cu
A	47	20	32.5	0.5
B	15	84	0.5	0.5
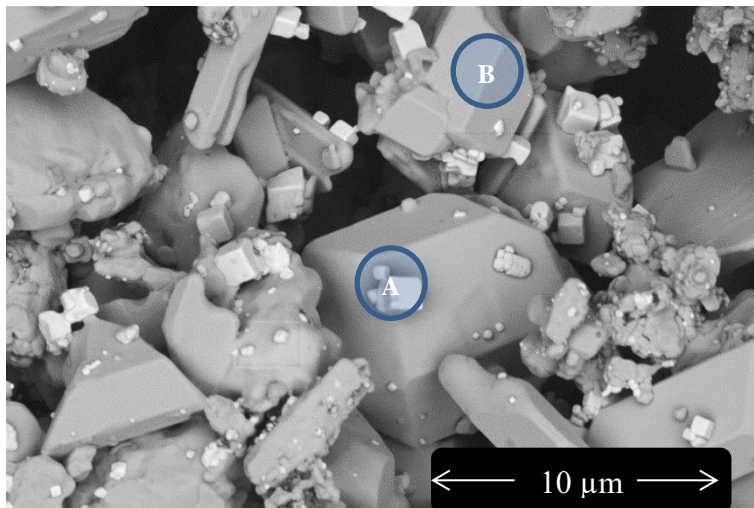
	Cs	O	I	Cu
A	46	22	31.5	0.5
B	69	27	3	1

Figure 4.7 - SEM images of milled Cs₂CO₃ at fresh (top), 2.5 hours (midde) and 5 hours (bottom). Elemental percentage composition as analysed by EDX given for the highlighted regions on the SEM images.

4.2.4.2. Acros Cs₂CO₃ Local Elemental Composition
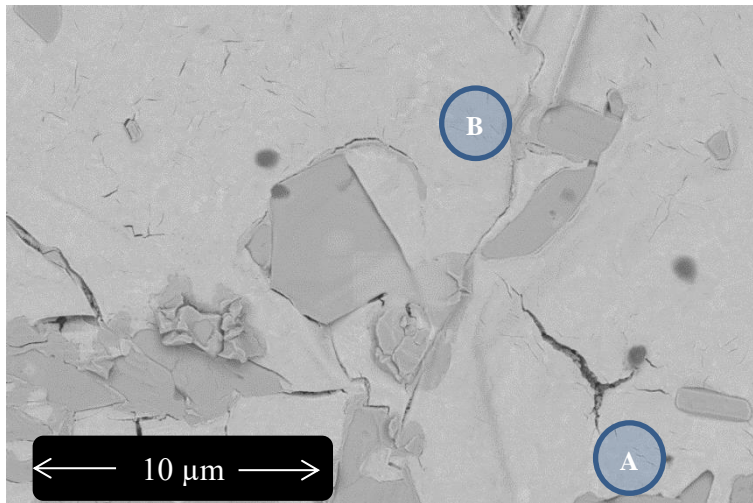
	Cs	O	I	Cu
A	22	78	0	0
B	26	74	0	0
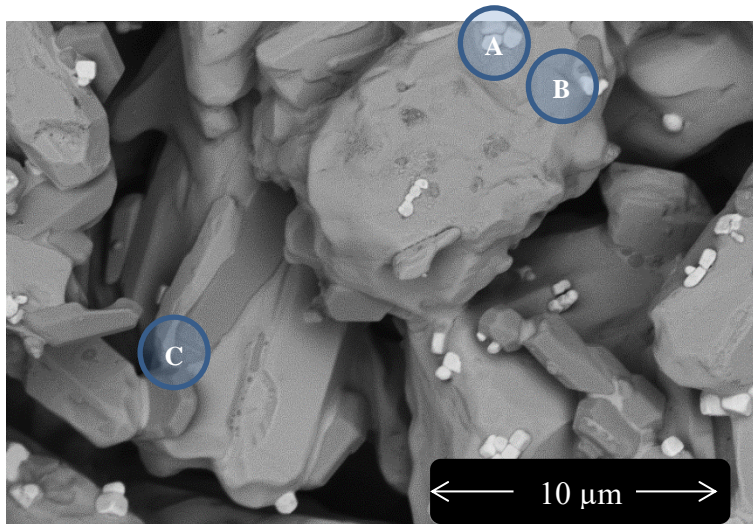
	Cs	O	I	Cu
A	29	57	13.3	0.7
B	17	80	1	2
C	24	53	14	9

	Cs	O	I	Cu
A	21	78	0.5	0.5
B	22	72	5	1

Figure 4.8 - SEM images of Acros Cs₂CO₃ at fresh (top), 2.5 hours (midde) and 5 hours (bottom). Elemental percentage composition as analysed by EDX given for the highlighted regions on the SEM images.

The SEM images show clear composition changes from the fresh base to that which has been isolated from the reactions. The appearance of small, mostly cuboid particles after reaction with the milled $Cs_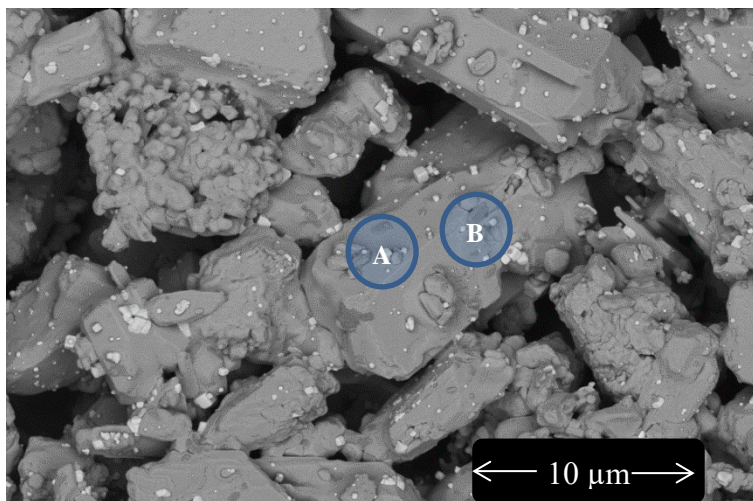2CO_3$ shows the formation of CsI, which is expected from the turnover of the catalyst. Elemental composition of the white particles in the images indicates a much higher iodine presence than the darker regions. In the reactions with the Acros base, which gave similar conversions to product, the CsI crystals are much smaller and well dispersed, particularly after 5 hours reaction. The oxygen content is also assessed, however distinguishing between $CsHCO_3$ and Cs_2CO_3 is not possible.

Unfortunately, the hygroscopic nature of the Cs_2CO_3 led to adsorption of water in the images of fresh samples, which caused clumping. The particles sizes are not seen to vary greatly over the course of the reaction with milled base. The average particle size does appear to decrease when using the Acros Cs_2CO_3 and there is a change in morphology compared with rounded edges seen in the images taken under stricter anaerobic conditions (Figure 4.9).
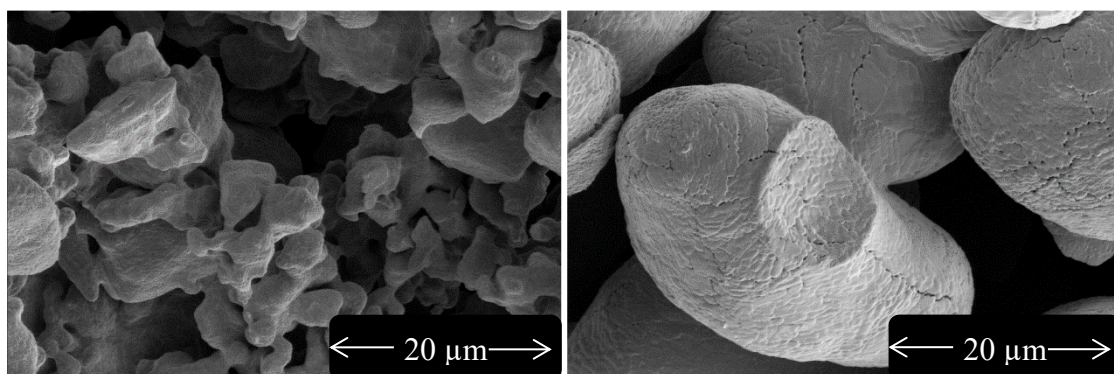
Figure 4.9 - SEM images of the fresh Cs_2CO_3 particles under anaerobic conditions. Chemmetal, milled (left) and Acros (right).

The use of elemental mapping helped discern whether the deposition of copper is linked with the formation of the CsI or $CsHCO_3$. By analysing the iodine, copper and oxygen mapping (Figure 4.10), it seen that the copper is very well distributed around the sample, whilst the iodine and oxygen distribution is seen to be more intense in some areas than others. As a result, it is unlikely that precipitation of the copper occurs with the formation of CsI and $CsHCO_3$ crystals as the reaction proceeds.
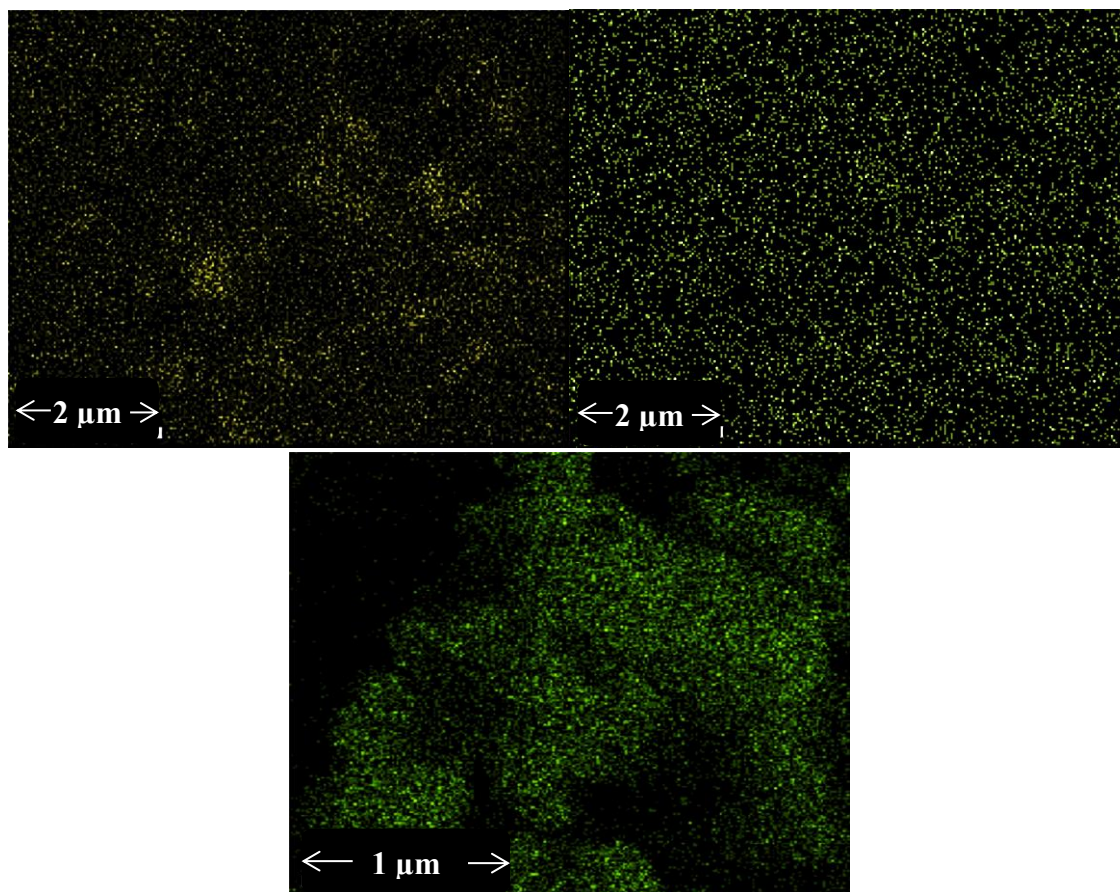
Figure 4.10 – Elemental mapping of post-reaction solid. **Top left** – Iodine. **Top right** – Copper. **Bottom middle** – Oxygen. Image brightness set to + 20% and contrast – 20%, to improve clarity of images.

Care was taken to ensure the recovered solid had been washed to remove any materials still in solution, so the presence of copper found in the EDX spectra is likely to be the cause for the blue colour of the solid. Although the exact percentages of the elemental composition figures have ~ 10 % error to them, the copper levels are found to be much lower than the Cs, I and O percentages. Nevertheless, the deposition of copper on the surface of the cesium compounds may mean the loss of active copper from the reaction solution, causing catalyst deactivation. Some alternative possibilities of this observation are that the deposited copper acts as a catalyst reservoir, which can dissociate back into solution for catalysis, or the reaction can proceed in a heterogeneous manner.

4.2.5. Powder Diffraction

Powder diffraction offered another method of analysing the base composition at the different stages of the reaction. Using the same procedure used for the SEM/EDX analysis, a sample of the coloured precipitate was prepared after 5 hours reaction (78 % conversion to product). Simple fingerprint analysis indicated that CsI and $CsHCO_3$ are present at this point, as would be expected (Figure 4.11). Surprisingly, literature Cs_2CO_3 patterns were not found to match the reaction data well, when Cs_2CO_3 should still be present after 78 % conversion to product. In running a sample of the fresh Cs_2CO_3, the signal obtained was poor, meaning that it is likely present, but with dilution by other cesium species, it is not visible.
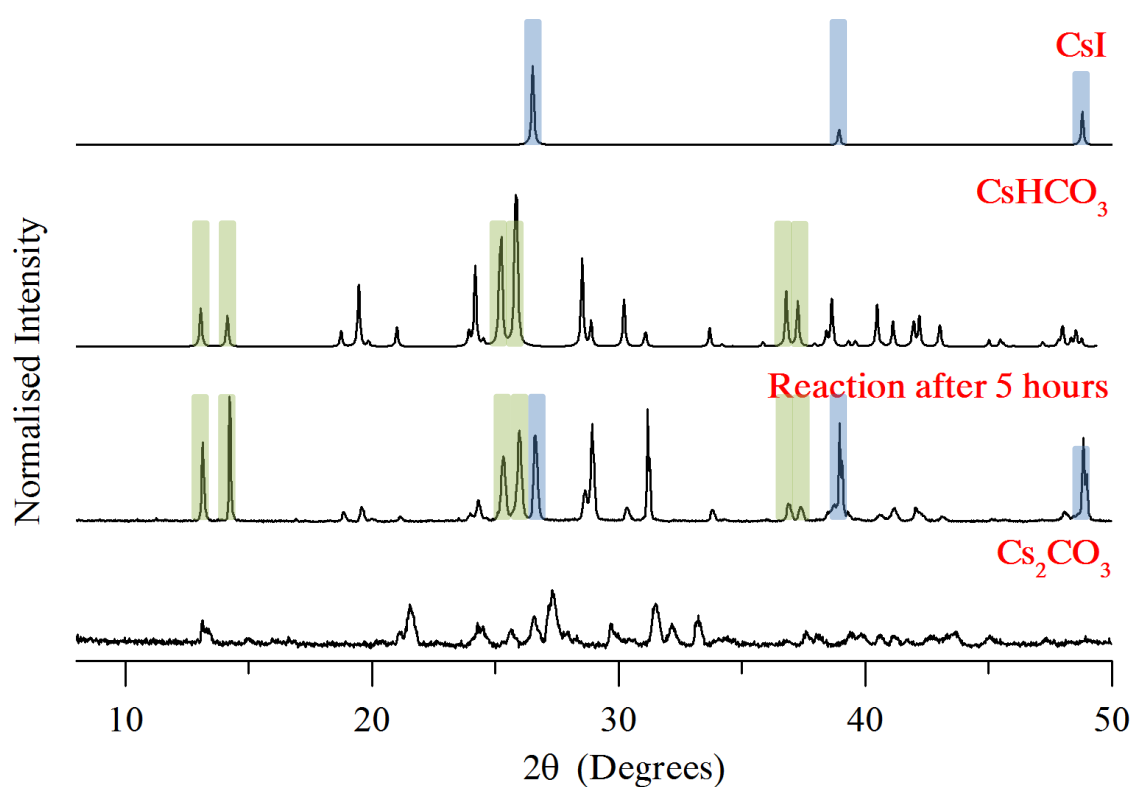
Figure 4.11 – Powder diffraction patterns for a various cesium species. CsI and $CsHCO_3$ patterns obtained from the Inorganic Crystal Structure Database.

Attempts to characterise the copper species on the surface of the particles were unsuccessful however. Fingerprinting possible crystal data for $CuCO_3$ and complex **71** showed no similarities and the low concentration of copper to the complex mixture of cesium species likely prevents characterisation of copper species *via* powder diffraction.

4.2.6. Atomic Absorption Spectroscopy (AAS)

Given that there is clear loss of the solution-based copper during the reaction, it is necessary to determine the extent of this loss. AAS has the benefit of being available for all elements if the necessary elemental lamp is available. A protocol for sampling and quenching reactions with HNO_3 was developed and analysis of the cesium and copper concentrations in these samples was determined. The kinetic profile in Figure 4.12 shows that the reaction had a short lag-time initially, similar to that seen in the work discussed in Chapter 3. The end point conversion does confirm that the reaction went to completion and the resulting data is relevant to turnover conditions.
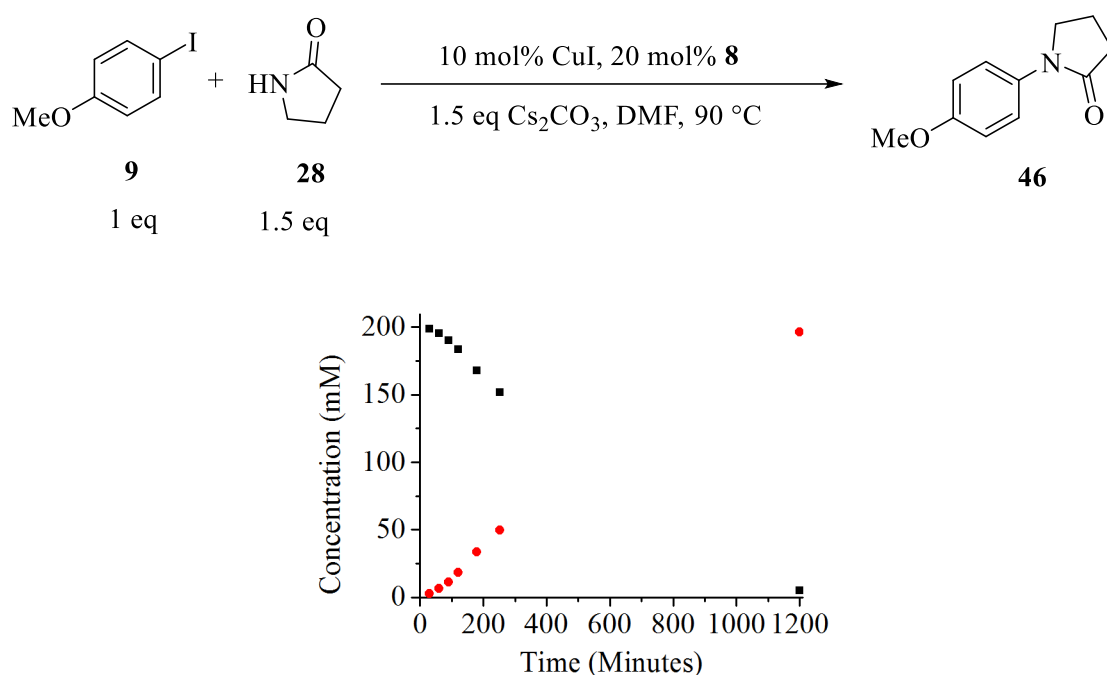
Figure 4.12 – Kinetic profile of the *N*-arylation reaction analysed by AAS. Only samples between 0 and 300 minutes were sent for analysis. ■ [**9**] ● [**46**]. The reaction was performed with 200 mM [**9**].

The results of the AAS is given in Table 4.2 with the relative conversions to product at each data point. The sampling and measurements of 100 µl for each sample was done with a 1 mL syringe and long needle, consequently, a small error must be associated with each sample. Taking this into account, it is difficult to claim the copper concentrations vary significantly through the reaction, where 75 – 80 % is found to be in solution consistently. These data correspond well with the observation of the blue precipitate

forming in the first 30 minutes of the reaction and this data suggests that around 2.5 mol% could be lost during this process.

An increase in cesium concentration may however be seen in this reaction and whilst this is only 4 - 5% of the possible cesium, this equates to up to 15 mmoles. A link between the rate of turnover increasing around 120 minutes and the increase in cesium concentration was considered. These data does however contradict those discussed regarding solubility of the base in Chapter 3 and so further answers were sought.

Table 4.2 - Amount of cesium and copper copper in solution at each data point of the reaction as a percentage of the maximum amount at full dissolution.

Entry	Time (minutes)	Conversion (% product)	Cesium (% in solution)	Copper (% in solution)
1	30	1.4	12.9	74.0
2	60	3.2	12.6	80.3
3	90	5.7	12.7	79.5
4	120	9.1	18.0	84.3
5	180	16.8	15.8	74.0
6	252	24.9	17.7	74.0

The solubility of Cs_2CO_3 is often anecdotally quoted as its main benefit over K_2CO_3, however the above data does not indicate good solubility, even at 90 °C. The reaction assessed does however contain numerous other compounds and salts which may affect this, so AAS data of Cs_2CO_3 stirred at 90 °C in anhydrous DMF, under a N_2 atmosphere was obtained. The result of these samples are given in Table 4.3 and show very low solubility of the Cs_2CO_3 in DMF. As such, the solubility of the cesium compounds formed in the reaction may be the cause of the increase in [Cs] seen in Table 4.2.

Table 4.3 - AAS data for solubility of Cs_2CO_3 in DMF. Maximum cesium concentration after dilution of 100 µL sample to 10 mL.

| Entry	Time (minutes)	Cesium (mg/L)	Cesium (% in solution)
1	30	5.2	1.3
2	120	21.2	5.3
3	240	15.0	3.8

4.2.7. ^{133}Cs NMR

^{133}Cs is not a common nuclei for NMR spectroscopy, however examples of its use can be found in the literature.[16-18] The 100 % abundance of the isotope and the narrow natural line width exhibited enable use of ^{133}Cs NMR despite the 7/2 spin of the nuclei. The anonymity of ^{133}Cs NMR spectroscopy in the literature is more likely due to a scarcity in requirement for it, where poor solubility of the cesium salts in organic solvents supersedes its use for many synthetic chemists. The ease of obtaining NMR spectra for many chemists does however make ^{133}Cs NMR a desirable technique if the need is there.

In order to address the question of which cesium species are likely to be in solution during catalysis, the solubility of Cs_2CO_3, $CsHCO_3$ and CsI were assessed by ^{133}Cs NMR (Figure 4.13). To do this, saturated solutions of the corresponding cesium salts were heated in DMF at 90 °C for 2 hours. 0.5 mL of the solutions were added to an NMR tube and a coaxial insert tube within the NMR tube containing 0.1 M aqueous solution of $CsNO_3$ in D_2O as external standard (Figure 4.14). The insert tube is used to act as a relative cesium reference, preventing Cs exchange between the standard and the sample.
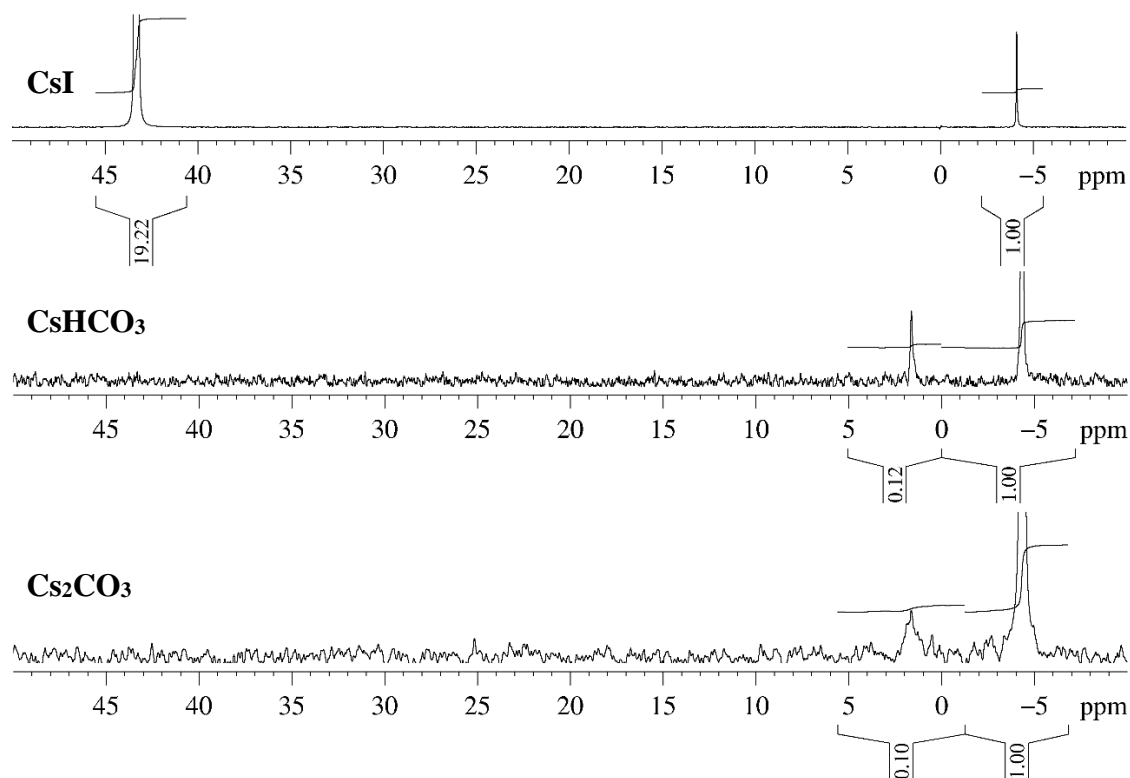
Figure 4.13 - ^{133}Cs NMR spectra (66 MHz) of saturated cesium salt solutions in DMF at 90 °C, using 0.1 M $CsNO_3$ in D_2O as a reference.
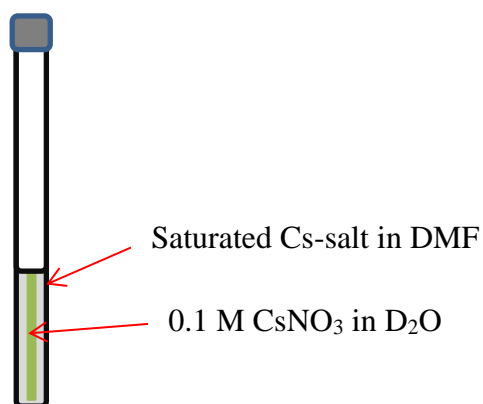
Figure 4.14 – Schematic of coaxial NMR tube for concentration experiments.

Exact concentrations are not possible to calculate based on the $CsNO_3$ standard due to the different diameters of the NMR tube and capillary tube, however relative concentrations of the cesium samples can be given (Table 4.4). As was seen in the AAS experiment, Cs_2CO_3 has very limited solubility in DMF under the reaction conditions, and similarly poor solubility is exhibited by $CsHCO_3$. CsI on the contrary, is almost three orders of magnitude more soluble than both Cs_2CO_3 and $CsHCO_3$. The increase in

cesium concentration throughout the course of the reaction discussed in Section 4.2.6. is likely to be caused by the increase in CsI in the system as the reaction proceeds.

Table 4.4 - Saturated concentrations of cesium salts at 90 °C in DMF.
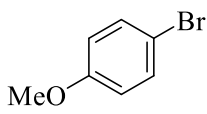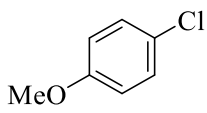
Cesium Salt	Relative Concentration
Cs_2CO_3	1
$CsHCO_3$	2.4
CsI	384

4.3. Halide inhibition

As the solubility of CsI is much greater than that of Cs_2CO_3, it is important to understand how this may affect reactivity in reactions in which CsI is formed over the course of a reaction. A simple set of experiments in which 1 equivalent of sodium or cesium halide was added to the standard reaction between **9** and **28** is shown in Table 4.5.

Table 4.5 – Addition of inorganic halide salts to the copper-catalysed *N*-arylation of **28**.
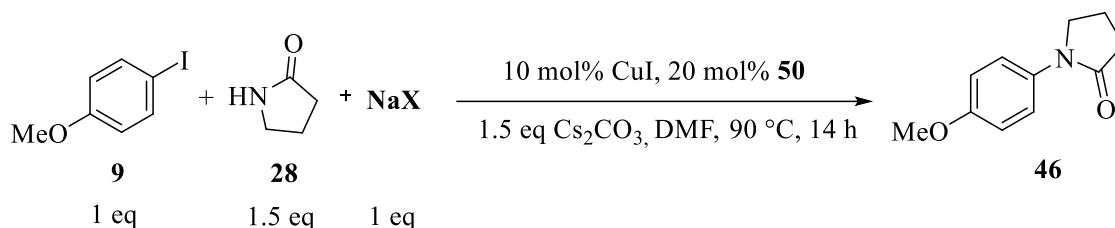
Entry	Halide additive	Conversion (% 9)	Conversion (% to 46)	Side products
1	None	87	87	None
2	CsI	32	32	None
3	NaI	14	14	None
4	NaBr	19	14	5 % **15**
5	NaCl	36	35	Trace **17**

141

The results detailed above show clear inhibition of the reaction by the halide additives. CsI, shown previously to be highly soluble in the DMF solvent at 90 °C, resulted in just 32 % conversion to product, much lower than 87 % when no additive was used. The halide salts of sodium inhibit the reaction in an order of I > Br > Cl, as judged by conversion of starting material. The observation of halogen exchange side products is noted in Entries 4 and 5, where significant formation of 4-bromoanisole was found. The presence of halogen exchange products could be related to an aromatic halogen exchange reaction, under similar conditions to that which Buchwald reported in 2002.[19]
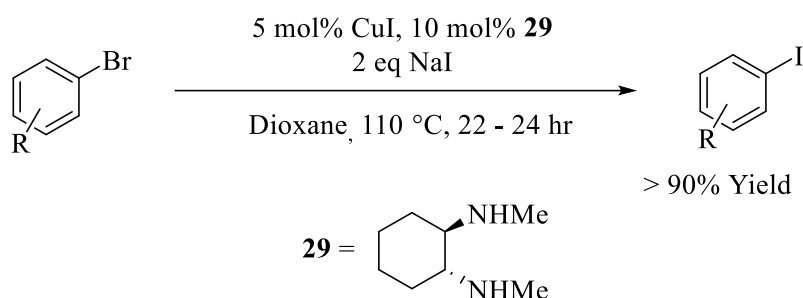
Scheme 4.8 – Copper-catalysed aromatic Finkelstein reaction reported by Buchwald.[19]

Although the reported reaction proceeds from aryl bromide to iodide, opposite to what was observed in this work, the pathway for halogen exchange from a copper iodide intermediate may be more favourable at high [NaBr]. The reaction would consequently reduce in rate due to the lower reactivity of the aryl bromide. Perhaps more likely is a reaction similar to that reported by Bacon,[20] in which under less similar conditions, aryl iodides have shown to be transformed to aryl bromides in DMF, at 153 °C with a Cu_2O additive.

Interestingly, the addition of 1.5 eq of 15-crown-5 to the reaction with NaI improved the yield drastically, giving 78 % conversion to product after 16 hours. Crown ethers have an affinity for cations, such as sodium, and it may be expected that inclusion of 15-crown-5 to the reaction would prevent interaction of sodium with the substrates and catalyst. The added iodide anion would therefore be more available for reaction and greater inhibition of the *N*-arylation was predicted. As the opposite of this is observed, it is possible that either the cation alone, or both sodium and iodide are the source of the inhibition.

A further experiment, looking at the effect of the addition of the larger 18-crown-6 shows the increase in conversion to product when using K_2CO_3 with no halide salt additive (Scheme 4.9). 18-Crown-6 was used due to its larger pore size and selectivity for the potassium anion, leading to improved solubility of the inorganic base and byproducts of the reaction. An alternative explanation for the increased reactivity in the *N*-arylation reactions which use crown ethers is that they change the copper speciation during the reaction. Aqueous KI, copper iodide and potassium crown ethers have previously shown to result in novel cluster formation when crystallised, indicating a possible influence on the solution behaviour.[21]
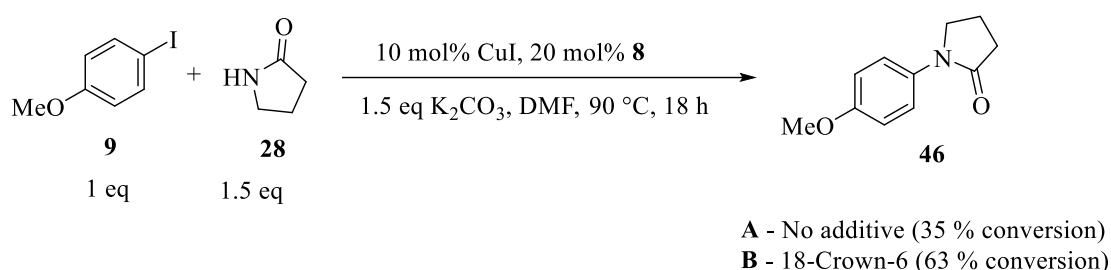
Scheme 4.9 - *N*-arylation of **28** with K_2CO_3 with and without crown ether.

4.3.1. Synthesis of a Cu(II) complex bearing a Cu-I-Cs motif

Probing further into the nature of the interactions between cations, anions and catalytic species, synthesis and analysis of catalytic intermediates were attempted. Under reaction conditions, CuI, **8** and Cs_2CO_3 were stirred in anhydrous DMF under N_2, the resulting blue solution was layered with THF : Et_2O (1 : 4) to yield crystals of **72** (Scheme 4.10) as blue monoclinic blocks. The formation of **72** occurred with the precipitation of an insoluble dark brown solid, assumed to be metallic Cu(O), indicating a disproportionation from Cu(I)-iodide.
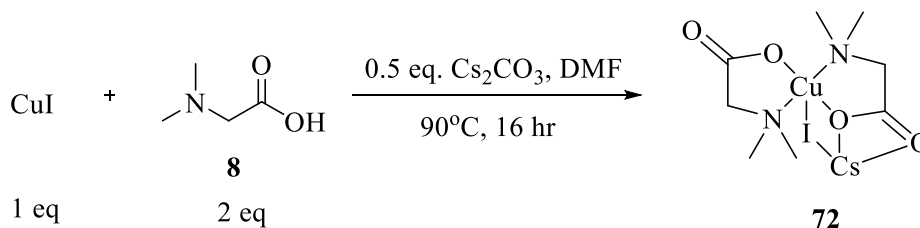
Scheme 4.10 – Synthesis of Cu-I-Cs complex **72** from CuI, **8** and Cs_2CO_3.

The complex exists as a penta-coordinate complex, with two ligands bound in a *trans*-orientation, with an axial iodide occupying the fifth coordination position. The coordination geometry around Cu is similar to that seen in **71**, with the iodide in place of H_2O. The Cu(1)-I(1) bond distance of 2.904(6) Å is much larger than the Cu-OH_2 distance in **71** (2.270 Å), and is also larger than the literature quoted value of ~ 2.6 Å.[22] The Cu-I bond distance is still significantly shorter than the sum of the Van Der Waals radii for Cu and I (3.38 Å). The Cs(1)-I(1) bond distance was measured to be 2.965 Å, within the range expected from the literature.[23, 24] Cs(1) and Cs(2) are crystallographically inequivalent, half of each Cs is found in the unit cell, being linked to the copper *via* a bridging iodide.
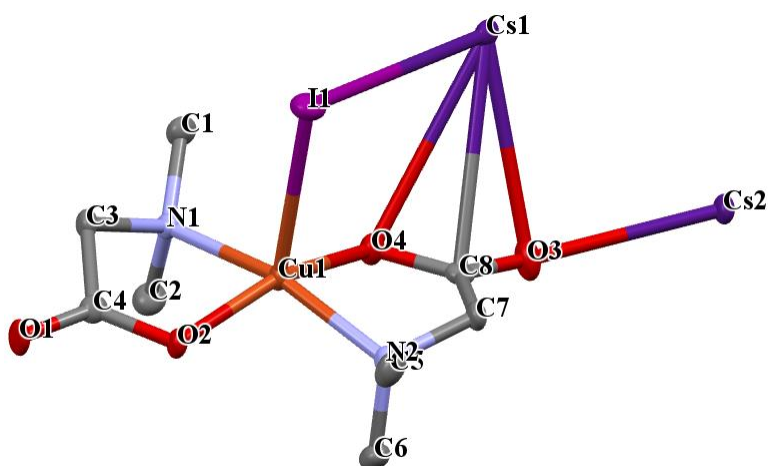
Figure 4.15 – Molecular structure of **72**. Atomic displacement parameters are drawn at the 50 % level, hydrogen atoms have been omitted for clarity.

The stability of the complex in the solid state appears to be a result of the extensive coordination around the Cs atoms, with numerous interactions with the ligand atoms. Cs(1) is coordinated to four CuL_2 units, two through the CO_2^- and iodide groups and two through the carbonyl oxygen (Figure 4.16). Cs(2) on the other hand coordinates to six CuL_2 units, four through the terminal oxygen atoms of the carboxylate and two further through the iodine groups. To understand whether the CsI motif remains coordinated to the Cu(II)-complex in solution, [133]Cs was used, with a similar setup to that described in Figure 4.14.
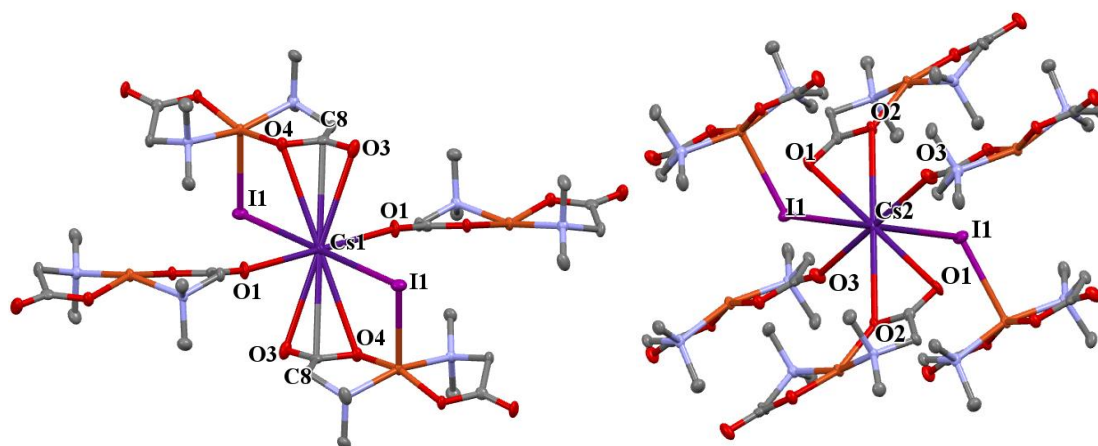
Figure 4.16 - Coordination environments of the two inequivalent Cs atoms in **72.**

The ^{133}Cs NMR spectra in Figure 4.17 are able to show that the complex and CsI have distinguishable chemical shifts, giving evidence that the CsI motif in the complex does not dissociate to give free CsI and a CuL$_2$ complex. When the spectrum of CsI and the complex mixture was recorded, both peaks shifted together and broadened, possibly a result of exchange between the complex and free CsI. An additional experiment was performed to prove the presence of Cu(II) with CsI does not cause the different signals seen for the complex and CsI (Figure 4.18Figure 4.17).
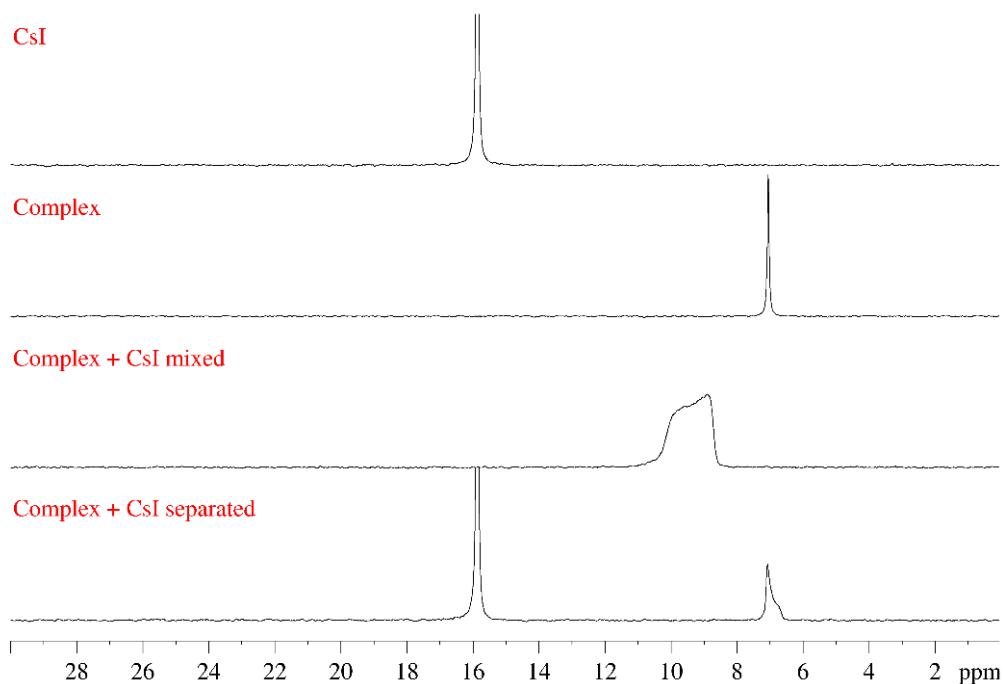
Figure 4.17 - ^{133}Cs NMR of cesium iodide and **72** combinations in *d$_7$*-DMF (66 MHz.
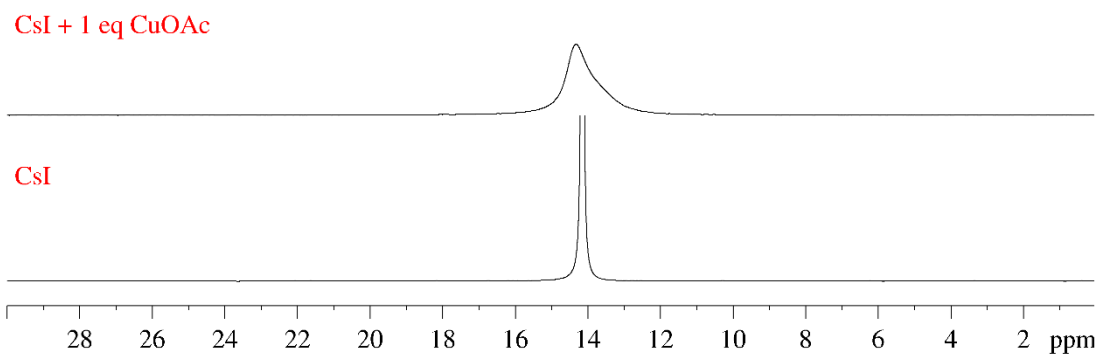
Figure 4.18 - ^{133}Cs NMR (d_7-DMF) of pure CsI and CsI with 1 eq of CuOAc added.

Catalytic competence of the complex was assessed by subjecting the catalyst to reaction conditions for the reaction previously shown to work well (Scheme 4.11). After 16 hours, no product was seen to have formed by ^{1}H NMR spectroscopy or GC/MS. The lack of turnover in the reaction is likely due to the complex existing in the Cu(II) oxidation state, where reduction to Cu(I) is expected to be needed to enter the catalytic cycle. It is also possible that the CsI provides a deactivating effect on the catalyst, preventing coordination and reaction with the substrates.
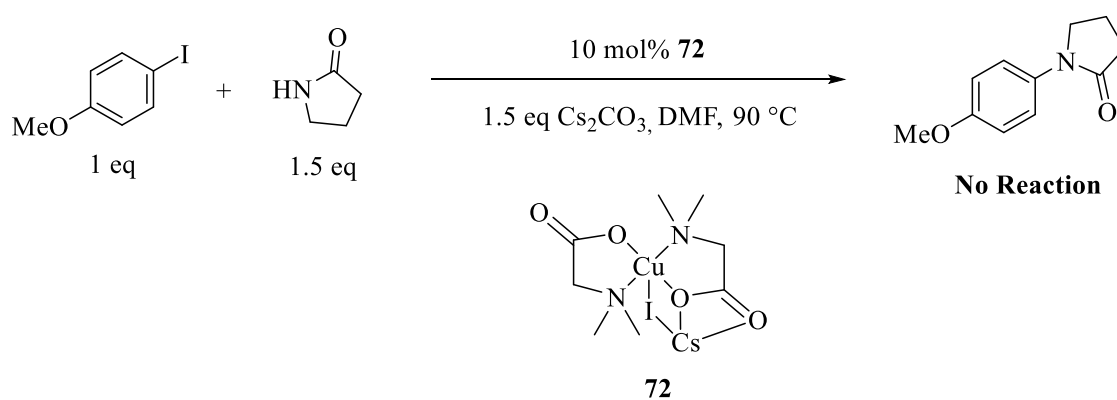
Scheme 4.11 – Catalytic testing of **72** in the C-N coupling between **9** and **28**.

This complex may provide insight into the halide inhibition that was seen when adding halide salts into the copper-catalysed systems. The coordination of the halogen salts to the copper centre in a fashion similar to that seen with **72** could explain the poor reactivity. Further examples of the Cu-I-Cs motif seen in **72** were sought, including attempts with the diketone ligand **13**, and another amino acid *L*-proline **(12)**. Subjecting **13** to the same synthesis as was used with **8** yielded complex **73** (Scheme 4.12), a Cu(II) complex adopting a square planar geometry with two O,O-donor ligands (Figure 4.19).
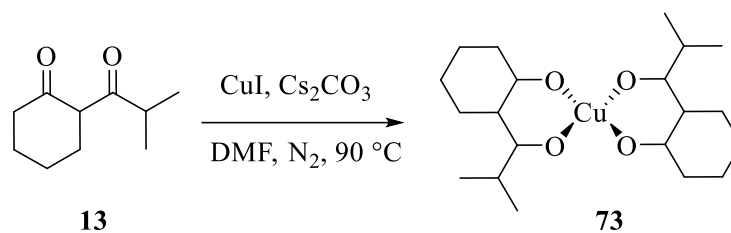
Scheme 4.12 - Conditions for the synthesis of Cu(II) complex **73**
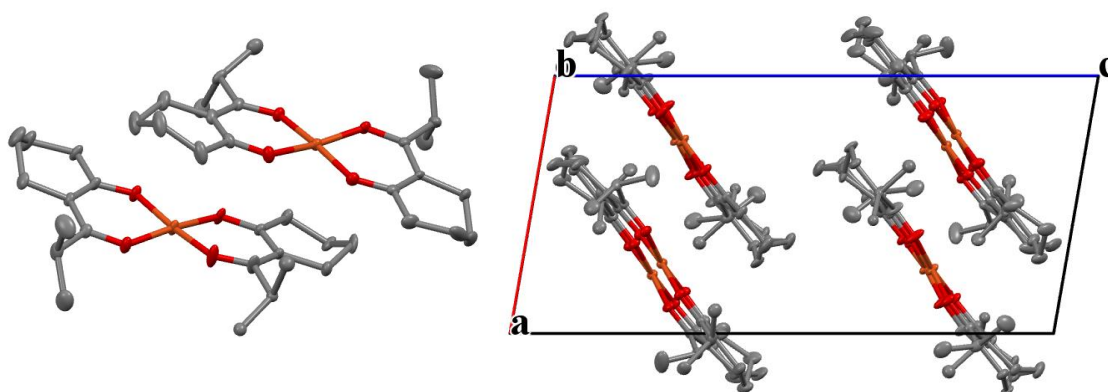

Figure 4.19 – Molecular structure of **73**. Atomic displacement parameters are drawn at the 50 % level, hydrogen atoms have been omitted for clarity. **A)** Asymmetric unit. **B)** Crystal packing, visualised along the crystallographic b axis.

Attempts to crystallise the complex formed with *L*-proline proved unsuccessful with no crystal structure obtained. HRMS analysis of the reaction mixture did give evidence for a species with the molecular mass corresponding to $C_{10}H_{16}CsCuIN_2O_4$, the expected neutral formula for the species **74** (Figure 4.20).
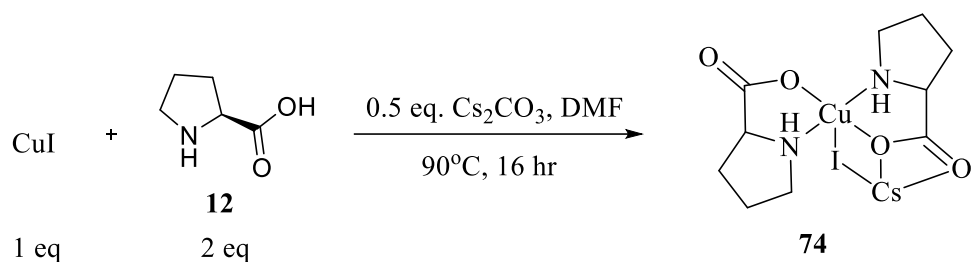
m/z (M + H$^+$) = 551.8578 (100.0 %), 553.8560 (44.6 %)

m/z + (M + Na$^+$) = 573.8398 (100.0 %), 575.8380 (44.6 %)
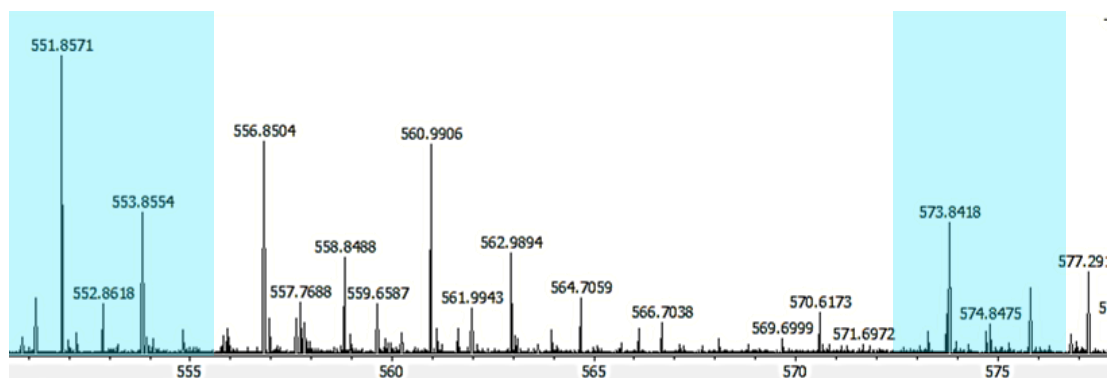
Figure 4.20 – (Above) Conditions attempted in formation of a (L$_2$Cu)I-Cs species (**74**) where L = *L*-proline. (Below) HRMS evidence for the formation of a species with the molecular formula C$_{10}$H$_{16}$CsCuIN$_2$O$_4$.

4.4. Investigating a heterogeneous catalyst

With evidence of an interaction between copper and cesium salts, and extraction of copper from solution onto the surface of the cesium bases, a significant question is raised of the homogeneity of the active catalyst. Heterogeneous copper systems for Ullmann-type couplings have been reported and shown to be useful, particularly with Cu(0) nanoparticles.[25-28] The reactions which use a CuI precursor and organic ligands are however expected to undergo homogeneous catalysis.

4.4.1. Hot filtrations

Investigation into the heterogeneity of the copper species is complicated by the dilution of any heterogeneous copper by the much larger quantity of solid cesium salts. An experiment was designed to explore whether the solution-based copper is catalytically active. This was done by a "hot filtration", using two B19 QuickFit Schlenk flasks which were connected *via* a sinter filter with two male joints on either side (Figure 4.21).
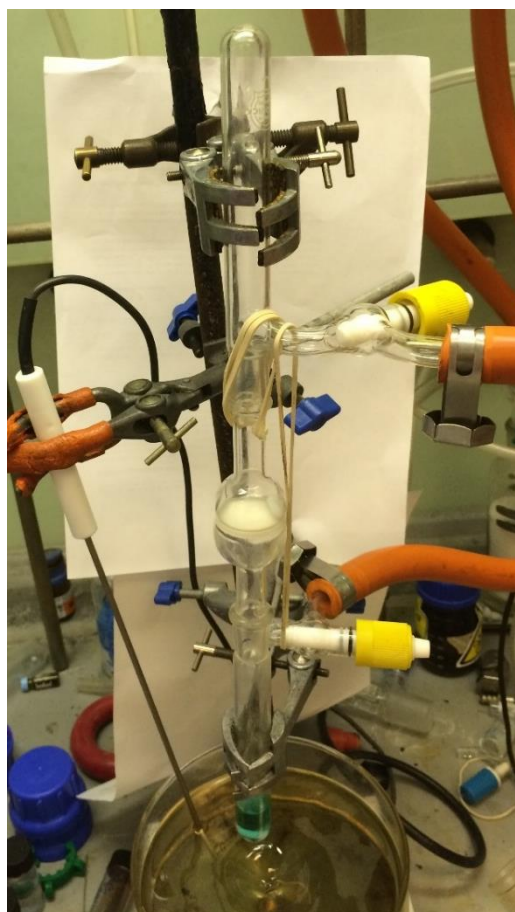
Figure 4.21 - Reaction set-up for hot filtration reactions.

The air stability of the filtration was ensured with a test reaction, shown in Scheme 4.13. In this experiment, the catalyst was allowed to form for 10 minutes at 90 °C with only enough Cs_2CO_3 to deprotonate the ligand. The reaction was initiated by filtration to the second Schlenk flask, containing the aryl halide and the rest of the Cs_2CO_3. The 58 % conversion to product shows that the filtration technique used does not kill the catalyst. Filtration after 10 minutes was intended to prevent the formation of the Cu/Cs precipitate, however a small amount of this was seen.
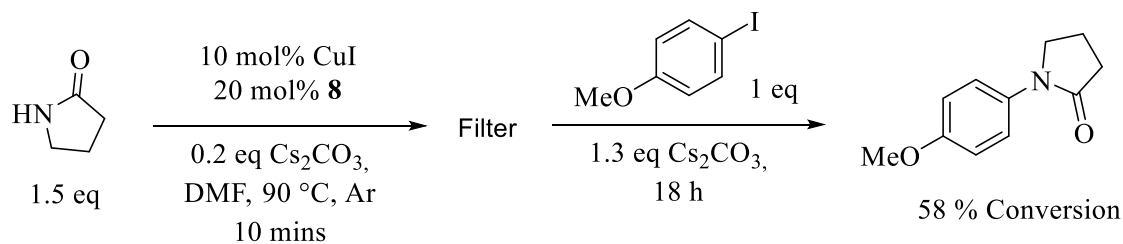
Scheme 4.13 - Reaction conditions for catalyst stability during hot filtration procedure.

If the active catalytic species remains in solution for the duration of the reaction, it was believed that the reaction would proceed following filtration. However, due to the limited solubility of Cs_2CO_3, the conversions may be limited by the amount of base in solution following the filtration.

Table 4.6 – Hot filtration experiment conditions. All reactions performed on 0.1 mmol ArI scale in 5 mL DMF.
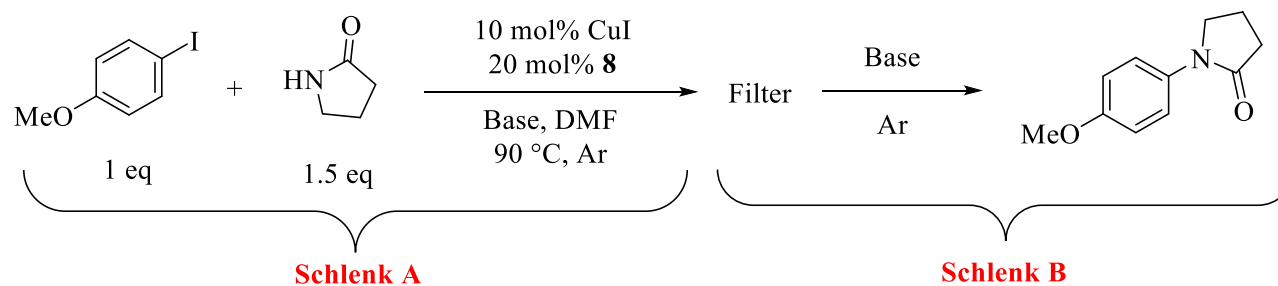
Entry	Schlenk A	Schlenk B	Filtration time	Conversion % (filtration)	End point	Conversion % (end)
1	CuI, **8**, **28**, **9**, Cs_2CO_3 (1.5 eq)	N/A	129 mins	48	19 hours	51
2	CuI, **8**, **28**, **9**, Cs_2CO_3 (1.5 eq)	N/A	33 mins	18	19 hours	25
3	CuI, **8**, **28**, **9**, Cs_2CO_3 (1.5 eq)	N/A	N/A	N/A	33 mins	19
4	CuI, **8**, **28**, **9**, Cs_2CO_3 (1.5 eq)	Cs_2CO_3 (1 eq)	30 mins	20	18 hours	50
5	CuI, **8**, **28**, **9**, K_2CO_3 (1.5 eq)	N/A	107 mins	21	217 mins	25

The full reaction was allowed to run in Schlenk A in the experiment detailed in Table 4.6. The results of the hot filtrations are able to show that some copper remains in solution and is able to catalyse the C-N coupling reaction after filtration. Reactions which were filtered and allowed to react without any added Cs_2CO_3 showed limited conversions from the time of filtration to the end point (Entries 1 and 2). It is apparent from comparing Entries 2 and 4, where addition of added Cs_2CO_3 to Schlenk 2 is explored, that this is a result of too little Cs_2CO_3 in solution during filtration, agreeing well with the poor Cs_2CO_3 solubility previously discussed. The reaction in Entry 5 compares Cs_2CO_3 with K_2CO_3 and whilst did not show a change in colour of the solid K_2CO_3 after 107 minutes. This indicates no Cu adsorption onto the base, however the poor solubility of K_2CO_3 still prevented significant further conversion.

The questions which remain unanswered from this experiment surround the nature of the active catalyst. Whilst there is enough copper in solution to promote the reactions following filtration, the solid Cs_2CO_3 in Schlenk B (Entry 4) became coloured over time and so it is not possible to rule out a scenario in which adsorbed Cu is performing the catalysis. It is also difficult to determine the amount of copper in solution during these reactions, use of further AAS analysis would perhaps provide quantification of this.

4.4.2. Reactions with pre-formed Cu/Cs precipitate

A final experiment was conducted in attempts to determine whether the copper precipitated from the reactions is still in an active state. The reaction outlined in Scheme 4.14 was performed, in which the mixture of CuI, ligand and Cs_2CO_3 caused formation of a dark purple solid when heated for 30 minutes, after a dark purple solution was initially formed. Removal of as much colourless solution as possible by syringe was followed by addition of a solution of organic reagents and reaction for 20 hours.
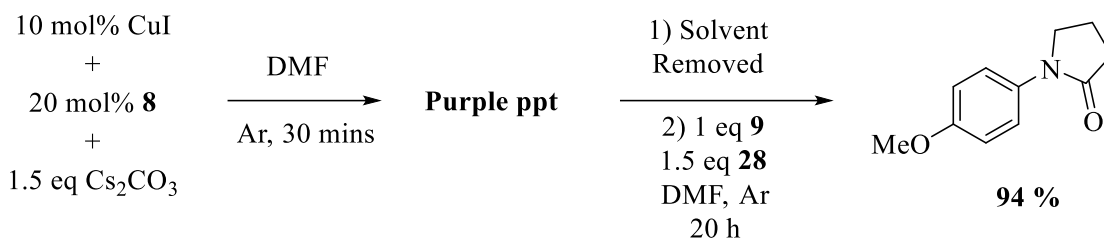
Scheme 4.14 - Procedure for preparation of Cu/Cs precipitate and use in C-N coupling reaction in the presence of ligand.
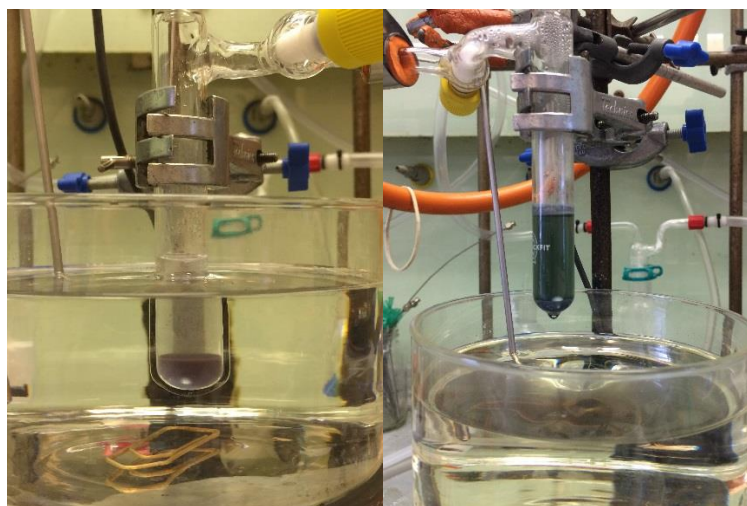
Figure 4.22 – Images taken of the reaction outlined in Scheme 4.14, taken at 30 minutes (left) and 20 hours (right).

Although the removal of all of the solution after 30 minutes proved difficult, only the wet solid remained. If 90 % of the solution was removed, and all copper was in solution, only 1 mol% copper would remain, which is unlikely to be sufficient to give the almost full conversion seen. The appearance of the reaction in Figure 4.22 after 20 hours indicates that the copper has leached back in to solution, which may be the source of the catalytic activity. A further reaction was performed with no ligand present, as it was expected that the ligand free reaction would not convert (Scheme 4.15). This reaction is shown in Figure 4.23 after 30 minutes, where a yellow precipitate is formed, and 20 hours, where it still appears as though no copper remains in solution. Given that turnover is still observed in these experiments, the Cs_2CO_3 which is likely "coated" in this copper species can still act as a base throughout the reaction.
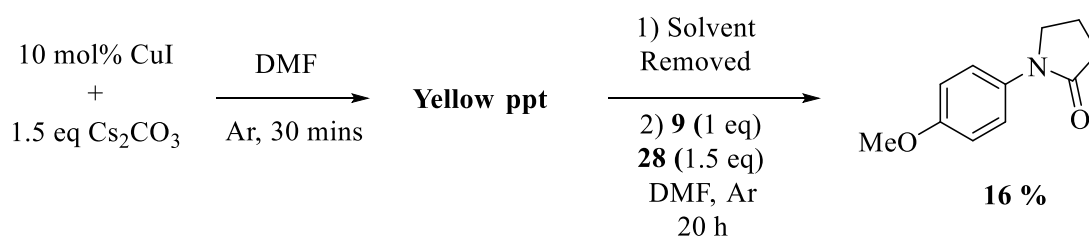
Scheme 4.15 - Procedure for preparation of Cu/Cs precipitate and use in C-N coupling reaction without the presence of ligand.
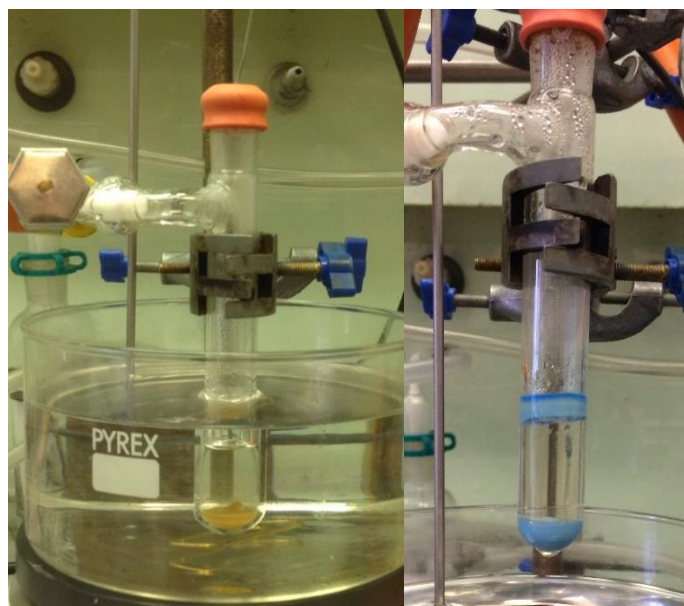
Figure 4.23 – Images taken of the reaction outlined in Scheme 4.15, taken at 30 minutes (left) and 20 hours (right).

The implication of this experiment is that the coloured precipitate which is seen to form during the copper-catalysed C-N coupling reactions using Cs_2CO_3 may be a source of active catalyst. The high conversion obtained when ligands is present, combined with the observation that the removed solution did not oxidise, indicates little or no copper remains in solution at this point. Whilst the hot filtration experiments in Section 4.4.1. indicate that active copper remains in solution for the duration of the experiment, the influence of the amide substrate may stabilise the catalyst in solution, preventing interaction with the cesium base.

Interestingly, it appears that having an excess of Cs_2CO_3 has a large effect on the interaction between copper and cesium, as when the reaction in Scheme 4.14 is performed with a 1 : 2 : 1 ratio of CuI : **8** : Cs_2CO_3, a blue solution, with red/brown precipitate is formed, as in the synthesis of **72**. This stability was assessed further through an experiment conducted similarly to that in Scheme 4.14, except isolation of the solid precipitate was performed after washing the precipitate three times with anhydrous MeCN. 450 mg solid was obtained from this procedure and weighed out in air, this equates to 85 % of the solids which were put into the reaction (489 mg Cs_2CO_3, 19 mg CuI and 21 mg **8**). The solid was put into a Schlenk flask and a solution of **9** and **28** added under argon. Stirring for 17 hours at 90 °C gave 22 % conversion of the aryl iodide to the product.
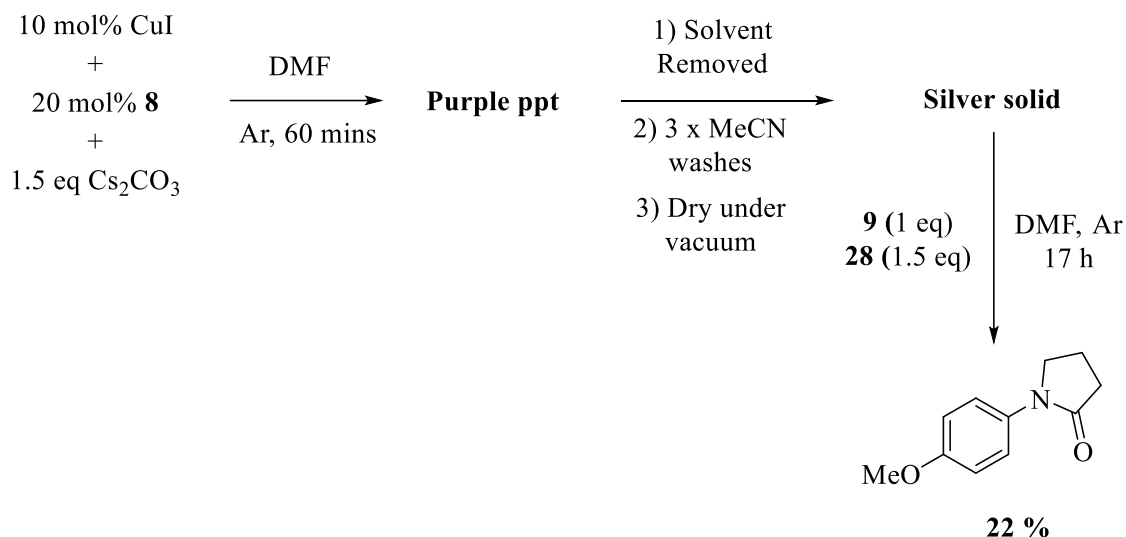
Scheme 4.16 - Procedure for preparation of Cu/Cs/**8** precipitate, isolation in air and use in C-N coupling reaction.

The ability of the isolated solid, to act as catalyst and base for the reaction introduces a possibility for air-stable catalytic precursor. Further work is necessary to understand whether the copper is "coating" the Cs_2CO_3, or a more complex matrix is formed, stabilising the Cu(I) from disproportionation to the Cu(II) complex **72**. Kinetic experiments and reaction optimisation will provide insight into the nature of the precipitate, and the role of cesium in the formation of it.

4.5. Summary and Conclusions

A variety of deactivation and inhibition pathways in the copper-catalysed C-N bond formation have been assessed using ^{1}H and ^{133}Cs NMR, EPR and atomic absorption spectroscopies, powder and single crystal X-ray diffraction analysis, SEM and EDX. The formation of a number of Cu(II) complexes of the type CuL_2 have been observed from reactions with Cu(I) salts, however EPR spectroscopy under turnover conditions showed that Cu(II) initially formed in solution quickly disappears upon heating. Despite this, without the presence of substrates, the Cu(II) signal in EPR does not disappear and so the substrates may be necessary to stabilise the Cu(I) species.

Precipitation of copper during turnover has been observed under numerous conditions and through the use of EDX, it is confirmed that interactions between the Cu species and Cs salts used in catalysis removes copper from solution. Under turnover conditions, AAS showed that a large proportion of copper remains in solution, whilst only very little cesium is in solution at any point. This poor solubility of Cs-salts was explored with ^{133}Cs NMR showing that at 90 °C, CsI has a much higher solubility than Cs_2CO_3. This has a negative impact on the reactivity in copper catalysis due to the inhibition effect which was seen when various halide salts were introduced to the reaction conditions. A combination of competitive halogen exchange and solubility may be the cause for this inhibition, although the use of crown ethers can improve reactivity.

It is possible that the interaction of the halide salts with the copper species can prevent formation of active catalyst, or encourage the formation of a Cu(II) complex such as the novel isolated Cu-I-Cs complex **72**. The formation of this complex may provide insight into the effect of various cations in catalysis, where coordination of the cation could have stabilisation or promoting effects in the catalytic cycle. Although the complex was shown to be catalytically inactive, formation of a similar complex whilst preventing the oxidation to Cu(II) may be possible with further work.

The complex interactions between copper and base led to investigations of the homogeneity of the active catalyst. Hot filtration experiments showed that despite the precipitation of copper, active copper does remain in solution. Alternatively, experiments in pre-forming a Cu/Cs species showed that the precipitated copper may

also be a source of active catalyst. It is therefore likely that exchange between copper in and out of solution is occurring on a reaction timescale when using Cs_2CO_3.

4.6. References

1. S. Sung, D. Sale, D.C. Braddock, A. Armstrong, C. Brennan and R.P. Davies, *ACS Catal.*, 2016, **6**, 3965-3974.

2. C. Sambiagio, R.H. Munday, S.P. Marsden, A.J. Blacker and P.C. McGowan, *Chem. Eur. J.*, 2014, **20**, 17606-17615.

3. C. He, G.H. Zhang, J. Ke, H. Zhang, J.T. Miller, A.J. Kropf and A.W. Lei, *J. Am. Chem. Soc.*, 2013, **135**, 488-493.

4. H. Weingarten, *J. Org. Chem.*, 1964, **29**, 3624-3626.

5. R. Cano, A.F. Schmidt and G.P. McGlacken, *Chem. Sci.*, 2015, **6**, 5338-5346.

6. D.A. Conlon, B. Pipik, S. Ferdinand, C.R. LeBlond, J.R. Sowa, B. Izzo, P. Collins, G.J. Ho, J.M. Williams, Y.J. Shi and Y.K. Sun, *Adv. Synth. Catal.*, 2003, **345**, 931-935.

7. P.J. Ellis, I.J.S. Fairlamb, S.F.J. Hackett, K. Wilson and A.F. Lee, *Angew. Chem. Int. Ed.*, 2010, **49**, 1820-1824.

8. A.J. Reay and I.J.S. Fairlamb, *Chem. Commun.*, 2015, **51**, 16289-16307.

9. I.J.S. Fairlamb and A.F. Lee, '*Fundamental Pd-0/Pd-II Redox Steps in Cross-coupling Reactions: Homogeneous, Hybrid Homogeneous-Heterogeneous to Heterogeneous Mechanistic Pathways for C-C Couplings*' Royal Society of Chemistry, United Kingdom, 2013, vol. 11.

10. R.H. Crabtree, *Chem. Rev.*, 2012, **112**, 1536-1554.

11. M. Parisien, D. Valette and K. Fagnou, *J. Org. Chem.*, 2005, **70**, 7578-7584.

12. D.S. Marlin, M.M. Olmstead and P.K. Mascharak, *Inorg. Chem.*, 2001, **40**, 7003-7008.

13. A.W. Addison, T.N. Rao, J. Reedijk, J. Vanrijn and G.C. Verschoor, *J. Chem. Soc., Dalton Trans.*, 1984, 1349-1356.

14. M. Kondo and M. Kubo, *J. Phys. Chem.*, 1958, **62**, 468-469.

15. J.D. Satterlee, *Concepts Magn. Reson.*, 1990, **2**, 119-129.

16. G. Dijkstra, W.H. Kruizinga and R.M. Kellogg, *J. Org. Chem.*, 1987, **52**, 4230-4234.

17. L.L. Soong, G.E. Leroi and A.I. Popov, *Inorg. Chem.*, 1990, **29**, 1366-1370.

18. W.J. Dewitte, R.C. Schoening and A.I. Popov, *Inorg. Nucl. Chem. Lett.*, 1976, **12**, 251-253.

19. A. Klapars and S.L. Buchwald, *J. Am. Chem. Soc.*, 2002, **124**, 14844-14845.

20.   R.G.R. Bacon and H.A.O. Hill, *J. Chem. Soc.*, 1964, 1108-&.

21.   N.P. Rath and E.M. Holt, *J. Chem. Soc., Chem. Commun.*, 1985, 665-667.

22.   A.G. Orpen, L. Brammer, F.H. Allen, O. Kennard, D.G. Watson and R. Taylor, *J. Chem. Soc., Dalton Trans.*, 1989, S1-S83.

23.   I.M. Muller and W.S. Sheldrick, *Z. Anorg. Allg. Chem.*, 1999, **625**, 443-448.

24.   M. Heller and W.S. Sheldrick, *Z. Anorg. Allg. Chem.*, 2003, **629**, 1589-1595.

25.   S. Jammi, S. Sakthivel, L. Rout, T. Mukherjee, S. Mandal, R. Mitra, P. Saha and T. Punniyamurthy, *J. Org. Chem.*, 2009, **74**, 1971-1976.

26.   J. Mondal, A. Biswas, S. Chiba and Y.L. Zhao, *Sci. Rep.*, 2015, **5**.

27.   L. Rout, T.K. Sen and T. Punniyamurthy, *Angew. Chem. Int. Ed.*, 2007, **46**, 5583-5586.

28.   Y. Isomura, T. Narushima, H. Kawasaki, T. Yonezawa and Y. Obora, *Chem. Commun.*, 2012, **48**, 3784-3786.

Chapter 5

XAS studies of an immobilised iridium transfer hydrogenation catalyst

---

5.1. Introduction

5.1.1. Transfer hydrogenation

The hydrogenation of organic compounds is a vital synthetic transformation in both research and industry. Heterogeneous catalysts such as palladium on carbon (Pd/C) are widely used for the hydrogenation of organic compounds under pressurised H_2. Whilst Pd/C is the most widely used catalyst for hydrogenation, it suffers from poor selectivity due to its high catalytic efficiency and the use of pressurised H_2 requires specialist equipment.[1]

A powerful alternative which avoids these issues is that of transfer hydrogenations; in which hydrogen atoms are supplied by a proton donor (Scheme 5.1). Transfer hydrogenations typically require transition metal catalysts, which can be tailored to provide greater chemo- and regiospecificity than that which is achievable by classic hydrogenation systems. The use of a simple alcohol or amine proton donors in these reactions such as 2-propanol (^{i}PrOH) is desirable due to the low cost and toxicity, whilst the resulting byproducts are often easy to remove.[2]
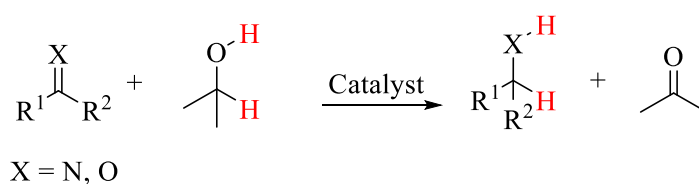
Scheme 5.1 - Simple transfer hydrogenation using ^{i}PrOH as a hydrogen donor.

Research into asymmetric hydrogenation catalysts by Knowles and Noyori led to the award of the Nobel Prize for chemistry in 2001. Noyori developed various chiral ruthenium complexes, with C_2-symmetry chiral ligands, as well as iridium complexes, giving very good yields an ee values in the asymmetric reduction of ketones.[3-6] Enantioselectivity can often be controlled through the choice of chiral ligands, for

example, Scheme 5.2 shows the asymmetric transfer hydrogenation of an acetophenone derivative to give the (*R*)-alcohol (**R-76**) in 99% yield with 95% ee using catalyst **77**,[6] whilst catalyst **78** gives the (*S*)-alcohol (**S-76**) in 98% yield with 98 ee.[4]
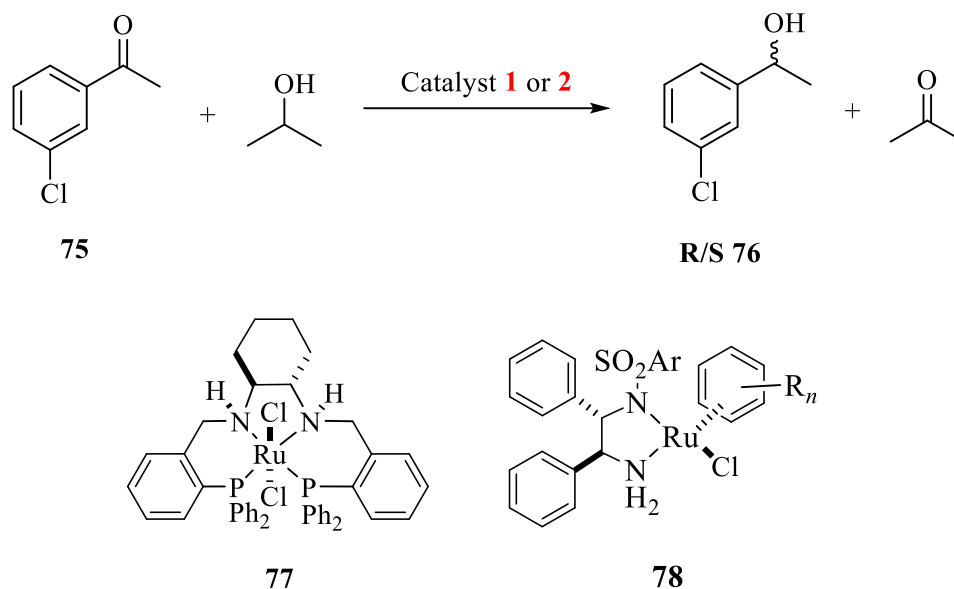
Scheme 5.2 – Hydrogenation of *m*-chloroacetophenone using ruthenium catalysts **77** and **78** to give different steroisomers.

5.1.2. Catalyst immobilisation

Metals such as palladium, iridium, ruthenium and rhodium offer wide applications in homogeneous catalysis. Transition metal complexes of these elements have been widely investigated and combined with intelligent ligand design can give high turnover numbers (TON) and turnover frequencies (TOF). The structures of many highly active catalysts are complex or use large, chiral ligands (Figure 5.1). Development of processes involving these catalysts in industry often focusses on minimising catalyst loading and maximising TONs.[7] This is a consequence of the cost associated with using these precious metals, whilst the "designer" ligands which may be necessary to improve reactivity can also be time consuming and expensive to synthesise.[7]

79   **80**
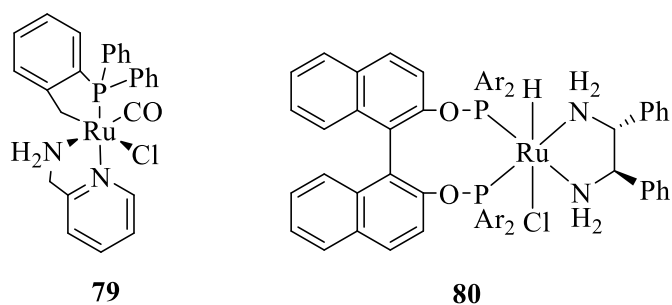
Figure 5.1 – Ruthenium catalysts developed for highly effective transfer hydrogenations of ketones.[8, 9]

Use of precious metal catalysts in industrial processes can also cause issues downstream, where the presence of residual metals may hinder reactivity or produce side products in further reactions. Guidelines for the acceptable levels of precious metals in active pharmaceutical ingredients (APIs) are also strict, so added processes such as the use of expensive metal scavengers are often required to adhere to these guidelines.[10]

Immobilisation methods for homogeneous catalysts provide a useful strategy in modern synthetic science to facilitate catalyst recovery and reuse, for example, the silica-immobilised TsDPEN ligand shown in Scheme 5.3 used in the Ru-catalysed enantioselective hydrogenation of aryl ketones.[11] The recycling of catalysts can reduce the cost of application of these often complex and sophisticated catalysts, particularly when precious metals are used.

81
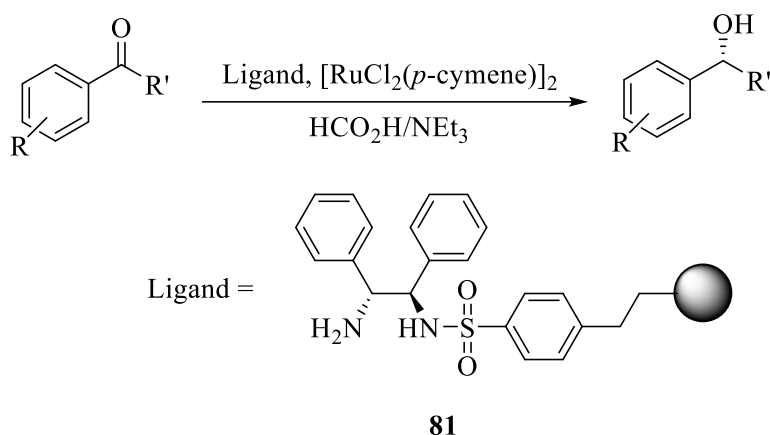
Scheme 5.3 – Chiral Ru-TsDPEN derived catalyst (**81**), immobilised onto amorphous silica gel for use up to 10 times in transfer hydrogenation reactions.[11]

Most immobilisation technology, however, is developed with limited understanding of the molecular behaviour, due to a lack of suitable and effective characterisation

techniques once the catalyst is immobilised. It can be expected that the behaviour of the catalyst will change upon immobilisation, through either interaction with the solid support or a change in the most facile catalytic pathways. Typically, activity and selectivity of the immobilised catalyst is negatively affected by the solid-support.[12] Often, this is a result of steric hinderance from the polymeric support, which prevents diffusion of the substrate through the catalyst.[7] The ability of a catalyst to undergo ligand exchange, substrate binding and dissociation of products is important to turnover, if these are limited by the polymeric support, activity of the catalyst is hindered.

5.1.3. A recyclable transfer-hydrogenation catalyst

Following on initial work on the immobilisation of cyclopentadiene ligands onto polymeric support,[13] in 2013, McGowan reported a method of immobilising group 9 metals onto a polystyrene support, Wang resin.[14] The work showcases the tethering of iridium and rhodium catalysts through a hydroxyl-group, whilst most examples reported for immobilisation of Noyori-type transfer hydrogenation catalysts do so through a diamine ligand, much like that shown in Scheme 5.3.[11, 15, 16] The strategy utilised for tethering the metal through hydroxyl groups was shown to be effective for various alkyl chain length and both iridium and rhodium (Scheme 5.4). It was proposed that by tethering by a covalent C-O bond, the metal would be resistant to leaching from the support, and the electronic properties of the ligand could still be controlled through ligand design. Although characterisation of the final catalysts was difficult, solid state ^{13}C $\{^1$H$\}$ NMR spectroscopy was utilised to confirm the presence of the Cp* ligand following immobilisation.

82a: M = Ir, n = 5
82b: M = Ir, n = 14
83a: M = Rh, n = 5
83b: M = Rh, n = 14

86a: M = Ir, n = 5
86b: M = Ir, n = 14
87a: M = Rh, n = 5
87b: M = Rh, n = 14
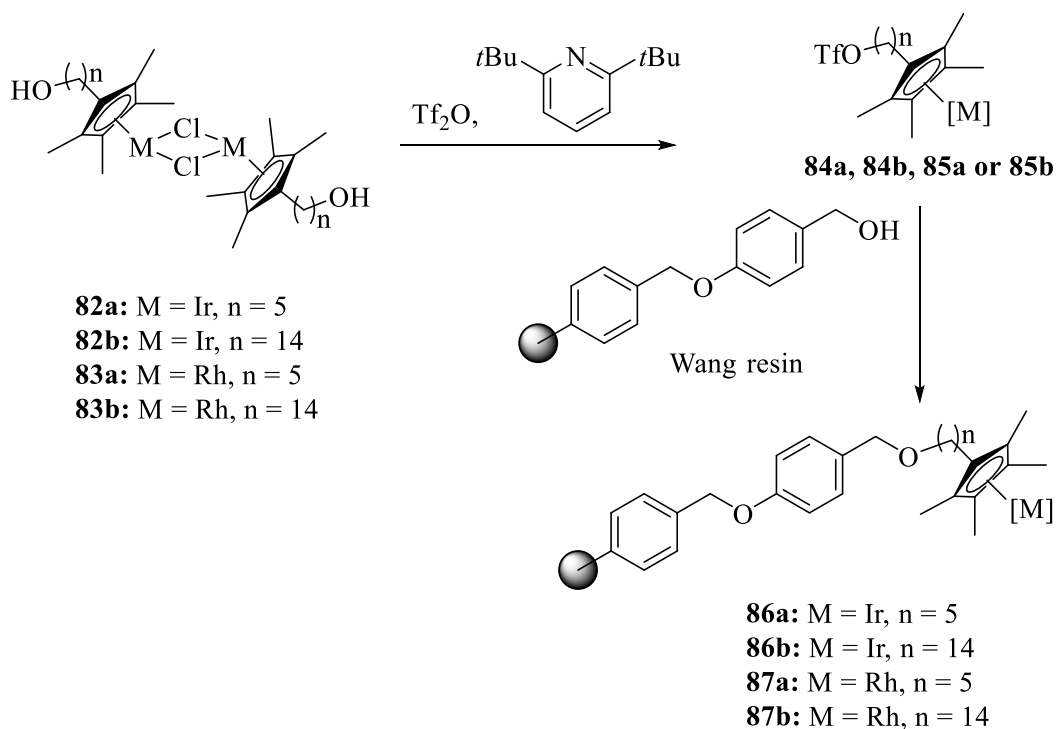
Scheme 5.4 - Immobilisation strategy reported by McGowan *et al.*[14]

The metal content and leaching of the resulting complexes was quantified by inductive coupled plasma (ICP) analysis. Two catalyst samples were subjected to consecutive washes with water, 1M HCl and MeOH at room temperature. One of the samples then underwent a protic wash (hot ^{i}PrOH) and the other a more aprotic wash (hot 1 : 1 DCM/^{i}PrOH, followed by room temperature acetone). ICP analysis showed a slight decrease in Ir content of the n = 5 complex from the protic wash (0.65 mmol g^{-1}) to the "aprotic" wash (0.61 mmol g^{-1}).

The catalytic competence of the different complexes was assessed in the transfer hydrogenation of benzadehyde (Table 5.1). It was found that stirring the catalyst with a catalytic quantity of KO^{t}Bu was necessary to induce full reactivity. Recycling of the catalyst was assessed by exposing the catalysts to the protic or aprotic washes detailed above and reusing the catalyst by adding in further substrates.

Table 5.1 - Catalytic screening of immobilised Ir and Rh catalysts in the transfer hydrogenation of benzealdehyde. Conversions after 24 hours.
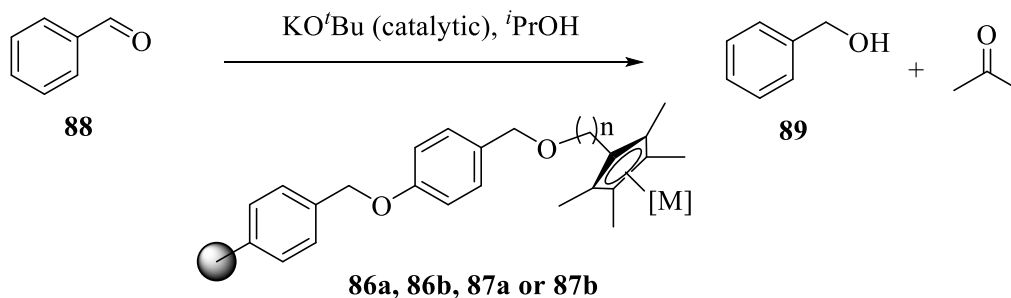
Entry	Catalyst	Wash regime	Conversion % (After 1 run)	Conversion % (After 3 runs)
1	**86a**	Protic	98	98
2	**86b**	Protic	>99	>99
3	**86a**	Aprotic	>99	>99
4	**87a**	Aprotic	60	43
5	**87b**	Aprotic	50	86
6	[RhCp*Cl$_2$]$_2$	Aprotic	97	-
7	[IrCp*Cl$_2$]$_2$	Aprotic	97	-

It was found in this study that the iridium catalysts all give comparable conversions after 24 hours to the standard [IrCp*Cl$_2$]$_2$ catalyst. The chain length of the irdium catalyst did not show a considerable change in reactivity (Entries 1 and 2), whilst the wash regime also did not affect reactivity significantly (Entry 3). It was however found that the rhodium catalysts (Entries 4 and 5) did not perform as well as the [RhCp*Cl$_2$]$_2$ or the analogous iridium catalysts. Recyclability was found to be extremely successful for both the n = 5 and 14 iridium catalysts after 3 runs, regardless of the wash regime used. Further recycling experiments showed that the catalyst was active for up to 26 uses, although it was found that after 20 uses, it became less efficient.

5.1.4. X-ray absorption spectroscopy (XAS) studies in catalysis

XAS, or XAFS (X-ray absorption fine structure) offers a useful tool throughout many areas of science, including geology, physics, biology and materials science, utilising synchrotron radiation to generate high-energy X-rays, which can be used to probe the state of a material or compound.[17, 18] XAFS has also found significant use in the field of catalysis, particularly with heterogeneous catalysts.[19] The technique benefits from the ability to tune the incident X-ray energy to specific elements, providing information on the local state of the desired element.

The XAFS spectrum consists of increase in signal intensity at the "edge" when the incoming X-ray has the same energy as the binding energy of a core electron. The absorbance of the X-ray and excitation of a photoelectron into an unbound state (continuum) causes a sharp rise in absorbance, referred to as the edge jump. This process, known as the photoelectric effect is represented in Figure 5.2.
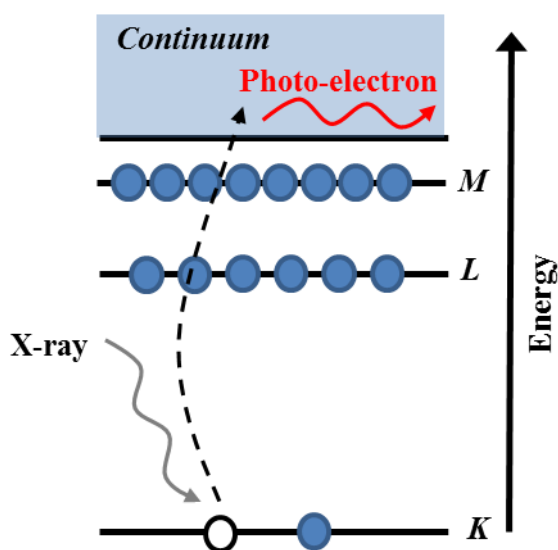
Figure 5.2 - Schematic representation of the photoelectic effect.

Figure 5.3 shows the scattering interactions which make up the spectra following the edge jump. Initially after the edge jump, the region of the spectrum known as the X-ray absorption near edge spectrum (XANES), this consists of numerous scattering interactions due to the low kinetic energy of the photoelectron. The EXAFS signal arises from the interference of the ejected photoelectron wave with the backscattered waves of surrounding atoms, causing constructive and destructive wave interference. This is

typically made up of single scattering contributions, and the scattered photoelectron returns directly to the excited atom[20]
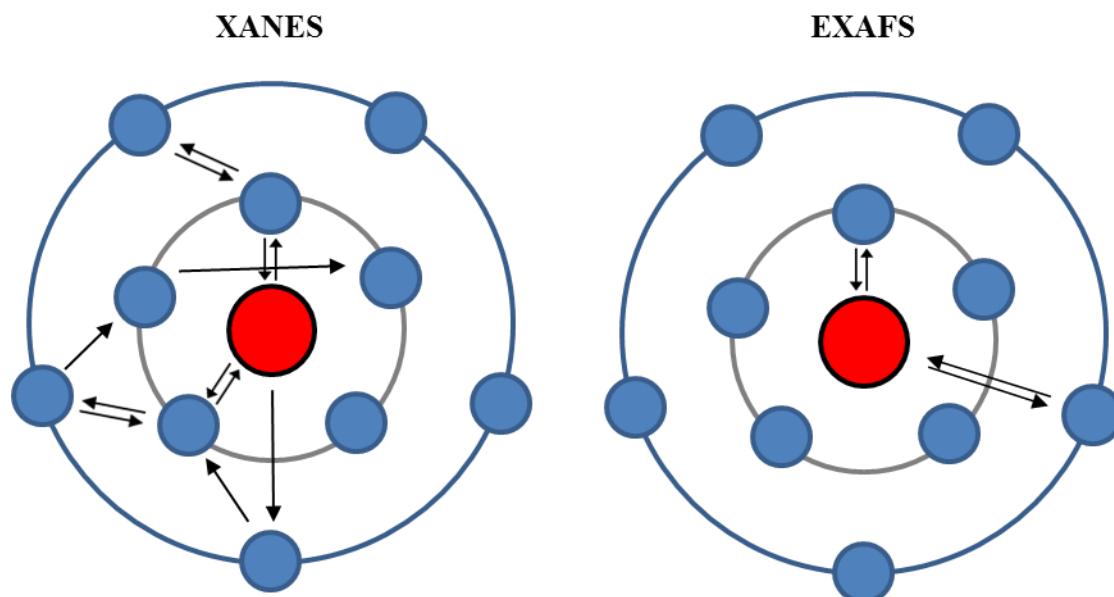
Figure 5.3 - Scattering of the ejected photoelectron which allows interpretation of XANES and EXAFS spectra. XANES spectra consists of multiple scattering interactions, whilst EXAFS is considered as single scattering contribution.

A typical XAFS spectrum is shown in Figure 5.4. In catalysis, the XANES region is often used to determine the formal oxidation state of the element and the coordination number of metals. The high-energy region of the spectrum is referred to as the X-ray absorption fine structure (EXAFS) region, typically extending for up to 1000 eV.[21] In chemistry, EXAFS is mainly utilised to provide highly accurate information into metal-ligand bond distances, as well as structural information about the ligands surround a metal centre.
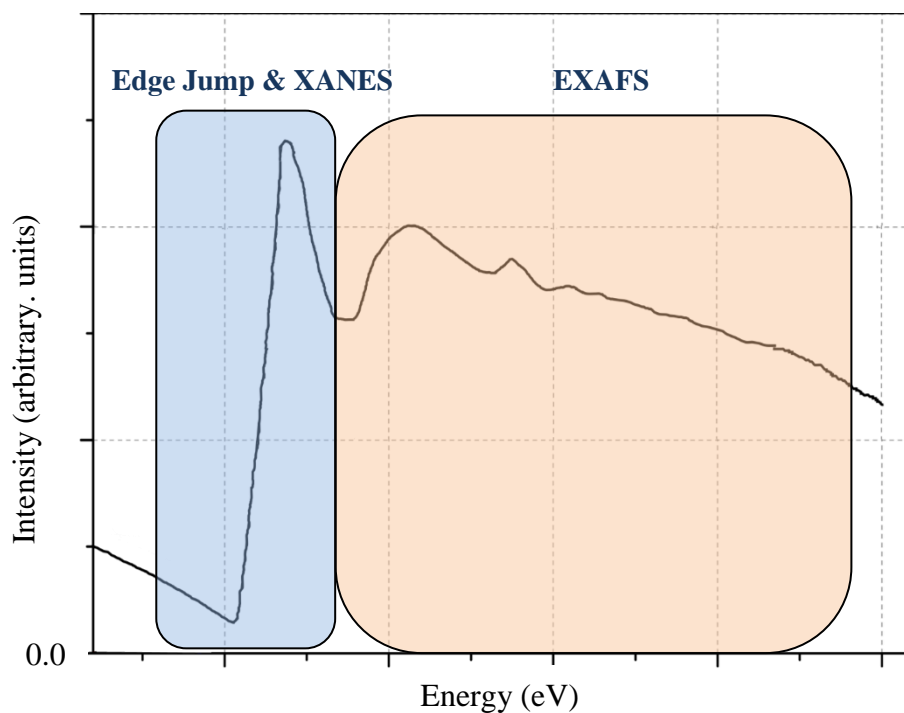
Figure 5.4 – Typical shape of a spectrum obtained from a XAFS study. X axis values dependant on the element being probed.

There are a broad range of applications of XAFS in heterogeneous catalysis, and it has been used to shed light on many metal/support systems. Some recent examples include; Au/Al$_2$O$_3$ catalysts for O$_2$ activation,[22] Cr/SiO$_2$ trimerisation catalysts,[23] molybdenum oxide dehydrogenation catalysts[24] and numerous metal nanoparticle systems.[25-28] Studies of homogeneous catalysts in solution are however more challenging, due to a poor signal to noise caused by low catalyst concentrations, difficulty in creating *in situ* sample environments and decomposition of the sample through radiation. Despite this, development of XAFS techniques and specialised reactors mean that examples of successful XAFS studies can be found, such as the determination of the oxidation state of gold in an Au-catalysed cyclobenzannulation reaction.[29] Tromp also utilised XAFS to uncover key intermediates in the Cu(II)-catalysed Chan-Lam reaction,[30] and deactivation pathways in a Cu(I)-catalysed C-C bond formation have also been studied.[31]

5.2. Project aims

A key issue with immobilised metal catalysts is the difficulty in determining structural information about the catalyst, such as resting state, intermediates and deactivation pathways. Whilst metal leaching is considered a major issue in the immobilisation of catalysts, the method of immobilisation reported by McGowan showed no significant

leaching, yet loss of activity for the hydrogenation of benzaldehyde was observed over time.[14] It was expected that XAFS would be a powerful tool which could develop the understanding of the activation, and deactivation of the immobilised iridium catalysts, using the n = C5-linker (**86a**) derivative. XAFS was considered a suitable technique due to the ability of this technique to study the iridium centre and the ligands directly, under turnover conditions.
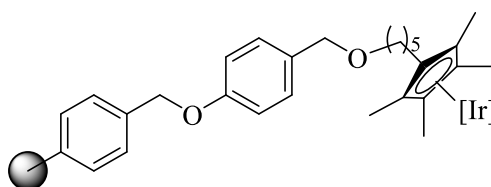
86a

Determination of the activation and deactivation pathways in catalysts is important to the design of more efficient and stable catalysts. A possible deactivation pathway of ligand dissociation/exchange offered a start point for the study. Using EXAFS, changes in ligand coordination around the iridium centre would be observable.

5.3. Solid state EXAFS at the Ir L-edge

Following the immobilisation of the iridium catalysts, as outlined in Scheme 5.4, limitations in characterisation of the metal species meant a lack of understanding of the active catalyst was available. The work done by McGowan *et al.* was able to show that the Cp* ligand is present in the immobilised catalyst, but more specialised techniques would be necessary for more in depth study.[14] One of the key questions regarding the iridium centre the amount of Ir-Cl bonds which were present, and whether the catalyst still existed as a dimer, as the precursors were. It is widely thought in Ru- and Ir-catalysed transfer hydrogenation reactions with monohalide precursors, that the first step of the mechanism is the removal of the halide with a base such as KO^{t}Bu.[32-34] Determination of the number of Ir-Cl bonds in the immobilised catalyst and deactivated catalyst could provide information into the speciation of the active catalyst and possible deactivation pathways.

5.3.1. Characterisation of freshly immobilised catalyst

Ex situ samples of **86a** and three iridium complexes of different monomeric and dimeric structures (**90, 91 and 92**) were analysed by EXAFS at the Ir L3-edge (11.2 KeV). The fourier transform of the data results in the radial distribution plots which are displayed in Figure 5.5A, in which two peaks are consistent between all four spectra at R ≈ 1.7 Å and R ≈ 2.2 Å). Comparison of the intensity of these peaks is possible when the spectra is normalised and overlaid (Figure 5.5B). The signals which arise at ≈ 1.7 Å are assigned to the Ir-C or Ir-N bonds, which are expected to be shorter than the Ir-Cl bonds based on the crystal structure of the non-immobilised n = C5 catalyst (**82a**).[14] The longer Ir-Cl bonds are therefore assigned to be responsible for the signals at ≈ 2.2 Å. Figure 5.5 shows a trend in intensity of this Ir-Cl signal where **90** and **92**, which have 3 Ir-Cl bonds per iridium centre, are stronger than **91**, which has 2 Ir-Cl bonds around the iridium centre. As **86a** gives a slightly weaker Ir-Cl signal than **91**, it is characterised as a monomeric species with 2 Ir-Cl bonds.
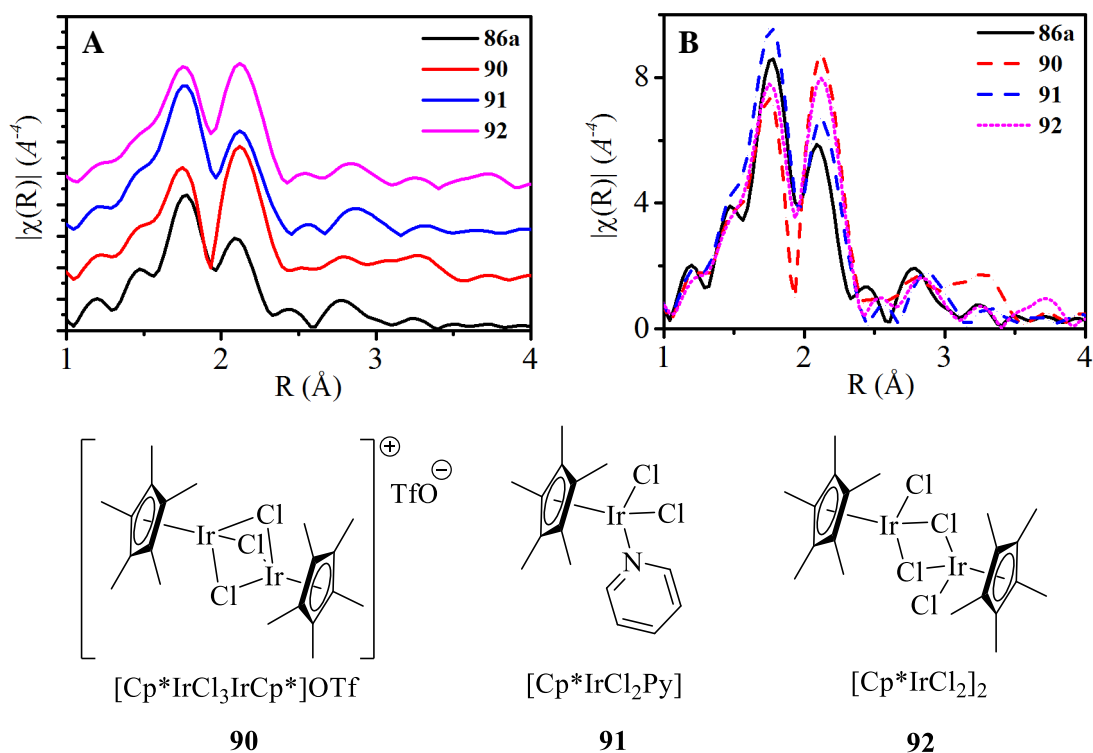

Figure 5.5 – Ir L-edge EXAFS – Stacked (**A**) and overlaid (**B**) radial distribution plots for selected iridium complexes.

5.3.2. Chloride content throughout catalyst lifetime

Four samples of the **86a** catalyst at different stages of its lifetime were also studied at the Ir L3-edge and the Cl K-edge by XAFS, in the solid state. The samples assessed in this experiment were the fresh, immobilised catalyst **86a**, and the same catalyst after 3 uses, and 30 uses in the transfer hydrogenation reaction shown in Table 5.1. The final sample was a "reactivated" catalyst, prepared when the deactivated 30 use sample was then stirred in 1 M aqueous HCl for 30 minutes. Unpublished results from Dr Stephanie Lucas showed that this procedure was able to restore its catalytic efficiency for 3 further reaction cycles.[35]

The fourier transformed Ir L3-edge EXAFS in Figure 5.6A shows the radial distributions of the four samples analysed. From this representation, it is seen that the Ir-Cl bond (2.2 Å) is lost throughout the lifetime of the catalyst, where the signal is significantly weaker in the 3-use sample and is not visible in the 30-use catalyst. Interestingly, the Ir-Cl bond is not seen to be restored after the reactivation procedure, indicating that the reactivated catalyst is not the same species as the initially active catalyst.

The Cl K-edge XANES shown in Figure 5.6B provides further information on the loss of the Ir-Cl bond. As the samples were prepared with a standard amount of catalyst, the Cl signal intensity should be indicative of the amount of chloride in the sample. From the fresh catalyst to the 3-uses catalyst, a very similar spectrum is seen, though the intensity is approximately halved after 3 uses, indicating a loss of one the initial 2 chlorides. The deactivated, 30-use sample provided almost no chloride signal, agreeing well with the loss of the Ir-Cl bond from the metal centre. The XANES spectrum of the reactivated catalyst shows that chlorine is reintroduced to the sample following the 1 M HCl wash, however the spectrum is not the same species as the fresh catalyst. Combining the Ir and Cl data, it can be concluded that the deactivation of the catalyst is linked with the loss of the Ir-Cl bonds around the metal centre. The reactivation of the sample restores chloride to the sample in a different form to the active catalyst, explaining why the reactivated catalyst is only able to be recycled for 3 further uses.
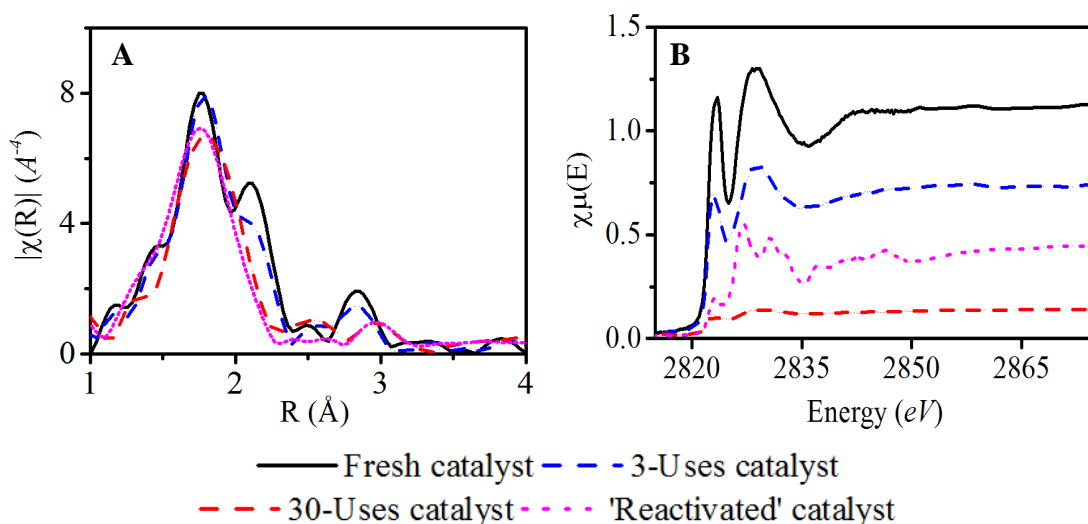
Figure 5.6 – **A -** Fourier-transformed Ir L3-edge EXAFS spectra of various stages of the catalyst lifetime. **B** – Cl K-edge XANES spectra.

Comparison of the Cl L-edge XANES spectrum of the reactivated catalyst with the literature spectrum of KCl shows very good agreement,[36] this is expected to form from either residual KO*t*Bu trapped in the Wang resin reacting with HCl, or the HCl reacting with potassium present in the deactivated catalyst.

5.4. Translation of catalysis to flow

As the catalyst is heterogeneous, to gather further information on the catalyst during turnover using XAFS, translation of the transfer hydrogenation to a flow chemistry set-up would allow study of the catalyst *in operando*. A stainless steel flow-cell, specifically designed for studying XAS at soft X-rays in fluorescence mode was developed to enable the *in operando* studies (Figure 5.7). The cell was developed with a catalyst bed of 100 µm depth, in which the immobilised catalyst can mounted with the help of a stainless steel grid. A cap with a window for the X-ray beams to reach the catalyst can be screwed on, with an O-ring and polypropylene film holding the lid in place and preventing the solution from leaking. A hole was drilled on the side of the cell for a thermocouple to enable heating during experiments.
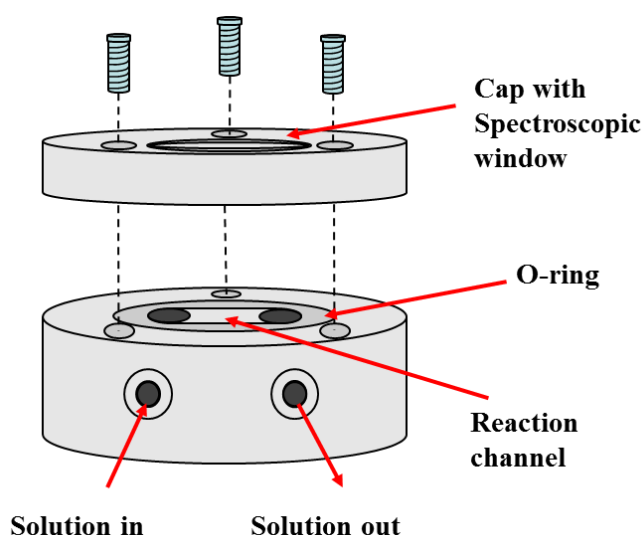
Figure 5.7 - Stainless steel flow cell for *in operando* XAFS measurements.

The flow reactions were performed with 1 mg of immobilised catalyst loaded onto a stainless steel grid, within the reaction channel and the solution flown over the catalyst using a milliGAT® positive displacement pump. Initial reactions in flow showed that conversion to product was very low as a result of the short residence times possible with a very small reaction channel volume (7 µl). The limitation of the pump set-up meant that if the flow rate was too slow, air bubbles would form in the PTFE tubing. As a result, 10.8 µL.min^{-1} was the found to be the optimal flow rate, giving a residence time of 39 seconds. The conditions that were used for subsequent kinetic and XAFS experiments are shown in Scheme 5.5. Typical conversions obtained under these conditions were ~ 1 – 2 %, however catalyst free reactions did show no conversion, indicating that some catalyst turnover is occurring.
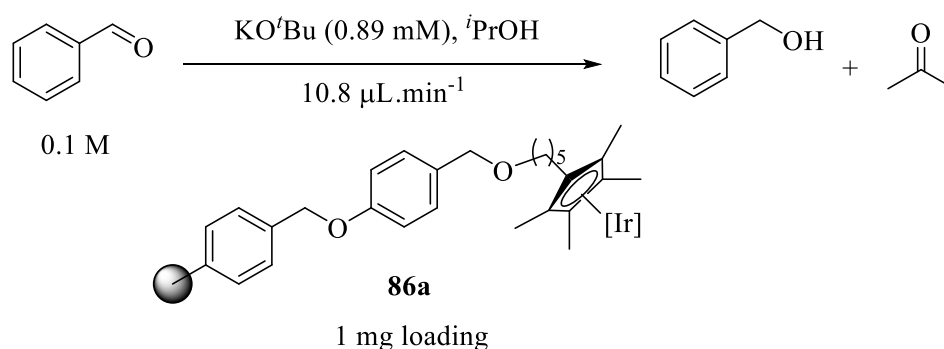
Scheme 5.5 – Reaction used for *in operando* monitoring of **86a**.

5.5. *In operando* XAFS monitoring

The reaction in Scheme 5.5 was assembled on the experiment beamline as illustrated in Figure 5.8. The cell was connected to a thermocouple, which allowed heating of the cell to 60 °C. The reaction was prepared with anhydrous solvent and the flow cell kept under an inert helium atmosphere throughout the duration of the reaction. The Cl K-edge exists at 2.82 KeV, in the "soft" X-ray region, typically these samples are run under vacuum due to the absorption of X-rays at this wavelength by air.[37] Test spectra at the Cl K-edge under helium suggested that these conditions were sufficient for *in operando* monitoring of the reaction.
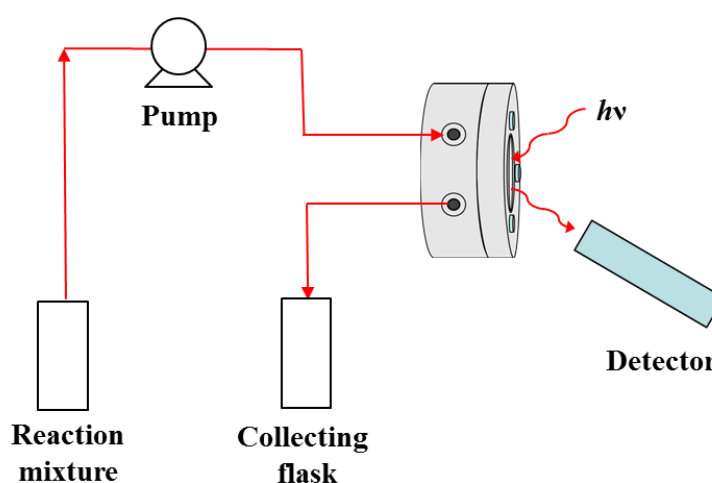
Figure 5.8 - Schematic of the flow cell set-up for *in operando* XAFS measurements

5.5.1. Monitoring the Cl and K K-edges

As the results of the *ex situ* Ir L3-edge experiments showed a loss of chlorine species throughout the course of the reaction, and KCl was seen to form after treatment of the catalyst with HCl, two experiments monitoring these under turnover conditions were performed. The edge jump intensity for both Cl and K is plotted over time in Figure 5.9. Both Cl and K content in the sample showed a significant trend throughout the reaction, with Cl content decreasing and K content increasing, agreeing well with the previous data.
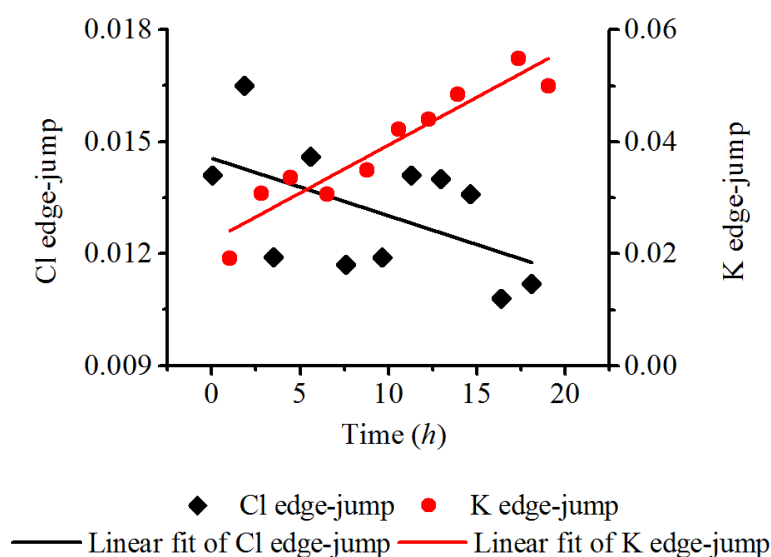
Figure 5.9 – Cl K-edge jump and K K-edge jump against time, under turnover conditions. Linear fit of the plotted data to show general trends.

The data displayed in Figure 5.10 shows the edge jump values for Cl and K at various points in the reaction procedure. Analysis of the Cl edge jump data shows that 50 % of the Cl signal is lost following the activation of the catalyst with KO^{t}Bu, indicating a loss of one of the two chlorides from the iridium centre. Decrease of the Cl edge jump intensity over the course of the reaction agrees well with the Ir L-edge data for the deactivated catalyst (Figure 5.6). The reactivation of the catalyst was performed by flowing 1 M HCl in ^{i}PrOH over the catalyst at 10.8 µL.min^{-1}, followed by a 30 mL ^{i}PrOH wash to remove any HCl from the catalyst and flow cell. An increase in the chlorine content is observed after the HCl wash, although the value is still low in comparison with the fresh catalyst.

The potassium edge-jump data shows that the build-up of potassium in the system can be followed using this method. Following the wash with KO^{t}Bu, a significant increase was observed, this built up over the 19 hours of the reaction. The reactivation procedure is efficient in removing the potassium from the sample, decreasing the edge-jump values almost to that of the fresh catalyst (residual). An explanation for the KCl seen in Section 5.3.2. is that the reactivation process in batch involves stirring in HCl, followed by filtration, causing formation of KCl, which is trapped in the polystyrene support. In flow, the constant flow of HCl is able to remove the KCl formed.
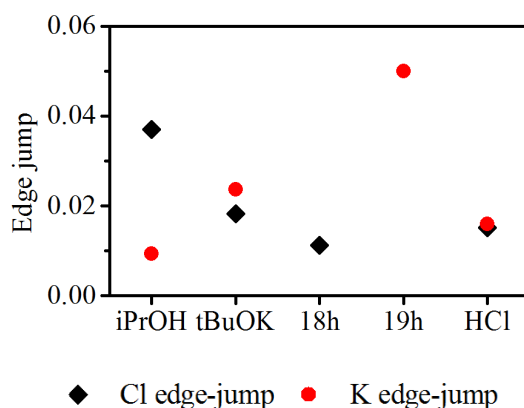
Figure 5.10 – Cl and K edge jump values for the catalyst during the *i*PrOH wash, KO*t*Bu wash, reaction and HCl wash.

The results of the *in operando* experiments, combined with the solid state Ir L3-edge and Cl K-edge measurements builds the picture for the pre-catalyst, activated, deactivated and reactivated catalyst. A proposal of the species of these is displayed in Scheme 5.6, which shows a monochloride species as the active catalyst (**93**), having displaced one of the chlorides of the pre-catalyst **86a** for an alkoxide ligand. The deactivation over time results in the loss of the second chloride and the formation of an anionic Ir(III) complex (**94**), with a potassium cation. By washing the deactivated catalyst with HCl, a cationic Ir(III) species is formed (**95**), in which the potassium cation is washed out, and chloride reintroduced as an anion. The presence of chloride as an anion is used to explain the Ir L-edge XANES data, in which it was shown that Ir-Cl bonds are not reintroduced to the metal centre.
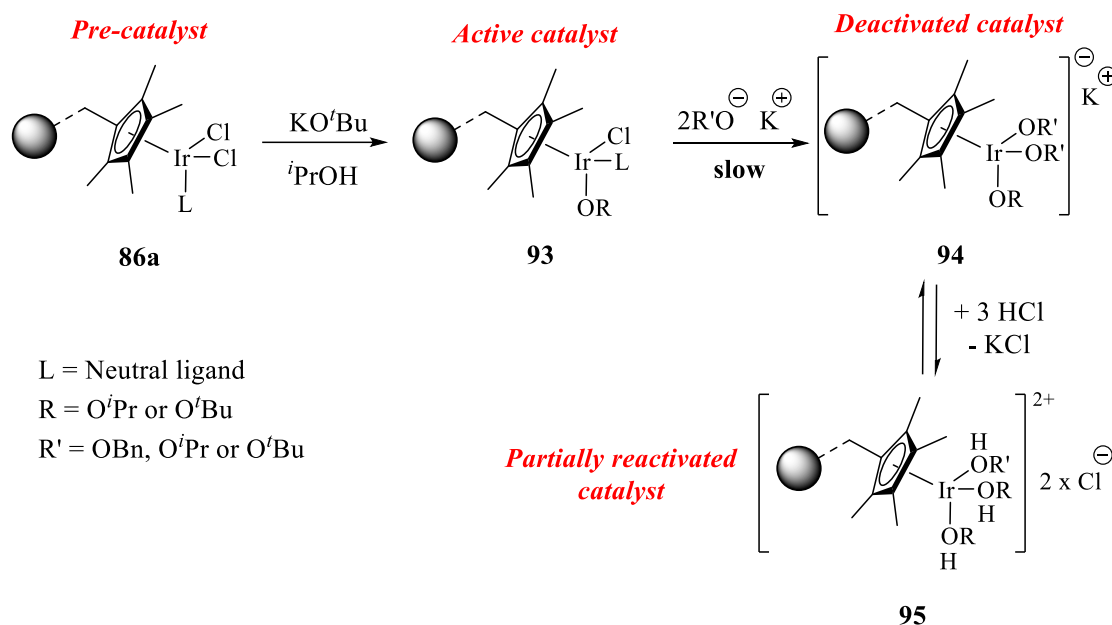
Scheme 5.6 - Proposed deactivation and reactivation pathways.

The strong Ir-OR bonds which are present in the deactivated catalyst are unlikely to be able to dissociate to provide the two coordination sites expected to be necessary for catalyst turnover.[34] It is proposed that the more labile Ir-O(R)H ligands which are formed in the reactivation will be more readily exchanged for benzaldehyde coordination, however will also be prone to exchange with the alkoxides.

5.6. Inhibition experiments

Three further experiments were performed to rule out the possibility that iridium nanoparticles are the active catalyst, and that residual H_2O may inhibit the reaction. These reactions were performed in batch mode, following the procedure outlined by McGowan (Scheme 5.7).[14]
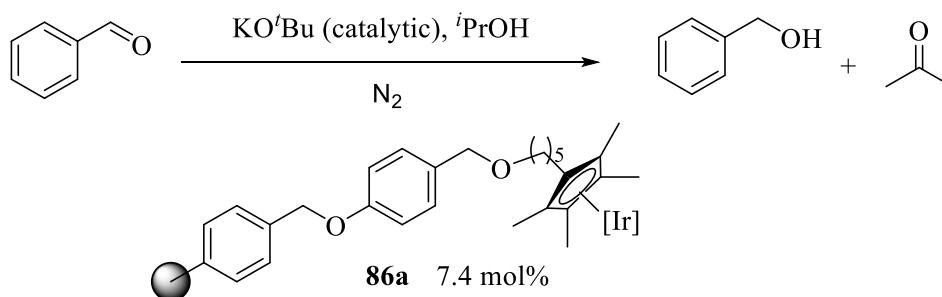
Scheme 5.7 – Transfer hydrogenation reaction of benzaldehyde used in batch deactivation experiments.

5.6.1. Hot filtration

A "hot filtration" experiment was designed in which the reaction in Scheme 5.7 was run and monitored by GC for 180 minutes, before filtration of half of the reaction through a 0.2 μm syringe filter. The remaining reaction mixture and the removed solution were monitored for a further 180 minutes. This experiment showed whether nanoparticles, which would be extracted through the syringe filter are the source of catalytic activity.
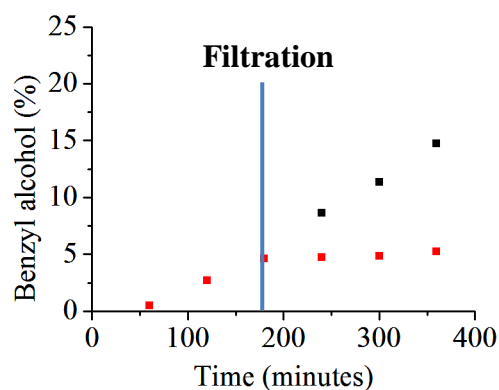
Figure 5.11 – Results of "hot filtration" experiment. Blue line represents the removal of 50 % of the reaction solution by a syringe fitted with a 0.2 μm syringe filter. ■ Reaction without filtration. ■ Filtered solution.

Figure 5.11 shows the results, whereby the filtered solution did not give any turnover, whilst the initial reaction mixture continues to react. This provides evidence that no catalytically active nanoparticles were passed through the filter, and it unlikely that they are the source of catalytic activity. As the reaction was stirred during the removal of half the reaction mixture, it should be expected that the rate of the reaction would remain the same. A slight increase in the rate of the initial reaction mixture is seen, this is likely to be a result of the solid catalyst particles being more difficult to draw through a needle than liquid.

5.6.2. Hg(0) poisoning

Complementary to the filtration experiment, a mercury poisoning experiment was performed, in which the same reaction set-up for the filtration experiment was spiked with a large excess of mercury metal. Mercury is well known to be an inhibitor for heterogeneous catalysts in the zero oxidation state, due to its tendency to "coat" the metallic particles.[38] If Ir(0) nanoparticles are present and catalytically active, a plateau in conversion would be observed in the kinetic profile (Figure 5.12).
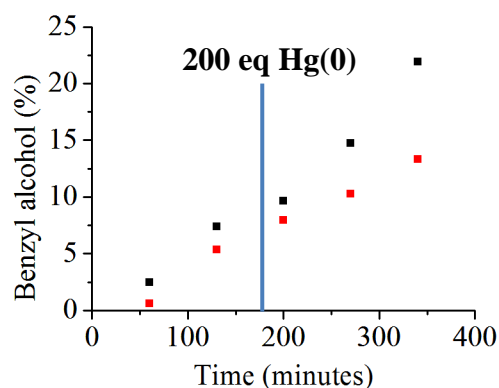
Figure 5.12 - Mercury poisoning experiment. Blue line represents the addition of 200 eq mercury metal ■ Reaction without Hg(0). ■ Reaction with Hg(0).

The results in Figure 5.12 show that this is not the case, and conversion continues following mercury addition. A small decrease in the rate of reaction after addition of mercury could be an influence of poorer mass transfer or stirring with mercury present. This and the "hot filtration" experiment rule out the possibility of Ir(0) nanoparticles forming and catalysing the transfer hydrogenation of benzaldehyde.

5.6.3. Effect of H_2O

The final inhibition experiment aimed to rule out the possibility of H_2O inhibition of the catalyst. Though all of these studies were performed with commercial anhydrous solvent, a possibility of residual water in the system was still present. By performing the reaction in Scheme 5.7 alongside an identical reaction with degassed H_2O (5 eq rel. to Ir) and monitoring the conversion by GC, determination of H_2O inhibition was possible (Figure 5.13).
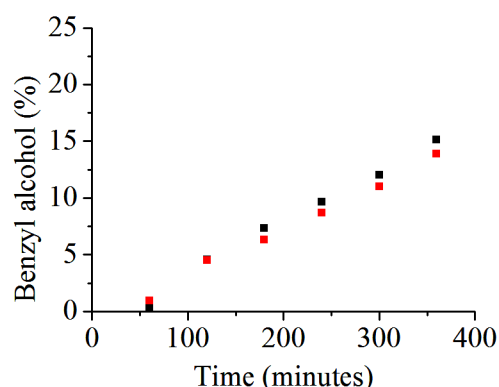
Figure 5.13 – H_2O inhibition experiment. ■ Reaction without H_2O. ■ Reaction with H_2O.

The kinetic profiles in Figure 5.13 show that there is minimal difference in the conversion with and without the H_2O, where it was expected that 5 eq relative to Ir would represent an extreme scenario for H_2O present.

5.7. Summary and conclusions

This work showcases a multi-element XAFS investigation of a robust immobilised iridium transfer hydrogenation catalyst. The results uncovered the nature of ligand-exchange on the iridium centre and led to the proposed pathways shown in Scheme 5.6. Experiments suggest that the base converts the pre-catalyst to an active species through the loss of a chloride however subsequent loss of a second chloride over time results in an inactive catalyst. The work showed that following reactivation of the catalyst, chloride is reintroduced to the sample, however it is not directly bound to the irdium centre, instead, weaker Ir-O bonds are hypothesised and the chlorides acting as anions.

This work highlights the importance of the Ir-Cl bond to catalyst stability, as it is lost, the catalyst is deactivated. The reactivated catalyst, which has a much shorter lifetime does not possess the Ir-Cl bond, explaining its instability. As the catalyst is currently recyclable for more the 20 cycles, it already offers an impressive option to industry, where recycling of catalysts is an important topic. If it is possible to regenerate the initial active catalyst from the deactivated state by reintroducing the Ir-Cl bond, infinite uses of the catalyst may be possible. Alternatively, the importance of the ligands to stability and activity may be useful in development of more active/stable catalysts.

A deactivation through ligand exchange with alkoxides, which are commonly used as bases with similar Cp*IrCl complexes will be of interest to homogeneous transfer hydrogenations. The results also have further implications on future development of immobilised catalysts, of which structural characterisation is difficult with most techniques. The methods displayed in this work can be applied to many other immobilised transition metal catalysts, due to the distinct advantages of XAFS.

5.8. References

1.	G. Brieger and T.J. Nestrick, *Chem. Rev.*, 1974, **74**, 567-580.

2.	D. Wang and D. Astruc, *Chem. Rev.*, 2015, **115**, 6621-6686.

3.	R. Noyori and T. Ohkuma, *Angew. Chem. Int. Ed.*, 2001, **40**, 40-73.

4.	R. Noyori and S. Hashiguchi, *Acc. Chem. Res.*, 1997, **30**, 97-102.

5.	S. Inoue, K. Nomura, S. Hashiguchi, R. Noyori and Y. Izawa, *Chem. Lett.*, 1997, 957-958.

6.	J.X. Gao, T. Ikariya and R. Noyori, *Organometallics*, 1996, **15**, 1087-1089.

7.	S. Hubner, J.G. de Vries and V. Farina, *Adv. Synth. Catal.*, 2016, **358**, 3-25.

8.	W. Baratta, P. Da Ros, A. Del Zotto, A. Sechi, E. Zangrando and P. Rigo, *Angew. Chem. Int. Ed.*, 2004, **43**, 3584-3588.

9.	R.W. Guo, C. Elpelt, X.H. Chen, D.T. Song and R.H. Morris, *Chem. Commun.*, 2005, 3050-3052.

10.	G. Reginato, P. Sadler and R.D. Wilkes, *Org. Process Res. Dev.*, 2011, **15**, 1396-1405.

11.	P.N. Liu, P.M. Gu, F. Wang and Y.Q. Tu, *Org. Lett.*, 2004, **6**, 169-172.

12.	S. Sabater, J.A. Mata and E. Peris, *ACS Catal.*, 2014, **4**, 2038-2047.

13.	J. Blacker, K. Treacher and T. Screen, *WO*, 2009/093059 A2, 2009.

14.	S.J. Lucas, B.D. Crossley, A.J. Pettman, A.D. Vassileiou, T.E.O. Screen, A.J. Blacker and P.C. McGowan, *Chem. Commun.*, 2013, **49**, 5562-5564.

15.	Y.C. Chen, T.F. Wu, J.G. Deng, H. Liu, X. Cui, J. Zhu, Y.Z. Jiang, M.C.K. Choi and A.S.C. Chan, *J. Org. Chem.*, 2002, **67**, 5301-5306.

16.	X.G. Li, X.F. Wu, W.P. Chen, F.E. Hancock, F. King and J.L. Xiao, *Org. Lett.*, 2004, **6**, 3321-3324.

17.	R.C. Nelson and J.T. Miller, *Catal. Sci. Tech.*, 2012, **2**, 461-470.

18.	R.A. Scott and C.M. Lukehart, '*Applications of physical methods to inorganic and bioinorganic chemistry*' Wiley, Chichester, 2007.

19.	S. Bordiga, E. Groppo, G. Agostini, J.A. van Bokhoven and C. Lamberti, *Chem. Rev.*, 2013, **113**, 1736-1850.

20.	B.K. Teo and D.C. Joy, '*EXAFS spectroscopy : techniques and applications*' Plenum, New York ; London, 1981.

21.	P.A. Lee, P.H. Citrin, P. Eisenberger and B.M. Kincaid, *Rev. Mod. Phys.*, 1981, **53**, 769-806.

22. J.A. van Bokhoven, C. Louis, J. T Miller, M. Tromp, O.V. Safonova and P. Glatzel, *Angew. Chem. Int. Ed.*, 2006, **45**, 4651-4654.

23. C.N. Nenu, J.N.L. van Lingen, F.M.F. de Groot, D.C. Koningsberger and B.M. Weckhuysen, *Chem. Eur. J.*, 2006, **12**, 4756-4763.

24. A.M. Beale, A.M.J. van der Eerden, K. Kervinen, M.A. Newton and B.M. Weckhuysen, *Chem. Commun.*, 2005, 3015-3017.

25. P. Glatzel, J. Singh, K.O. Kvashnina and J.A. van Bokhoven, *J. Am. Chem. Soc.*, 2010, **132**, 2555-2557.

26. M.A. Newton, M. Di Michiel, A. Kubacka, A. Iglesias-Juez and M. Fernandez-Garcia, *Angew. Chem. Int. Ed.*, 2012, **51**, 2363-2367.

27. M.A. Newton, J.B. Brazier, E.M. Barreiro, S. Parry, H. Emmerich, L.A. Adrio, C.J. Mulligan, K. Hellgardt and K.K. Hii, *Green Chem.*, 2016, **18**, 406-411.

28. P.J. Ellis, I.J.S. Fairlamb, S.F.J. Hackett, K. Wilson and A.F. Lee, *Angew. Chem. Int. Ed.*, 2010, **49**, 1820-1824.

29. B.N. Nguyen, L.A. Adrio, E.M. Barreiro, J.B. Brazier, P. Haycock, K.K. Hii, M. Nachtegaal, M.A. Newton and J. Szlachetko, *Organometallics*, 2012, **31**, 2395-2402.

30. M. Tromp, G.P.F. van Strijdonck, S.S. van Berkel, A. van den Hoogenband, M.C. Feiters, B. de Bruin, S.G. Fiddy, A.M.J. van der Eerden, J.A. van Bokhoven, P.W.N.M. van Leeuwen and D.C. Koningsberger, *Organometallics*, 2010, **29**, 3085-3097.

31. C. He, G.H. Zhang, J. Ke, H. Zhang, J.T. Miller, A.J. Kropf and A.W. Lei, *J. Am. Chem. Soc.*, 2013, **135**, 488-493.

32. K. Mashima, T. Abe and K. Tani, *Chem. Lett.*, 1998, 1199-1200.

33. D.A. Alonso, P. Brandt, S.J.M. Nordin and P.G. Andersson, *J. Am. Chem. Soc.*, 1999, **121**, 9580-9588.

34. J.S.M. Samec, J.E. Backvall, P.G. Andersson and P. Brandt, *Chem. Soc. Rev.*, 2006, **35**, 237-248.

35. S.J. Lucas, ′The synthesis of group 9 complexes for use as transfer hydrogenation catalysts and anti-cancer agents′, *Ph.D. thesis, University of Leeds*, 2013.

36. K. Nakanishi and T. Ohta, *J. Phys.: Condens. Matter*, 2009, **21**.

37. M. Honda, Y. Baba, I. Shimoyama and T. Sekiguchi, *Rev. Sci. Instrum.*, 2015, **86**.

38.   P.D. Landre, D. Richard, M. Draye, P. Gallezot and M. Lemaire, *J. Catal.*, 1994, **147**, 214-222.

Experimental

6.1. General methods and materials

6.1.1. Reagents and materials

Unless otherwise stated, all reactions were performed under an atmosphere of nitrogen, using flame-dried glassware. Reactions were set up using air-sensitive techniques on a Schlenk manifold or in a nitrogen-filled glovebox. Anhydrous solvents were dried by passing the solvent over activated alumina via the Dow-Grubbs solvent system (Pure Solv™) unless otherwise specified. Anhydrous *N,N*-dimethylformamide and acetonitrile (99.8%) were purchased from Sigma Aldrich. Reaction solvents were degassed by bubbling of nitrogen through for a minimum of 30 minutes. Anhydrous NMR solvents for air sensitive products were degassed using three freeze-thaw cycles. All other reagents were obtained from commercial suppliers and used without further purification.

6.1.2. General analytical data

^{1}H and ^{13}C NMR data were performed using deuterated chloroform (CDCl$_3$), unless otherwise stated and recorded on either an Avance 300 (Brüker Biospin GmbH), or Avance 500 (Brüker Biospin GmbH). All kinetic data was obtained on the Avance 500 and ^{133}Cs NMR was run on an Avance 400 or 500 MHz spectrometer. Microanalysis data was obtained by Tanya Marinko-Covell of the University of Leeds. Hydrogenation of amides was performed using a 300 mL Parr Pressure Reactor. High resolution mass spectra were collected on a Brüker Daltonics (microTOF) instrument operating in the electrospray mode. GC/MS data was obtained using Agilent HP2890 series GC system, with an Agilent HP5973 mass selective detector on EI mode. Column chromatography was performed using Geduran© Si 60 silica gel with the stated solvents. FT-IR spectroscopy measurements were taken on a Brüker Alpha Platinum-ATR. HPLC data was collected from an Agilent 1200 HPLC system using a 30 x 4.6 mm Waters Acquity BEH C18 1.7 µm column and UV/Vis detector set at 285 nm. GC data was obtained from

an Agilent Technologies 7890B gas chromatograph using an Agilent J&W HP-5 GC Column, 30 m, 0.32 mm, 0.25 µm.

Single crystal X-ray data for complexes **71, 72 and 73** were collected at 100K using an Agilent SuperNova diffractometer equipped with an Atlas CCD detector using mirror monochromated Mo-Kα (λ = 0.71073 Å) or Cu-Kα (λ = 1.54184 Å) radiation and processed using CrysAlis Pro software. The structures were solved using SHELXS direct methods, and the structural model refined by full matrix least squares on F^2 using SHELXL97.[1] Hydrogen atoms were placed using idealised geometric positions (with free rotation for methyl groups), allowed to move in a "riding model" along with the atoms to which they were attached, and refined isotropically. Molecular graphics and preparation of tables of bond lengths was carried out using Olex2.[2]

6.2. Chapter 2

6.2.1. General procedures

6.2.1.1. General procedure for synthesis of organic bases

The procedures for the formation of tetrabutylammonium salts were performed according to the procedure of Liu *et al.*[3] Tetrabutylammonium or tetrabutylphosphonium hydroxide (40% solution in H_2O or 1 M in MeOH) was added with a stoichiotmetric quantity of the corresponding acid in a round bottomed flask and 5 mL solvent added. The reaction was stirred under an atmosphere of nitrogen at room temperature overnight and upon completion, water was removed by lyophilisation and MeOH by vacuum. The resulting solid was dried under high vacuum without further purification and stored under a nitrogen atmosphere.

6.2.1.2. General procedure for screening reactions with organic bases

CuI (9.5 mg, 0.05 mmol, 10 mol%), *N,N*-dimethylglycine (**8**) (10.3 mg, 0.1 mmol, 20 mol%), 4-iodoanisole (**9**) (117.0 mg, 0.5 mmol) and tetrabutylammonium adipate (472.0 mg, 0.75 mmol) were added to a flame dried Schlenk flask. The vessel was evacuated and backfilled with nitrogen three times before **10** (74.0 µL, 0.75 mmol) and 2 mL degassed DMF were added by syringe. The reaction flask was sealed and the reaction stirred at 90 °C for 18 hours. Upon completion, the reaction mixture was filtered over a short pad of silica with 200 mL ethyl acetate and evaporated to give the organic

compounds in DMF. The resulting solution was diluted with 20 mL water and extracted with 4 x 20 mL of diethyl ether, with the organic layers combined and evaporated to dryness to give the crude product for ^{1}H NMR analysis.

6.2.2. Synthesis of materials

6.2.2.1. Tetrabutylammonium adipate (TBAA) - 3
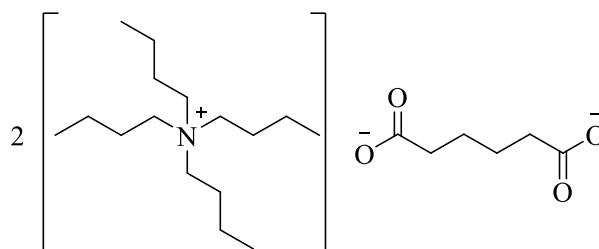
Tetrabutylammonium hydroxide (1M solution in MeOH, 3.4 mL, 3.42 mmol) was added with adipic acid (250 mg, 1.71 mmol) in a round bottomed flask with activated 4 Å molecular sieves. The reaction was stirred under an atmosphere of nitrogen at room temperature for 18 hours and upon completion, the solution was filtered over a short pad of Celite with 50 mL MeOH. The majority of the solvent was removed using a rotary evaporator and the resulting thick slurry dried on a Schlenk line to give a white solid. **3** was isolated as a white solid, dried further under vacuum for 9 hours and stored under a nitrogen atmosphere without further purification.

^{1}H NMR (500 MHz, D$_2$O) δ (ppm) = 3.21 (t, J = 9.0 Hz, 16H), 2.20 (m, 4H), 1.66 (m, 16H), 1.56 (m, 4H), 1.39 (dt, J = 21.2, 7.3 Hz, 16H), 0.93 (t, J = 7.3 Hz, 24H).

Literature Values:[3] 1H NMR (300 MHz, D$_2$O): δ (ppm) 3.12 (t, J = 9.1 Hz, 16H), 2.11 (m, 4H), 1.54 (m, 16H), 1.43 (m, 4H), 1.27 (dt, J = 21.6, 7.2 Hz,16H), 0.89 (t, J = 7.2 Hz, 24H).

6.2.2.2. *N,N*-Dimethylglycine - 8
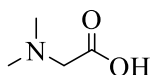
Synthesis was performed as outlined by Makriyannis *et al.*[4] A mixture of glycine (10.0 g 0.133 mmol), formaldehyde (37% w/v in H$_2$O, 32.0 mL, 0.361 mmol) and palladised charcoal (10% w/w Pd, 4.0 g) was stirred in ethanol (150 mL) under 3 bar H$_2$ using a Parr

pressure reactor for 12 hours. The resulting mixture was filtered over Celite with ethanol and evaporated to dryness. The product was crystallised from ethanol/diethyl ether and dried *in vacuo*, yielding **8** as a white solid (11.8 g, 86%).

^{1}H NMR (500 MHz, D$_2$O) δ (ppm) = 3.73 (s, 2H), 2.94 (s, 6H); ^{13}C NMR (125 MHz, D$_2$O) δ = 60.0, 43.7; vmax (neat)/cm^{-1} 3386, 3025, 1607 (C=O), 1470, 1391, 1356; HRMS (ESI+) *m/z* [M+Na]$^+$ Calcd for C$_4$H$_9$NNaO$_2$: 126.0531. Found: 126.0525.

Literature values:[4] ^{1}H NMR (D$_2$O) δ = 3.96 (s, 2 H), 2.80 (s, 6H)

6.2.2.3. Synthesis of 1-(4-methoxyphenyl)-piperidine - 11
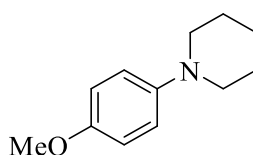
CuI (19.0 mg, 0.1 mmol), **8** (20.8 mg, 0.2 mmol), **9** (236.0 mg, 1.0 mmol) and tetrabutylammonium adipate (942.0 mg, 1.5 mmol) were added to a flame dried Schlenk flask. The vessel was evacuated and backfilled with nitrogen three times before **10** (158.0 μL, 1.5 mmol) and 4 mL of degassed anhydrous DMF were added by syringe. The Schlenk flask was sealed and the reaction stirred at 90 ºC for 71 hours. Upon completion, the reaction mixture was filtered over a short pad of silica with ethyl acetate and evaporated to give the organic compounds in DMF. The resulting solution was dilute with 50 mL water and extracted with 4 x 20 mL of diethyl ether, with the organic layers combined and evaporated to dryness to give the crude product. The crude product was purified by column chromatography, eluting with a 2:1 mixture of petroleum ether and diethyl ether (R$_f$ = 0.82) to yield **11** as a yellow oil (73 mg, 38 % yield).

^{1}H NMR (500 MHz, CDCl$_3$) δ (ppm) = 6.92 (d, *J* = 9.0 Hz, 2H), 6.83 (d, *J* = 9.1 Hz, 2H), 3.77 (s, 3H), 3.02 (t, *J* = 5.4 Hz, 4H), 1.72 (quint, 5.5 Hz, 4H), 1.54 (quint, 6.0 Hz, 4H); ^{13}C NMR (125 MHz CDCl$_3$) δ = 153.5, 146.9, 118.8, 114.4, 55.6, 52.3, 26.1, 24.2; HRMS (ESI+) *m/z* [M+H]$^+$ Calcd for C$_{12}$H$_{18}$NO: 192.1388. Found: 192.1394.

Literature values:[5] ^{1}H NMR (600 MHz, CDCl$_3$) δ 6.91 (d, *J* = 9.0 Hz, 2H), 6.82 (d, *J* = 9.0 Hz, 2H), 3.76 (s, 3H), 3.02 (t, *J* = 5.5 Hz, 4H), 1.72 (quint, *J* = 5.7 Hz, 4H), 1.54

(quint, $J = 6.1$ Hz, 2H); ^{13}C NMR (150 MHz, CDCl₃) δ 153.5, 146.9, 118.7, 114.3, 55.5, 52.3, 26.1, 24.2.

6.2.3. *In situ* ^{1}H NMR kinetic study

6.2.3.1. General procedure for NMR experiments
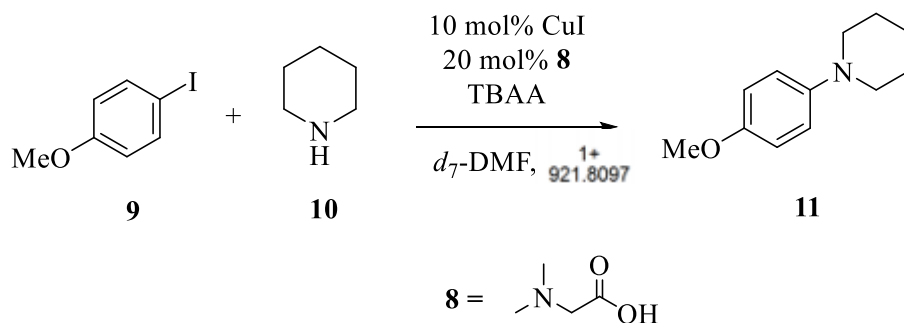
CuI (1.2 mg, 0.0063 mmol) was added with **8** (1.3 mg, 0.0126 mmol) to a dry NMR tube with a Young valve and taken in to a nitrogen filled glovebox. Inside the glovebox, a solution of TBAA (59.0 mg, 0.0938 mmol) and **10** (9.0 μL, 0.0911 mmol) in d_7-DMF (0.25 mL) was added. The reaction was initiated when a solution of **9** (14.6 mg, 0.0625 mmol) in d_7-DMF (0.25 mL) was added. The NMR tube was removed and shaken to ensure homogeneity before the NMR experiment began.

6.2.3.2. Procedure for obtaining kinetic data

The NMR sample is prepared as outlined above and is then placed into the NMR machine. A scan is taken at 25 ℃ to measure t_0 for the reaction, before the temperature probe is heated to the desired temperature (70 ℃). After this temperature is reached, an NMR spectrum is collected every 10 minutes.

The resulting spectra are processed using the TopSpin[TM] package and the integrals of all aromatic species (6 – 8 ppm) are normalised to 100. The conversions are noted for each known compound and the concentration of each species calculated based on the starting concentration of **9**. Rate data were generated using differential function in Origin Pro 9.0.

6.2.3.3. Example spectra – *d₇*-DMF

Figure 6.1 – ¹H NMR of *in situ* reaction in *d₇*-DMF. Spectra collected at 70 °C after 4 hours.
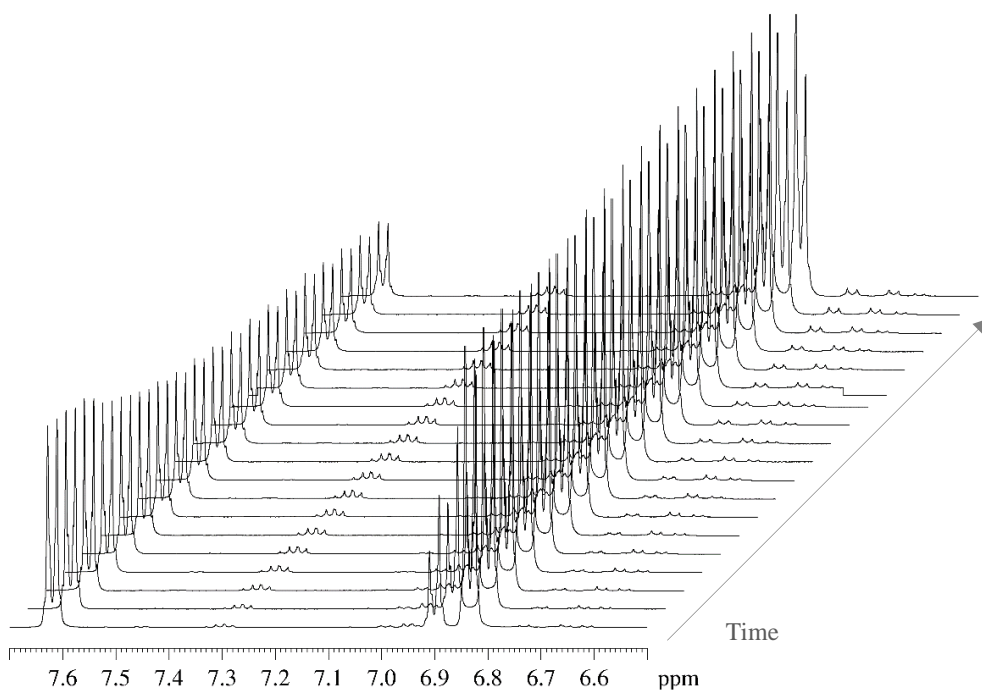
Figure 6.2 – Time-lapse of *in situ* kinetic measurements. Each spectrum represents 10 minutes time gap.

6.2.3.4. Example spectra – d_3-MeCN
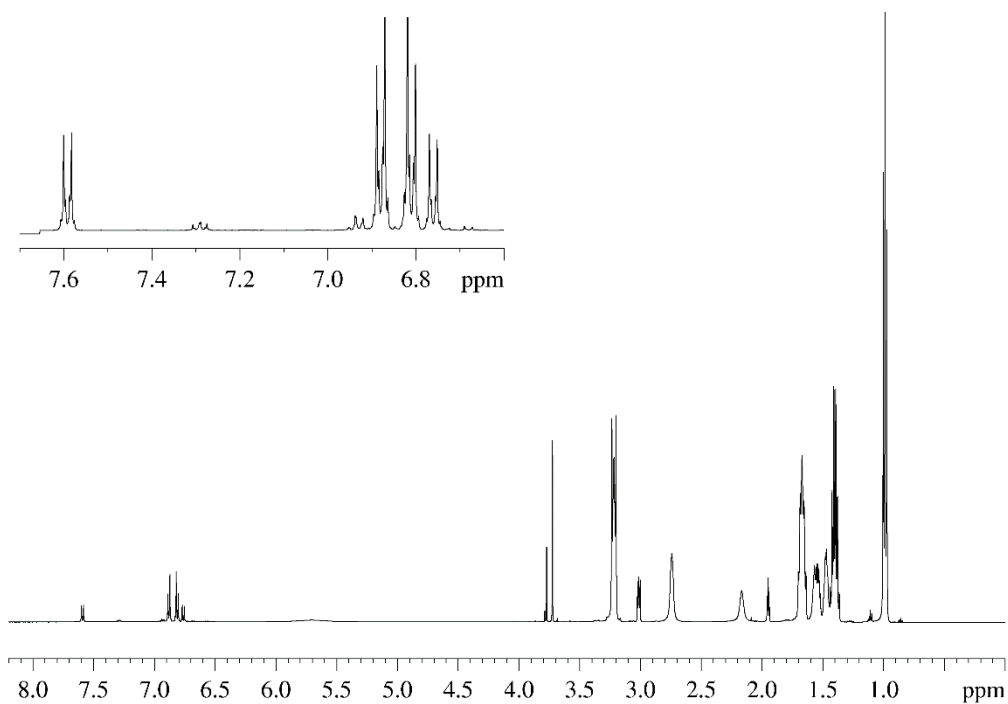
Figure 6.3 -^{1}H NMR of *in situ* reaction in d_3-DMF. Spectra collected at 70 °C after 4 hours.

6.2.3.5. Reaction conditions for *in situ* study in *d₇*-DMF

Quantities given in mg.

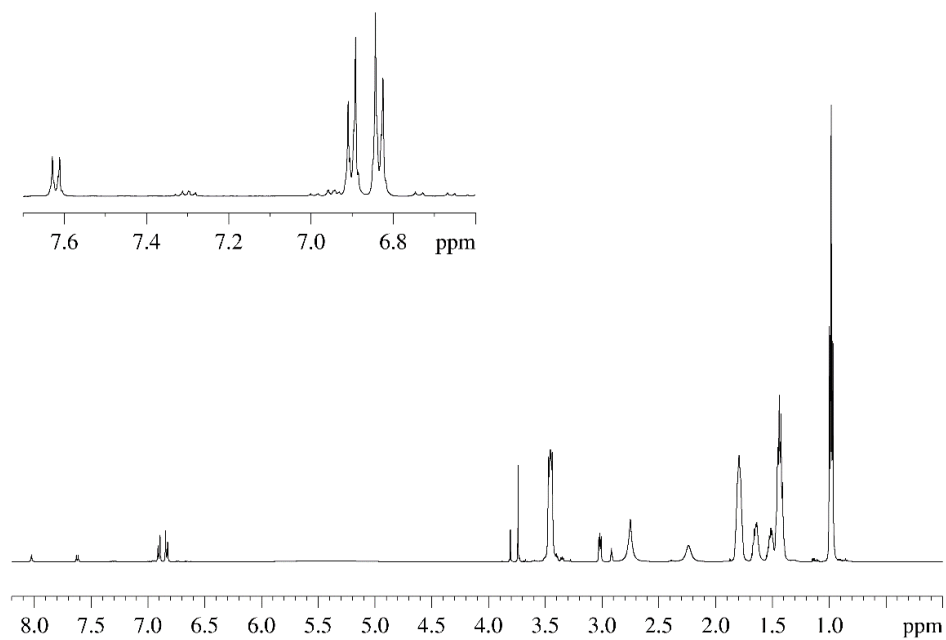|	MW	Density	Standard	2x [10]	2x [TBAA]	2x [8]	0.5x [9]	Product Inhibition	Same "Excess"	0.5x CuI/8
CuI (mg)	190.44		1.2	1.2	1.2	1.2	1.2	1.2	1.2	0.6
8 (mg)	103.12		1.3	1.3	1.3	2.6	1.3	1.3	1.3	0.7
TBAA (mg)	629.07		59.0	59.0	118.0	59.0	59.0	59.0	39.3	59.0
d₇-DMF (µL)			500	500	500	500	500	500	500	500
9 (mg)	234.03		14.6	14.6	14.6	14.6	7.3	14.6	14.6	14.6
10 (µL)	85.15	0.862	9	18	9	9	9	9	6	9
11 (mg)	191.27						7.4			

6.2.3.6. Product inhibition experiment
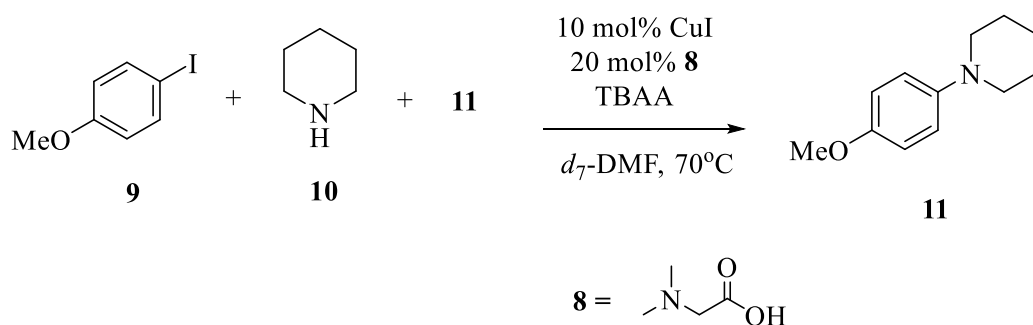
CuI (1.2 mg, 0.0063 mmol) was added with **8** (1.3 mg, 0.0126 mmol) to a dry NMR tube with a Young valve and taken in to a nitrogen filled glovebox. Inside the glovebox, a solution of TBAA (59.0 mg, 0.0938 mmol) and **9** (14.6 mg, 0.0625 mmol) in d_7-DMF (0.50 mL) was added by syringe. A microsyringe was used to inject 9.0 μL product and the reaction was sealed and removed from the glovebox. A room temperature ^{1}H NMR spectra (Figure 6.4) was taken to determine [**11**] before transfer back into the glovebox. **10** (9.0 μL, 0.0911 mmol) was added and the reaction initiated when a solution of in d_7-DMF (0.25 mL) was added. The NMR tube was removed and shaken to ensure homogeneity before the NMR experiment began.
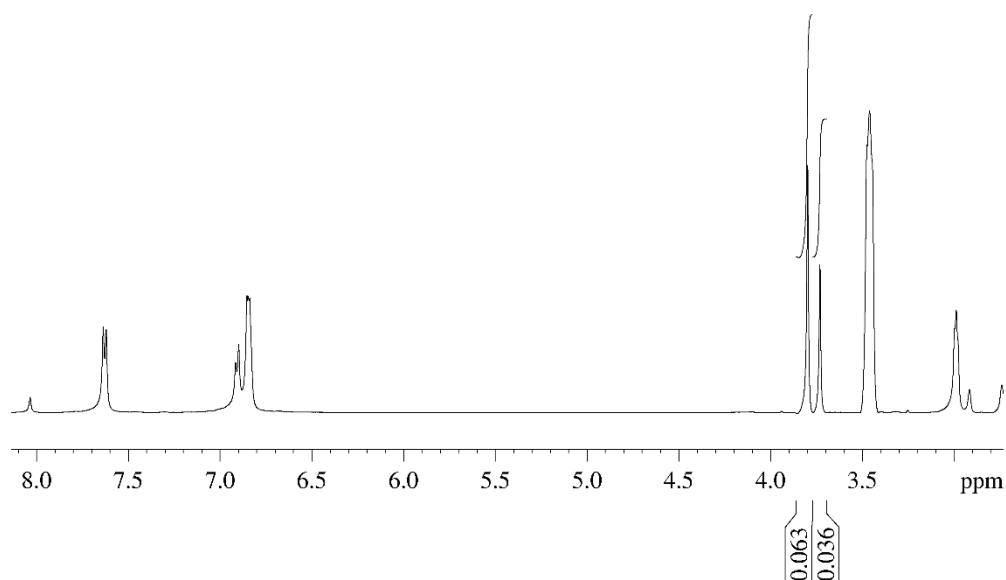
Figure 6.4 – ^{1}H NMR spectrum to determine concentration of **11** at t_0 in product inhibition experiment. OMe protons used due to broadened peaks in the aromatic region at room temperature.

6.2.3.7. Reaction conditions for *in situ* study in *d₃*-MeCN

	MW	Density	Standard	2x [10]	2x [TBAA]	2x [8]	0.5x [9]
CuI (mg)	190.44		1.2	1.2	1.2	1.2	1.2
8 (mg)	103.12		1.3	1.3	1.3	2.6	1.3
TBAA (mg)	629.07		59.0	59.0	118.0	59.0	59.0
d₃-MeCN (μL)			500	500	500	500	500
9 (mg)	234.03		14.6	14.6	14.6	14.6	7.3
10 (μL)	85.15	0.862	9	18	9	9	9

6.3. Chapter 3

6.3.1. General procedures

6.3.1.1. Reactions with automated sampling

All experiments were performed as outlined in general procedure above. Reactions were performed in a 4 mL vial with a stirrer disk in a 24 well plate within a glovebox filled with an N_2 atmosphere. Heating, solution additions and sampling were executed by a Freeslate automation robot.

Inside a nitrogen-filled glovebox reaction vials containing magnetic stirrer disks were loaded with the corresponding amounts of CuI (0.1 eq., 0.05 mmol), ligand (**8** or **37**, 0.1 mmol) and base (Cs_2CO_3 or K_3PO_4, 1.5 eq., see table below for quantities). Into separate vials, a solution of **9** (0.625 M) in and a solution of **28**/1,1'-biphenyl (0.441 M and 0.0294 M, respectively) were made up in degassed and anhydrous DMF. The reaction vials were loaded into a 24 well stainless steel heating plate and loosely fitted with septum seal caps to prevent pressure fluctuations during charging and sampling. The reaction vials were each charged with the **28**/1,1'-biphenyl solution (1.7 mL), heated to 90 °C before being left to equilibrate for 30 minutes. The solution of **9** was pre-heated to 90 °C and the reaction initiated through the addition of this solution (0.8 mL) to each vial.

For analysis, HPLC vials were loosely fitted with caps and injected with 500 µl MeCN by the Freeslate automation robot. Sampling of reactions was also performed by the robot at the desired time intervals, whereby 30 µl of reaction mixture was added to the MeCN. The samples were removed from the glovebox and filtered using Whatman Mini-UniPrep syringeless filters (0.2 µm pore size) prior to analysis.

For experiments varying the quantities of **9** and **28**, separate solutions were made to adjust the reaction concentrations without changing the volume of the reaction mixtures.

6.3.1.2. Screening reactions

All solids were added to a flame dried Schlenk flask and 3 vacuum purge and nitrogen flush cycles were performed before addition of liquid substrates or ligands and 5 mL degassed, anhydrous solvent and heated under an N_2 atmosphere overnight. The resulting solutions were filtered through a short silica plug using 50 mL ethyl acetate and concentrated to give the crude product, to be analysed by ^1H NMR spectroscopy.

6.3.1.3. Formylation of piperidine

CuI (19.0 mg, 0.1 mmol), **8** (20.6 mg, 0.2 mmol), biphenyl (15.4 mg, 0.1 mmol) and base (1.5 mmol) were added to a flame dried Schlenk flask and 3 vacuum purge and nitrogen flush cycles were performed. **10** (158 µL, 1.5 mmol) was added *via* microsyringe, followed by 5 mL degassed, anhydrous DMF. The reactions were heated under an argon atmosphere for the designated time before being allowed to cool to room temperature and analysed by ^1H NMR.

6.3.2. Base suppliers, purity, and drying protocols

Cesium carbonate was obtained from three individual sources; Sigma Aldrich (99 %, Lot # BCBP3311V), Acros Organics (99.5 %, Lot # A0359643) and Chemetall (Milled, D_{50} = 20 µm, D_{90} = 50 µm, Bx # 27091B032) and oven dried at 80 °C before being used. Prior to SEM analysis, all bases were dried at 75 °C for a period of at least 24 hours, ensuring consistency between samples.

6.3.3. Synthesis of materials

6.3.3.1. Synthesis of 1-(4-methoxyphenyl)pyrrolidin-2-one - 46
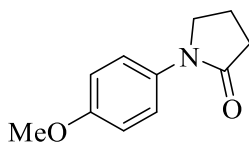
CuI (19.0 mg, 0.1 mmol), **8** (20.6 mg, 0.2 mmol), Cs_2CO_3 (489.0 mg, 1.5 mmol) and **9** (234.0 mg, 1 mmol) were added to a flame dried Schlenk flask. 3 vacuum purge and nitrogen flush cycles were performed before addition of **28** (114 µL, 1.5 mmol) and 5 mL DMF and heated to 90 °C for 16 hours. The resulting brown liquid was filtered through a short silica plug using 50 mL ethyl acetate and concentrated to give the crude product, which was purified by column chromatography, eluting with a 7 : 3 mixture of

n-hexane and ethyl acetate (R_f = 0.74) to yield **46** as a cream coloured solid (172.9 mg, 90% yield).

^{1}H NMR (500 MHz, CDCl$_3$) δ (ppm) = 7.49 (d, *J* = 9.2 Hz, 2H), 6.90 (d, *J* = 9.1 Hz, 2H), 3.83 (t, *J* = 7.1 Hz, 2H), 3.80 (s, 3H), 2.58 (t, *J* = 8.0 Hz, 2H), 2.15 (quint, *J* = 7.8 Hz, 2H); ^{13}C NMR (125 MHz CDCl$_3$) δ (ppm) = 173.9, 156.6, 132.7, 121.9, 114.1, 55.5, 49.2, 32.5, 18.1; vmax (neat)/cm^{-1} 2951, 1883, 1677 (C=O), 1508, 1391, 1223, 1125; Anal. Calcd for C$_{11}$H$_{13}$NO$_2$: C, 69.09; H, 6.85; N, 7.32. Found: C, 68.20; H, 6.80; N, 7.20; HRMS (ESI+) *m/z* [M+H]$^+$: Calcd for C$_{11}$H$_{13}$NNaO$_2$: 214.0844. Found: 214.0845.

Literature values:[6] ^{1}H NMR (400 MHz, CDCl3): δ (ppm) = 7.49 (d, *J* = 9.1 Hz, 2H), 6.90 (d, *J* = 9.1 Hz, 2H), 3.83 (t, *J* = 7.1 Hz, 2H), 3.80 (s, 3H), 2.59 (t, *J* = 8.1 Hz, 2H), 2.15 (quint, *J* = 7.6 Hz, 2H); ^{13}C NMR (100MHz, CDCl3): δ (ppm) = 173.9, 156.6, 132.6, 121.9, 114.0, 55.5, 49.2, 32.5, 18.0.

6.3.3.2. Synthesis of sodium pyrolidinide – Na-28
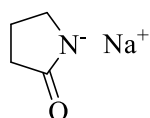
NaH (60 % dispersion in mineral oil, 1.048 g, 26.2 mmol) was weighed out into a flame-dried round bottom flask kept under nitrogen. The NaH was washed with three 10 mL batches of degassed pentane and the pentane removed via syringe. 20 mL of anhydrous THF was added at the NaH stirred as a suspension before being cooled down to 0 °C. **28** (2.0 mL, 26.2 mmol) was added dropwise and the reaction stirred at 0 °C until no further bubbles were observed to evolve. The colourless solution was allowed to warm up to room temperature and stirred for 30 minutes further before the solvent was removed *in vacuo*. 2.35 g (84 % yield) of an insoluble white solid was obtained and stored in an N$_2$ filled glovebox. ^{1}H NMR spectroscopy in *d*$_3$-MeCN showed no starting material peaks, indicating all **28** had reacted.

6.3.3.3. Synthesis of sodium *N,N*-dimethylglycinate – Na-8
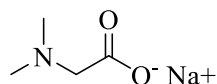
NaH (60 % dispersion in mineral oil, 77.6 mg, 1.94 mmol) was weighed out into a flame-dried round bottom flask kept under nitrogen. The NaH was washed with three 6 mL batches of degassed pentane and the pentane removed via syringe. 2.5 mL of anhydrous THF was added at the NaH stirred as a suspension before being cooled down to 0 °C. **8** (200 mg, 1.94 mmol) was suspended in 2.5 mL MeCN and added slowly to the NaH, the reaction was stirred at 0 °C until no further bubbles were seen to evolve. The colourless solution was allowed to heat to room temperature and stirred for 30 minutes further before the solvent was removed *in vacuo*. The off-white solid was washed three times with degassed MeCN, giving 80 mg (33 % yield) of an insoluble white solid was obtained and stored in an N_2 filled glovebox. ^{1}H NMR spectroscopy in d_3-MeCN showed no starting material peaks, indicating all **8** had reacted. Further characterization of this salt was unsuccessful due to its low solubility in organic solvents.

6.3.4. HPLC calibration

Calibrations were run based on the 200 mM reactions being diluted (30 µL reaction mixture diluted with 0.5 mL solvent).

4-Iodoanisole	Product	Internal Standard
8	**46**	**IS**
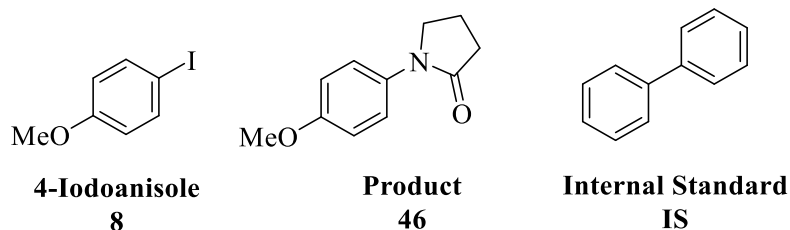
UV lamp set at 285 nm and concentration of 1,1-biphenyl (IS) held at 1.13 mM.

[46] (mM)	1.1	2.8	5.7	8.5	10.2	11.3
Area **46**	129665.5	323057.9	646656.8	929430.4	1136975.0	1257801.0
Area IS	53605.9	54349.68	55026.88	54723.1	55208.0	55779.7
Area **46**/IS	2.4	5.9	11.7	17.0	20.5	22.5

	Value	Standard Err
Intercept	0.0238	0.04637
Slope	2.2528	0.00539
R Squared	0.9999	--
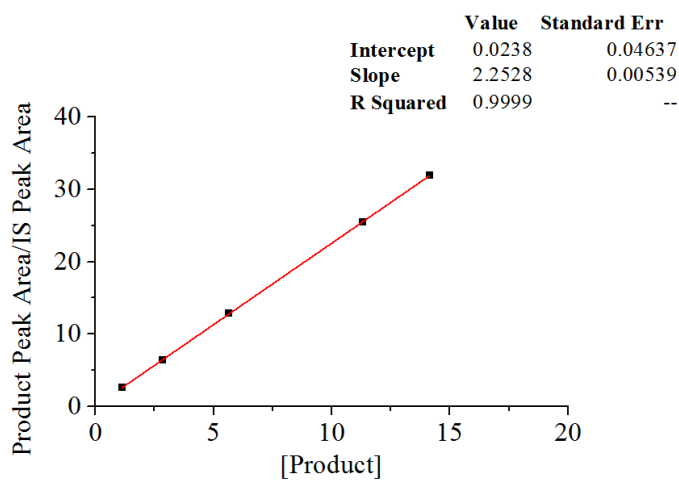
Figure 6.5 - HPLC calibration curve for 46.

[9] (mM)	1.1	2.8	5.7	8.5	10.2	11.3
Area **9**	82035.7	207296.1	419618.7	605277.8	745358.8	842654.1
Area IS	53605.9	54349.68	55026.88	54723.1	55208.0	55779.7
Area **9**/IS	1.5	3.8	7.6	11.1	13.5	15.1

	Value	Standard Err
Intercept	-0.30404	0.16884
Slope	1.59237	0.01964
R Squared	0.99939	
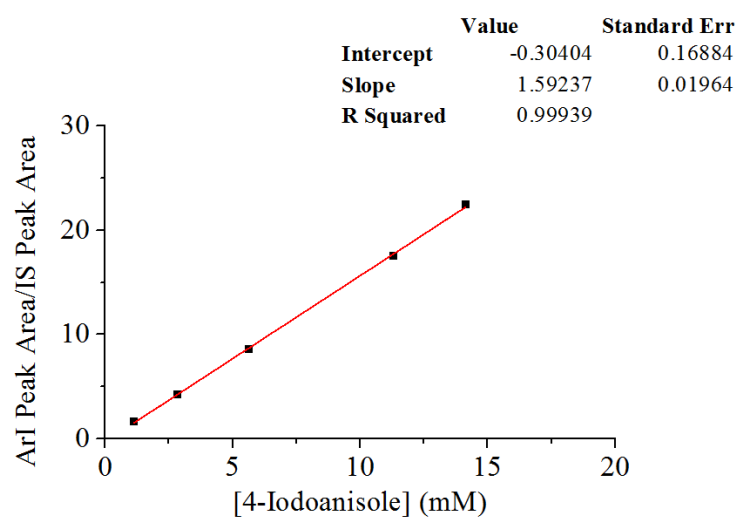
Figure 6.6 - HPLC calibration curve for **9.**

6.3.5. Kinetic reaction with inorganic bases

6.3.5.1. Reaction conditions – experiment 1 (8/Cs$_2$CO$_3$)

	MW (g.mol^{-1})	Density (g.mL^{-1})	Standard	0.5x [CuI/8]	2x [28]	Standard Duplicate	0.5x CuI	Product Inhibition	1eq H$_2$O
CuI (mg)	190.44		9.5	4.8	9.5	9.5	4.7	9.5	9.5
8 (mg)	103.12		10.3	5.2	10.3	10.3	10.3	10.3	10.3
1,1'-Biphenyl (mg)	154.21		7.7	7.7	7.7	7.7	7.7	7.7	7.7
Cs$_2$CO$_3$ (mg)	325.82		244	244	244	244	244	244	244
DMF (µL)			2500	2500	2500	2500	2500	2500	2500
9 (mg)	234.03		117	117	117	117	117	117	117
46 (mg)	191.23							47.8	
28 (µL)	85.15	1.116	57	57	114	57	57	57	57
H$_2$O (µL)	18.02	1.000							9

Conditions for reactions repeated in experiments with *N,N*-diethylsalicylamide (**37**)/K$_3$PO$_4$.

6.3.6. Sampling air-sensitive reactions

To ensure no oxygen is introduced into the reaction system by standard sampling techniques, enough needles for the desired amount of samples are introduced prior to the vacuum/inert gas cycles, with each needle thoroughly flushed. The set-up as shown below has been found to be a simple method of obtaining kinetic data with these reactions.

Figure 6.7 – Set-up of reaction for sampling under an inert atmosphere, avoiding introduction of O_2.

6.3.7. GC calibrations

Calibrations were run based on the 200 mM reactions being diluted (100 µL reaction mixture diluted with 1.4 mL solvent).

| 4-Iodoanisole | Product | Internal Standard |
| 8 | 46 | IS |
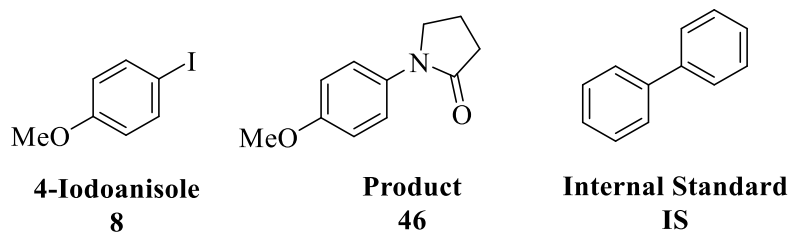
6.3.7.1. Compound 9

[9] (mM)	1.3	3.3	6.7	13.3	16.7
Area 9	1138.4	903.8	450.6	225.7	82.9
Area IS	181.9	180.7	180.5	179.1	177.8
Area 9/IS	6.3	5.0	2.5	1.3	0.5

	Value	Standard Error
Intercept	-0.01638	0.01303
Slope	0.37657	0.00129
R Squared	0.99995	
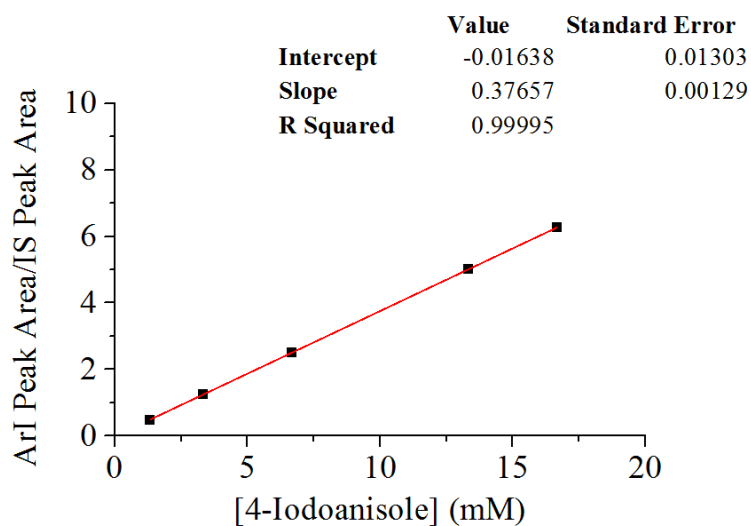
Figure 6.8 - GC calibration curve for starting material.

6.3.7.2. Compound 46

[46] (mM)	1.3	3.3	6.7	13.3	16.7
Area 46	1739.1	1387.1	688.3	345.6	125.9
Area IS	181.9	180.7	180.5	179.1	177.8
Area 46/IS	9.6	7.7	3.8	1.9	0.7

	Value	**Standard Error**
Intercept	-0.02697	0.02468
Slope	0.57636	0.00244
R Squared	0.99993	--
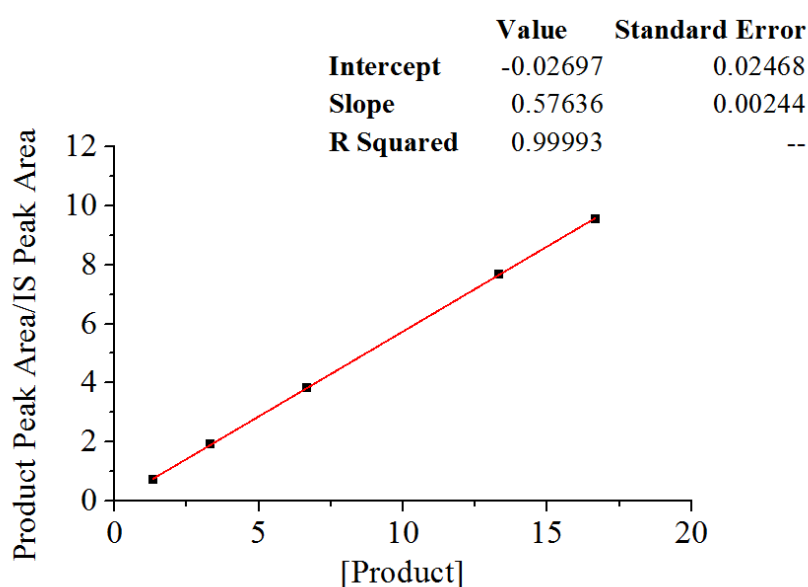
Figure 6.9 - GC calibration curve for **46**.

6.3.8. Experiment with portioned addition of Na-pyrrolidinone (Na-28)

CuI (19 mg, 0.1 mmol), **50** (36 mg, 0.2 mmol), 1,1'-biphenyl (15.4 mg, 0.1 mmol) and **9 1** (234 mg, 1 mmol) were added to a flame-dried Schlenk flask under nitrogen. Three purge/flush cycles were performed prior to addition of degassed DMF (2.5 mL). In a separate flask, **Na-28** (160 mg, 1.5 mmol) was mixed with degassed DMF (2.5 mL) under nitrogen to give a suspension. Both flasks were heated to 90 °C and the **Na-28** suspension was added in three portions at 0, 1 and 2 hours. The reaction was stopped after 20 hours and GC analysis showed 60 % conversion to product.

6.4. Chapter 4

6.4.1. Synthesis of materials

6.4.1.1. Preparation of cesium adipate - 48
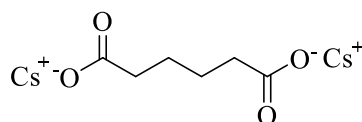
Adipic acid (1.00 g) and Cs_2CO_3 (2.23 g) were stirred at 50 °C in MeOH for 16 hours. The solvent was removed under reduced pressure to give a solid, which was dried under high vacuum for 4 hours, yielding 2.60 g of **48** as a free flowing white powder.

HRMS (ESI-) *m/z* $[C_6H_9O_4]^-$ calcd. 145.0512. Found: 145.0509; $[C_6H_8O_4Cs]^-$ calcd. 276.9477. Found: 276.9482.

6.4.2. Isolation of Cu(II)-complexes

6.4.2.1. Bis-(*N*,*N*-dimethylglycinato)copper(II) monohydrate - 71
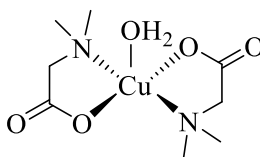
Following the same procedure detailed in Section 6.3.3.1. with Cs_2CO_3 replaced with 417 mg cesium adipate. Following elution of the organic compounds through a silica plug with EtOAc, the plug was flushed with 50 mL EtOH to yield a blue solution. The solvent was removed by evaportation and the blue oil was crystallised to give X-ray quality single crystals by vapour diffusion (MeOH/Et$_2$O).

^{1}H NMR (500 MHz, MeOD) δ (ppm) = 3.73 (s, 2H), 2.94 (s, 6H);

6.4.2.2. Bis-(*N*,*N*-dimethylglycinato)copper(II)-CsI adduct 72

Procedure 1
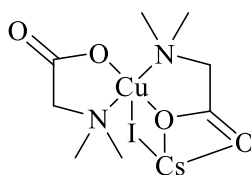
CuI (54 mg, 0.284 mmol), **8** (123 mg, 1.194 mmol) and Cs_2CO_3 (48 mg, 0.147 mmol) were added to a flame-dried Schlenk flask under N_2. The flask was flushed and evacuated three times with N_2 and 5 mL anhydrous DMF added. The mixture was stirred at 90 °C for 16 hours and upon cooling, some red/brown precipitate was seen to settle from the blue reaction solution. The blue solution was syringed out of the Schlenk flask and crystallisations were prepared. Single crystals suitable for X-ray diffraction were obtained by allowing diethyl ether to diffuse into a saturated solution of the complex in a 1:4 mixture of THF : DMF.

The complex crystallised as blue blocks in a monoclinic cell and was solved in the $P2_1/n$ space group, with one monomer unit in the asymmetric unit. In the solid state the compound forms a polymeric type structure.

Procedure 2

CuI (54 mg, 0.284 mmol), **8** (123 mg, 1.194 mmol) and Cs_2CO_3 (48 mg, 0.147 mmol) were added to a flame-dried Schlenk flask under N_2. The flask was flushed and evacuated three times with N_2 and 5 mL anhydrous DMF added. The mixture was stirred at 90 °C for one hour, after which the reaction was cooled to room temperature. The resulting blue solution was separated from the brown solid formed during the reaction *via* cannula filtration, and concentrated to 1 mL. 10 mL of Et_2O was added to precipitate the complex as a blue powder. The air-stable solid was collected, further washed with Et_2O and dried under vacuum to yield 71 mg, (45% yield) of the complex.

Anal. calcd for $C_8H_{16}CuN_2O_4CsI$: C, 18.21; H, 3.06; N, 5.31; Found: C, 18.20; H, 3.00; N, 5.20. HRMS (ESI+) *m/z* $[Cs]^+$ calcd. 132.9054. Found: 132.9035; $[Cu(MeCN)_2]^+$ calcd. 144.9827. Found: 144.9822; $[\mathbf{8} + Cs]^+$ calcd. 235.9688. Found: 235.9752; HRMS (ESI-) *m/z* $[\mathbf{8}\text{-}\mathbf{H}]^-$ calcd. 102.0561. Found: 102.0639; $[I]^-$ calcd. 126.9045. Found:

126.9035; [CuI$_2$]$^-$ calcd. 316.7385; Found: 316.7392. ^{133}Cs NMR (66 MHz, d_7-DMF) δ (ppm) – 9.0 (rel. to CsI).

6.4.2.3. Bis-(2-isobutyrylcyclo)copper(II) - 73
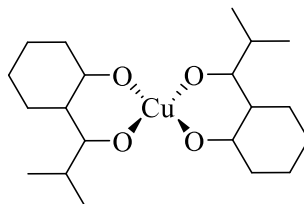
CuI (57 mg, 0.30 mmol), 2-isobutyrylcyclohexanone (197 µL, 1.20 mmol) and Cs$_2$CO$_3$ (49 mg, 0.15 mmol) were added to a flame-dried Schlenk flask under N$_2$. The flask was flushed and evacuated three times with N$_2$ and 5 mL anhydrous DMF added. The mixture was stirred at 90 °C for 60 hours, after which the reaction was cooled to room temperature. The resulting green solution was filtered through silica under N$_2$ *via* cannulae. 0.6 mL anhydrous THF was added and the solution was layered with 3 mL anhydrous Et$_2$O. The complex crystallised as green blocks and the single-crystal X-ray diffraction solved to show the complex **73**.

6.4.3. Isolation of Cs-bases post-reaction

Following completion of the reaction, the solution stopped stirring and was removed *via* syringe at 90 °C, the solid was then washed three times with hot, anhydrous Et$_2$O and evaporated to dryness. The dried solid was stored under argon until analysis was performed.

6.4.4. EPR measurements

EPR measurements were performed at the Leibniz-Institut für Katalyse with reactions prepared by Dr Bao Nguyen and data collected and processed by Mr Sven Adomeit.

6.4.4.1. *In situ* experiment

2.50 g (10.7 mmol) **9**, 0.221 g (2.14 mmol, 20 mol%) **8** and 5.23 g (16.05 mmol) Cs$_2$CO$_3$ were added to a jacketed glass reactor and flushed with argon. 54 mL anhydrous, degassed DMF and 1.25 mL **28** were added and the reaction allowed to equilibrate at 80 °C.

CuI was added last to the pre-equilibrated reaction mixture containing all other components to enable EPR background measurements. The reaction was performed under argon at 80 °C and the solution (with *in situ* filtration) was circulated through the EPR cavity using an FEP tube (ID 0.8 mm) using a Milligat pump at a flow rate of 3.0 mL/min. EPR spectra were recorded on a Brücker ELEXYS spectrometer at room temperature in X-band with a microwave power of 6.9 mW, a modulation frequency of 100 kHz and modulation amplitude of up to 5 G.

6.4.4.2. CuI/8/DMF experiment

The sample was prepared using a standard EPR tube in a glovebox with degassed DMF and measured using the same equipment as described above. The sample was cooled with liquid nitrogen during this measurement.

6.4.5. SEM imaging and EDX measurements

All samples were mounted in powder form, under exclusion of ambient moisture, on SEM sample stubs using adhesive carbon film. The samples were then coated with a thin layer of iridium using a Cressington 208HR sputter coater. Samples were imaged using an FEI Nova NanoSEM 450 operating typically at 3 kV. The gun voltage was increased to 10 keV to collect EDX point spectra.
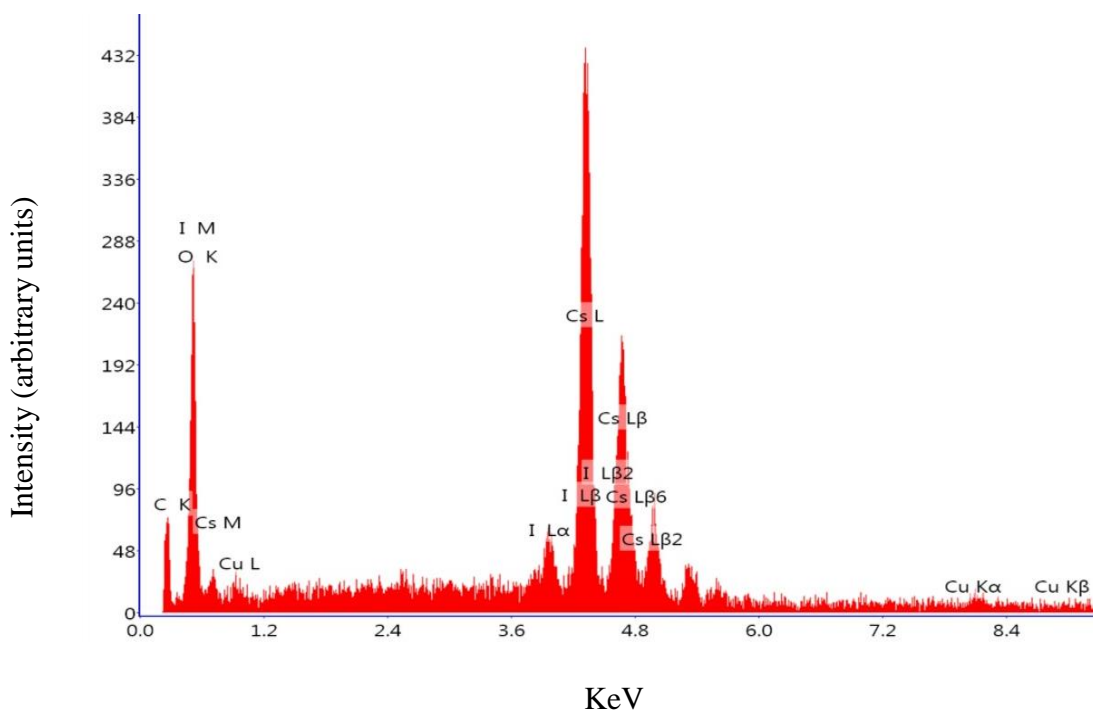
Figure 6.10 – EDX spectrum of solid obtained post-reaction.

6.4.6. Powder diffraction

X-Ray powder diffraction data was collected on a Bruker D2Phaser Diffractometer. Powdered samples were mounted on a silicon wafer by evenly distributing the powder over the wafer. All samples were rotated during data collection to ensure more homogeneous (i.e. isotropic) diffraction patterns. Data collection was carried out at room temperature, using Cu Kα radiation (λ = 1.54184 Å). Diffraction patterns were recorded in step-scan mode with a step size of (2θ) 0.7°, from (2θ) 5° to 55° (30 secs per step) using a 0.1 or 0.6mm divergent slit. Samples showed no significant evidence of degradation within the X-ray beam. The software package Diffrac.Suite Eva14 was used to process the experimental powder X-ray diffraction data collected, and Mercury 3.3 was used to simulate the powder diffraction pattern of the single crystal structures taken from literature.

6.4.7. Atomic absorption spectroscopy

Reactions were prepared as described in Section 6.3.3.1. and sampled as in Section 6.3.6. After allowing all solids to settle to the bottom of the reaction, a 100 µL sample of the solution was taken from the reaction. The sample was quenched by 1 mL of conc. HNO_3 and the sample made up to 10 mL in a volumetric flask with deionised water. The samples were run by Mr. Simon Lloyd at Leeds School of Engineering. Cu samples were run at a wavelength of 324.8 nm with a slit width of 0.5 nm and Cs samples were run at a wavelength of 852.1 nm and slit width of 1.0 nm.

6.4.8. ^{133}Cs NMR – Solubility

^{133}Cs NMR spectra were collected on a Bruker Avance III HD-400 (AV400) at 90 °C in DMF. An insert tube was used to include 0.1 M solution of $CsNO_3$ in D_2O as external standard and solvent for locking, while preventing Cs exchange between the standard and the sample.

Samples were prepared by stirring saturated solutions of CsI, $CsHCO_3$ and Cs_2CO_3 (Acros Organics, Lot A0359643) in anhydrous DMF at 90 °C for 2 hours. After the mixture was allowed to settle, the supernatants (0.5 mL) were transferred to an NMR tube via a syringe fitted with a metal needle (pre-flushed with hot DMF). An insert tube filled with 0.1 M $CsNO_3$ in D_2O was inserted into the NMR tube and the samples kept at

90 °C. The samples were inserted to the NMR spectrometer at 70 °C and quickly heated to 90 °C before data acquisition.

6.4.9. General procedure for hot filtrations

Flame-dried glassware was assembled as shown in Figure 6.11 with two B19 QuickFit Schlenk flasks which connected *via* a sinter filter with two male joints on either side. Solids of the reaction were added to the bottom Schlenk flask (side A) and three vacuum/argon fush cycles were performed. In reactions with added Cs_2CO_3, this was added to side B. A solution of 0.3 M **28** in anhydrous, degassed DMF was added to side A by syringe, with a high flow of argon. After the desired reaction time, the apparatus was inverted to allow filtration through the sinter glass into side B, and the reaction allowed to proceed. Conversion at the time of inversion was assessed by washing the collected solid with $CDCl_3$ following completion of the reaction, and NMR analysis of the washings.
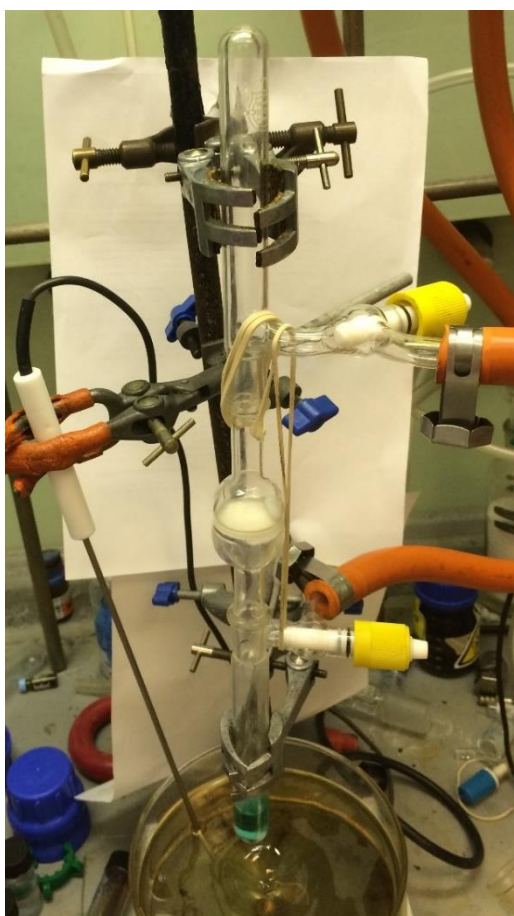
Figure 6.11 - Reaction set-up for hot filtration reactions. Side A – below sinter glass. Side B – above sinter glass.

6.4.10. General procedure for reactions with Cu/Cs precipitate - A

CuI (19 mg, 0.1 mmol), **8** (21 mg, 0.2 mmol) and Cs_2CO_3 (489 mg, 1.5 mmol) were added to a flame-dried Schlenk flask under N_2. The flask was flushed and evacuated three times with N_2 and 5 mL anhydrous DMF added. The mixture was stirred at 90 °C for one hour, allowed to settle, and as much solution as possible was removed with a syringe, without disturbing the solid. 5 mL of a solution of **28** (0.3 M), **9** (0.2 M) and biphenyl (0.02 M) was added to the solid and the reaction heated at 90 °C overnight.

6.4.11. General procedure for reactions with Cu/Cs precipitate - B

CuI (19 mg, 0.1 mmol), **8** (21 mg, 0.2 mmol) and Cs_2CO_3 (489 mg, 1.5 mmol) were added to a flame-dried Schlenk flask under N_2. The flask was flushed and evacuated three times with N_2 and 5 mL anhydrous DMF added. The mixture was stirred at 90 °C for one hour, allowed to settle, and as much solution as possible was removed with a syringe, without disturbing the solid. The remaining solid was washed three time with 5 mL degassed, anhydrous MeCN, allowed to settle and the washings removed and the solid dried under vacuum. 450 mg of silver/grey powder was obtained, and 350 mg was weighed into a Schlenk flask. Following a typical anaerobic procedure, 2.5 mL of a solution of **28** (0.3 M), **9** (0.2 M) and biphenyl (0.02 M) was added to the solid and the reaction heated at 90 °C overnight.

6.5. Chapter 5

6.5.1. General Procedures

Experiments involving air sensitive reagents or products were performed under an atmosphere of nitrogen, using oven-dried glassware. The XAS flow-cell was assembled and flushed with nitrogen for 30 minutes before experiments. Anhydrous 2-propanol (<50 ppm water) and all other reagents were obtained from commercial suppliers and used without further purification. Reaction solvents were degassed by bubbling nitrogen through for a minimum of 30 minutes. All glassware was dried in oven (120 °C) overnight prior to use. GC analyses were performed using a Bruker 430-GC equipped with a CP-8400 autosampler.

Complexes [Cp*Ir(μ^2-Cl)$_3$IrCp*]OTf (**90**) and [Cp*IrCl$_2$(Py)] (**91**) were synthesised by members of the McGowan group at the University of Leeds according to literature procedures.[7] Immobilised catalysts were provided by Yorkshire Process Technology.

6.5.2. Synthesis of Materials

6.5.2.1. [Cp*IrCl$_2$]$_2$ - 92

25 mL of degassed methanol was added to iridium trichloride hydrate (1.00 g, 2.70 mmol), followed by 1,2,3,4,5-pentamethylcyclopentadiene (0.75 mL, 6.33 mL) and the mixture heated at reflux under N$_2$ for 36 hours. An orange powder precipitated from the solution, which was removed by syringe and the solid washed three times with 10 mL methanol. The orange solid was dried under vacuum to yield **92** (0.96 g, 1.21 mmol, 89 % yield).

^{1}H NMR (400 MHz, CDCl$_3$) δ (ppm) = 1.59 (s, 15H); ^{13}C NMR (101 MHz CDCl$_3$) δ (ppm) = 86.2, 9.36.[8]

6.5.3. Typical batch reaction

In a vial, the immobilized pre-catalyst **86a** (0.057 g, 0.035 mmol Ir), KO^{t}Bu (0.50 mg, 0.004 mmol) and anhydrous ^{i}PrOH (5 mL) were added. The mixture was stirred at 60 °C for one hour for catalyst activation. Benzaldehyde (**88**) (0.05 mL, 0.5 mmol) was then added. The mixture was stirred at 60° C and the reaction was monitored by GC. Further

runs were conducted by decanting the solution, and recharging the resin with KO^{t}Bu (0.5 mg, 0.004 mmol), ^{i}PrOH (5 mL) and **88** (0.05 mL, 0.5 mmol) immediately.

6.5.4. Mercury poisoning experiment

Two identical batch reactions were performed at the scale described in 6.5.3. at 60 °C. After 3 hours, mercury (2.1 g, 10.5 mmol) was added to one reaction. GC samples were taken from both reactions at regular intervals with 1,1'-biphenyl as internal standard.

6.5.5. 'Hot filtration' experiment

A batch reaction as described in 6.5.1. was performed at 60 °C. After 3 hours, half of the reaction mixture was taken up by a syringe and filtered through a Whatman® cellulose acetate syringe filter (0.2 mm) into another vial. Both vials were continued to be stirred at and GC samples were taken at regular intervals with 1,1'-biphenyl as internal standard.

6.5.6. Effect of water experiment

Two batch reactions were performed based on the typical anhydrous batch reaction in 6.5.3. using 57 mg of **86a** (0.035 mmole Ir), with water (3.3 mL, 0.18 mmole) added to one. Reaction progress was monitored over 6 hours using GC.

6.5.7. Beamline Details

Solid state XAS measurements of various iridium catalysts and standards at the Ir L-edge were acquired on beamline B18 at Diamond Light Source using a Si(111) monochromator at 3 GeV and 300 mA. Samples were prepared as 8 mm cellulose pellets (80 mg of cellulose) with 10 mg of the immobilised catalyst samples and 5 mg for the iridium complexes. Signal was recorded using an ionisation chamber and intensity monitoring.

Cl and K K-edge XAS measurements were performed on beamline BM28 of the ESRF using a Si(111) double crystal monochromator at 6 GeV and 200 mA. Ir L-edge, *ex situ* Cl K-edge and K K-edge spectra were collected in fluorescence mode using solid sample mounted on carbon tape under vaccum. *In operando* experiments are described in more details in section 0 and 0. Signal was recorded using MCA and a Vortex Silicon Drift detector.

Data processing was conducted using the IFFEFIT software package by Dr Bao Nguyen.[9]

6.5.8. XAFS spectroscopy flow-cell

A flow-cell for XAS at low energy in fluorescence mode was developed for this study (Figure 6.12). The cell was constructed from stainless steel, with a catalyst bed of 100 µm depth and a polypropylene window (6 µm thickness). The immobilised catalyst was mounted with the help of a stainless steel grid. Two Swagelok connectors were used to connect the cell with a pump for reaction solution and a reservoir for reaction output using 1/8" PTFE tubing. The cell is mounted on a heating unit, for temperature control, which is subsequently connected to a *x,y,z*-motorised mount inside a vacuum/helium chamber. A hole was drilled on the side of the cell for a thermocouple.

Figure 6.12 - Flow-cell with catalyst and window

6.5.9. *In operando* XAS experiment at Cl and K K-edge

The reaction solutions were prepared following the protocol outlined below at 60 $^{\circ}$C using a milliGAT$^{®}$ positive displacement pump and 1/8" PTFE tubing.

Step 1: A solution of anhydrous 2-propanol was passed through the flow reactor (volume = 6.9 µL) containing **86a** (1 mg, 12% Ir w/w) on a stainless steel mesh support at 10.8 µLmin^{-1} (residence time = 39 seconds) at 60 $^{\circ}$C for 30 minutes. XANES spectra at Cl K-edge or K K-edge were collected.

Step 2: A solution of anhydrous 2-propanol (60 mL) containing KO^{t}Bu (6.0 mg, 0.89 mM) was passed through the flow reactor at 10.8 µL.min^{-1} and 60 $^{\circ}$C for 30 minutes to

generate active catalyst. This was followed by washing with anhydrous 2-propanol (0.33 mL) at flow-rate 10.8 µL.min^{-1}. XANES spectra at Cl K-edge or K K-edge were collected.

Step 3: A solution of anhydrous 2-propanol (60 mL) containing KO^{t}Bu (6 mg, 0.89 mM) and **88** (0.637 g, 0.10 M) was passed through the flow reactor 10.8 µL.min^{-1} (residence time = 39 seconds) at 60 °C. This was continued for 24 hours, and XANES spectra at Cl K-edge and K K-edge were collected alternatively. The total runtime for each scan was approximately 60 minutes.

Step 4: Anhydrous 2-propanol (30 mL) was passed through the flow-cell at flow rate mL.min-1 to wash off residue of the reaction mixture. XANES spectra at Cl K-edge or K K-edge were collected.

Step 5: The flow-cell was allowed to cool to room temperature. A solution of HCl 1M in 2-propanol (1 mL) was flowed through the cell at 10.8 µL.min^{-1}. This was followed immediately by 2-propanol (30 mL) to remove the acid from the stainless steel flow-cell. XANES spectra at Cl K-edge or K K-edge were then collected.

Table 6.1 - *In operando* edge jump data at Cl K-edge and K K-edge *vs* time

Time (h)	Cl edge-jump	K edge-jump
0.05	0.0141	
1.00		0.0192
1.85	0.0165	
2.80		0.0307
3.51	0.0119	
4.47		0.0336
5.59	0.0146	
6.54		0.0306
7.61	0.0117	
8.80		0.0349
9.64	0.0119	
10.59		0.0422
11.30	0.0141	
12.26		0.044
12.97	0.014	
13.92		0.0485
14.64	0.0136	
15.60		0.017
16.39	0.0108	
17.34		0.0549
18.09	0.0112	
19.04		0.05

6.5.9.1. GC calibration and calculations

GC was performed using a BR-5 column (30 m x 0.25 mm (ID) x 0.25 µm film thickness) with carrier gas flow rate of 2.0 mL.min^{-1} and a temperature ramp from 50 to 310 °C at 20 °C.min^{-1}. The injection volume was 5 µL with a split ratio of 10. The response factors for the internal standard, substrate and product were calculated using an appropriate calibration for this GC and column.

Calibration was performed for between 0.1 % and 1.25 % of the reaction product, benzylalcohol (**89**), using 0.001 M biphenyl as an internal standard (Table 6.2). All calibration samples were made up using 0.001 M biphenyl solution in 2-propanol.

Table 6.2 - GC calibration of **89** against 1,1'-biphenyl as internal standard (IS).

| [89] (M)	0.0001	0.00025	0.0005	0.001	0.00125
Peak Area (BnOH)	54.0	168.7	350.7	638.9	757.3
Peak Area (IS 0.001 M)	165.7	170.9	145.8	121.6	123.6
Peak Area ratio (89/IS)	0.326	0.987	2.405	5.254	6.127

The calibration curve is shown below:
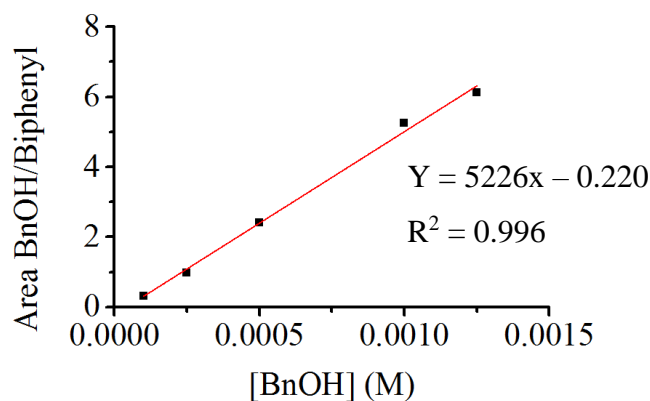
Figure 6.13 - Calibration curve for BnOH response factor against internal standard.

The concentration of **89** was calculated as:

$$[89] = \frac{(Area_{89}/Area_{Biphenyl}) + 0.22}{526.66}$$

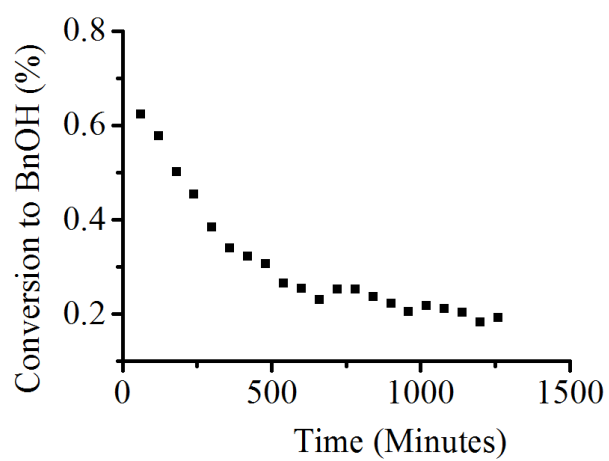### 6.5.9.2. Catalytic activity *vs* time experiment

The experiment was carried out as described in Section 0, to monitor the conversion of **88** to **89** over time. 1,1'-Biphenyl (0.001 M) was added to the reaction mixture as internal standard for GC. Samples were collected for every 60 minutes (0.65 mL) for 21 hours and analysed by GC without further purification. Conversion data was calculated based on the concentration of the product against the concentration of starting material flown into the cell (0.1 M **88**).
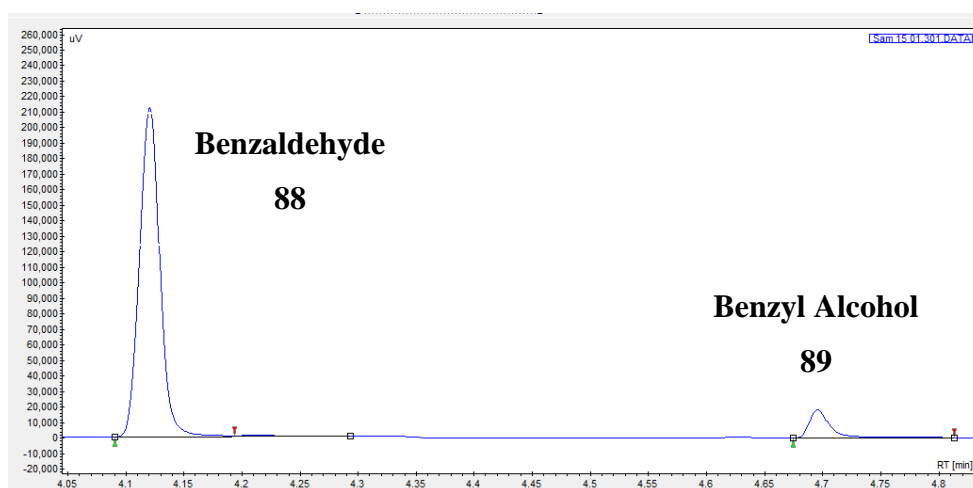
Figure 6.14 - Example GC chromatogram from catalytic activity *vs* time experiment.

Table 6.3 - Results from catalytic activity *vs* time experiment

Sample	Time (Minutes)	Time (Hours)	Area$_{89}$/ Area$_{Biphenyl}$	[89] (mM)	Conversion (%)
1	60	1	3.034281	0.623	0.623
2	120	2	2.798548	0.578	0.578
3	180	3	2.397136	0.501	0.501
4	240	4	2.150478	0.454	0.454
5	300	5	1.78777	0.384	0.384
6	360	6	1.555456	0.340	0.34
7	420	7	1.466791	0.323	0.323
8	480	8	1.380987	0.306	0.306
9	540	9	1.164112	0.265	0.265
10	600	10	1.105163	0.254	0.254
11	660	11	0.980291	0.230	0.23
12	720	12	1.094952	0.252	0.252
13	780	13	1.100872	0.253	0.253
14	840	14	1.015635	0.237	0.237
15	900	15	0.941104	0.222	0.222
16	960	16	0.852471	0.205	0.205
17	1020	17	0.912715	0.217	0.217
18	1080	18	0.885246	0.212	0.212
19	1140	19	0.843333	0.204	0.204
20	1200	20	0.735398	0.183	0.183
21	1260	21	0.789517	0.193	0.193

Figure 6.15 - Conversion vs time in catalytic activity vs time experiment

6.6. References

1. G.M. Sheldrick, *Acta. Crystallogr. A*, 2008, **64**, 112-122.

2. O.V. Dolomanov, L.J. Bourhis, R.J. Gildea, J.A.K. Howard and H. Puschmann, *J. Appl. Crystallogr.*, 2009, **42**, 339-341.

3. C.T. Yang, Y. Fu, Y.B. Huang, J. Yi, Q.X. Guo and L. Liu, *Angew. Chem. Int. Ed.*, 2009, **48**, 7398-7401.

4. S.Y. Lin, R.I. Duclos and A. Makriyannis, *Chem. Phys. Lipids*, 1997, **86**, 171-181.

5. J. Jeong, D. Lee and S. Chang, *Chem. Commun.*, 2015, **51**, 7035-7038.

6. F.-F. Yong, Y.-C. Teo, G.-L. Chua, G.S. Lim and Y. Lin, *Tetrahedron Lett.*, 2011, **52**, 1169-1172.

7. H.-H. Gortz, G. Luinstra, M. Forster, A. Baumann and E. Lindner, 2003, U.S. Patent Application No. 10/510,475.

8. F. Li, C.L. Sun and N.N. Wang, *J. Org. Chem.*, 2014, **79**, 8031-8039.

9. M. Newville, *J. Synchotron Radiat.*, 2001, **8**, 322-324.

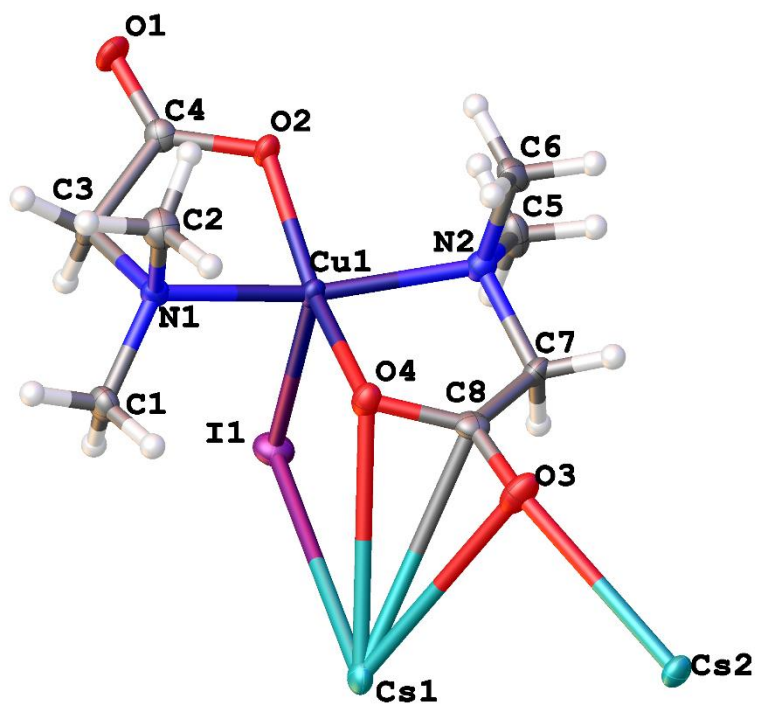# *Appendix*

A.1. Crystal structure data

Complex 71
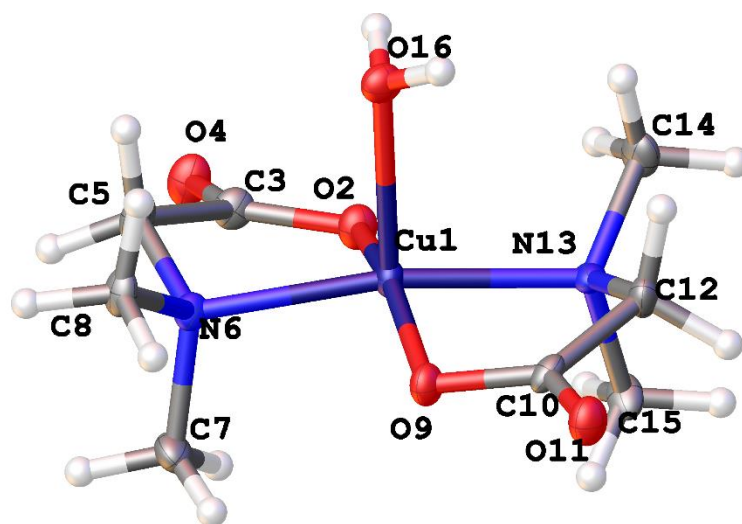
Crystal data and structural assignment

Identification code	GS130blue_Mo
Empirical formula	$C_8H_{18}CuN_2O_5$
Formula weight	285.78
Temperature/K	120.02(10)
Crystal system	monoclinic
Space group	Cc
a/Å	15.7025(6)
b/Å	9.5363(4)
c/Å	7.9857(3)
α/°	90
β/°	97.745(4)
γ/°	90
Volume/Å^3	1184.90(8)
Z	4
ρ_{calc}g/cm^3	1.602
μ/mm^{-1}	1.852

F(000)	596
Crystal size/mm^3	$0.24 \times 0.15 \times 0.11$
Radiation	MoKα ($\lambda = 0.71073$)
2Θ range for data collection/°	6.92 to 56.56
Index ranges	$-20 \leq h \leq 20$, $-12 \leq k \leq 12$, $-10 \leq l \leq 10$
Reflections collected	6125
Independent reflections	2866 [$R_{int} = 0.0646$, $R_{sigma} = 0.0910$]
Data/restraints/parameters	2866/4/157
Goodness-of-fit on F^2	1.038
Final R indexes [I>=2σ (I)]	$R_1 = 0.0474$, w$R_2 = 0.0934$
Final R indexes [all data]	$R_1 = 0.0544$, w$R_2 = 0.0994$
Largest diff. peak/hole / e Å^{-3}	0.99/-0.54
Flack parameter	-0.017(17)

Complex 72

Crystal data and structural assignment

Identification code	GS111blue_Mo
Empirical formula	$C_8H_{16}CsCuIN_2O_4$
Formula weight	527.58
Temperature/K	120.00(10)
Crystal system	monoclinic
Space group	$P2_1/n$
a/Å	8.5389(6)
b/Å	12.8281(9)
c/Å	14.4332(10)
α/°	90
β/°	97.972(6)
γ/°	90
Volume/Å^3	1565.71(19)
Z	4
ρ_{calc}g/cm^3	2.238
μ/mm^{-1}	5.662
F(000)	988

Crystal size/mm^3	$0.12 \times 0.07 \times 0.05$
Radiation	MoKα (λ = 0.71073)
2Θ range for data collection/°	6.14 to 52.74
Index ranges	-10 ≤ h ≤ 10, -13 ≤ k ≤ 16, -18 ≤ l ≤ 15
Reflections collected	10099
Independent reflections	3196 [R_{int} = 0.0461, R_{sigma} = 0.0494]
Data/restraints/parameters	3196/0/161
Goodness-of-fit on F^2	1.037
Final R indexes [I>=2σ (I)]	R_1 = 0.0305, wR_2 = 0.0551
Final R indexes [all data]	R_1 = 0.0389, wR_2 = 0.0593
Largest diff. peak/hole / e Å^{-3}	0.60/-0.78

Complex 73
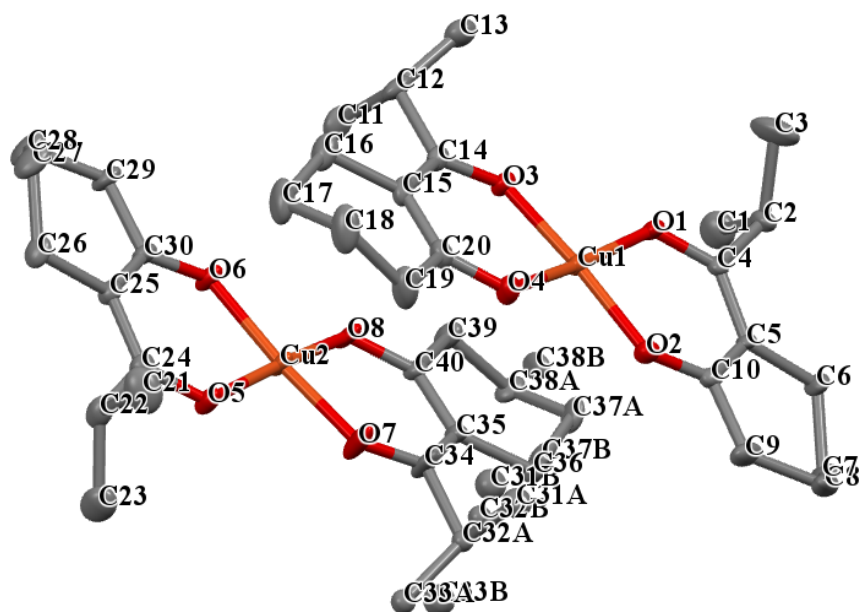
Crystal data and structural assignment

Identification code	GS131_Mo_d
Empirical formula	$C_{20}H_{30}CuO_4$
Formula weight	397.98
Temperature/K	120.00(19)
Crystal system	monoclinic
Space group	$P2_1/n$
a/Å	9.6080(3)
b/Å	20.0328(4)
c/Å	20.0278(6)
α/°	90
β/°	99.901(3)
γ/°	90
Volume/Å^3	3797.43(17)
Z	8
ρ_{calc}g/cm^3	1.392
μ/mm^{-1}	1.171
F(000)	1688

Crystal size/mm^3	$0.18 \times 0.09 \times 0.07$
Radiation	MoKα ($\lambda = 0.71073$)
2Θ range for data collection/°	5.48 to 56.56
Index ranges	-12 ≤ h ≤ 12, -26 ≤ k ≤ 26, -26 ≤ l ≤ 26
Reflections collected	28894
Independent reflections	9415 [R_{int} = 0.0335, R_{sigma} = 0.0365]
Data/restraints/parameters	9415/2/476
Goodness-of-fit on F^2	1.27
Final R indexes [I>=2σ (I)]	R_1 = 0.0736, wR_2 = 0.1433
Final R indexes [all data]	R_1 = 0.0852, wR_2 = 0.1473
Largest diff. peak/hole / e Å^{-3}	1.31/-1.14